The c-Rel transcription factor regulates host defence against neurotropic and cardiac virus infections

MATHIEU MANCINI

Department of Human Genetics
McGill University, Montréal
August, 2020

A thesis submitted to McGill University in partial fulfilment of the requirements of the degree of Doctor of Philosophy.

ABSTRACT

Infection with herpes simplex virus 1 (HSV-1) can result in an acute inflammatory condition of the brain called herpes simplex encephalitis (HSE). While relatively rare, HSE is the most common form of sporadic viral encephalitis worldwide. On the other hand, coxsackievirus B3 (CVB3) can establish productive infection in the heart, and is the most frequent cause of viral myocarditis. The onset of both HSE and CVB3-induced myocarditis is influenced in part by host genetics. While the genetic causes of viral myocarditis in humans are unclear, recent studies have established that inborn single gene errors are responsible for disease onset in cases of childhood HSE, where most discovered mutations compromise antiviral type I interferon signaling in the brain. Mouse models of viral infection have been instrumental to define the many layers of genetic regulation that govern host defence responses.

To identify novel genetic determinants of HSE that may extend beyond cell-intrinsic interferon signaling, we screened *N*-ethyl-*N*-nitrosourea (ENU)-mutagenized mice for susceptibility to HSE, and have discovered a homozygous C307X mutation in the reticuloendotheliosis oncogene (*Rel*), encoding a premature truncation of the NF-κB transcription factor subunit c-Rel, as a cause of lethal encephalitis. Upon HSE symptom onset, moribund mutant mice demonstrated elevated viral replication, neuroinflammation, and cell death in the hindbrain, resulting from defects in cell-mediated immunity. We next applied dual RNA sequencing of both host and viral transcripts, together with flow cytometry, to investigate early effects of the Rel^{C307X} mutation in the HSV-1-infected brain. At least one day prior to symptom onset, mutant brainstems were characterized by elevated viral RNA transcription and by excess interferon-dependent and inflammatory gene expression, predictive of later infiltration of pathological T lymphocytes and myeloid cells that drove fulminant HSE. Thus, Rel^{C307X}-dependent regulation of gene expression in the brain was detrimental in mouse HSE and involves distinct mechanisms from known cases of human childhood HSE. Conversely, the Rel^{C307X} mutation was protective against CVB3-induced myocarditis, resulting in improved control of viral transcription, and a later reduction in infectious CVB3 viral load in the heart. Compared to susceptible wild-type mice, the mutation also resulted in dampened inflammatory and cell-mediated gene expression, suggesting that while T lymphocytes and myeloid cells infiltrated the infected heart, these cells were attenuated in their ability to cause pathological damage to the heart, and allowed the virus to be efficiently cleared.

Ultimately, these findings support a role for the c-Rel transcription factor as a key regulator of inflammation during viral infection—protective during HSE, and detrimental to CVB3-induced myocarditis. This work also provides a framework, through the combination of dual host-pathogen transcriptomic profiling with flow cytometric analysis, to evaluate the effect of single gene defects in the context of whole infected tissues, which often vary in their capacity to support viral infection and tolerate inflammatory responses. The Rel^{C307X} model also highlights the potential for further investigations into the therapeutic modulation of inflammation through c-Rel or its regulators.

RÉSUMÉ

L'infection au virus *Herpes simplex* de type 1 (HSV-1) peut conduire à l'encéphalite herpétique (*herpes simplex encephalitis* ou HSE), une maladie marquée par une inflammation aiguë du cerveau. Bien que plutôt rare, le HSE représente la forme la plus courante parmi les encéphalites sporadiques d'origine virale recensées à l'échelle mondiale. D'autre part, le virus Coxsackie de type B3 (CVB3) peut causer une infection productive au niveau du cœur, et représente l'étiologie la plus importante de la myocardite virale. Chez l'hôte, divers facteurs génétiques peuvent contribuer en partie à la survenue du HSE et de la myocardite induite par le CVB3. Alors que les causes génétiques de la myocardite virale chez l'humain sont incertaines, des études récentes ont démontré que des lésions monogéniques et congénitales provoquent le HSE de l'enfant, avec la plupart de ces mutations causant un déficit dans la voie de signalisation de l'interféron qui assure normalement une protection antivirale au cerveau. Les modèles-souris de l'infection virale ont été déterminants pour comprendre les multiples niveaux de régulation génétique qui dirigent les nombreux mécanismes de défense de l'hôte.

Afin de découvrir de nouveaux facteurs génétiques qui peuvent contrôler la survenue du HSE et qui pourraient s'étendre au-delà de la voie de l'interféron de l'immunité intrinsèque, nous avons employé une stratégie de mutagénèse à la *N*-ethyl-*N*-nitrosourée (ENU) chez la souris. Parmi les souris mutées qui se sont avérées susceptibles au HSE, nous avons identifié une mutation homozygote C307X dans le gène *reticuloendotheliosis oncogene* (*Rel*), qui encode une forme tronquée du facteur de transcription c-Rel appartenant à la famille NF-κB, et qui entraîne une susceptibilité au HSE. Dès l'apparition de symptômes du HSE, les souris mutantes ont démontré des taux élevés de réplication virale, d'inflammation cérébrale et de mort cellulaire dans le cerveau postérieur, provenant de déficits reliés à l'immunité à médiation cellulaire. Le double séquençage de l'ARN de l'hôte et du virus, conjugué à la cytométrie en flux, nous ont permis d'examiner les effets précoces de la mutation Rel^{C307X} dans le contexte du cerveau infecté au HSV-1. Avec au moins un jour d'avance sur l'apparition des symptômes du HSE, les troncs cérébraux mutants étaient marqués par une augmentation importante de la transcription d'ARN virale, et d'une expression démesurée de gènes liés aux voies de l'interféron et de l'inflammation, indicatives de la future infiltration pathologique de lymphocytes T et de cellules myéloïdes qui ont conduit au HSE fulminant. Ainsi, cette régulation anormale de l'expression de gènes au cerveau, liée à la mutation Rel^{C307X}, était défavorable au HSE chez la souris, d'après des mécanismes distincts au

HSE de l'enfance. En revanche, la mutation *Rel*^{C307X} a eu un effet protecteur contre la myocardite induite par le CVB3, notamment en assurant un meilleur contrôle de la transcription virale, et ultérieurement en réduisant le titre infectieux du CVB3 dans le cœur. Comparée aux souris de type sauvage susceptibles au CVB3, la mutation a été responsable d'une diminution marquée de l'expression de gènes inflammatoires et de gènes liés à l'immunité à médiation cellulaire, ce qui suggère que malgré une infiltration de lymphocytes T et de cellules myéloïdes au cœur, la capacité de ces dernières à induire des dommages pathologiques au cœur était atténuée, permettant un contrôle efficace du virus.

En conclusion, nos résultats corroborent le rôle important du facteur de transcription c-Rel en tant que régulateur essentiel de la réponse inflammatoire à l'infection virale : c-Rel contribue aux mécanismes de défense de l'hôte contre le HSE, et nuit à la survenue de la myocardite induite par le CVB3. De plus, ces travaux font la preuve de l'utilisation en tandem du double séquençage de l'ARN de l'hôte et du virus avec la cytométrie en flux afin de bien évaluer la contribution de lésions monogéniques dans le cadre d'un tissu infecté; ce dernier pourrait varier en fonction de sa capacité à supporter une infection virale ou de tolérer une réponse inflammatoire trop prononcée. Enfin, le modèle *Rel*^{C307X} nous rappelle que c-Rel et ses potentiels régulateurs en amont pourraient faire l'objet de cibles thérapeutiques afin de moduler l'inflammation, et donc mériteraient de plus amples recherches.

TABLE OF CONTENTS

LIST OF ABBREVIATIONS

Gene and protein names follow standard nomenclature. For example: human gene *MYD88*; mouse gene *Myd88*; protein MYD88.

Abbreviation	Definition
ANOVA	Analysis of variance
APC	Allophycocyanin
ATP	Adenosine triphosphate
B10	C57BL/10J
B6	C57BL/6J
BBB	Blood-brain barrier
BH	Benjamini-Hochberg method
BMDC	Bone marrow–derived dendritic cells
BMDM	Bone marrow–derived macrophages
BSC	Brainstem and cerebellum
c-Rel (*Rel*)	Reticuloendotheliosis oncogene; c-Rel proto-oncogene
cAMP	Cyclic adenosine monophosphate
CAR (*Cxadr*)	Coxsackievirus and adenovirus receptor
CCL; CCR	C-C motif ligand; receptor
CD	Cluster of differentiation
cDNA	Complementary DNA
cGAMP	Cyclic guanosine monophosphate/adenosine monophosphate
cGAS (*Mb21d1*)	Cyclic GAMP synthase
CNS	Central nervous system
CPM	Counts per million
CRB	Cerebrum
CREB	Cyclic adenosine monophosphate/cAMP response element-binding
CT-1 (*Ctf1*)	Cardiotrophin-1
CVB3	Coxsackievirus B3
CX3CL; CX3CR	C-X3-C motif ligand; receptor
CXCL; CXCR	C-X-C motif ligand; receptor
DAF (*Cd55*)	Decay-accelerating factor
DC	Dendritic cells
DEG	Differentially expressed gene
DMEM	Dulbecco's Modified Eagle Medium
DN	Double negative

Abbreviation	Definition
DNA	Deoxyribonucleic acid
EAE	Experimental autoimmune encephalomyelitis
EDTA	Ethylenediaminetetraacetic acid
ENU	*N*-ethyl-*N*-nitrosourea
FBS	Fetal bovine serum
FC	Fold change
FITC	Fluorescein isothiocyanate
Foxp3	Forkhead box P3
FSC-A; H	Forward scatter-area; -height
G0; G1; G2; G3	Generation
Gapdh	Glyceraldehyde 3-phosphate dehydrogenase
GM-CSF (*Csf2*)	Granulocyte macrophage colony stimulating factor
GO	Gene ontology
GSEA	Gene set enrichment analysis
H2A	Histone 2A
HBSS	Hank's balanced salt solution
HHV	Human herpesvirus
HSE	Herpes simplex encephalitis
HSV-1	Herpes simplex virus 1
HSV-2	Herpes simplex virus 2
HVEM (*Tnfrsf14*)	Herpes virus entry mediator
i.n.	Intranasal
i.p.	Intraperitoneal
IFI16	IFN-γ-inducible protein-16
IFN; IFN-I; IFN-II	Interferon; type I interferon; type II interferon
IFNAR	Type I interferon receptor
Ig	Immunoglobulin
IKKα; β; γ; ε	I kappa B kinase α; β; γ; ε
IL	Interleukin
iPSC	Induced pluripotent stem cell
IRAK4 (*Irak4*)	Interleukin-1 receptor associated kinase 4
IRES	Internal ribosome entry site
IRF	Interferon regulatory factor
ISG	Interferon-stimulated gene
ISGF3	IFN-stimulated gene factor 3
JAK1	Janus kinase 1
kDa	Kilodalton

Abbreviation	Definition
KLRG1	Killer cell lectin-like receptor subfamily G member 1
LDH	Lactate dehydrogenase
LOD	Limit of detection
LPS	Lipopolysaccharide
Ly6	Lymphocyte antigen 6
M-CSF	Macrophage colony stimulating factor
MAVS (*Mavs*)	Mitochondrial antiviral-signaling protein
MDA5 (*Ifih1*)	Melanoma differentiation-associated protein 5
MEF	Mouse embryonic fibroblasts
MFI	Median fluorescence intensity
MHC-I; MHC-2	Major histocompatibility complex class I; class 2
MMP	Matrix metalloprotease
MOI	Multiplicity of infection
mRNA	Messenger RNA
MYD88 (*Myd88*)	Myeloid differentiation primary response 88
NEMO	NF-κB essential modulator (also known as IKKγ)
NF-κB	Nuclear factor κ-light-chain-enhancer of B cells
NI	Non-infected
NK	Natural killer
NLRP3	NOD-like receptor family pyrin domain containing 3
NOD	Nucleotide-binding oligomerization domain
OB	Olfactory bulb
p.i.	Postinfection
PAMP	Pathogen-associated molecular patterns
PBMCs	Peripheral blood mononuclear cells
PBS	Phosphate-buffered saline
PC	Principal component
PCA	Principal component analysis
PE	Phycoerythrin
PerCP	Peridinin-chlorophyll-protein complex
PFU	Plaque forming unit
PI3K	Phosphoinositide 3-kinase
PMA	Phorbol 12-myristate 13-acetate
PRR	Pattern recognition receptors
RBC	Red blood cell
RHD	REL homology domain
RID	REL inhibitory domain

Abbreviation	Definition
RIG-I	Retinoic acid-induced gene 1
RLR	RIG-I-like receptors
RNA	Ribonucleic acid
RORγt	RAR-related orphan receptor gamma t
RPMI	Roswell Park Memorial Institute 1640 medium
rRNA	Ribosomal RNA
SD	Standard deviation
SEM	Standard error
SSC-A; H	Side Scatter-area; height
STAT	Signal transducer and activator of transcription
STING (*Sting*)	Stimulator of IFN genes
TAD	Transactivation domain
TBK1 (*Tbk1*)	TANK-binding kinase 1
TCR	T cell receptor
TG	Trigeminal ganglia
Th	T helper
TLR	Toll-like receptors
TMM	Trimmed mean of M-values
TNF-α	Tumour necrosis factor alpha
TRAIL	TNF-related apoptosis-inducing ligand
Treg	Regulatory T cell
TRIF (*Ticam1*)	Toll/interkeukin-1 receptor domain-containing adapter-inducing interferon-β
TYK2	Tyrosine kinase 2
UNC93B1 (*Unc93b1*)	Unc-93 Homolog B1, TLR Signaling Regulator
USP18 (*Usp18*)	Ubiquitin Specific Peptidase 18
UTR	Untranslated region
WT	Wild-type

LIST OF FIGURES

CHAPTER 1

CHAPTER 2

CHAPTER 3

CHAPTER 4

CHAPTER 4 (continued)

CHAPTER 5

LIST OF TABLES

CHAPTER 1

CHAPTER 2

CHAPTER 4

ACKNOWLEDGEMENTS

I must first thank my supervisor, Dr. Silvia Vidal, for her guidance and support. Her encouragement to always explore new ideas, adopt new technologies, and shift perspectives have shaped me into the scientist that I am today. I am also grateful to Dr. Grégory Caignard and Dr. David Langlais for their mentorship. Greg taught me the many rudiments of working at the bench and of sound experimental design, and how best to dissect a complex immune pathway. David taught me to delve deeper into transcriptomics, to always treat data with diligence, and to always be generous with advice. They are both responsible for my work ethic today, and I am indebted to them.

I also wish to thank Dr. Danielle Malo and Dr. Martin Olivier, who have guided me through many supervisory committee meetings, and through their advice and support, have shaped this work.

A big thank you to Benoît Charbonneau for his immense help with so many experiments and necropsies, this work would not have been possible without him and his early morning assistance, or without our early morning coffee! Thank you to Barbara Mindt with whom I shared many other coffees in between, and Marianne Provost for welcoming quick pop-in conversations during my experimental downtime. I am grateful to all of you for your friendship and support.

I also thank past members of the Vidal lab, including Dr. Jennifer Marton, Anne Dumaine, Dr. Nassima Fodil, Dr. Gregory Boivin, Dr. Gabriel Leiva, and Dr. Peter Moussa for showing me the ropes when I first joined the lab, and to everyone throughout the years who helped make the lab and floor such a welcoming and vibrant place. A special thank you to the members of the Langlais lab who welcomed me into their fold over the past year; I really appreciated our weekly exchanges, especially during these last few months of research ramp-down.

I must also acknowledge the expert assistance of Dr. Odile Neyret at the Plateau de biologie moléculaire at the Institut de recherches cliniques de Montréal (IRCM) in the preparation and sequencing of our sample libraries, support with animal experiments from Patricia D'Arcy, and Julien Leconte and Camille Stegen for their help at the Life Sciences Complex flow cytometry core facility. My experimental work would not have been possible without them.

Not least, thank you to my parents and my sister. Your support means everything, and I am lucky to always have you in my corner. And finally, to my *nonno*—who as it turned out, was the first to encourage me in the pursuit of this endeavour—thank you.

CONTRIBUTION TO ORIGINAL KNOWLEDGE

This doctoral thesis presents the following distinct and original contributions to knowledge:

First, Chapter 2 outlines the discovery of an *N*-ethyl-*N*-nitrosourea (ENU)-induced nonsense mutation in the reticuloendotheliosis oncogene, or *Rel* gene, encoding the c-Rel transcription factor. This mutation, Rel^{C307X}, backcrossed at least four times to the C57BL/6J background, results in the expression of a c-Rel protein that is truncated at amino acid position 307. This novel recessive Rel^{C307X} allele is now listed as Rel^{Coby} on the Mouse Genome Informatics (MGI) database (http://www.informatics.jax.org/allele/MGI:6287253) under the accession number MGI:6287253, and is further characterized in Chapters 2, 3 and 4.

Second, the *Rel* gene is a novel genetic etiology for herpes simplex encephalitis (HSE) in mice. This finding, presented in Chapters 2 and 3, involved the infection of homozygous Rel^{C307X} mice and of $Rel^{-/-}$ knockout mice with herpes simplex virus 1 (HSV-1), resulting in increased susceptibility to HSE compared to wild-type controls. In Rel^{C307X} mice, regulatory defects in cell-mediated immunity led to increased viral replication and pathological immune cell infiltration, as are further described in Chapters 2 and 3.

Third, the *Rel* gene is a host genetic determinant of coxsackievirus B3 (CVB3)-induced myocarditis in mice. Chapter 4 describes the infection of Rel^{C307X} mice with CVB3, resulting in their increased resistance to cardiac infection and inflammation compared to susceptible wild-type controls. In the heart, the Rel^{C307X} mutation was associated with reduced CVB3 viral transcription and dampened the pathological inflammatory response, as further described in Chapters 4.

Fourth, Chapter 3 presents an original transcriptome profiling experiment using dual virus-host RNA sequencing of HSV-1 infected Rel^{C307X} and $Rel^{+/+}$ brainstem tissue. To our knowledge, this represents the first RNA sequencing dataset to include total viral and host gene transcripts in the HSV-1-infected brain during mouse herpes simplex encephalitis. The quantification of viral RNA transcripts to further subdivide mice into high and low responders to infection was an original methodological step to reveal the impact of the mutation on HSE development.

Lastly, Chapter 4 presents an original transcriptome profiling experiment using dual virus-host RNA sequencing of HSV-1 infected Rel^{C307X} and $Rel^{+/+}$ cardiac tissue. To our knowledge, this represents the first RNA sequencing dataset to include total viral and host gene transcripts in the CVB3-infected mouse heart.

THESIS FORMAT

This doctoral thesis contains seven chapters. Chapter 1 consists of a general introduction, Chapters 2, 3 and 4 comprise three manuscripts; the first of was previously published, and the latter two are in preparation for submission towards publication. Chapter 5 consists of a general discussion, and Chapter 6 presents future directions and a conclusion. Chapter 7 contains a master reference list, collecting references for all in-text citation included in Chapters 1, 5 and 6. However, for each manuscript (Chapters 2, 3 and 4), references to in-text citations are included separately within their respective chapters. A bridging statement is included between Chapters 2, 3 and 4 to bring further context to each chapter.

AUTHOR CONTRIBUTIONS

Of the three original manuscripts presented in this thesis, Chapter 2 has previously been published; Chapters 3 and 4 will soon be submitted for publication. Unless otherwise indicated, I, Mathieu Mancini, designed, performed, and analyzed the following experiments under the supervision of Dr. Silvia Vidal. The specific contributions of co-authors are outlined below:

Chapter 2: *Rel*-dependent immune and central nervous system mechanisms control viral replication and inflammation during mouse herpes simplex encephalitis.

Mathieu Mancini, Grégory Caignard, Benoît Charbonneau, Anne Dumaine, Nila Wu, Gabriel A. Leiva-Torres, Steve Gerondakis, Angela Pearson, Salman T. Qureshi, Robert Sladek, and Silvia M. Vidal. 2019. *J Immunol* 202: 1479-93. https://doi.org/10.4049/jimmunol.1800063.

Grégory Caignard performed the ENU mutagenesis screen outlined in Figure 1 with assistance from Patricia D'Arcy, Benoît Charbonneau and Gabriel Leiva-Torres. Grégory Caignard also designed, performed, and analysed the experiments outlined in Figure 1, Figure 2A-C, and Figure 3A-B. Benoît Charbonneau assisted me with tissue harvesting for samples included in Figures 4, 5, 7, 8 and 9 as well as Supplemental Figures 1-3. Patricia D'Arcy assisted with most infections and with bone marrow chimera transfers. Anne Dumaine performed the Western blot in Figure 2D. Nila Wu contributed to the experiments in Figure 6A by performing an independent replication. Steve Gerondakis provided $Rel^{-/-}$ mice. Angela Pearson provided HSV-1 strain 17 virus stocks and reagents. Salman Qureshi provided $Unc93b1^{Letr/Letr}$ mice. Robert Sladek performed the exome sequencing alignment and variant calling analysis. Silvia Vidal conceived, supervised and financed the study. I designed, performed and analysed all other experiments (Figure 2E, Figure 3C-E, Figures 4-9 and Supplemental materials), prepared figures, and wrote the manuscript.

Chapter 3: c-Rel-regulated pathways protect mice from herpes simplex encephalitis by limiting pathological interferon responses and neuroinflammation.

Mathieu Mancini, Benoît Charbonneau, David Langlais, and Silvia M. Vidal.

Benoît Charbonneau assisted with infections and tissue harvests for samples included in most experiments. David Langlais contributed to the design of the RNA sequencing experiment and assisted with the alignment and differential gene expression analysis. Silvia Vidal conceived, supervised and financed the study. I designed, performed and analysed all experiments and data, prepared figures, and wrote the manuscript.

Chapter 4: A truncating mutation in the c-Rel transcription factor protects mice from lethal coxsackieviral myocarditis

Mathieu Mancini, Benoît Charbonneau, Jennifer Marton, Steve Gerondakis, David Langlais, and Silvia M. Vidal.

Benoît Charbonneau assisted with infections and tissue harvests for samples included in most experiments. Jennifer Marton and I performed a pilot CVB3 infection on mice included in Figure 1. In addition, Jennifer Marton produced the CVB3 H3 viral stock. Steve Gerondakis provided *Rel*$^{-/-}$ mice. David Langlais contributed to the design of the RNA sequencing experiment and assisted with the alignment and differential gene expression analysis. Silvia Vidal conceived, supervised and financed the study. I designed, performed and analysed all experiments and data, prepared figures, and wrote the manuscript.

In addition to the preceding manuscripts, I have co-authored the following published review articles in the context of my doctoral work:

Mechanisms of natural killer cell evasion through viral adaptation.

Mathieu Mancini and Silvia M. Vidal. 2020. *Annual Review of Immunology* 38:511-39. https://doi:10.1146/annurev-immunol-082619-124440

This review article describes various genes and factors that allow herpesviruses, poxviruses, flaviviruses, retroviruses and others to evade natural killer cell-mediated recognition and immunity. Silvia Vidal and I conceived and wrote the article. Furthermore, I designed and prepared the figures and table.

Insights into the pathogenesis of herpes simplex encephalitis from mouse models.

Mathieu Mancini and Silvia M. Vidal. 2018. *Mammalian Genome*. 29(7-8): 425-445, https://doi.org/10.1007/s00335-018-9772-5

This review article describes the contribution of various mouse gene knockout models to our understanding of herpes simplex encephalitis. Silvia Vidal and I conceived and wrote the article. Furthermore, I designed and prepared the figures and tables. Figure 1, Figure 2, and Table 1 presented in Chapter 1 of this doctoral thesis are adapted in part from the figures and table published in this review article.

I, Mathieu Mancini, have read, understood, and abided by all norms and regulations of academic integrity of McGill University.

CHAPTER ONE: GENERAL INTRODUCTION

Viruses are infectious pathogens and consist of a nucleic acid genome bundled in a protein capsid, and sometimes a further lipid envelope. Viruses are obligate cellular parasites, meaning that they depend on a host organism and its cellular machinery to replicate themselves and ultimately infect new cells or hosts. Some virus species are endemic to humans, while others are transmitted by vertebrate hosts (zoonotic viruses) or by arthropod vectors (arboviruses). Certainly, many viruses have co-evolved with humans, where an estimated 5-8% of the human genome is of viral origin, and conversely, viruses are pressured and shaped by the immune system to develop their own evasion and virulence strategies (1, 2). Viruses are especially known as the cause of various infectious diseases. However, their long-term success often lies in their capacity to adapt to the host, and to replicate while limiting pathology and avoiding host lethality. While virus-encoded factors play an important role in determining virulence, viral infections are complex diseases, where severity is influenced by host genetic variation, and by environmental factors including age or diet.

This thesis will focus on two very different viruses, herpes simplex virus 1 and coxsackievirus type B3, each with opposite genome types, structures and tissue tropisms, but both well-adapted and widespread in human populations, and notable for the complex inflammatory diseases they can elicit in some individuals.

1.1 HERPES SIMPLEX VIRUS

1.1.1 Discovery and classification

Herpesviruses are enveloped viruses with large double-stranded DNA genomes. The *Herpesviridae* family is ancient; with infections in humans, mammals and other vertebrates attested for millions of years, these viruses have evolved alongside humans (3). While herpetic sores and blisters had been described since antiquity, herpes simplex virus 1, or human herpesvirus-1 (HSV-1; HHV-1), was first isolated in the laboratory by A. Löwenstein in 1919, proven as an infectious agent derived from “fever sores,” and later detected in cellular inclusions observed in a case of lethal encephalitis (4, 5). Other alpha herpesviruses include HSV-2 (HHV-

2) and varicella zoster virus (VZV; HHV-3), that like HSV-1 are set apart by their ability to establish latent infection in neurons. Beta herpesviruses (HHV-5, 6, 7) can instead enter latency broadly in leukocytes, and include cytomegalovirus (CMV; HHV-5) first identified and isolated and propagated in mouse salivary glands by Margaret G. Smith in 1956 (6). Only later was Epstein-Barr virus (EBV; HHV-4) recognized as a founding member of the gamma herpesviruses subfamily (7), which also includes Kaposi's sarcoma-associated herpesvirus (KSHV; HHV-8).

HSV-1 has since been propagated in laboratory settings in a number of different strains, which vary based on their origin and accumulated mutations. KOS strain first isolated from lip lesions by Kendall O. Smith (8), McKrae strain from ocular lesions (9), and strain 17 in Glasgow, Scotland (10). Strain 17 and McKrae strain viruses are noted for their high *in vivo* neurovirulence compared to KOS strain (11-13). HSV-1 strain 17 was also the first to be fully sequenced by 1988 (14), with a double-stranded DNA genome consisting of 152,222 base pairs (bp) and at least 75 coding sequences spread across sense and anti-sense DNA strands (15, 16). These many viral gene products, like other herpesviruses, allow HSV-1 to cycle between lytic and latent stages, determine tissue tropism, and provide numerous strategies to evade recognition by the host immune response.

1.1.2 Structure, life cycle, tropism and immune evasion

HSV-1 virions consist of an icosahedral protein capsid surrounded by a viral tegument and a lipid envelope. Its linear double-stranded DNA genome consists of a long and a short region, each encoding unique coding genes, and each flanked by inverted repeats, such that each HSV-1 genome encodes two copies of *LAT*, *RL1* (ICP34.5), *RL2* (ICP0), and *RS1* (ICP4) genes (17). HSV-1 entry is accomplished through the binding of envelope glycoproteins gB and gC to heparan sulfate residues on the host cell membrane, and attachment of glycoprotein gD to host receptors herpes virus entry mediator (HVEM) or nectin-1 (18). Further HSV-1 glycoproteins facilitate the fusion of the envelope with the cell membrane or endosomal membranes, releasing tegument proteins and capsids into the cytoplasm. Capsids are transported to the nuclear membranes where HSV-1 DNA enters the nucleus as a circular episome, while tegument protein *UL48* (VP16) associates with host factors to promote transcription of immediate-early HSV-1 genes (19). From here, ICP0 and ICP4 orchestrate the transcription of early phase genes (including viral DNA polymerase *UL30*) and late phase genes (encoding ICP34.5 and most glycoproteins (15)). During this lytic cycle, factors including *UL41* (Vhs) and *UL49* (ICP22) work to limit host transcription

and splicing, while the task of replicating the HSV-1 genome falls to a virus-encoded polymerase complex with an estimated fidelity of 1.38 x 10^{-7} mutations per nucleotide, similar to eukaryotic polymerases (20). Finally, the linear DNA genome is packaged into a new capsid in the nucleus, followed by their cellular egress and envelopment.

As for which cells are preferentially infected, host entry receptors are only part of what determines tissue tropism. HVEM and nectin-1 are both expressed in epithelial keratinocytes and fibroblasts to support infection in the skin or mucosa, while nectin-1 is also expressed on the surface of neurons (21). HSV-1 infection of neurons is well-documented, where the capsid is shuttled by retrograde transport along the axon to reach the soma and nucleus, and the expression of the *LAT* transcript, encoded in anti-sense to ICP0 and ICP4, works to inhibit the expression of intermediate-early genes altogether and promote latency (22). To promote long-lasting infection, the *LAT* transcript also functions to limit apoptosis in neurons, while the *RL1*-encoded factor ICP34.5 inhibits autophagy and is essential in neurovirulent strains (23-25). Finally, HSV-1 also encodes multiple strategies to evade the host immune response, ranging from inhibition of antiviral type I IFN production through ICP34.5 and ICP0, and by ICP47-dependent restriction of the transport of host major histocompatibility complex (MHC) molecules to the cell surface, effectively cloaking infected cells from recognition by $CD8^+$ T cells (26-28).

1.1.3 Epidemiology and transmission

All these strategies allow herpes to effectively replicate in humans without causing overt sickness, and latency can ensure its survival for years, contributing to the success of HSV-1 as a pathogen. HSV-1 infections are therefore ubiquitous in human populations, and it is estimated that over 3 billion people have been infected with HSV-1, compared with over 400 million people with the related HSV-2 (29, 30). While the number of worldwide HSV-1 and HSV-2 cases are decreasing in the United States, HSV-1 remains predominant worldwide, with HSV-2 being prominent on the African continent and disproportionately affecting women (31). HSV-1 is commonly considered to cause orolabial lesions (“cold sores”) and HSV-2, genital lesions, however both viruses can cause similar diseases, and are transmitted through contact with lesions, body fluids or mucosal surfaces (32). HSV-1 and HSV-2 can also be transmitted to newborns post-partum (33). While normally relatively benign, HSV-1 infection can also result in ocular keratitis, and in rare cases, infection and inflammation of the central nervous system, or herpes simplex

encephalitis. These complications are thought to occur mainly during primary infection, but can also arise from reactivation events from a latent infection (32).

1.2 COXSACKIEVIRUSES

1.2.1 Discovery and classification

Coxsackieviruses belong to the *Picornaviridae* family of small RNA viruses, and more specifically to the *Enterovirus* genus. Polioviruses were the first discovered *Enterovirus* species, and as causal agents of poliomyelitis, are arguably the most well-known. Later isolated in the 1940s, coxsackieviruses were named upon the discovery of novel filterable agents responsible for non-epidemic cases of childhood paralysis in Coxsackie, New York (34). They were first classified into A and B subtypes based on lesions and paralysis induced by intracranial inoculation of suckling mice (35). In humans, they are now recognized as the cause of various diseases, ranging from relatively benign Hand-Foot-and-Mouth disease to more severe cases of myocarditis, pancreatitis, or aseptic meningitis (36). In particular, CVB3 is the most common cause of viral myocarditis. Of the many wild-type CVB3 strains (Nancy strain) maintained in the laboratory, pathogenicity can often deviate between virus stocks due to the high mutation rate of CVB3, estimated from poliovirus at an average 4.68 mutations per new genome (37, 38). For example, plaque-purified viruses like CVB3 H3 (Woodruff) strain, originating from a single passage from an infected mouse heart, generate more consistent myocarditis in genetically susceptible mice (37); the availability of the original complete genomic sequence for the CVB3 H3 (Woodruff) strain, published in 1996 (39), allows recent virus stocks to be tested for the emergence of new mutations.

1.2.2 Structure, life cycle, tropism and immune evasion

CVB3, like other coxsackieviruses, consist of a short (7,400 bp) non-segmented, single-stranded positive-sense RNA genome. A long 742 bp 5' untranslated region (UTR) is integral to the translation of its single open reading frame; the 5' UTR is characterized by a large hairpin structure and internal ribosome entry site (IRES) that, like other enteroviruses, ensures cap-independent translation (40). The CVB3 genome is translated as a single polyprotein, later processed by virus-encoded proteases ($2A^{Pro}$ and $3C^{Pro}$) into 11 protein products (39). The CVB3

genomes is polyadenylated at the end of its short 3' UTR. The CVB3 genome is packaged in a small, non-enveloped protein capsid (consisting of viral proteins VP1-4).

As enteroviruses are normally transmitted by the fecal-oral route, CVB3 is quickly exposed to gut epithelial cells, where CVB3 virions will first bind to the decay-accelerating factor (DAF, or CD55) accessible at the apical cell surface (41). This first interaction is thought to trigger actin-mediated reorganization of the apical surface to shuttle DAF-bound virions closer to tight junctions, where they can engage the coxsackievirus and adenovirus receptor (CAR), normally only accessible at the basolateral surface (42). Once CVB3 has interacted with both receptors, virions can enter the cell by caveolin-mediated endocytosis. Viral replication occurs in the cytoplasm via a negative-sense RNA template intermediate, upon formation of a replication complex surrounding the RNA-dependent RNA polymerase (viral protein 3D). These replication events occur in clusters within lipid-rich replication organelles, derived by the virus from the cell membrane (41). Replicated genomes are finally re-packed into non-enveloped capsids and are likely released upon cell lysis, whereby virions are commonly detected in fecal samples (41).

As CVB3 can enter circulation upon initial gut epithelial cell infection, cardiac tropism depends at least in part on CAR expression in cardiomyocytes, the striated cells that comprise the heart muscle (43, 44). Furthermore, CVB3 and its encoded proteases can also help evade the immune system, although to a lesser extent than large DNA viruses. For example, RNA-sensors RIG-I, MDA5 and MAVS are cleaved by $2A^{Pro}$ and $3C^{Pro}$ to reduce type I IFN signaling (45), while non-structural viral protein 2C can interact with protein phosphatase 1 to limit IKKβ phosphorylation and NF-κB activation (46). CVB3 has also been reported to reduce surface MHC-I expression, where a concerted effort between viral proteins 3A, 2B and 2BC upregulates endocytosis and limits Golgi trafficking (47). Thus, CVB3 is equipped with mechanisms to reduce type I IFN signaling and to avoid recognition by antigen-specific $CD8^+$ T cells.

Enteroviruses are further advantaged by their high mutability, with an average error rate of 6.3×10^{-4} mutations per base per replication, compared to higher fidelity herpesviral polymerases at 1.38 mutations per 10^{-7} bp, or eukaryotic polymerases at 1 mutation per 10^{-8} or 10^{-9} bp (20, 38, 48). Therefore, enteroviral RNA-dependent RNA polymerase can generate multiple CVB3 quasi-species within an infected host, while recombination events between RNA genomes also contribute to CVB3 diversity (49). These quasi-species can enhance the infection, where a diverse population of viruses with improved fitness or virulence can significantly increase pathogenesis. However,

their high mutation rate can also result in so-called error catastrophe, where too many detrimental mutations accumulate to stifle CVB3 replication or invasion of new tissues (50).

1.2.3 Epidemiology and transmission

Coxsackieviruses are easily transmissible from person to person by the fecal-oral route and are widespread in the global population. Seropositivity rates for CVB3 in the United States are estimated at 4% of total confirmed *Enterovirus* cases between 2014-2016 as reported by the National Enterovirus Monitoring System (51). Population-wide CVB3 seropositivity rates are reported to be as low as 33% in Italy (52) and as high as 66% in the United Kingdom (53), and at greater than 50% in persons of 15 years and over in Yantai, China (54). Furthermore, in areas where selenium is poorly available in soil and crops, dietary selenium deficiency has long been associated with increased rates of CVB3-induced myocarditis, referred to as Keshan disease (55). Selenium-deficient and selenoenzyme *GPx1*$^{-/-}$ deficient mice are both susceptible to a non-virulent CVB3 strain, suggesting that as an antioxidant, selenium may protect against reactive oxygen species-induced mutations that would otherwise drive pathogenic viral evolution (56, 57).

1.3 HOST DEFENCE

1.3.1 Cell-intrinsic responses to viruses

The non-specific innate immune response is initiated as a viral pathogen enters its target cell. At first, these signaling pathways are intrinsic to the infected cells, also called cell-autonomous responses, and centre on the production of type I interferon (IFN) to limit viral replication. Secreted IFN later orchestrates the activation of surrounding immune cells until an efficient cellular immune response is achieved.

Pattern recognition receptors (PRR) allow the host to detect viral infections by engaging pathogen-associated molecular patterns (PAMPs) derived from an invading virus. Among PRR, cell membrane-bound Toll-like receptors (TLRs) TLR1, TLR2 and TLR6 canonically recognize lipopeptides and glycolipids, and TLR4, lipopolysaccharide (LPS) (58). Additionally, TLR3, TLR7, TLR8 and TLR9 are targeted to endosomal membranes by UNC93B1, where they can detect viral nucleic acids including double-stranded RNA (TLR3), single-stranded RNA (TLR7

and TLR8), and CpG-rich unmethylated DNA (TLR9) (58). Endosomal TLRs are especially important for the detection of enveloped viruses and play non-redundant roles in the control of viral pathogens. Most TLRs associate with adaptor proteins such as MYD88 or TRIF on the cytoplasmic side, initiate signaling cascades that result in the activation and translocation of transcription factors including IRF3, IRF7, or NF-κB to the nucleus, where they may induce IFN and proinflammatory cytokine gene expression (as illustrated in Figure 1).

Cytoplasmic sensors of DNA or RNA are also employed by mammalian cells to detect nucleic acid by-products and intermediates of viral replication. Viral RNA containing 5' trisphosphate or 5' diphosphate features are recognized by RIG-I, and double-stranded RNA by MDA5, which both signal through the MAVS adapter to activate IRF3 through TBK1 and IKKε, or through NF-κB, resulting in IFN expression (59-62). On the other hand, cytosolic viral DNA can be processed by cyclic GAMP synthase (cGAS) to produce cyclic guanosine monophosphate/adenosine monophosphate cGAMP molecules, which are in turn detected by STING to induce IFN through the TBK1/IRF3 axis (63, 64). Double-stranded viral DNA can also be recognized in the cytoplasm or nucleus by IFI16 in humans, whereas IFI200-family genes (including *Ifi204*) are homologs in mice (65, 66). Ultimately, STING is involved in all above responses as a direct sensor, or as a scaffold facilitating the phosphorylation and activation of IRF3 (67-69).

Type I IFN is released from infected cells as a result of most of the above sensing cascades. These cytokines are expressed in 13 isoforms for IFN-α and one for IFN-β, each with their own tissue and cellular tropisms (70). Secreted type I IFN molecule can bind to the dimeric IFN I receptor IFNAR, comprised of IFNAR1 and IFNAR2 subunits. This interaction triggers the recruitment of Janus kinase 1 (JAK1) and tyrosine kinase 2 (TYK2) to the cytoplasmic end of IFNAR, whereby these kinases phosphorylate STAT1 and STAT2 (71). These STAT1 and STAT2 transcription factors, in complex with IRF9, are referred to as IFN-stimulated gene factor 3 (ISGF3), which translocates to the nucleus to induce transcriptions of various IFN-stimulated genes (72). Mx GTPase proteins can sequester viral proteins or viral RNA-protein complexes in the cytoplasm or nucleus (73). Other IFN-stimulated genes (ISGs) act as modulators and even negative regulators of IFN production, including the ubiquitin mimic ISG15, and deubiquitinase USP18 (74). For example, both *Usp18*$^{-/-}$ mice and human cases of *ISG15* deficiency result in interferonopathies, characterized by excess and pathological IFN production. Finally, other ISGs

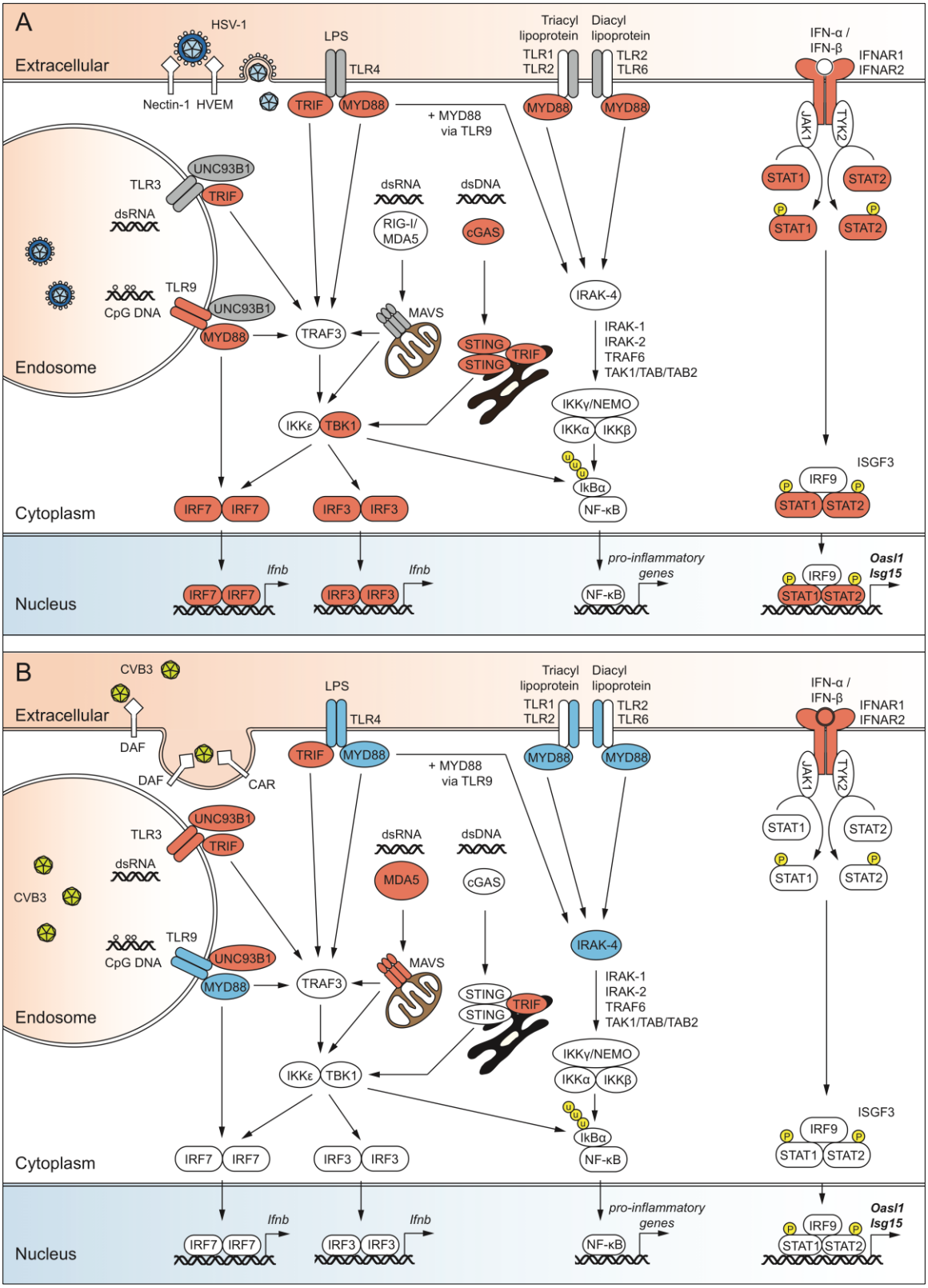

FIGURE 1. Genetic contribution to cell-intrinsic responses against HSV-1 and CVB3 infections in mice.

FIGURE 1. Genetic contribution to cell-intrinsic responses against HSV-1 and CVB3 infections in mice.

(A) Signaling downstream of HSV-1 infection. (B) Signaling downstream of CVB3 infection. Red factors red indicated that a gene defect causes susceptibility to infection compared to wild-type mice; blue factors indicate resistance; grey factors indicate that knockout mice behave like wild-types. Adapted from (75).

including IFIT2 commonly induce apoptosis in infected cells, to better curb viral spread (76).

1.3.2 Cell-mediated responses to viruses

The production of type I IFN and expression of ISGs triggers a cascade of highly regulated cellular interactions that drive immune cell activation, proliferation and antiviral function. Infected cells and peripheral dendritic cells (DCs) or macrophages will produce type I IFN and chemoattractant molecules (chemokines) that will attract and initiate signaling in monocytes, natural killer (NK) cells and other leukocytes (77). NK cells will be quick to recognize and kill virus-infected cells by secreting membrane-disrupting cytotoxic factors like perforin and granzyme. As one of the most useful innate effectors against viral infection, NK cell activation is tightly regulated by multiple activating and inhibitory receptors, guaranteeing that only infected cells are recognized and targeted for cytotoxic killing (2). Activated NK cells also express elevated levels of the proinflammatory cytokine IFN-γ, which together with other cytokines help to activate and regulate other immune cells. For example, cytokines like IFN-γ, TNF-α and interleukin (IL)-12 may polarize immune cells towards a type I profile that classically promotes cell-mediated immunity, while a humoural response is favoured by type 2 cytokines like IL-4, IL-5 or IL-13 (78). Finally, many ISGs are also chemokines, whose secretion will attract leukocytes that express cognate chemokine receptors (for example, CCL2:CCR2, CCL5:CCR5, CXCL9/10:CXCR3, CX3CL1:CX3CR1).

Here, the innate response yields to adaptive immune cells. Briefly, T and B lymphocytes are equipped via their T or B cell receptors (TCR, BCR) to recognize peptide antigens presented on major histocompatibility complex class I or II (MHC-I, MHC-II) molecules expressed on the surface of antigen presenting cells (APC) (79). These APCs include macrophages, DCs or B cells that can process viral particles into short antigenic peptides fit for cross-presentation to B or T cells. These peptide/MHC to TCR or BCR interactions are integral to the activation of effector T and B cells. In the context of viral infection, the activated B cell response involves the generation of antigen-specific immunoglobulin (Ig)-type antibodies that can bind and neutralize viruses directly, or mark infected cells for targeted killing by NK cells (antigen-dependent cell-mediated cytotoxicity) (2). On the other hand, antigen-specific $CD8^+$ T cells will recognize and kill infected cells via perforin and granzyme-mediated cytotoxicity, while antigen-specific $CD4^+$ T cells can support immune cell activation by producing factors including IFN-γ (80). Helper $CD4^+$ T cells

(Th) are also polarized in part by their expression of lineage-defining transcription factors and by their cytokine milieu into various subtypes (78). In general, Th1 cells are typical of the IFN-γ-dependent protective response to viral infections, while Th2 cells are important for defence against extracellular pathogens, wound healing or allergic responses. IL-17 secreting RORγt$^+$ Th17 cells also contribute to the inflammatory response (81), while Foxp3$^+$ regulatory T cells (Tregs) typically suppress inflammation and T cell activation (82).

Altogether, while the general responses described above are typical of viral infections in the periphery, a protective host defence response will vary depending on the tissue context, where specialized tissues like the brain, heart, lungs or gut include unique resident and infiltrating cell types, and differ in their sensitivity to infection and inflammation.

1.3.3 Antiviral response and inflammation in the brain

Despite its long-standing characterization as "immune-privileged," the brain does in fact host a wide range of sophisticated immune cell-mediated and pathogen sensing mechanisms to defend against infection (Figure 2). The blood-brain barrier (BBB) physically separates the peripheral circulatory system from the CNS parenchyma to allow selective entry of molecules and cells into the brain; the BBB consists of endothelial cells joined by tight junctions and supported by specialized astrocytes and pericytes on the side of the parenchyma (83). However, many small RNA viruses, as well as herpesviruses, are known to circumvent the BBB and cause encephalitis in humans. Viruses will employ various invasion routes alone or in combination, transiting through cells that line the BBB, across tight junctions, within phagocytosing immune cells, or directly through sensory neuron axons, to ultimately replicate in different parts of the brain including the brainstem, choroid plexus (ventricles), meninges or cortex (83, 84). Thus, the glial cells that populate the brain, including resident macrophage-like microglia, astrocytes, and oligodendrocytes, as well as the neurons that they work to support, are all involved in pathogen sensing and contribute to the activation of an inflammatory response. Ultimately, viral infection of the brain involves the delicate regulation of inflammation to achieve an effective antiviral response, at the risk of generating an excessively strong pathological inflammatory response that may result in permanent tissue damage or lethal encephalitis.

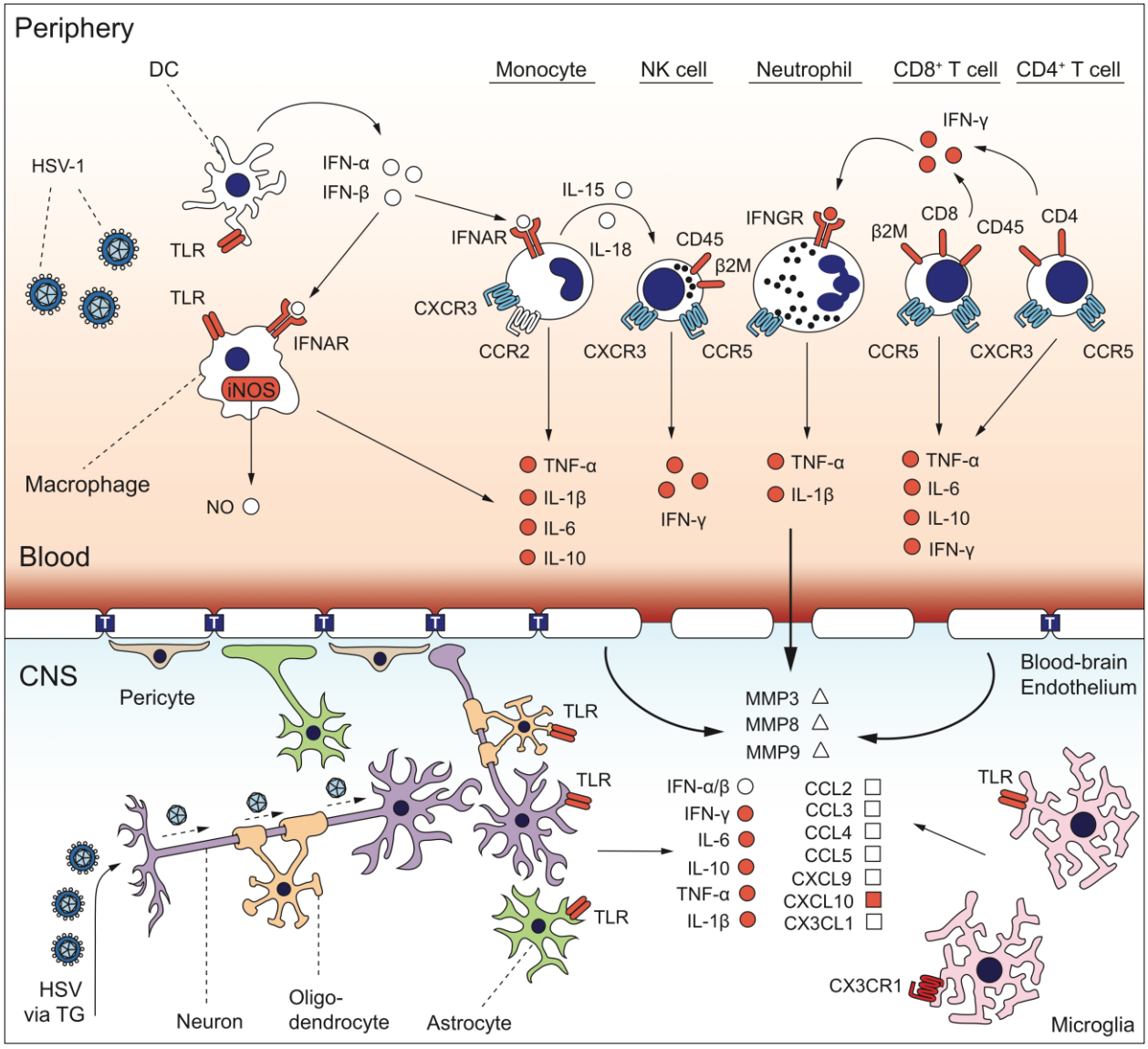

FIGURE 2. Genetic contribution to the cell-mediated response in the HSV-1-infected mouse brain.

Immune cell activation in the periphery is shown above; immune cell infiltration into the CNS parenchyma is shown below. Red factors or receptors indicate that a gene defect causes susceptibility to infection compared to wild-type mice; blue indicates resistance; grey indicates that knockout mice behave like wild-types. T's in blue boxes refer to tight junctions between endothelial cells. Adapted from (75).

TLRs are expressed throughout the brain at homeostasis, particularly in microglia. Activated microglia can further induce TLR2, TLR3 and TLR4 expression in astrocytes, while neurons and oligodendrocytes have been shown to rely on TLR3 signaling and type I IFN production to counter HSV-1 replication (85-87). TLR2 and TLR9 are also upregulated in the neuron-rich trigeminal ganglia during HSV-1 infection in mice (88). As a result of effective pathogen sensing, type I IFN production in glial cells is generally required to control coronavirus and West Nile virus replication and even limit damage to the BBB (89, 90). HSV-1 infection of microglia is self-limiting and triggers early caspase-3-dependent apoptosis, while infected astrocytes undergo Fas receptor-mediated cell death to limit viral spread (91). On the other hand, neurons are not generally capable of renewal, and therefore have been shown to promote autophagy instead of apoptosis in response to type I IFN signaling during HSV-1 infection (92, 93).

In addition to type I IFN, glial cells and endothelial cells are keen producers of a variety of proinflammatory cytokines (TNF-α, IL-1β, IL-6, IFN-γ), and chemokines (CCL2, CCL5, CXCL9, CXCL10, CX3CL1) during viral infection (75, 94). Beyond their usual functions in the activation and polarization of immune signals, TNF-α, IL-6 and CCL2 contribute to a weakening of the tight junctions of the BBB (95, 96). Increased matrix metalloprotease production has also been noted in virus-infected endothelial cells, which reduces BBB integrity and facilitates the entry of peripheral immune cells into the brain (97). Chemokine production will attract NK cells that will produce elevated amounts of IFN-γ and destroy infected cells, functions that are essential to HSV-1 clearance in the brain (98). Invading IFN-γ-producing Th1 $CD4^+$ and cytotoxic $CD8^+$ T cells are also required for HSV-1 clearance in the brain (80, 88, 99). However, excessive $CXCR3^+$ T cell and monocyte infiltration, coupled with uncontrolled inflammatory cytokine production, can also be pathological in various models of brain infection (100-104).

1.3.4 Antiviral response and inflammation in the heart

The heart is an altogether different organ in structure and function, but also in its response to viral infection and inflammation (Figure 3). Human and mouse hearts consist primarily of contractile cardiac muscle cells (cardiomyocytes), and together with specialized pacemaker cells, fibroblasts and endothelial cells, comprise the myocardium or heart muscle (105). The mechanical

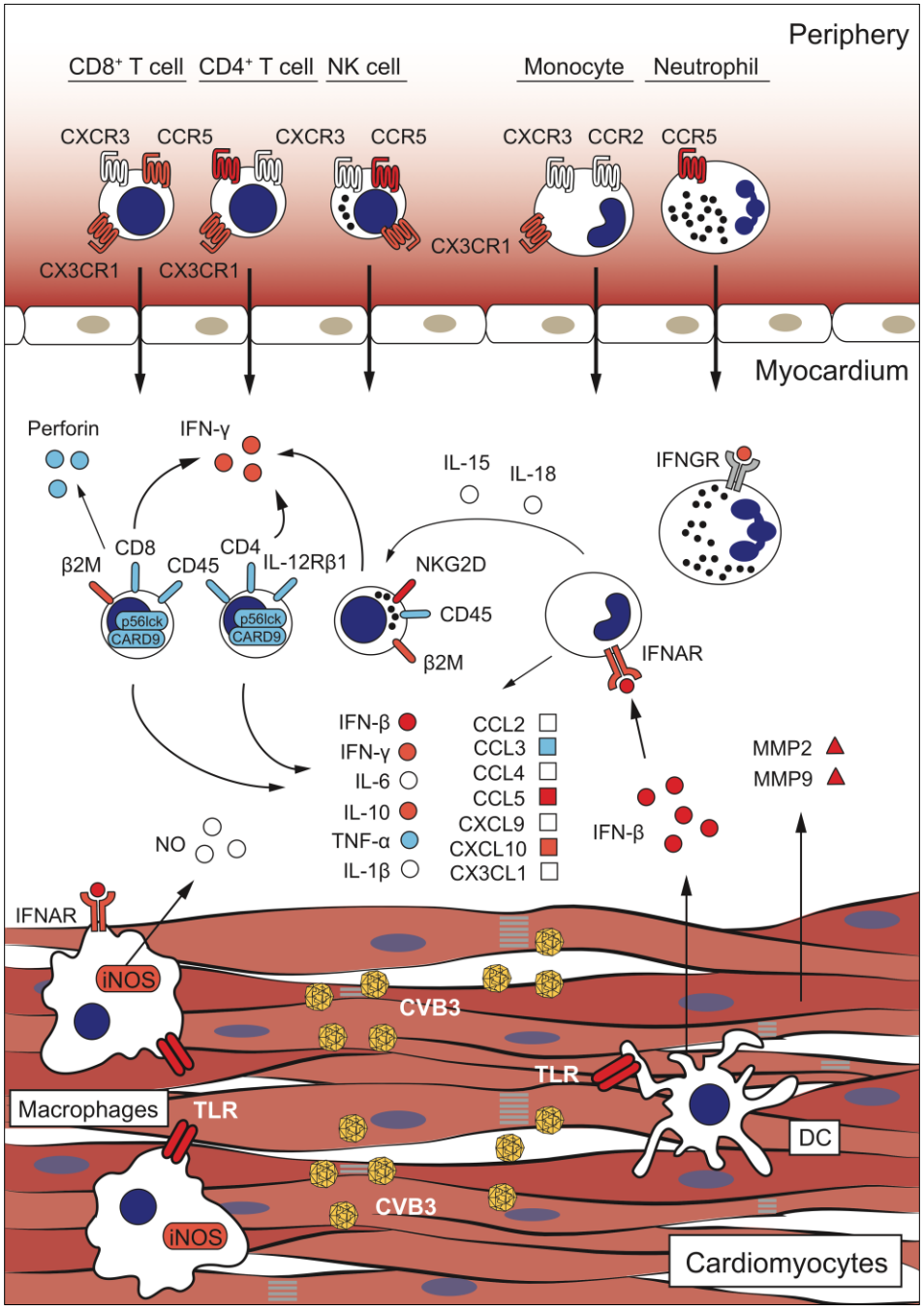

FIGURE 3: Genetic contribution to the cell-mediated response in the CVB3-infected mouse heart.

Immune cell infiltration into the myocardium is shown above, while macrophages and DCs patrolling near infected cardiomyocytes is shown below. Red factors or receptors indicate that a gene defect causes susceptibility to infection compared to wild-type mice; blue indicates resistance; grey indicates that knockout mice behave like wild-types.

contraction of the myocardium, from atria to ventricles, pumps blood through the body. Cardiomyocytes are connected to one another via intercalated disks, which allow for coordinated contractions and further contain gap junctions that allow for rapid intercellular signaling (106). While CAR and DAF-expressing cardiomyocytes are preferentially infected by CVB3, human induce pluripotent stem cell (iPSC)-derived cardiomyocytes have been shown to be poor producers of type I IFN in response to CVB3 infection (107). Cardiomyocytes are capable, however, of producing IFN-β via a MAVS-dependent mechanism under homeostatic conditions (108). Otherwise, heart-surveying macrophages and DCs and resident cardiac fibroblasts express multiple TLRs, known to be essential for type I IFN-dependent CVB3 viral clearance (109-111). In addition, cytoplasmic RNA sensing and its downstream TBK1/STING/IRF3 signaling axis are essential components of the protective antiviral response (112).

As cardiomyocytes play host to replicating virus, they must undergo necrotic cell death to release virions into the surrounding tissue environment (113). Notably, the CVB3-encoded 2A protease can cleave dystrophin, disrupting the cardiomyocyte cell membrane and its support of the contractile sarcomere, killing the cell (114). The regulation of programmed necrotic cell death during cardiac viral infection is an emerging area of study. These pathways include necroptosis (dependent on various kinases) or pyroptosis (dependent on IL-1β and IL-18 activity) (113). Both cascades result in a release of proinflammatory damage-associated molecular patterns, recognized in the cytoplasm by NOD-like intracellular receptors to direct NLRP3-mediated inflammation (115-117); lytic cell death may lead to calcification of the heart muscle (118). On the other hand, non-lytic caspase-3-dependent apoptosis of cardiomyocytes occurs during early CVB3 infection in mice, and peaking at day 5 postinfection (p.i.) (119). Cardiomyocytes cell death can also be triggered by the infiltration of cytotoxic immune cells into the inflamed heart (120). Ultimately, cardiomyocytes have limited regenerative capacity, and are normally replaced by cardiac fibroblasts, particularly in ventricular tissue (121). Hypertrophic remodeling, matrix metalloprotease expression and subsequent fibrosis are central to the wound healing response (122). However, this build-up of fibrotic scar tissue dilates and stiffens the ventricle, meaning the heart may become more prone to failure.

Regarding the cell-mediated immune response, macrophages and DCs patrol the myocardium at steady-state, and respond to infection by producing type I IFN and proinflammatory cytokines and chemokines, removing debris and dying cells, and processing viral

antigen for cross-presentation to lymphocytes. Chemokines including CXCL10 attract NK cells to the heart to fulfill their essential cytotoxic function and produce large amounts of IFN-γ (123-125). Neutrophils are attracted by IL-8 and recognize CVB3 via TLR8, whereas invading macrophages and monocytes are attracted by CCL2 or CCL3 production (126, 127). Overall, the pathologically inflamed CVB3-infected heart exhibits a type 1 cytokine profile, IFN-γ and IL-12 over type 2 IL-4, IL-5 and IL-13 cytokines, along with other inflammatory cytokines including TNF-α, IL-6, and IL-10 (128-130). In such an environment, type 1-polarized macrophages are thought to be pathological, and type 2, protective (131, 132). Specific to the heart milieu, IL-6-family cytokine cardiotrophin-1 (CT-1, *Ctf1* mouse gene) is expressed at high levels during early infection, and signals through the STAT3 transcription factor to promote cardiac cell survival and reduce inflammatory cytokine production by macrophages (133, 134). However, long-term activation of STAT3 may also induce cardiac hypertrophy and remodeling that may impede heart function (135).

Incoming $CCR5^+$, $CXCR3^+$ or $CX3CR1^+$ T cells attracted by CCL5, CXCL10 or CX3CL1 are also polarized by the cytokine milieu (124, 136, 137). Antigen-specific responses notwithstanding, the invasion of T cells in the infected myocardium is invariably pathological, where T cell-deficient animals exhibit improved outcomes to CVB3 infection (138-140). However, the roles and dynamics of various T cell subsets remain more controversial. During acute infection, Th1 $CD4^+$ T cells are considered pathological through their contribution to damaging inflammation (128, 132, 141-143). In complete contrast however, mouse models of chronic infection have provided evidence that Th1 responses are protective, as they actively suppress Th2 responses that are required to trigger ventricular remodeling, fibrosis, and heart failure (144). Among other T cell subtypes, IL-17-producing Th17 cells are detrimental to viral control in the heart (144-146), while the role of regulatory T cells (Treg) is less understood, where they may promote or limit disease (147, 148). Finally, B cell deficient mice are sensitive to CVB3 infection, suggesting that unlike T cells, B cells are protective (149).

1.4 HERPES SIMPLEX ENCEPHALITIS

1.4.1 Incidence, presentation and treatment

Herpes simplex encephalitis (HSE) is a rare complication of herpes simplex virus infection in humans. HSV-1 is the most common cause of sporadic viral encephalitis worldwide, and accounts for an average of 2 to 4 HSE cases per 100,000 individuals per year (150). Otherwise, some 10% of HSE cases are traced back to HSV-2 infection (151). HSE incidence is bimodally distributed, with approximately one third of cases occur in children and young adults under 20 years of age, and the remaining two thirds in adults aged 60 years or over (32). In both cases, inflammatory or necrotic focal lesions are typically detected in the frontal or temporal lobe, and occasionally in the brainstem (152, 153). Clinical presentation also involves fever, focal seizures, or altered level of consciousness (154). Additionally, HSV infections can occur in newborns, predominantly by way of post-partum HSV-2 infection acquired from the mother during delivery, but also through contact with an HSV-1-infected caregiver in 10% of cases. Neonatal HSV encephalitis is typically generalized throughout the brain, with an incidence of 10 to 60 cases per 100,000 live births per year in the United States (33).

Once a largely fatal disease, daily administration of intravenous acyclovir for up to 14 days has been the standard treatment for HSE for the past 30 years and has significantly reduced the risk of mortality (154). Early detection and antiviral treatment is critical to improve outcomes, however, many patients develop long term neurological sequelae. Furthermore, a third of reported pediatric HSE patients presented with acute clinical relapses, sometimes related to a rebound in viral replication. In the absence of detectable virus, these relapses are thought to be the result of an inflammatory or immune reaction. In older adults, cases of post-HSE autoimmune encephalitis have also been reported in 27% of patients in an HSE cohort (N=54), where neuroinflammation was correlated with the generation of anti-*N*-methyl-*D*-aspartate receptor (NMDAR) antibodies that may have been generated during the initial HSE course (155).

1.4.2 Human genetic determinants

Using next-generation sequencing, several genetic etiologies for childhood HSE have been identified in the last 20 years, with most related to the TLR3/type I IFN signaling axis. A homozygous loss-of-function mutation was first identified in the *STAT1* transcription factor

causing mendelian susceptibility to mycobacterial disease and HSE, while a second mutation in the IKK complex subunit *NEMO* led to susceptibility to HSE, mycobacterial disease, and various bacterial infections (156, 157). Since these two initial cases, further single gene defects in *UNC93B1*, *TLR3*, *TRIF*, *TRAF3*, *TBK1* and *IRF3* have been found to uniquely cause HSE; all belong to the TLR3 signaling cascade (158-163). Most of these mutations are autosomal dominant, consistent with the sporadic nature of HSE onset (164). Curiously, in the absence of HSV infection, these latter defects are otherwise silent, and led to no other infectious phenotypes. Thus, TLR3 appears to play a non-redundant role in the brain, that is essential to the protective IFN response against HSV-1 in childhood HSE. These gene defects, however, only explain a minority of ascertained HSE cases.

Other gene mutations have recently been associated with childhood HSE, including in the small nucleolar RNA-encoding *SNORA31* gene, with unclear function, but involved in protective IFN-β production in neurons (165). Unlike the previous childhood cases with frontal or temporal lobe HSE, further mutations in the RNA lariat debranching enzyme *DBR1* results in HSE, as well as influenza and norovirus encephalitis, in the brainstem (166). Finally, two unique autosomal dominant mutations in the mannan-binding lectin serine protease *MASP2* were identified in adult forebrain HSE patients (age 60 and 24 years), resulting in a dampened complement system activation (167). These recent findings reveal that immune pathways other than TLR3/type I IFN play a role in HSE onset, in cases that deviate from previous forebrain/childhood studies.

1.4.3 Mouse genetic determinants

Mouse models of HSV infection have greatly contributed to our understanding of HSE disease pathogenesis and of the genes that underlie the protective host response (75). However recent studies have typically employed different routes of inoculation—subcutaneous, intranasal, corneal, intravenous or intracranial for HSV-1, intravaginal for HSV-2. For example, the ocular route is often used to study HSV-1 infection in the trigeminal ganglia (TG). Intravaginal or subcutaneous routes are well-suited to peripheral studies of DCs or NK cells. Intranasal infection perhaps best recapitulates HSE in the brainstem, with HSV-1 thought to accede to the hindbrain via the trigeminal nerve (168). No model, however, recapitulates the frontal or temporal lesions characteristic of many childhood HSE cases. A further consideration should be made for viral dosage and genetic background. Thus, studies usually compare deleterious alleles with wild-type

alleles on the same background, in mice receiving an identical dose. Commonly used backgrounds include naturally resistant C57BL/6 or 129 strains or susceptible BALB/c mice (169).

Overall, mouse genetic studies have confirmed the importance of TLRs and of type I IFN signaling in HSE resistance (Figure 2, Table 1). While *Tlr3*$^{-/-}$ mice are susceptible to HSV-2, *Tlr3*$^{-/-}$ and *Unc93b1* mutants behave as wild-type following intranasal or intracranial HSV-1 infection (170-172). Furthermore, *Tlr9*$^{-/-}$, *Tlr2*$^{-/-}$*Tlr9*$^{-/-}$, *Ticam1*$^{-/-}$ (TRIF), *Myd88*$^{-/-}$, *Tbk1*$^{-/-}$, *Stat1*$^{-/-}$, *Irf3*$^{-/-}$ and *Isg15*$^{-/-}$ mice are all susceptible to i.n. HSV-1 (74, 93, 94, 172-176). Also, cytoplasmic DNA sensing pathways (cGAS, STING) play a role in HSE protection, while RNA sensors (MAVS) appear to have no effect in HSE (67, 174, 177). Thus, mouse HSE models implicate additional TLR and DNA sensors in the CNS response.

The importance of the inflammatory and immune response is especially underscored by mouse HSE studies. Deletion of *Ifng*, *Tnf*, *Il6*, *Il10*, *Il1b*, and *Nos2* cytokine and effector genes all result in HSE susceptibility, as do T cell-related genes *Ptprc* (CD45), *B2m* (MHC-I), *Cd4* and *Cd8*, suggesting that the regulation of Th1 responses is protective during HSV-1 infection in the brain (80, 88, 99, 175, 178-181). However, it is also clear from chemokine and chemokine receptor gene studies while CX3CR1 expression on microglia and T cell chemoattractant CXCL10 are protective, CXCR3 and CCR5 expression contribute to the pathological HSE response, indicating that infiltration of activated T cells into the brain may be detrimental to the host and auxiliary to damaging inflammation (101, 182-184). Overall, the genetic regulation of the immune response appears to be a driver of HSE in mice, and may hint at an important contribution of inflammatory mechanisms in unresolved or adult cases of human HSE.

1.5 COXSACKIEVIRAL MYOCARDITIS

1.5.1 Incidence, presentation and treatment

Myocarditis is a disease that involves inflammation of the heart muscle (the myocardium) detrimental to heart function. Myocarditis accounts for up to 20% of sudden cardiovascular deaths in young adults (185). However, the actual incidence of myocarditis is difficult to estimate given the heterogeneity of the disease, its nonspecific symptoms, and the generally poor sensitivity

TABLE 1. Comparison of survival phenotypes for selected antiviral and immune gene defects in HSV-infected mice, CVB3-infected mice, and humans.

Gene defect	Protein	HSV-1 phenotype*	CVB3 phenotype*	Human Gene	Infectious phenotypes	References***
Pathogen-associated molecular pattern sensing						
Tlr2$^{-/-}$	TLR2	As WT	R	*TLR2*		(173, 186)
Tlr3$^{-/-}$	TLR3	As WT	S	*TLR3*	HSV-1	(110, 172) OMIM 603029
Tlr4$^{-/-}$	TLR4	As WT	R	*TLR4*		(123, 187, 188)
Tlr9$^{-/-}$	TLR9	S	R	*TLR9*		(173, 188)
Tlr2$^{-/-}$*Tlr9*$^{-/-}$	TLR2/9	S		*TLR2/9*		(173)
Unc93b1^{3d} or $^{Letr/Letr}$	UNC93B1	As WT	S	*UNC93B1*	HSV-1	(171, 172, 189) OMIM 608204
Ticam1$^{-/-}$	TRIF	S	S	*TICAM1*	HSV-1, HSV-2	(171, 174, 190) OMIM 607601
Myd88$^{-/-}$	MYD88	S	R	*MYD88*	Pyogenic bacteria	(172, 175, 191) OMIM 602170
Irak4$^{-/-}$	IRAK4		R	*IRAK4*	Bacterial infections	(136) OMIM 606883
Tbk1$^{-/-}$*Tnfr1*$^{-/-}$	TBK1	S**		*TBK1*	HSV-1	(176) OMIM 604834
Mb21d1$^{-/-}$	cGAS	S		*CGAS*		(177)
Sting$^{-/-}$	STING	S		*STING1*		(67, 177)
Ifih1$^{-/-}$	MDA5		S	*IFIH1*		(192)
Mavs$^{-/-}$	MAVS	As WT	S	*MAVS*		(172, 174, 192)
IFN response and transcription factors						
Ifnb$^{-/-}$	IFN-β		S	*IFNB1*		(111)
Ifng$^{-/-}$	IFN-γ	S	S	*IFNG*	*Mycobacterium*	(123, 175, 178) OMIM 147570
Ifnar$^{-/-}$	IFNα/βR1	S	S	*IFNAR2*	Disseminated vaccine measles, HBV	(171, 193) OMIM 602376
Ifngr$^{-/-}$	IFNγR	S	As WT	*IFNGR1*	*Mycobacterium* and *Salmonella*	(193, 194) OMIM 107470
				IFNGR2	*Mycobacterium* and *Salmonella*	OMIM 147569
Stat1$^{-/-}$	STAT1	S		*STAT1*	*Mycobacterium*	(93, 94) OMIM 614892
					HSV-1, EBV, VZV	OMIM 613796
					Candidiasis	OMIM 614162
Stat3$^{-/-}$ *(cardiac)*	STAT3		S	*STAT3*	Hyper-IgE recurrent infection syndrome	(134) OMIM 102582
Irf3$^{-/-}$	IRF3	S		*IRF3*	HSV-1	(172, 195) OMIM 616532
Irf7$^{-/-}$	IRF7	S		*IRF7*	Severe influenza disease	(195) OMIM 605047
Irf3$^{-/-}$*Irf7*$^{-/-}$	IRF3/IRF7	S		*IRF3/IRF7*		(195)
Isg15$^{-/-}$	ISG15	S	S	*ISG15*	*Mycobacterium*	(74, 196) OMIM 147571

TABLE 1. Continued

Gene defect	Protein	HSV-1 phenotype*	CVB3 phenotype*	Human Gene	Infectious phenotypes	References***
Cytokines, chemokines, enzymes and metalloproteases						
Tnf$^{-/-}$	TNF-α	S	R	*TNF*		(128, 179, 180)
Il1b$^{-/-}$	IL-1β	S		*IL1B*		(180)
Il6$^{-/-}$	IL-6	S		*IL6*		(181)
Il10$^{-/-}$	IL-10	S	S	*IL10*		(130, 178)
Prf1$^{-/-}$	Perforin		R	*PRF1*		(197, 198)
Nos2$^{-/-}$	iNOS	S	S	*NOS2A*		(88, 199)
Il12rb1$^{-/-}$	IL-12Rβ1		R	*IL12RB1*	*Mycobacterium*	(143) OMIM 601604
Ccl3$^{-/-}$	CCL3		R	*CCL3*		(127)
Ccl5$^{-/-}$	CCL5		S	*CCL5*		(136)
Cxcl10$^{-/-}$	CXCL10	S	S	*CXCL10*		(124, 183)
Ccr5$^{-/-}$	CCR5	R	S	*CCR5*	Resistance to HIV-1 (32-bp DEL)	(136, 200) OMIM 601373
Cxcr3$^{-/-}$	CXCR3	R		*CXCR3*		(101, 104)
Cx3cr1$^{-/-}$	CX3CR1	S	S	*CX3CR1*		(137, 182)
Mmp2$^{-/-}$	MMP2		S	*MMP2*		(201)
Mmp9$^{-/-}$	MMP9		S	*MMP9*		(122)
Cell-mediated responses						
Rag1$^{-/-}$	RAG-1	S		*RAG1*	HCMV	(88)
Rag2$^{-/-}$	RAG-2	S		*RAG2*	Respiratory infections	(178) OMIM 233650
Nkg2d$^{-/-}$	NKG2D		S	*KLRK1*		(125)
Ptprc^{L3X} *or* $^{-/-}$	CD45	S	R	*PTPRC*		(80, 140)
Cd4$^{-/-}$	CD4	S	R	*CD4*		(99, 138)
Cd8$^{-/-}$	CD8	S		*CD8*	Recurrent bacterial infections	(88, 138) OMIM 186910
Cd4$^{-/-}$*Cd8*$^{-/-}$	CD4/CD8		R	*CD4/CD8*		(138)
p56lck$^{-/-}$	LCK (p56)		R	*LCK*		(139)
Card9$^{-/-}$	CARD9		R	*CARD9*	Candidiasis	(202) OMIM 607212
B2m$^{-/-}$	β2M	S	S	*B2M*	Sinopulmonary infections	(99, 198) OMIM 109700

* "R" indicates resistance compared to wild-type controls; "S" indicates susceptibility compared to wild-type controls; "As WT" indicates that knockouts and wild-types behave similarly.

** *Tbk1*$^{-/-}$*Tnfr1*$^{-/-}$ mice are compared here to *Tnfr1*$^{-/-}$ control mice (176).

*** OMIM accession numbers for human gene deficiencies are available at the Online Mendelian Inheritance in Man (OMIM) database (http://www.omim.org/).

This table is adapted from (75).

of invasive myocardial biopsies (144). Myocarditis has been suggested to be more common in children compared to adults (107). Among cases of myocarditis, some 20% can be traced back to viral origin, including enteroviruses, adenoviruses or human immunodeficiency virus 1 infections (144). CVB3 infection is involved in 25-40% of childhood and adolescent cases of myocarditis, making it the most common cause of viral myocarditis (144, 203). Cardiac infiltration of T lymphocytes and of other inflammatory mediators is a hallmark of viral myocarditis, as well as the detection of autoantibodies and autoreactive T cells (204). In response to inflammation and tissue fibrosis, viral myocarditis can progress to dilated cardiomyopathy. Dilated cardiomyopathy has an estimated incidence of 5 to 8 cases per 100,000 individuals annually in the United States; among which viral genomes have been identified in some 10-34% of these cases (205). Treatment for dilated cardiomyopathy consists of supportive care to reduce vascular resistance, or in the case of severe symptoms, implantation of ventricular assist devices or heart transplant.

1.5.2 Human genetic determinants

Several genetic factors have been associated with dilated cardiomyopathy, including polymorphisms in genes encoding cardiac actin, myosin, titin and cardiac muscle troponin (206). However, scarcely any genetic studies have been performed for patients with acute myocarditis, particularly of viral origin. In these cases of viral myocarditis, where disease severity is not a function of the viral agent (most commonly CVB3, but also other enteroviruses, adenoviruses, and parvoviruses), disease may be influenced by host genetics (107). A rare non-synonymous substitution mutation in *TLR3* was associated in an adult patient with acute CVB3 myocarditis (207). However, while the variant expressed in HEK293 cells resulted in lower type I IFN upon CVB3 infection, *TLR3* deficiency in cardiomyocytes does not render them more sensitive to CVB3 infection, nor do wild-type cardiomyocytes induce ISGs upon infection (107, 207). Otherwise, in a whole-exome sequencing screen of 42 children with acute myocarditis, 7 patients carried rare homozygous variants in genes associated with inherited cardiomyopathies, of which variants in plakophilin-2 (*PKP2*), ryanodine receptor 2 (*RYR2*) and troponin I3 (*TNNI3*) corresponded with herpesviral, enteroviral, and parvoviral etiologies, respectively (107). Further investigation into these variants is required to determine their penetrance and contribution to the development of acute viral myocarditis.

1.5.3 Mouse genetic determinants

Inbred mouse models of CVB3-induced myocarditis have been especially useful to define the genetic contribution to disease onset and severity (Figure 3 and Table 1). Studies over the past 30 years have focused on single gene knockout mice, spread primarily across naturally CVB3-susceptible A/J or BALB/c strains, and more resistant C57BL/6 or 129 strains, but nearly always comparing deficient mice to wild-type mice of the same genetic background. As a first important finding, an intact type I IFN response is essential to CVB3 control. Mice deficient in *Tlr3*, *Unc93b1*, *Ticam1* (TRIF), *Ifih1* (MDA5) and *Mavs* RNA sensing cascade genes, as well as IFN-β and IFNα/βR1 receptor, are all susceptible to CVB3 myocarditis (110, 189, 190, 192). As a notable exception, non-TLR3 related MYD88 and IRAK4 factors are detrimental to the host response in the heart (136, 191). In addition to dampening type I IFN in the heart, MYD88 has been proposed to exacerbate pathological T cell activation, while IRAK4 leads to reduced infiltration of protective CCR5+ myeloid cells in the heart (136, 191).

Second, secreted immune factors play a major role in disease pathogenesis. IFN-γ and iNOS deficient mice fail to control infection, likely pointing to a failure of NK cell and macrophage-mediated antiviral control (123, 199). On the other hand, *Tnf*$^{-/-}$ mice are more resistant compared to wild-type littermates, an important indication that NF-κB/TNF-α-mediated inflammation is pathological in the heart (128). From chemokine and chemokine receptor knockout mice, the recruitment of T, NK and myeloid effector cells is a requirement for viral clearance (124, 136, 137). However, the cell-mediated response can be harmful to the infected host. Mouse genetic models have shown that T cells are pathological, where *Ptprc*$^{-/-}$, *Cd4*$^{-/-}$, *Cd4*$^{-/-}$*Cd8*$^{-/-}$, *p56lck*$^{-/-}$, *Card9*$^{-/-}$ and perforin-deficient mice all overcome CVB3 myocarditis, and exhibit dampened cardiac inflammation (138-140, 202). *Il12rb1*$^{-/-}$ mice are also resistant to CVB3 infection, suggesting that Th1-supporting IL-12 and IL-23 cytokines may play a role in T cell-mediated acute myocardial inflammation (143).

Third, mouse models have revealed an additional genetic contribution of factors involved in the regulation of cell death and of cardiac remodeling. Matrix metalloprotease MMP2 and MMP9 knockout mice are susceptible to CVB3 due to their limited ability to repair cardiac injury (122, 201). Necroptosis and pyroptosis are also hallmarks of damaging CVB3-induced inflammation, where expression of the damage-associated molecular pattern sensor NOD2 (*Nod2*)

or cathepsin B (*Ctsb*) are detrimental, while the function of the NLRP3 inflammasome is protective (115-117). Finally, the loss of *Abcc6*, an ATP binding cassette transporter of ATP, results in increased permeability of the mitochondrial outer membrane, tissue calcification and necrotic cell death; this effect can be reversed by pharmacological inhibition of the mitochondrial permeability transition pore using cyclosporin A (118).

As a final consideration, the cell-mediated response to cardiac viruses is affected by the sex of the murine host. Male mice are particularly sensitive to myocarditis, in part by their relatively higher expression of *Tlr4*, more pronounced Th1 responses, and endocrine differences related to testosterone (143, 186). A more frequent incidence of heart failure and dilated cardiomyopathy in men has also been reported in clinical studies (208).

1.6 FORWARD GENETIC APPROACHES IN INBRED MOUSE MODELS

Inbred mouse strains, and their range of natural resistances to different pathogens, have proven useful to the study and modeling of infectious disease. The various knockout allele mouse models of HSV-1 and CVB3 infection discussed in the previous sections have especially contributed to our understanding of how inflammatory and cell survival mechanisms are essential to the development of HSE or viral myocarditis, and expand upon the relatively few human genetic etiologies that have been identified in a minority of total disease cases. While these models primarily use reverse genetic approaches—altering genes to assess resulting phenotypes—forward genetic strategies that ask which genes might underlie a known phenotype have also been instrumental in identifying new functions for genes in host defence. Thus, genetic crosses between inbred mouse strains have helped to identify genes like *Nramp1*, *Tlr4* and *Irf8* as essential to control various bacterial and parasitic infections, phenotypes which have also been associated with human *NRAMP*, *TLR4* and *IRF8* variants (209).

Of these forward genetic approaches, *N*-ethyl-*N*-nitrosourea (ENU) chemical mutagenesis has also revealed the contribution of novel genes, or of new functions of known genes, to host defence. ENU is an alkylating agent and carcinogen, mediating the addition of ethyl groups to various nucleobases can trigger faulty DNA repair and single nucleotide substitutions (210). AT to GC transition mutations (45% of induced mutations) and AT to TA transversion mutations (28.5%) are more likely to occur (211). Thus, for ENU-treated male mice, ENU introduces to the

germline an average of 1.5 point mutations per megabase of genomic DNA, or roughly 4,000 variants over the 2.7 gigabase mouse genome, and some 40 to 80 variants falling within protein coding regions (212). From these ENU-treated male mice, these mutations can be bred to homozygosity in multiple third generation pedigrees and screened for recessive phenotypes following infection with a pathogen (80, 213, 214). Next-generation whole exome sequencing can be employed in phenotype-deviant mice to identify causal mutations that might explain differential susceptibility or resistance to infection compared with wild-type littermate mice (213, 214). This thesis will focus on an ENU-induced mutation in the reticuloendotheliosis oncogene (*Rel*) encoding the c-Rel transcription factor, whose known functions and targets will be introduced in the following section.

1.7 THE c-REL TRANSCRIPTION FACTOR

1.7.1 c-Rel and the NF-κB signaling pathway

NF-κB (nuclear factor κ-light-chain-enhancer of B cells) refers to a family of transcription factors (RelA/p65, RelB, c-Rel, NFκB1/p50, and NFκB2/p52) that associate in homo- or heterodimeric complexes to modulate transcription of various genes, including many proinflammatory genes (215). These subunits are constitutively expressed in diverse cell types, including hematopoietic cells, and are maintained inactive by bound IκBα molecules in the cytoplasm. Phosphorylation of IκBα by the I kappa B kinase (IKK) complex (consisting of α, β, and NEMO subunits), and the subsequent ubiquitination and proteomic degradation of IκBα, releases NF-κB dimers and allows them to transit to the nucleus and modulate transcription. This canonical NF-κB signaling cascade can occur downstream of TNF-α, IL-1β or TLR stimulation, and while RelA/p50 heterodimers are usually involved, other pairs including RelA/c-Rel, c-Rel/p50 or even c-Rel/c-Rel homodimers can occur (216). All NF-κB subunits contain a nuclear localization signal, an inhibitory domain, and a crucial *REL* homology domain which allows for binding of DNA and of other *REL* homology domain-containing factors; only RelA, RelB and c-Rel contain transactivation domains to induce transcription (215, 217). While most subunit dimers recognize an NF-κB consensus sequence 5′ GGGRNWYCC 3′, c-Rel has been noted to recognize

more varied sequences compared to RelA or RelB, and specifically a 5′ NGGRNWTTCC 3′ , where R = A or G, W = A or T, Y = C or T, and N represents any nucleotide (216, 217). Thus, c-Rel-containing dimers may target additional genes and carry out unique regulatory functions.

Recent studies are beginning to define how various upstream signals and stimuli preferentially modulate the expression of c-Rel over other NF-κB subunits. In general, c-Rel nuclear translocation and activity are induced in fibroblasts and macrophages upon *in vitro* stimulation with multiple TLR agonists, and especially upon TLR1, TLR2, and TLR4 stimulation in macrophages, and TLR1, TLR2, TLR7 and TLR8 in fibroblasts (218). In the context of the above single cell analysis however, c-Rel induction is slightly inferior to RelA and of lesser duration. Upon TCR engagement, members of the NFAT transcription factor family induce c-Rel transcription, which in turn increases c-Myc expression to regulate T cell proliferation (219). Other factors including the cellular nucleic acid–binding protein (CNBP) are required to promote nuclear translocation and DNA binding activity of c-Rel to the *Il12b* promoter, where *Cnpb*$^{-/-}$ macrophages fail to elicit c-Rel activity (220). Finally, during infection, the HIV-1 Tat viral product has been shown to bind to NF-κB motifs in the *Rel* promoter, and repressing c-Rel expression in infected T cells (221).

1.7.2 c-Rel target genes

Many inflammatory genes, including proliferation, survival and development genes required for the generation of cell-mediated immune responses, have been shown to be direct and specific targets of c-Rel. Among T cell-modulating cytokine genes, chromatin immuno-precipitation has confirmed that *Il12p40*, *1l2p35*, and *Il23p19* transcription is induced upon c-Rel promoter binding, and is required for IL-12 and IL-23 expression by DCs and myeloid cells (222-224). The transcription of the IL-21-encoding gene is also reliant on c-Rel, where *Rel*$^{-/-}$ mice develop fewer follicular helper T cells resulting in altered lymph node germinal centre structures (225). Upon TCR activation in effector T cells, c-Rel is recruited to the *Il2* promoter and engages in chromatin remodeling to *Il2* expression and promote IL-2-dependent T cell proliferation (226, 227). The expression of the granulocyte macrophage colony stimulating factor (GM-CSF) cytokine is similarly regulated by c-Rel at the level of the *Csf2* promoter during T cell activation (228). Finally, c-Rel induction of *Foxp3*, *Rorc*, *Rorg* transcription factor expression is also required

for the development of thymic Foxp3$^+$ Tregs and of RORγt$^+$ Th17 cells, where *Rel*$^{-/-}$ mice exhibit reductions in these mature cell populations (81, 82, 229).

As for B cells, c-Rel plays a role in immunoglobulin class-switching to IgG1 and IgE isotypes (226), and further enhances mature B cell proliferation and cell cycle progression in part by inducing c-Myc transcription factor expression (230). B cell survival is further promoted by c-Rel through its induction of anti-apoptotic BCL2-family genes, including *Bcl2a1* (A1/Bfl-1) and *Bcl2l1* (Bcl-xL) (231, 232). Interestingly, a prosurvival role for c-Rel, countering an anti-apoptotic role of RelA, has been reported in neurons upon injury (233). In heart-resident cardiomyocytes, c-Rel also appears to have a role in limiting cellular and ventricular hypertrophy (234).

Finally, both the upregulation and deletion of c-Rel in human T cells results in the modulation of *Cxcl10*, *Cd40*, *Il4* and *Il13* expression, among genes that were not previously mentioned above (235). Classically, c-Rel is considered an activator of transcription, however, it remains to be determined to what extent or in which contexts c-Rel may act as a transcriptional repressor.

1.7.3 c-Rel in inflammatory diseases

Finally, c-Rel has been implicated in several inflammatory diseases in humans. Genome wide association studies have demonstrated that single nucleotide variants in the *REL* locus are associated with rheumatoid arthritis, psoriatic arthritis, psoriasis, vitiligo, ulcerative colitis, Crohn's disease and multiple sclerosis (236-241). These chronic inflammatory disorders all generally involve pathological cell-mediated inflammation or autoimmunity, target diverse tissues including the skin, gut and CNS, and represent an elevated disease burden in Canada (242). In mice, the *Rel*$^{-/-}$ mouse has proven a useful tool to validate and dissect some of the mechanisms by which c-Rel may regulate immunity and inflammation (226). For example, c-Rel-deficient mice are more resistant to induction of experimental autoimmune encephalomyelitis (EAE) and to experimental colitis induced by anti-CD40 antibody treatment, but susceptible to azoxymethane/dextran sodium sulfate-induced colitis-associated colorectal cancer (81, 243, 244). With the implication that similar mechanisms will govern inflammation and the host response to infection, the role of c-Rel in response to HSV-1 and CVB3 viral infections will be explored in the context of our own c-Rel mutant model in the following chapters.

1.8 RATIONALE, HYPOTHESIS, AND OBJECTIVES

Rationale

HSV-1 and CVB3 are both widespread in human populations. In contrast, the incidence of HSE and CVB3-induced myocarditis is relatively low, and only affect a minority of individuals exposed to these viruses. Specifically, host genetics are known to play an important role in the onset of these diseases. For HSE, whole exome sequencing has revealed that inborn genetic defects in the TLR3/type I IFN axis explain a subset of childhood cases. However, these cases do not capture the full spectrum of HSE disease, which can also develop in adults or manifest as post-HSE autoimmune encephalitis. Mouse models have proved useful to recapitulate HSE phenotypes and implicate genes related to diverse antiviral and inflammatory pathways in HSE pathogenesis. Forward genetic approaches are particularly well-suited to the discovery of new loci and genes, or ascribe new roles for known genes in mediating susceptibility or resistance to infection.

Hypothesis

Thus, in our implementation of a chemical ENU mutagenesis screen for HSV-1 susceptibility, we expected to identify new genetic determinants of HSE beyond type 1 interferon-related genes. When our screen revealed a deleterious mutation in the NF-κB transcription factor c-Rel, known for its expression in hematopoietic cells and for its association with human inflammatory diseases, we hypothesized that the Rel^{C307X} mutation would disrupt immune cell-mediated responses to viral infection. We tested our hypothesis in both neurotropic HSV-1 and cardiotropic CVB3 infection models, with a focus on exploring the effect of c-Rel-dependent regulation on tissue-specific immunity, along the three following objectives:

Objective 1. To establish the effect of the ENU-induced Rel^{C307X} mutation on viral replication, production of inflammatory markers, and cell survival in the CNS of HSV-1 infected animals.

We first tested the impact of the mutation on survival in an intranasal model of HSV-1 infection, compared to heterozygous and wild-type littermates, and to compound heterozygous mice. Bone marrow chimeric mice, quantification of peripheral immune cells, and *ex vivo* infection of primary cell cultures were used to evaluate the contribution of immune cells or of resident cells

to the host response. Finally, we assessed HSV-1 viral replication, neuroinflammation and cell death in the *Rel*^{C307X} brainstem and cerebellum at both transcript and protein levels.

Objective 2. To identify specific hematopoietic or resident cell types that contribute to HSE through c-Rel-dependent dysregulation of gene expression and of inflammatory pathways, prior to clinical symptom onset.

We favoured a two-pronged approach, first by using dual RNA sequencing to capture host and viral gene transcripts in non-infected or HSV-1 infected brainstem tissue. After determining changes in the *Rel*^{C307X} and viral transcriptomes, we complemented these findings with flow cytometry in the brain to determine which tissue-infiltrating cells were present in the sequenced tissue, and which populations had later infiltrated the brain at the height of HSE disease in response to earlier changes in gene expression.

Objective 3. To investigate the role of the truncating *Rel*^{C307X} mutation in cell-mediated immunity in a model of CVB3-induced myocarditis.

We applied an intraperitoneal model of CVB3 infection in *Rel*^{C307X} and littermate mice to evaluate the contribution of the mutation to viral control and to the inflammatory response in the heart. Using a similar experimental approach to Objective 2, heart infiltrating immune cells were compared to changes in host or viral gene expression in the infected heart to assess the effect of c-Rel-dependent dysregulation on pathological inflammation and CVB3 replication.

CHAPTER TWO: *Rel*-DEPENDENT IMMUNE AND CENTRAL NERVOUS SYSTEM MECHANISMS CONTROL VIRAL REPLICATION AND INFLAMMATION DURING MOUSE HERPES SIMPLEX ENCEPHALITIS

Mathieu Mancini,[*,†] Grégory Caignard,[*,‡] Benoît Charbonneau,[*,†] Anne Dumaine,[*,†] Nila Wu,[*,†] Gabriel A. Leiva-Torres,[*,†] Steve Gerondakis,[§,¶] Angela Pearson,[||] Salman T. Qureshi,[†,#] Robert Sladek,[*,**] and Silvia M. Vidal[*, †, ††]

∗ Department of Human Genetics, McGill University, Montréal, Québec, Canada

† McGill Research Centre on Complex Traits, McGill University, Montréal, Québec, Canada

‡ Laboratoire de Santé Animale d'Alfort, Université Paris Est, ANSES, ENVA, INRA, UMR 1161 VIROLOGIE, Maisons-Alfort, France.

§ Biomedicine Discovery Institute, Monash University, Clayton, Victoria, Australia

¶ Department of Biochemistry and Molecular Biology, Monash University, Clayton, Victoria, Australia

| | INRS-Institut Armand-Frappier, Laval, Québec, Canada

Division of Experimental Medicine, Department of Medicine, McGill University, Montréal, Québec, Canada

∗∗ McGill University and Genome Québec Innovation Centre, Montréal, Québec, Canada

†† Corresponding author: Silvia M. Vidal, Tel. (514) 398-2362, Fax (514) 398-2603, Email silvia.vidal@mcgill.ca

Originally published in The Journal of Immunology:

Mancini M, Caignard G, Charbonneau B, Dumaine A, Wu N, Leiva-Torres GA, Gerondakis S, Pearson A, Qureshi ST, Sladek R, Vidal SM. 2019. *Rel*-Dependent Immune and Central Nervous System Mechanisms Control Viral Replication and Inflammation during Mouse Herpes Simplex Encephalitis. *J Immunol* 202: 1479-93. https://doi.org/10.4049/jimmunol.1800063

2.1 ABSTRACT

Herpes simplex encephalitis (HSE), caused by HSV type 1 (HSV-1) infection, is an acute neuroinflammatory condition of the CNS and remains the most common type of sporadic viral encephalitis worldwide. Studies in humans have shown that susceptibility to HSE depends in part on the genetic make-up of the host, with deleterious mutations in the TLR3/type I IFN axis underlying some cases of childhood HSE. Using an *in vivo* chemical mutagenesis screen for HSV-1 susceptibility in mice, we identified a susceptible pedigree carrying a causal truncating mutation in the *Rel* gene (Rel^{C307X}), encoding for the NF-κB transcription factor subunit c-Rel. Like $Myd88^{-/-}$ and $Irf3^{-/-}$ mice, Rel^{C307X} mice were susceptible to intranasal HSV-1 infection. Reciprocal bone marrow transfers into lethally irradiated hosts suggested that defects in both hematopoietic and CNS-resident cellular compartments contributed together to HSE susceptibility in Rel^{C307X} mice. Although the Rel^{C307X} mutation maintained cell-intrinsic antiviral control, it drove increased apoptotic cell death in infected fibroblasts. Moreover, reduced numbers of $CD4^+CD25^+Foxp3^+$ T regulatory cells, and dysregulated NK cell and $CD4^+$ effector T cell responses in infected Rel^{C307X} animals, indicated that protective immunity was also compromised in these mice. In the CNS, moribund Rel^{C307X} mice failed to control HSV-1 viral replication in the brainstem and cerebellum, triggering cell death and elevated expression of *Ccl2*, *Il6*, and *Mmp8* characteristic of HSE neuroinflammation and pathology. In summary, our work implicates c-Rel in both CNS-resident cell survival and lymphocyte responses to HSV-1 infection and as a novel cause of HSE disease susceptibility in mice.

2.2 INTRODUCTION

Herpes simplex virus type 1 (HSV-1) is a neurotropic, dsDNA virus for which humans are the only natural reservoir. Primary infection with HSV-1 usually occurs in epithelial cells and keratinocytes, in which actively replicating viral particles can be shed in the saliva and transmitted through close personal contact (1, 2). Like other viruses of the *Herpesviridae* family, HSV-1 can switch away from this lytic replication cycle to establish life-long latency in the nuclei of sensory neurons. Both primary infection and reactivation from latency can lead to the infection of the corneal epithelium and ocular herpes simplex keratitis (3), or in rare cases, HSV-1 can travel along the axons of the trigeminal ganglia (TG), bypassing the blood-brain barrier (BBB) to invade the

CNS and cause herpes simplex encephalitis (HSE). The peak age of HSE onset is bimodally distributed, occurring either in early childhood following primary HSV-1 infection or in adults frequently upon reactivation of latent virus (4, 5). Human HSE is characterized by elevated lytic replication of HSV-1 in the CNS and involves the recruitment of mononuclear cells to infected neuronal and glial cells, leading to the formation of necrotic and inflammatory lesions in the temporal or frontal lobes (6).

In children, host genetic factors play a role in determining HSE susceptibility and converge around inborn defects of innate immune type I IFN signaling that together account for ~5% of childhood cases (7). HSV-1 nucleic acids are recognized by pattern recognition receptors, including endosomal TLR 3, 7, 8, and 9, that initiate production of type I IFN notably via the transcription factors NF-κB and IRF3 (8). In CNS cells, the engagement of the type I IFN receptor (IFNAR) by IFN-α or IFN-β, initiating downstream JAK/STAT signaling, will trigger increased expression of various IFN-stimulated genes to limit HSV-1 replication and spread (9). Several identified etiologies for HSE fall directly within the TLR3 pathway, including *UNC93B1*, *TLR3*, *TRIF*, *TRAF3*, and *TBK1* (10-14). Additionally, HSE patient mutations in the transcription factor genes *STAT1* and *IRF3* (15, 16), as well as in the essential NF-κB modulator *NEMO* (17), further reinforce the importance of IFN in mounting a protective response to HSV-1 neuroinvasion. Although antiviral therapy is used to control CNS viral replication and treat HSE, it cannot mitigate the risk of sequelae incurred through the breakdown of the BBB, infiltration of leukocytes, or elevated caspase-dependent neuronal cell death at sites of infection and neuroinflammation (18, 19). Even in patients who have fully recovered from HSE, the extensive infiltration of activated $CD68^+$ myeloid cells and of $CD3^+$ T cells, including many cytotoxic $CD8^+$ T cells, may persist long after HSV-1 viral clearance from the CNS (20).

Similarly, HSE in mice is characterized by inflammatory cell infiltrate and by concurrent, acute viral replication in the CNS. Susceptibility in mice can be driven by aberrant IFN signaling; for example, *Stat1*$^{-/-}$ mice fail to upregulate IFN-stimulated gene expression in the brainstem, leading to elevated viral replication (21). Furthermore, mice lacking UNC93B1 or MyD88, adaptor proteins employed by various endosomal TLR cascades, in addition to *Irf3*$^{-/-}$ mice, have been reported as susceptible to certain routes of HSV-1 inoculation (22-24). Essential to the clearance and control of viral replication are $CD8^+$ cytotoxic T cells, supported by IFN-γ–secreting $CD4^+$ T cells (25). Other immune cells such as NK cells and $CX3CR1^+$ microglia have protective roles (26,

27), whereas $CXCR3^+$ infiltrating monocytes and leukocytes have been shown to be detrimental and auxiliary to this pathologic condition (28, 29). Considering this known involvement of various immune and CNS-resident cell types in the protective response to HSV-1 infection in mice, experimental HSE is a good model to explore novel genetic deficiencies or cellular mechanisms related to the antiviral or inflammatory host response to infection.

N-Ethyl-*N*-nitrosourea (ENU), a potent mutagen that randomly induces point mutations in the germline of a male mouse, is often used in mouse forward genetic screens for genes that affect resistance or susceptibility to pathogens (30-32). We applied an ENU mutagenesis screen for HSV-1 susceptibility and have previously uncovered the *Ptprc* gene (CD45) as a cause of HSE in mice that implicates a protective T cell response in the peripheral control of viral replication (25). In this study, we characterize a new pedigree from the same mutagenesis screen that identifies an HSV-1–susceptible mouse carrying an ENU-induced mutation in the reticuloendotheliosis oncogene (*Rel*) gene, resulting in elevated CNS viral replication, neuroinflammation, and cell death. These data point to a role for Rel, in hematopoietic and resident cells, in the control of virus replication in the CNS, and as a novel mediator of HSE resistance.

2.3 MATERIAL AND METHODS

Ethics statement

The experiments in this study were performed in compliance with the guidelines and regulations of the Canadian Council on Animal Care. All experiments were approved under protocol number 4792 by the McGill University Animal Care Committee. All animals were housed and maintained under specific pathogen-free conditions at McGill University.

Virus strain and measurement of viral titer

HSV-1 strain 17 was amplified on Vero cells (ATCC CCL-81; American Type Culture Collection), whereas the titers of stock virus, infected tissue homogenates, and infected primary cells were measured by standard plaque assay on confluent Vero cell monolayers, as previously described (33).

Infected tissues were homogenized at speed 6000 for 40 s with a MagNA Lyser Instrument (Roche) in 1 ml DMEM; infected cells were resuspended in 1 ml DMEM. Confluent Vero cell

monolayers in 12- or 24-well culture plates were inoculated in duplicate with 10- or 5-fold serially diluted samples, respectively. After 1 h, cells were overlaid with DMEM, 2% FBS, 1% penicillin/streptomycin (p/s), and 0.35% methylcellulose. After 3 d, wells were fixed with 10% phosphate-buffered formalin, stained with 0.5% crystal violet in 70% ethanol, and counted for viral plaques. PFU were calculated by averaging counts between two duplicate wells. The limit of detection denotes the viral titer corresponding to a single detectable PFU at the lowest sample dilution.

Mouse strains and infections

Inbred C57BL/6J (B6), C57BL/10J (B10), BALB/c, A/J, *Myd88*$^{-/-}$, and *Tlr3*$^{-/-}$ mice were purchased from The Jackson Laboratory (Bar Harbor, ME). *Rel*$^{-/-}$ knockout mice were kindly provided by Dr. S. Gerondakis (34), and *Unc93B1*$^{Letr/Letr}$ mice were a kind gift of Dr. S. T. Qureshi (35). All mice were maintained as breeding colonies at McGill University. Seven-week-old or older mice were each infected via i.p. injection with 1 x 10^4 PFU of HSV-1 strain 17 in 200 μl PBS. Alternatively, mice aged 7 wk or older were first anesthetized (i.m. or i.p. ketamine and xylazine injection) and each infected via intranasal (i.n.) inoculation at 5 x 10^4 PFU of HSV-1 strain 17 per 20 g of weight, or as otherwise indicated. For a 20 g mouse, the weight-adjusted viral dose was delivered in 10 μl of sterile PBS in the left nostril and allowed to be inhaled. Mice were monitored at least once daily postinfection (p.i.), at least three times daily between days 6 and 10 p.i., and at least twice daily until end point at day 14. Mice that demonstrated either HSE-like symptoms (hunched posture, reduced mobility, neurologic symptoms) or weight loss above 15% of initial weight were euthanized and considered susceptible to HSV-1. B6 and B10 animals were used as resistant controls, whereas A/J or BALB/c animals were used as susceptible controls. At clinical or experimental end point, mice were euthanized and spleen, olfactory bulbs (OB), TG, brainstem and cerebellum (BSC), and/or cerebrum tissue were excised and collected in 1 ml DMEM for viral titer measurement or flow cytometry or snap-frozen in liquid nitrogen pending RNA or protein extraction.

ENU mutagenesis and whole-exome sequencing

ENU mutagenesis was performed as previously described (25). Briefly, male B6 mice (G0) were mutagenized with ENU and out-crossed to B10 females to generate first-generation (G1) mice, which were further outcrossed to B10 females to generate G2 offspring. Per pedigree, two G2 females were backcrossed with their G1 father to generate G3 animals. G3 mice were screened for susceptibility to i.p. HSV-1 infection. Whole-exome sequencing was performed on genomic DNA isolated from 3 HSV-1-susceptible G3 animals. Using the Canadian Centre for Computational Genomics pipeline and the BROAD Institute Genome Analysis Toolkit (GATK) best practices, raw sequencing reads were trimmed using Trimmomatic (36) and aligned to a reference genome (build GRCm38) using the Burrows–Wheeler transform aligner BWA-mem (37). Mapped reads were further refined using the GATK and Picard program suites (38) to improve mapping near insertions and deletions (indels: GATK IndelRealigner), remove duplicate reads with the same paired start site (Picard mark duplicates), and improve quality scores (GATK base recalibration). Variants were called using the GATK haplotype caller in gvcf mode to allow efficient downstream merging of multiple samples into one variant file. Variant and functional annotation was performed with SnpEff (39).

Bone marrow transfers

Eight-week-old mice were subjected to two rounds of full-body lethal radiation (900 Rad total; two doses of 450 Rad) within 3 h intervals using an X-Ray RS-2000 biological irradiator. The next day, mice were reconstituted by i.v. injection with 5 x 10^6 RBC-depleted bone marrow cells from sex- and age-matched donors. Paired donors and recipients were either $CD45.1^+$, $CD45.2^+$, or $CD45.1^+CD45.2^+$ to track engraftment after transfer. Mice were maintained on antibiotic water 1 wk prior through 3 wk post-irradiation. Reconstitution of the hematopoietic compartment was assessed in blood and collected by cheek bleed at 6 wk post-irradiation by flow cytometry for CD45.1 and CD45.2 expression (gating strategy detailed in Supplemental Fig. 3E). At 8 wk post-irradiation, mice were infected i.n. with HSV-1 and monitored for survival.

Flow cytometry and ex vivo cell stimulation

Leukocytes were isolated from whole spleen or thymus tissue following manual dissociation of tissue in RPMI 1640 10% FBS 1% p/s and treatment with 2 ml of RBC Lysing Buffer Hybri-Max (no. R7757; Sigma-Aldrich). Blood was collected via cheek bleed in tubes containing 1.6 mg/ml EDTA, and samples were treated twice with 2 ml of RBC Lysing Buffer Hybri-Max. A total of 5 x 10^6 splenocytes or thymocytes were stained extracellularly, fixed and permeabilized using the Foxp3/Transcription Factor Staining Buffer Set (no. 00-5523-00; eBioscience) as per the manufacturer's instructions, and finally stained intracellularly for Foxp3 expression. For *ex vivo* stimulations, 5 x 10^6 splenocytes or 5 x 10^6 blood leukocytes were incubated for 5 h at 37°C in RPMI 10% FBS 1% p/s medium, completed with either 1) Cell Stimulation Cocktail (dilution 1:500, no. 00-4975-93, containing PMA/ionomycin and protein transport inhibitors; eBioscience) or 2) purified CD3ε Ab (clone 145-2C11, dilution 1:250), purified CD28 Ab (36.51, 1:500), brefeldin A (1:500, no. 00-4506-51; eBioscience), and monensin (1:500, no. 00-4505-51; eBioscience). These stimulated cells were first stained extracellularly, fixed and permeabilized using the BD Cytofix/Cytoperm Kit (BD Biosciences no. 554714) as per the manufacturer's instructions, and finally stained intracellularly for IFN-γ expression.

For extracellular and intracellular staining, the following fluorochrome-conjugated Abs (clone, working dilution) were used from eBioscience: CD3 eFluor780 (17A2, 1:200), CD4 FITC (GK1.5, 1:200), CD8a eFluor450 (53-6.7, 1:200), CD11b eFluor450 (M1/70, 1:300), CD25 PerCP-cyanine5.5 (PC61.5, 1:500), CD44 allophycocyanin (IM7, 1:500), CD45.1 PE (A20, 1:300), CD45.2 PerCP-cyanine5.5 (104, 1:300), CD62L FITC (MEL-14, 1:200), CXCR3 PE-cy7 (CXCR3-173, 1:200), F4/80 PE (BM8, 1:250), Foxp3 allophycocyanin (FJK-16s, 1:100), KLRG1 PE (2F1, 1:200), and NK1.1 PE-cy7 (PK136, 1:200); and from BioLegend: CD3 Brilliant Violet 605 (17A2, 1:200), CD4 Brilliant Violet 510 (GK1.5, 1:200), CD27 PE-cy7 (LG.3A10, 1:100), I-A/I-E (MHC type II [MHCII]) AlexaFluor700 (M5/114.15.2, 1:500), and IFN-γ Brilliant Violet 711 (XMG1.2, 1:50). Fixable Viability Dye eFluor506 and eFluor780 (no. 65-0866-14 and no. 65-0865-14, respectively; eBioscience) were used to identify dead cells. A total of 1 x 10^6 events per sample were acquired on a BD LSRFortessa or BD FACSCanto II cytometer and gated as described in Supplemental Fig. 3 with FlowJo Version 10.1 software.

Primary cell culture and infection

Both femurs and tibias were collected from mice aged 8 wk or older, and RBC-depleted bone marrow cells were cultured in RPMI 10% FBS, 1% p/s, and 30% M-CSF medium for 5 d to collect bone marrow–derived macrophages (BMDM). Mouse embryonic fibroblasts (MEF) were prepared from embrionic day 14.5–17.5 embryos as previously described (40) and expanded in DMEM 10% FBS and 1% p/s. In 48-well plates, BMDM were infected with HSV-1 for 1 h at a multiplicity of infection (MOI) of 0.1 and MEF for 1 h with at MOI = 0.01 HSV-1 in free medium. After 1 h, at T = 0 h, the inoculum was removed, cells were washed with PBS, and fresh complete medium was added to each well. At each time point, adherent BMDM or MEF were detached and cell suspensions were collected and subjected to three freeze/thaw cycles, in which total virus was measured by plaque assay. Lactate dehydrogenase (LDH) activity was measured in cell supernatants using the Cytotoxicity Detection Kit^{PLUS} kit (Roche). For RNA and protein extraction at various time points, BMDM and MEF cells were seeded in six-well plates and infected with HSV-1 strain 17 at MOI = 0.1 or MOI = 0.01, respectively.

Protein extraction and Western blots

Snap-frozen tissues were homogenized at speed 6000 for 40 s with a MagNA Lyser Instrument in 1 ml T-PER Tissue Protein Extraction Reagent (no. 78510; Thermo Fisher Scientific) containing protease inhibitor. BMDM or MEF cells were resuspended and lysed in 500 µl CelLytic M reagent (no. C2978; Sigma-Aldrich) containing protease inhibitor. Subcellular fractionation was performed as previously described (41) on 1 x 10^7 RBC-depleted total splenocytes, with all buffers containing protease inhibitor. All samples were probe-sonicated for 15 s at 60% amplitude. Protein was quantified using the Bio-Rad Protein Assay (no. 500-0006). Twenty micrograms of protein per tissue or BMDM sample, or 10 µg of protein per MEF sample, were separated on 8 or 10% polyacrylamide gels, with a 3% polyacrylamide stacking gel. Proteins were wet transferred onto nitrocellulose membranes. For immunoblotting, membranes were probed with the following primary Abs from Santa Cruz Biotechnology (SC) or Cell Signaling Technology (CST) (product number, working dilution): mouse monoclonal anti-c-Rel (SC no. 373713, 1:500), rabbit polyclonal anti-Gapdh-HRP (SC no. 25778, 1:2000), rabbit monoclonal anti-H2A (CST no. 12349, 1:1000), rabbit monoclonal anti–cleaved caspase-3 (Asp175) (CST no.

9664, 1:1000), and rabbit monoclonal anti–β-Actin (CST no. 4970, 1:10,000). For MEF and BMDM samples, individual protein band intensities were quantified using ImageJ software and normalized to β-actin expression. Protein quantities are represented as the mean ± SD of three individual mice.

RNA extraction and real-time quantitative PCR

Snap-frozen tissues were homogenized in 1 ml TRIzol reagent (no. 15596; Invitrogen) at speed 6000 for 40 s with a MagNA Lyser Instrument. BMDM or MEF cells were lysed directly in 500 μl TRIzol reagent. Total RNA was isolated from tissue and cells using a standard protocol outlined by the manufacturer. Using M-MLV reverse transcriptase (no. 28025013; Thermo Fisher Scientific), 1 μg of total RNA was reverse transcribed into cDNA according to the protocol outlined by the manufacturer. Real-time quantitative PCR was performed using the StepOnePlus Real-Time PCR system by Applied Biosciences, using Power SYBR Green PCR master mix (no. 4367659; Thermo Fisher Scientific), and cycle threshold (cT) values were measured in duplicate samples. The following primer pairs were used: *Hprt* (5'-CAGGCCAGACTTTGTTGGAT-3', 5'-TGGCGCTCATCTTAGGCTTT-3'), *Rel* (5'-AGTGACTCACCCCACCTCAC-3', 5'-AGGCC-CTTCTAGGAATGGAA-3'), *ICP4* (5'-CGACACGGATCCACGACCC-3', 5'-GATCCCCCTC-CCGCGCTTCGTCCG-3'), *Ccl2* (5'-AGGTGTCCCAAAGAAGCTGTA-3', 5'-TCTGGACCC-ATTCCTTCTTG-3'), *Bcl2l1* (5'-ATGCAGGTATTGGTGAGTCG-3', 5'-CCCGTAGAGATC-CACAAAAG-3'), *Sod2* (5'-GCTGGCTTGGCTTCAATAAG-3', 5'-TAGTAAGCGTGCTCC-CACAC-3'), *Mmp8* (5'-TTTGATGGACCCAATGGAAT-3', 5'-GAGCAGCCACGAGAAA-TAGG-3'), *Il6* (5'-CATGTTCTCTGGGAAATCGTG-3', 5'-TTCTGCAAGTGCATCATCG-3'), *Usp18* (5'-CGTGCTTGAGAGGGTCATTTG-3', 5'-GGTCGGGAGTCCACAACTTC-3'). Target gene expression in each sample was first normalized to the expression of housekeeping gene *Hprt*, then to the target gene expression of uninfected samples to calculate $2^{-\Delta\Delta cT}$ relative expression values, as specified in each figure legend.

Multiplex protein assays

Fresh or snap-frozen tissue samples were homogenized in 1 ml of PBS containing protease inhibitor at speed 6000 for 40 s with a MagNA Lyser Instrument (Roche). Multiplexing Laser

Bead assays were performed on undiluted tissue homogenates to detect a 32-plex panel of cytokines and chemokines and a 5-plex panel of matrix metalloproteases (Eve Technologies, Calgary, Canada). LOG2-transformed fold changes of the average protein concentrations in each experimental group over the noninfected wild-type (WT) group were visualized after hierarchical clustering, with average Euclidean distance performed in R using the "gplots" package.

Statistical analysis

Statistical significance for all experiments was assessed using the statistical package in GraphPad Prism, version 6, with tests detailed in each figure legend. Survival curves were compared using a log-rank (Mantel– Cox) test, and one or two-way ANOVA were performed with, respectively, Tukey or Sidak multiple corrections testing between groups. A significant p value cut-off of $p < 0.05$ was used for all tests (*$p < 0.05$, **$p < 0.01$, ***$p < 0.001$, ****$p < 0.001$).

2.4 RESULTS

Identification of a novel ENU-induced Rel mutation in HSV-1 susceptible mice

To discover novel genes and alleles that may underlie HSE risk, chemically mutagenized mice were screened for susceptibility to HSV-1 infection. Briefly, male mice on an HSV-1-resistant B6 background were treated with ENU to induce germline point mutations. In discrete pedigrees, G1 male offspring were crossed with their G2 daughters to generate G3 mice that were homozygous for a single ENU-induced mutation at a predicted frequency of 25% (Fig. 1A). Upon i.p. infection with HSV-1, 26.3% (10 out of 38) of *Coby* pedigree G3 mice succumbed by day 14 p.i., compared with 7.7% of G3 animals issued from all other pedigrees or resistant B6 and B10 controls (Fig. 1B). Furthermore, no sex-specific differences were observed between all 21 female and 17 male *Coby* mice upon infection. Thus, an ENU-induced mutation had likely increased susceptibility to infection in the *Coby* pedigree.

Although suggestive linkage was detected at loci on chromosomes 8 and 11 (data not shown), whole-exome sequencing was performed on genomic DNA isolated from three susceptible G3 animals to identify the mutation underlying the susceptible phenotype. A minimum 10-fold depth was achieved over the entire exome. Within protein-coding genes, 16 homozygous mutations were shared between at least two susceptible animals, of which a single mutation,

Rel^{C307X}, was predicted to be damaging and was located in exon 8 of the *Rel* gene at position 23,644,438 of chromosome 11 (Supplemental Table 1). Two susceptible mice were homozygous and one was heterozygous for this non-sense adenine to thymine transversion mutation, which substituted cysteine for a stop codon at amino acid position 307 of the c-Rel protein (Fig. 1C). Furthermore, additional *Coby* pedigree G3 mice were infected i.p. with HSV-1; Sanger sequencing confirmed that the homozygous *Rel*^{C307X} mutation segregated with a partially penetrant susceptible phenotype (Fig. 1D). Susceptibility did not correlate with other shared homozygous ENU-induced mutations identified by exome sequencing. The potential impact of the mutation on the integrity of the c-Rel protein, a subunit of the NF-κB family of transcription factors that acts downstream of previously discovered HSV-1 susceptibility loci, further supported *Rel*^{C307X} as the most likely candidate ENU-induced homozygous mutation that led to HSV-1 susceptibility.

A truncated c-Rel protein is expressed in both cytoplasmic and nuclear compartments of Rel^{C307X} *cells*

Rel is expressed in both hematopoietic and stromal cells and, as an NF-κB family transcription factor, is implicated in both inflammatory and cell survival pathways (42). In the c-Rel peptide, the mutation mapped to a region immediately C-terminal of the *Rel* homology domain (RHD), a sequence highly conserved among other NF-κB subunits in vertebrates that ensures DNA binding and dimerization and encompasses a nuclear localization signal (Fig. 2A, 2B) (43). However, given that the stop codon occurs before the *Rel* inhibitory domain (RID) and both transactivation domains (TAD1, TAD2), we predicted that a truncated protein encoded by this allele might lose transactivation and inhibitory activity while retaining its ability to bind DNA and to dimerize with other NF-κB subunits.

In tissues including spleen, liver, brain, heart, kidney, lung, and thymus, relative expression of *Rel* mRNA was comparable between *Rel*^{C307X}, *Rel*$^{C307X/+}$, and *Rel*$^{+/+}$ littermate mice, indicating that the mutation did not promote the nonsense–mediated decay of Rel transcripts (Fig. 2C). Given the elevated expression of Rel in spleen hematopoietic cells, c-Rel protein expression was measured in the spleen. Although *Rel*$^{+/+}$ mice produced a full-length c-Rel protein (588 aa) of a predicted 66-kDa molecular mass, only a 35-kDa species was observed in the *Rel*^{C307X} spleen, a size consistent for a 307 aa truncated protein encoded by the mutant allele (Fig. 2D). Furthermore, truncated c-Rel was detected in *Rel*^{C307X} nuclei upon subcellular fractionation, despite the absence

of full-length nuclear c-Rel in $Rel^{+/+}$ splenocytes at steady-state (Fig. 2E). Of note, both c-Rel isoforms were detected in heterozygous $Rel^{C307X/+}$ mice. Together, these data suggest that either a loss-of-function of the full-length c-Rel protein or residual function associated with the constitutive nuclear expression of the truncated C307X c-Rel protein may directly contribute to HSV-1 susceptibility in Rel^{C307X} mice.

Rel^{C307X} confers susceptibility to i.p. and i.n. HSV-1 infection

To confirm that homozygous Rel^{C307X} mice were susceptible to HSV-1 infection, following two backcrosses on the parental B6 background, Rel^{C307X}, $Rel^{C307X/+}$, and $Rel^{+/+}$ littermates were infected i.p. with 1 x 10^4 PFU HSV-1. The same virus strain used in the initial infectious screen, strain 17, was chosen for its high neurotropism (44); doses were titrated as a function of the sensitivity of resistant B6 and susceptible BALB/c control mice and chosen for the best partition between controls (data not shown). Approximately 60% of Rel^{C307X} mice succumbed by day 8 p.i., compared with mostly resistant $Rel^{C307X/+}$ and $Rel^{+/+}$ littermates (Fig. 3A). Using an alternate model of infection to better recapitulate CNS infection and pathogenesis, littermates were challenged i.n. with HSV-1, and over 60% of Rel^{C307X} mice were susceptible by day 10 p.i. (Fig. 3B). Although the mutation had similar penetrance with both inoculation routes, Rel^{C307X} mice succumbed to i.n. infection over a wider period, between days 6 and 9 p.i.

In applying this i.n. model of HSV-1 infection to mouse strains lacking genes encoding factors upstream of NF-κB, $Tlr3^{-/-}$ mice and $Unc93b1^{Letr/Letr}$ mice (35) were only slightly more susceptible than resistant controls, whereas $Myd88^{-/-}$ mice succumbed at a similar level to Rel^{C307X} mice (Fig. 3C). Downstream of TLR3 and other MyD88-dependent TLRs, $Irf3^{-/-}$ mice were partially susceptible, whereas mice lacking MAVS, which is involved in several nucleic acid sensing pathways, including RIG-I, were completely resistant (Fig. 3D). As a result, this i.n. inoculation model of HSV-1 strain 17 infection implicated MyD88, NF-κB, and IRF3 in the protective host response to infection.

To further exclude the potential contribution of other ENU-induced mutations to the HSV-1 susceptibility of Rel^{C307X} mice, we performed an allele complementation test with $Rel^{-/-}$ knockout mice (34) challenged by i.n. infection with 5 x 10^4 PFU/20 g. $Rel^{-/-}$ mice were susceptible to i.n. infection, and the survival of compound heterozygous $Rel^{C307X/-}$ mice was comparable to both $Rel^{-/-}$ and Rel^{C307X} mice (Fig. 3E). Thus, the lack of complementation between the Rel^{C307X} and

Rel$^{-/-}$ phenotypes, both partially penetrant, provided strong evidence to implicate the *Rel* gene and the *Rel*^{C307X} mutation in HSV-1 susceptibility. Furthermore, the lack of allelic complementation suggested that *Rel*^{C307X} is a loss-of-function mutation.

Hematopoietic and tissue-resident cell compartments together mediate HSE susceptibility in Rel^{C307X} *mice*

Although the BBB normally excludes peripheral immune cells from the CNS, both hematopoietic cells and CNS-resident glial or stromal cells are known to have roles in the control of HSV-1 infection and ensuing inflammation. To determine if cell types of hematopoietic and/or nonhematopoietic origin promote HSE susceptibility in *Rel*^{C307X} mice, we performed reciprocal bone marrow transfers into lethally irradiated recipient mice. Engraftment of donor cells was assessed in the blood of recipient hosts at 6 wk post-irradiation (Fig. 4A, Supplemental Fig. 1A, 1B). Upon i.n. HSV-1 challenge at 8 wk postirradiation, chimeras involving the transfer of *Rel*^{C307X} (CD45.2$^+$) cells into *Rel*$^{+/+}$ (CD45.1$^+$ or CD45.1$^+$CD45.2$^+$) hosts ($p = 0.0074$) or *Rel*$^{+/+}$ (CD45.1$^+$ or CD45.1$^+$CD45.2$^+$) bone marrow into *Rel*^{C307X} (CD45.2$^+$) recipients ($p = 0.0010$) were resistant, compared with the susceptible *Rel*^{C307X} into *Rel*^{C307X} control group (Fig. 4B). These data support a model where both hematopoietic and tissue-resident cells expressing the *Rel*^{C307X} mutation contribute together to susceptibility. Alternatively, either compartment might compensate for the other defective *Rel*^{C307X} expressing compartment to resolve the infection and rescue the mouse. Of note, all groups of male chimeric mice were generally more susceptible to infection, and lost more weight, than female groups (Supplemental Fig. 1C, 1D). Collectively, these data indicate that susceptibility to HSE in mice depends on both hematopoietic and CNS-resident cells.

Altered NK cell, CD4$^+$ *T cell, and regulatory T cell responses to HSV-1 infection in Rel*^{C307X} *mice*

Lymphoid and myeloid cells of hematopoietic origin contribute to protective immune responses to HSV-1 infection. Upon their activation via cytokines, NK cells, along with CD4$^+$ and CD8$^+$ T cells, are especially critical to viral clearance in resistant mice (25, 26). CD4$^+$CD25$^+$Foxp3$^+$ regulatory T cells (Tregs) have also emerged as an important cell population involved in the protective response to HSV-1 infection (45, 46). c-Rel itself is directly required for Treg development and function (47) and in promoting IL-2 production to support effector T cell proliferation (34).

To determine the impact of the *Rel*^{C307X} mutation on the immune response, we quantified peripheral hematopoietic cell populations in the spleen at steady-state (day 0), and following HSV-1 infection at the acute stage (days 4 or 5 p.i.), or after resolution (day 14 p.i.). Although there were equivalent numbers of NK, effector CD4$^+$, and CD8$^+$ T cells, and macrophages at steady-state, splenic NK cells were markedly reduced in both numbers and percentages at day 4 p.i. near the height of the infection in *Rel*^{C307X} mice (Fig. 5A, Supplemental Fig. 2A). The mutation did not, however, lead to defects in NK cell maturation (CD11b$^+$CD27$^-$ expression), activation (KLRG1$^+$ expression), or IFN-γ production in response to PMA/ionomycin stimulation (Fig. 5B, 5C). Furthermore, elevated CD4$^+$ T cells were detected both near the peak of the infection and at day 14 in the spleens of surviving *Rel*^{C307X} mutants (Fig. 5D, Supplemental Fig. 2B), whereas *Rel*^{C307X} CD8$^+$ cells were lower in percentage but unchanged in numbers (Fig. 5G, Supplemental Fig. 2C). Although generally increasing in both genotype groups over the course of the infection, there were no significant differences in the level of activation (CD44$^+$CD62L$^-$ or CXCR3$^+$ expression) or IFN-γ production in response to anti-CD3/CD28 or to PMA/ionomycin stimulation in both CD4$^+$ T cells (Fig. 5E, 5F, Supplemental Fig. 2E) and CD8$^+$ T cells (Fig. 5H, 5I, Supplemental Fig. 2F). Numbers and percentages of CD11b$^+$F4/80$^+$MHCII$^+$ macrophages were also unaffected by the mutation (Fig. 5J, Supplemental Fig. 2D).

Furthermore, in keeping with previous reports of *Rel*$^{-/-}$ knockout mice, *Rel*^{C307X} mutant mice had important reductions in splenic CD4$^+$CD25$^+$Foxp3$^+$ Tregs at steady-state and during infection compared with *Rel*$^{+/+}$ mice (Fig. 5K). Yet no differences were observed in the development of double negative, CD4$^+$CD8$^+$ double positive, or single positive CD4$^+$ or CD8$^+$ T cells at steady-state in the thymus (Supplemental Fig. 2G, 2H). Finally, in the blood, the *Rel*^{C307X} CD4$^+$ T cell compartment was augmented at steady-state but also at day 4 p.i., concordant with changes in the spleen (Supplemental Fig. 2I). Blood CD8$^+$ T cells were comparable in *Rel*^{C307X} and *Rel*$^{+/+}$ animals (Supplemental Fig. 2J). As with the spleen, stimulated total blood leukocytes had equal levels of IFN-γ production in *Rel*^{C307X} and *Rel*$^{+/+}$ CD4$^+$ or CD8$^+$ T cells (Supplemental Fig. 2K, 2L). Thus, *Rel*^{C307X} mice responded to HSV-1 infection in the periphery with increased CD4$^+$ T cells and reduced NK cells that otherwise did not differ in their activation, maturity, or capacity to produce IFN-γ. These differences at the cell compartment level, along with a *Rel*^{C307X} -dependent Treg deficit at steady-state and during infection, are indicative of an unbalanced immune response that fails to adequately control viral replication in HSE-susceptible mice.

Intact IFN response and elevated apoptosis ensure intrinsic control of HSV-1 in Rel^{C307X} primary cells

In stromal cells, cell-intrinsic control of viral replication depends on effective cytokine signaling (notably type I IFN) and on the controlled apoptosis of infected cells, which together limit viral spread (48). Studies have implicated c-Rel in *IFNb* gene transcription at steady-state conditions and in the prosurvival responses of neurons subject to cytokine stimulation (49, 50).

To evaluate the role of the *Rel*^{C307X} mutation in cell-intrinsic virus control, both viral titers (Fig. 6A) and viral transcriptional regulator *ICP4* gene expression (Fig. 6B) were measured in primary MEF and BMDM cells infected *ex vivo* with subsaturating doses of HSV-1. Although MEF were more permissive to productive infection, compared with BMDM that mostly controlled and limited infection, viral titers in both *Rel*^{C307X} MEF and *Rel*^{C307X} BMDM were comparable to WT cells. These outcomes in *Rel*^{C307X} cells were further supported by the equivalent expression of *Ifnb* in both groups of infected cells (Fig. 6C). Together, these data indicate that the mutation does not negatively impact cell-intrinsic control of viral replication.

Although the intrinsic antiviral response was effective, a defect in cell survival may have further reduced the pool of *Rel*^{C307X} cells available to the replicating virus. Relative LDH activity was measured as a read-out of membrane integrity and was found to be higher in *Rel*^{C307X} MEF at 36 and 48 h p.i. (Fig. 6D, left panel). In contrast, BMDM could limit membrane damage and LDH release at time points later than 12 h (Fig. 6E, right panel). Additionally, in later stages of the infection (48 h), *Rel*^{C307X} MEF expressed significantly more cleaved caspase-3 compared with *Rel*$^{+/+}$ ($p < 0.01$) (Fig. 6E). Infected MEF were also generally quicker to undergo apoptosis and showed cytotoxic effects as of 36 h p.i. and reduced levels of β-actin housekeeping protein at 48 h p.i. As expected, infected BMDM did not express cleaved caspase-3 (Fig. 6F), indicating that the *Rel*^{C307X} mutation did not impact the general survival of BMDM during later replicating stages of HSV-1 infection. Thus, these *ex vivo* experiments show that cell-intrinsic virus control is maintained in mutant cells but may also implicate elevated caspase-3-dependent apoptosis in the progression of the pathological condition of HSE in the susceptible *Rel*^{C307X} model.

HSV-1 replication in the CNS induces inflammatory, IFN, and prosurvival responses

Upon i.n. infection in mice, HSV-1 first replicates in the nasal epithelium and then spreads either directly to the OB or through the TG to reach the BSC. To understand the kinetics of HSV-1 replication in the susceptible Rel^{C307X} model, we measured viral replication in these tissues at days 1, 3, 5, and 7 after i.n. infection. No productive viral gene expression was detected in OB tissue at these time points (data not shown). In the TG, viral *ICP4* expression was first detected at day 1 p.i., peaking at day 3 in both Rel^{C307X} and $Rel^{+/+}$ mice (Fig. 7A). In the BSC, *ICP4* expression increased through day 5 and remained elevated at day 7, when susceptible Rel^{C307X} had started to show clinical symptoms of HSE (Fig. 7B). As in the TG, there were no statistically significant differences in viral replication between mutant and WT mice. However, in the BSC at day 7, four out of eight Rel^{C307X} mice exhibited higher *ICP4* expression. This increase, observed in 50% of Rel^{C307X} mice, may reflect the susceptibility phenotype (~40% survival) of infected mutant mice. Taken together, these data suggest that viral replication may be higher in moribund Rel^{C307X} BSC than in mutants and WT mice that survive and ultimately clear the virus, in turn hinting at the essential role of virus control in BSC tissues for HSE resistance.

Next, we measured the expression of key genes involved in inflammatory, IFN, and cell death pathways to assess any defects that might compromise viral control mediated by various cell types of the Rel^{C307X} CNS. The expression of *Ccl2*, a signature HSE chemokine gene and proxy for CNS inflammation, increased over time in both groups and peaked by day 5 in the BSC, closely tracking viral replication (Fig. 7C). Further, Rel^{C307X} and $Rel^{+/+}$ mice both mounted a robust type I IFN response over the course of the infection, measured through the expression of *Usp18*, which is strongly induced in the CNS by type I IFN signaling (Fig. 7D). Despite comparable inflammatory and IFN signaling profiles in both groups, a significant decrease in expression of prosurvival genes *Bcl2l1* (Bcl-xL) ($p < 0.01$) and superoxide dismutase *Sod2* ($p < 0.05$) occurred at day 3 p.i. in Rel^{C307X} BSC (Fig. 7E, 7F). This outcome agreed with the elevated apoptosis observed in *ex vivo* HSV-1–infected mutant MEF cells, and when taken together suggest that a failure to upregulate prosurvival genes may be driven by the Rel^{C307X} mutation in the infected CNS.

CNS viral replication drives acute type 1 Th cell–like inflammation and cell death in moribund HSE-susceptible Rel^{C307X} mice

As noted above, four of eight Rel^{C307X} mice distinguished themselves by their poor control of viral replication at day 7 in the BSC. Given the partial penetrance of the susceptible phenotype in Rel^{C307X} animals, we hypothesized that this group included mice that would succumb to infection, whereas others that would ultimately clear the infection. This heterogeneity was reinforced by the varying and sudden onset of disease; susceptible mice normally present with HSE-like symptoms only hours prior to the clinical end point. To better determine if viral replication, inflammation, or both drove susceptibility in Rel^{C307X} mice, we collected infected BSC tissue in moribund Rel^{C307X} and $Rel^{+/+}$ mice at their corresponding clinical end points (from days 6 to 10 p.i.), compared with BSC tissue collected from healthy Rel^{C307X} and $Rel^{+/+}$ mice that survived the infection by day 14 (Fig. 8A). In terms of gene expression, moribund Rel^{C307X} had elevated viral replication (*ICP4* expression), high levels of neuroinflammatory markers (*Ccl2* and *Il6* expression), and increased expression of Mmp8, which was suggestive of damage to the integrity of the BBB (Fig. 8B). Furthermore, viral transcript expression correlated with the expression of *Ccl2* (r^2 = 0.3750), *Il6* (r^2 = 0.4481), and *Mmp8* (r^2 = 0.5396), which tended to increase together in all infected samples (Fig. 8C). However, in moribund Rel^{C307X} mice (n = 9), there was no correlation between viral replication and HSE-signature genes; high *Ccl2*, *Il6*, or *Mmp8* expression coincided with varying levels (between 1 and 3 LOG) of *ICP4* expression in these samples.

In infected BSC collected from age- and sex-matched littermate (Rel^{C307X} and $Rel^{+/+}$) or bone marrow chimeric mice ($Rel^{C307X} > Rel^{C307X}$ and $Rel^{+/+} > Rel^{+/+}$), both CCL2 and IL-6 protein levels were augmented in moribund Rel^{C307X} mice, whereas MMP8, although highly expressed, was at the same level as controls (Fig. 8D). Among 30 detectable proteins, CCL2 and IL-6 were further grouped with other type 1 Th cell (Th1) inflammatory cytokines, including IFN-γ and G-CSF, and with T cell and myeloid cell chemoattractants CXCL9, RANTES, CXCL10, MIP-1β, and eotaxin, all highly expressed in moribund Rel^{C307X} BSC tissue (Fig. 8E). In addition, high cleaved caspase-3 expression was detected in two moribund Rel^{C307X} BSC collected at days 8 and 9 p.i. and further into the cerebrum at day 9 p.i. (Fig. 8F). These findings were further replicated in chimeric animals, where only moribund Rel^{C307X} BSC demonstrated both elevated cell death and high HSV-1 viral titer between days 6 to 8 p.i. (Fig. 8G). Altogether, these data suggest that

replicating virus in the CNS triggered elevated neuroinflammation and cell death in susceptible Rel^{C307X} mice.

To confirm that ineffective viral control only occurred in the moribund subset of mice expressing the Rel^{C307X} mutation, we tested infected TG, BSC, and OB for productive virus load by HSV-1 plaque assay. Between groups of infected animals (n = 15) matched for sex, age, and clinical end point, only moribund Rel^{C307X} mice had elevated virus load in both TG and BSC when compared with healthy Rel^{C307X} and $Rel^{+/+}$ littermates (Fig. 9). No viral replication was detected in the OB tissue of these infected animals. Thus, aberrant c-Rel-dependent responses, in both immune and resident CNS cell types, led to inadequate viral control in CNS tissue, which drove lethal neuroinflammation and cell death characteristic of HSE.

2.5 DISCUSSION

Common as HSV-1 infections are in humans, HSE has a strong genetic component characterized by rare defects in nonredundant innate immune pathways. We screened ENU-mutagenized mice for susceptibility to HSV-1 infection, with the aim of identifying new host genetic etiologies for HSE. In this article, we report a loss-of-function mutation (Rel^{C307X}) in the *Rel* gene that causes HSE-like disease in Rel^{C307X} mice. This mutation led to ineffective viral control, profound neuroinflammation, and increased cell death in the CNS of susceptible mice, phenotypes to which both immune and resident cells may have contributed.

In this study, mice were infected with neurotropic HSV-1 strain 17, and viral replication was localized to the CNS in the i.n. infection model. Viral *ICP4* expression detected in the TG and the BSC supported transport along the axons of the TG, rather than through the OB, as the mechanism of viral entry to the CNS (51, 52). HSV-1 virus titer was especially high in the TG and BSC of moribund Rel^{C307X} mice. Because productive virus was seldom detected in the OB or in the cerebrum, virus was unlikely to have crossed the cribriform plate to invade the CNS in our model, as similarly reported for other HSV-1 strains (53). Thus, although Rel^{C307X} mice were susceptible to both i.p. and i.n. infection routes, we chose to characterize the mutation in the context of i.n. HSV-1 infection to more directly recapitulate CNS viral invasion.

In childhood disease, genetic defects in the TLR3/type I IFN innate response are implicated in the progression of HSV-1 infection to HSE. Our *in vivo* infections of various knockout animals

suggest that i.n. HSV-1 infection triggers both MyD88/NF-κB and IRF3 signaling, with mice lacking *Myd88*, *Rel*, or *Irf3* succumbing to infection. *Tlr3*$^{-/-}$ and *Unc93b1*$^{Letr/Letr}$ mice were mostly resistant, revealing a different aspect of HSE pathogenesis in which TLR3 signaling is less important in the i.n. model of infection.

In the context of viral infection, a first consequence of defects in NF-κB signaling might involve ineffective type I IFN signaling. In both glial and neuronal cells, previous studies have shown that control of infection depends on the TLR3/type I IFN axis (9, 54-56). IFN-β and IFN-λ production is also deficient in fibroblasts derived from HSE-susceptible patients carrying loss-of-function mutations in NF-κB pathway regulator *NEMO* (17). However, *Rel*^{C307X} mice had a normal type I IFN response (*Usp18* expression) over the course of infection in the CNS. Furthermore, the capacity of *Rel*^{C307X} MEF and BMDM to express *Ifnb* and to control HSV-1 viral replication, at least as well as *Rel*$^{+/+}$ cells, indicated that cell-intrinsic antiviral control mechanisms were effective in mutant animals. Thus, as a novel cause of HSE in mice, *Rel* may have an essential role in pathways independent of the TLR3/type I IFN axis.

Rather, defects in *Rel*-dependent pathways, in both CNS-resident cells and in immune cells of hematopoietic origin, led to HSE susceptibility in *Rel*^{C307X} mice. First, regarding non-hematopoietic cells, the mutation drove increased apoptotic cell death in infected *Rel*^{C307X} MEF. Apoptosis is a well-established mechanism of antiviral defense which, especially in a limited culture environment, ensures that dying cells can no longer play host to replicating virus. Yet in the context of CNS infection, active caspase-3-expressing apoptotic neurons and glia are also features of an acute HSE pathological condition (48, 57). c-Rel itself, when overexpressed in neurons, has also been shown to dampen cell death responses, notably by inducing the transcription of antiapoptotic genes *Bcl2l1* and *Sod2* (58-60). In *Rel*^{C307X} mice, we observed lower expression of both *Bcl2l1* and *Sod2* in the BSC early during infection (day 3). By clinical end point, expression in the BSC and cerebrum of cleaved caspase-3 was also detected in two of three moribund *Rel*^{C307X} mice, and in the BSC of moribund *Rel*^{C307X} chimeric mice. Altogether, elevated cell death in *Rel*^{C307X} neuronal or glial cells may directly contribute to decreased survival.

Second, immune cells of hematopoietic origin also contributed to the susceptibility phenotype of *Rel*^{C307X} mice. On one hand, although the mutation did not affect IFN-γ production by NK cells, the observed reduction in mutant NK cells in the spleen during acute infection was responsible, in part, for the insufficient viral clearance in susceptible mice, as reported in other

HSV infection models (26, 61). On the other hand, splenic and circulating $CD4^+$ T cells were significantly augmented in infected Rel^{C307X} mice, which is further indicative of a dysregulated response to infection. More interestingly, with its normal capacity for expression of activation markers and of IFN-γ, this increased $CD4^+$ T cell compartment may directly contribute to the heightened Th1 inflammatory and pathological response in the CNS, and further compromise viral replication control. As measured in the BSC of moribund Rel^{C307X} mice, matrix metalloprotease (Mmp8) and proinflammatory *Il6* and *Ccl2* gene expression were both elevated like in other models of murine viral encephalitis (62-65); cytokine (IFN-γ) and chemokine (CCL2, CXCL9, CXCL10) production was also increased in the Rel^{C307X} CNS. A Th1 inflammatory environment is also known to induce tight junction disruption at the BBB and may promote cellular infiltration (66, 67). Further investigation will reveal if NK and $CD4^+$ T cells are disproportionately infiltrating the CNS of susceptible mice in our model. Finally, Rel^{C307X} mice have low peripheral Treg numbers, both at steady-state and during infection; c-Rel is directly required for the expression of Treg-specific transcription factor Foxp3 (68). Although Tregs have been implicated in protective responses against HSV-1 (45, 69), their role in CNS infection is not fully understood, and further work is required to determine how they counter neuroinflammation and promote viral clearance in the Rel^{C307X} CNS.

Ultimately, the resistance of both bone marrow chimera groups (Rel^{C307X} into $Rel^{+/+}$, $Rel^{+/+}$ into Rel^{C307X}) indicated to us that hematopoietic and CNS-resident cells, together, contributed to the failure of viral control in HSE-susceptible of Rel^{C307X} mice. This finding contrasts with other mouse studies of genetic susceptibility to HSV-1 infection in which major defects constrained to one cellular compartment were enough to cause viral escape, for example in hematopoietic NK or T cells (25, 26) or in CNS-resident cells expressing CX3CR1 (27). Yet despite their many defects, Rel^{C307X} hematopoietic cells were able to maintain sufficient antiviral control in WT irradiated hosts and ensure mouse survival. The converse was also true, in which cell death-prone mutant CNS-resident cells were still able to clear the infection with the contribution of WT immune cells. One interpretation for these resistant outcomes would be that a Rel^{C307X}-dependent defect in an antiviral mechanism in one compartment is superseded or rescued by another antiviral pathway belonging to the WT compartment. Another interpretation would be that Rel acts primarily in a regulatory role, rather than in an effector role, and participates in essential cross-talk between immune and CNS-resident cells to achieve an antiviral state. This interpretation fits the Rel^{C307X}

model well, where a narrow interplay between glial and infiltrating immune cells to produce elevated cytokines, an increase in caspase-3-dependent cell death in CNS cells, and a loss of regulatory activity normally provided by Tregs could together tip the scale toward HSE susceptibility. In other models of infection, whereas c-Rel had no direct incidence on the generation of Ag-specific T effector cells, the regulatory role of c-Rel also emerged as the main contributor to protective host responses (70-72).

In the context of human neuroinflammation, the underlying mechanisms are only partly defined and vary depending on the clinical type of HSE. In acute childhood HSE, most often caused by defects in type I IFN signaling, the active replication of HSV-1 induces neuronal cell death and recruits peripheral leukocytes to inflammatory lesions. In contrast, the role of these infiltrating immune cells is better understood in adult HSE, which may stem from reactivation or primary infection (4). Specifically, the long-term activation of $CD8^+$ cytotoxic T cells and activation of microglia in the CNS, often years after primary viral replication has been cleared, might contribute both to pathological sequelae and to HSV-1 reactivation and relapse (18, 20). For human survivors of HSE, the development of long-term adaptive T cell-mediated responses can even limit the occurrence of mucocutaneous HSV-1 infections in the periphery (73). Nevertheless, there is a second peak of HSE incidence at later time points (5), which cannot be explained by type I IFN-dependent innate immunity. Importantly, HSV-1 infectious screens of ENU-mutagenized mice have since revealed gene defects independent of type I IFN, first in CD45 (*Ptprc* gene) (25) and now in c-Rel. Thus, i.n. HSV-1 infection in mice appears to better address the importance of hematopoietic responses, implicated in cases of relapsing or primary HSE in older adults, rather than provide a model of innate immune-dependent childhood disease.

In summary, this study highlights the role of *Rel* in HSE susceptibility and reinforces the importance of these pathways in neuroinflammation. *REL* has been identified in several genome-wide association studies for human inflammatory diseases, including inflammatory bowel disease, and psoriatic and rheumatoid arthritis (74-76), and in a larger meta-analysis for multiple sclerosis (77). Further investigations to identify possible *REL* mutations or polymorphisms occurring in HSE and other viral encephalitis patients, and particularly in the older adult population, would help to establish a broader regulatory role for *REL* in host defense.

2.6 ACKNOWLEDGMENTS

We thank Patricia D'Arcy, Geneviève Perreault, Leigh Piercey-Brunet, Cynthia Villeda-Herrera, and Vanessa Guay for expert technical assistance. We are grateful to Dr. Philippe Gros for kindly providing *Irf3*$^{-/-}$ and *Mavs*$^{-/-}$ mice. We thank the following core facilities: the Life Science Complex Cell Vision Core Facility for flow cytometry (McGill University), the Comparative Medicine and Animal Resources Centre (McGill University), the Centre for Phenogenomics, TCP Infection and Inflammation Core, and the Next-Generation Sequencing Facility at the Centre for Applied Genomics (SickKids, Toronto). We also acknowledge the Canadian Centre for Computational Genomic Innovation Network, supported by the Canadian Government through Genome Canada.

This work was supported by funds from the Fonds de Recherche du Québec-Santé (to M.M.). G.C. was supported by the Canadian Institutes for Health Research. S.M.V. was supported by the Canada Research Chair Program. This project was conducted with the support of Canadian Institutes for Health Research Grants CTP-87520 and MOP-238757. The authors have no financial conflicts of interest.

2.7 FIGURES AND LEGENDS

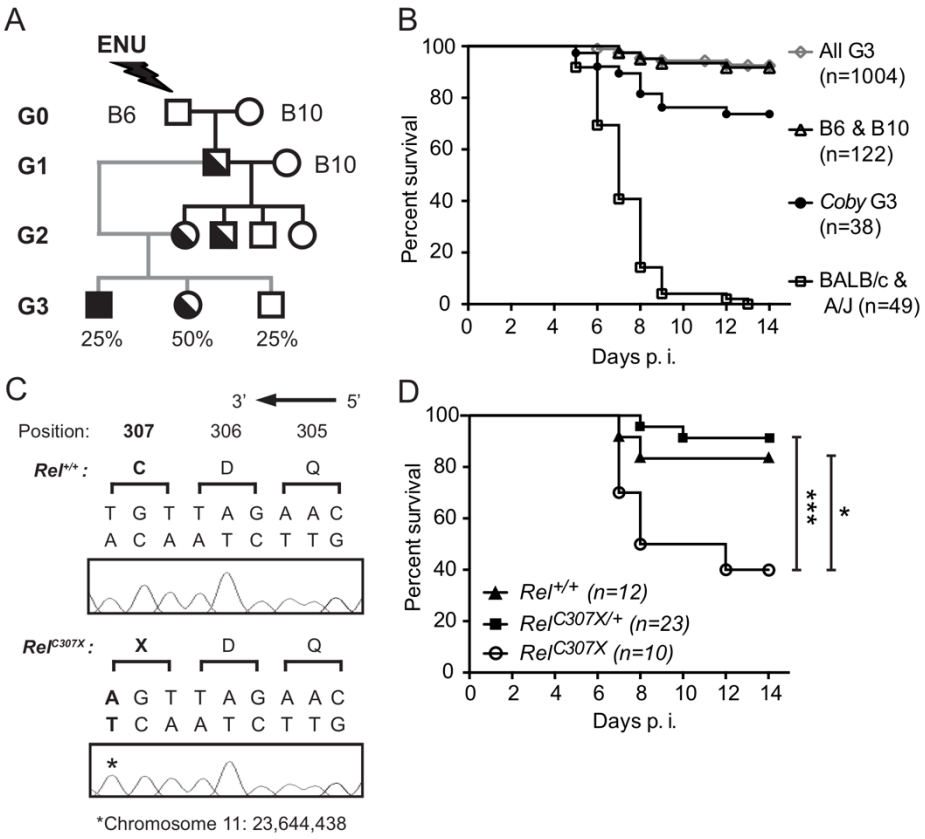

FIGURE 1. HSV-1–susceptible mice carry an ENU-induced mutation in Rel.

(A) Breeding scheme detailing the generation of homozygous ENU mutations. G3 *Coby* pedigree animals were generated by backcrossing two G2 females to their G1 father (*Coby*). (B) Survival of *Coby* G3 offspring (from either G2a or G2b mothers) compared with all G3 pedigree animals, resistant B6, and susceptible A/J controls following i.p. infection with 1 x 10^4 PFU HSV-1 per mouse. (C) Whole-exome sequencing revealed that three susceptible mice carried an adenine to thymine transversion mutation in exon 8 of *Rel*, at position 23,644,438 of chromosome 11, which introduced a cysteine to stop codon mutation at amino acid position 307. (D) Coby G3 offspring (from both G2 mothers, $n = 45$) were genotyped for the Rel^{C307X} mutation by Sanger sequencing and infected i.p. with 1 x 10^4 PFU HSV-1 per mouse. Statistical tests: (D) log-rank (Mantel–Cox) tests. *$p < 0.05$, ***$p < 0.001$.

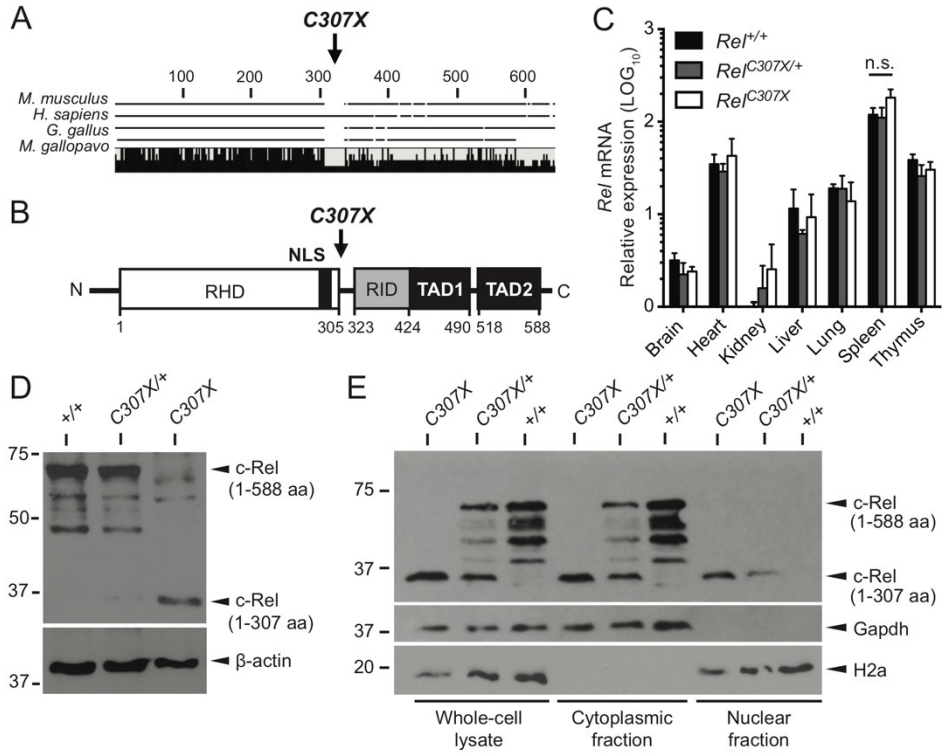

FIGURE 2. Rel^{C307X} mice express a truncated c-Rel protein.

(A) In the c-Rel peptide sequence, the *Rel*^{C307X} mutation is positioned immediately downstream of a highly conserved region among vertebrate species, corresponding to the RHD. (B) Within the c-Rel protein, the *Rel*^{C307X} mutation is located between the N-terminal RHD and nuclear localization signal (NLS), and the C-terminal *Rel* inhibitory domain (RID) and transactivation domains (TAD1, TAD2). (C) Relative expression of *Rel* mRNA was measured in *Rel*^{C307X} and littermate tissues and normalized to *Hprt* expression and to *Rel*$^{+/+}$ kidney tissue, with $n = 3$ mice per group. (D) Whole-cell lysate from spleen tissue was probed for c-Rel by Western blot. Expression of β-actin served as a protein loading control. Protein sizes are indicated on the left in kilodaltons and on the right in amino acid (aa) length. (E) Whole-cell, cytoplasmic, and nuclear lysates from fractionated total splenocytes were probed for c-Rel by Western blot. Expression of Gapdh and H2A served as both protein loading and fractionation controls. Data represent mean ± SD. Statistical tests: (C) one-way ANOVA with Tukey multiple comparison test for spleen samples. n.s., nonsignificant.

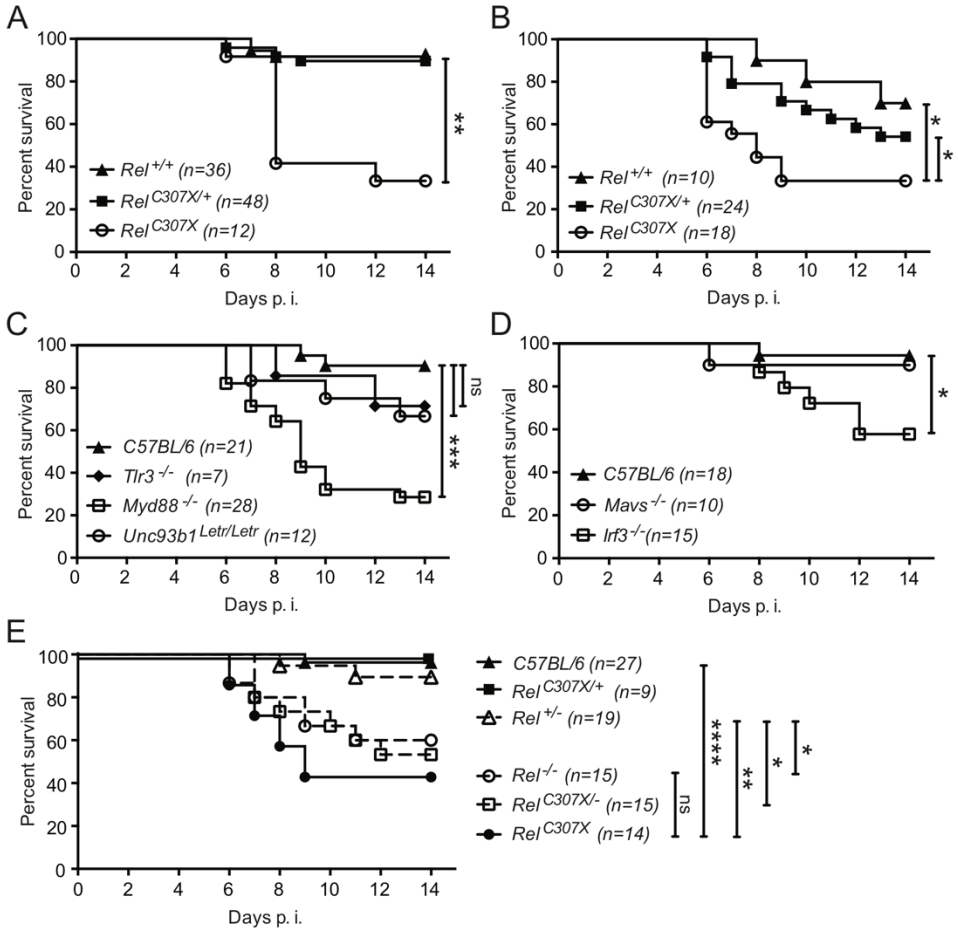

FIGURE 3. Rel^{C307X} mice are susceptible to both i.p. and i.n. models of infection.

Rel^{C307X}, *Rel$^{C307X/+}$* , and *Rel$^{+/+}$* littermates were infected (A) i.p. with 1 x 10^4 PFU HSV-1 and (B) i.n. with 1 x 10^5 PFU/ 20 g HSV-1 and monitored for 2 wk for survival and presentation of clinical HSE-like symptoms. (C) *Tlr3$^{-/-}$*, *Myd88$^{-/-}$*, *Unc93b1$^{Letr/Letr}$*, and B6 mice and (D) *Mavs$^{-/-}$*, *Irf3$^{-/-}$*, and B6 mice were infected i.n. between 1 x 10^4 PFU/20 g and 1 x 10^5 PFU/20 g HSV-1. (E) *Rel^{C307X}*, *Rel$^{C307X/+}$* , and *Rel$^{+/+}$* littermates, along with *Rel$^{-/-}$* knockout mice and compound heterozygotes *Rel$^{C307X/-}$* and *Rel$^{+/-}$*, were infected i.n. with 5 x 10^4 PFU/20 g HSV-1 and monitored for 2 wk. Statistical tests: log-rank (Mantel– Cox) tests. *$p < 0.05$, **$p < 0.01$, ***$p < 0.001$, ****$p < 0.0001$. ns, nonsignificant.

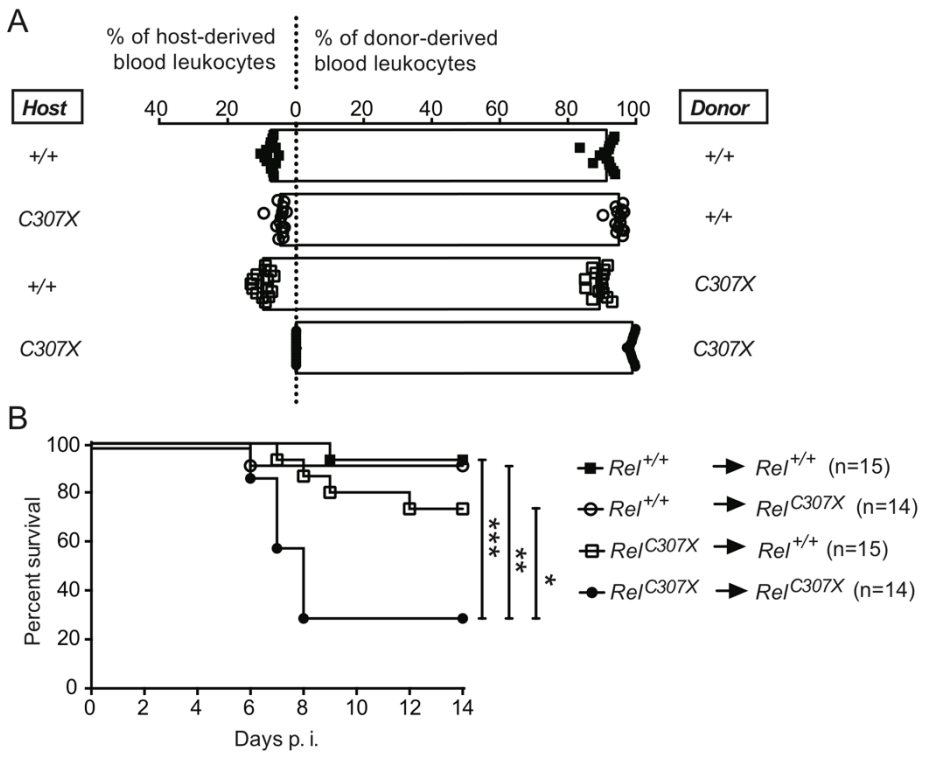

FIGURE 4. HSV-1 susceptibility depends on both hematopoietic and nonhematopoietic Rel^{C307X} cellular compartments.

(A) Reciprocal bone marrow transfers between sex- and age-matched Rel^{C307X} and $Rel^{+/+}$ were performed in lethally irradiated mice. Proportions of donor and host blood leukocytes were measured by flow cytometry in chimeric animals at 6 wk post-irradiation using congenic CD45.1 and CD45.2 markers. (B) At 8 wk postirradiation, chimeric animals were infected i.n. with 5 x 10^4 PFU/20 g HSV-1. Both Rel^{C307X} into $Rel^{+/+}$ and $Rel^{+/+}$ into Rel^{C307X} groups were resistant to infection compared with the susceptible Rel^{C307X} into Rel^{C307X} control group. Data represent mean ± SD. Statistical tests: (B) log-rank (Mantel–Cox) test. $^{**}p < 0.01$, $^{***}p < 0.001$.

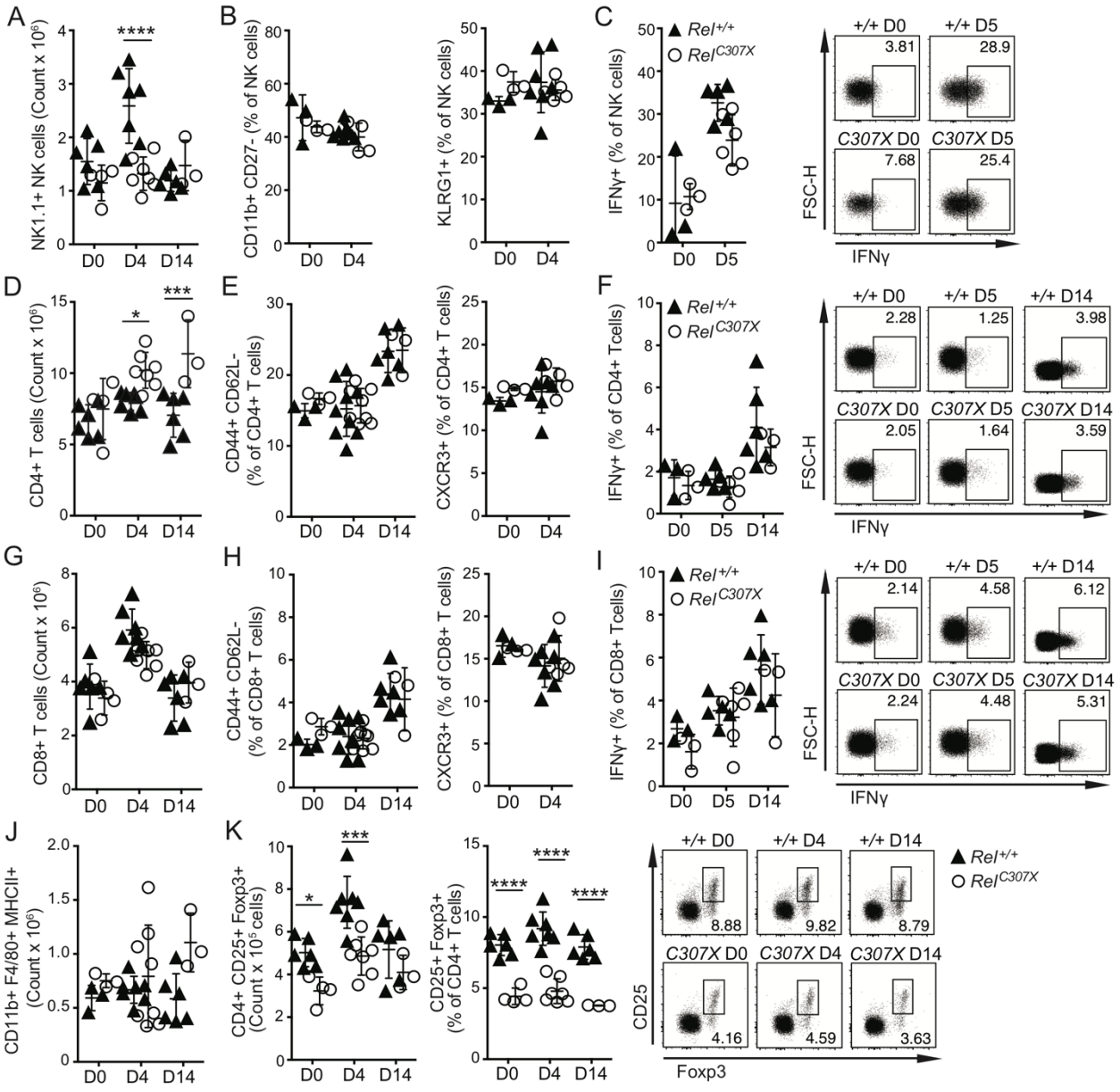

FIGURE 5. Rel^{C307X}-specific defects in splenic NK and T cell populations following HSV-1 infection.

FIGURE 5. Rel^{C307X}-specific defects in splenic NK and T cell populations following HSV-1 infection.

Rel^{C307X} and $Rel^{+/+}$ mice were infected i.n. with 5 x 10^4 PFU/20 g HSV-1. Whole splenocytes were isolated from noninfected (day [D] 0) and infected mice at D4 and D14 cells ($n \geq 3$ per group), and cell populations were identified by flow cytometry. Whole splenocytes isolated from D0-, D5-, and D14-infected mice were stimulated *ex vivo*, and IFN-γ production was measured by flow cytometry. (A) Splenic $NK1.1^+$ NK cells were measured in total cell number. (B) Mature $CD11b^+CD27^-$ and activated $KLRG1^+$ NK cells and (C) PMA/ionomycin–stimulated IFN-γ^+ NK cells are shown as a percentage of total NK cells. (D) Splenic $CD4^+$ and (G) $CD8^+$ T cells were measured in total cell number. (E and H) Activated $CD44^+CD62L^-$ and $CXCR3^+$ T cells and (F and I) anti-CD3/CD28– stimulated IFN-γ^+ T cells are shown as a percentage of total $CD4^+$ or $CD8^+$ T cells. (J) Splenic $CD11b^+F4/80^+MHCII^+$ macrophages were measured in total cell number. (K) Splenic $CD3^+CD4^+CD25^+Foxp3^+$ Tregs were quantified in cell number and in percentage of splenic $CD4^+$ T cells. Data represent mean ± SD. Representative flow cytometry plots show IFN-γ^+ populations as percentages of parent NK, $CD4^+$, or $CD8^+$ T cells and show $CD25^+Foxp3^+$ populations as a percentage of parent $CD4^+$ T cells. Statistical tests: two-way ANOVA with Sidak multiple correction test. *$p < 0.05$, ***$p < 0.001$, ****$p < 0.0001$.

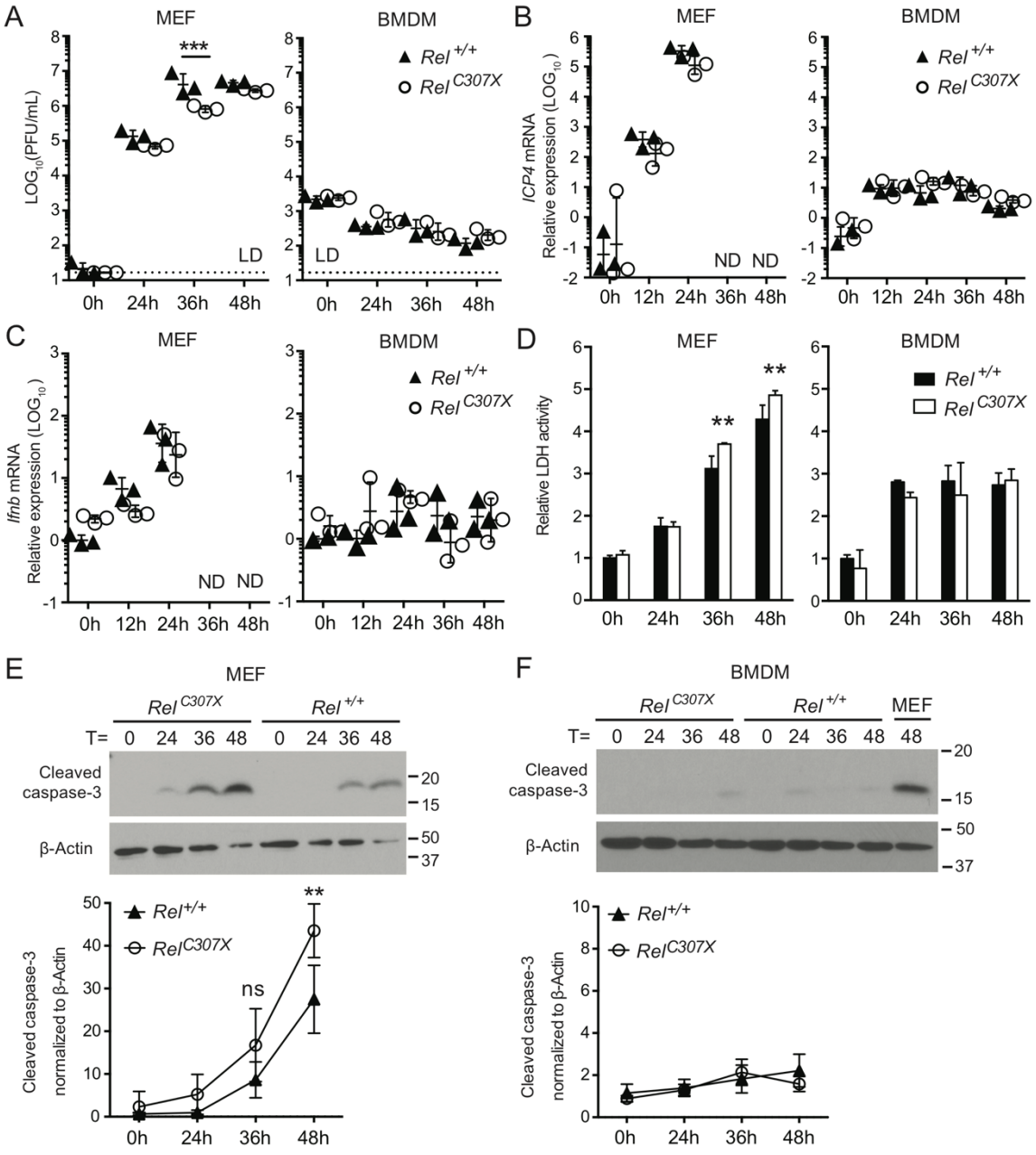

FIGURE 6. Intrinsic viral control and elevated apoptosis in HSV-1–infected Rel^{C307X} primary cells.

FIGURE 6. Intrinsic viral control and elevated apoptosis in HSV-1–infected Rel^{C307X} primary cells.

MEF cells and BMDM cells were cultured from Rel^{C307X} and $Rel^{+/+}$ mice (n = 3 independent embryos/mice per genotype), and infected *ex vivo* with HSV-1 at subsaturating doses (MOI = 0.01 for MEF, MOI = 0.1 for BMDM). (A) Total viral titer (both secreted and cell-associated virus) was quantified in PFU/ml of cell homogenate by plaque assay. Expression of (B) viral *ICP4* mRNA and (C) *Ifnb* mRNA were measured and normalized to cell *Hprt* mRNA expression. *ICP4* expression in MEF cells at 36 and 48 h p.i. was not determined (ND) because of low RNA yield and undetectable *Hprt* expression. (D) LDH activity relative to $Rel^{+/+}$ cells at 0 h was measured in infected cell supernatants. (E) MEF and (F) BMDM whole-cell protein lysates were probed for expression of cleaved caspase-3 by Western blot. Protein sizes are indicated in kilodaltons. A protein lysate from Rel^{C307X} MEF at 48 h p.i. was included in (F) as a positive control for cleaved caspase-3 protein expression. Representative blots are shown for one mouse out of three tested per genotype, with cleaved caspase-3 protein quantification for n = 3 experiments normalized to β-actin protein loading control. Data represent mean ± SD. Statistical tests: two-way ANOVA with Sidak multiple correction test. $^{**}p < 0.01$, $^{***}p < 0.001$. LD, limit of detection of viral PFU.

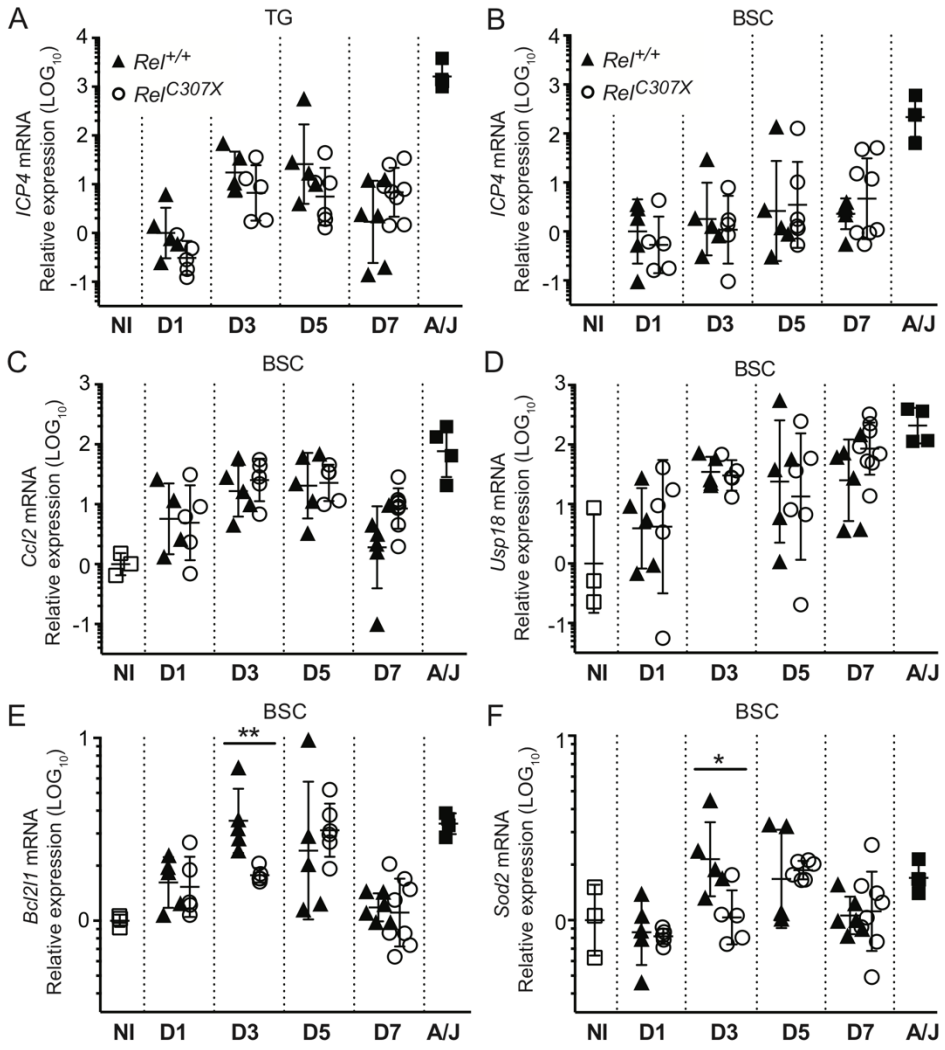

FIGURE 7. HSV-1 infection kinetics in CNS tissue.

TG and BSC tissues were collected from *Rel*^{C307X} and *Rel*$^{+/+}$ mice infected i.n. with 5 x 10^4 PFU/20 g HSV-1 at days 1, 3, 5, and 7 p.i. (n = 3–8 per group). Corresponding tissues from infected A/J mice at day 5 p.i. were included as positive controls for the infection, and noninfected (NI) *Rel*$^{+/+}$ mice were included as negative controls. *ICP4* viral mRNA expression was measured in (A) TG and (B) BSC relative to host *Hprt* mRNA expression. (C) *Ccl2*, (D) *Usp18*, (E) *Bcl2l1*, and (F) *Sod2* mRNA expression was measured in BSC and normalized to *Hprt* expression and *Rel*$^{+/+}$ NI controls. Data represent mean ± SD. Statistical tests: two-way ANOVA with Sidak multiple correction test. *$p < 0.05$, **$p < 0.01$.

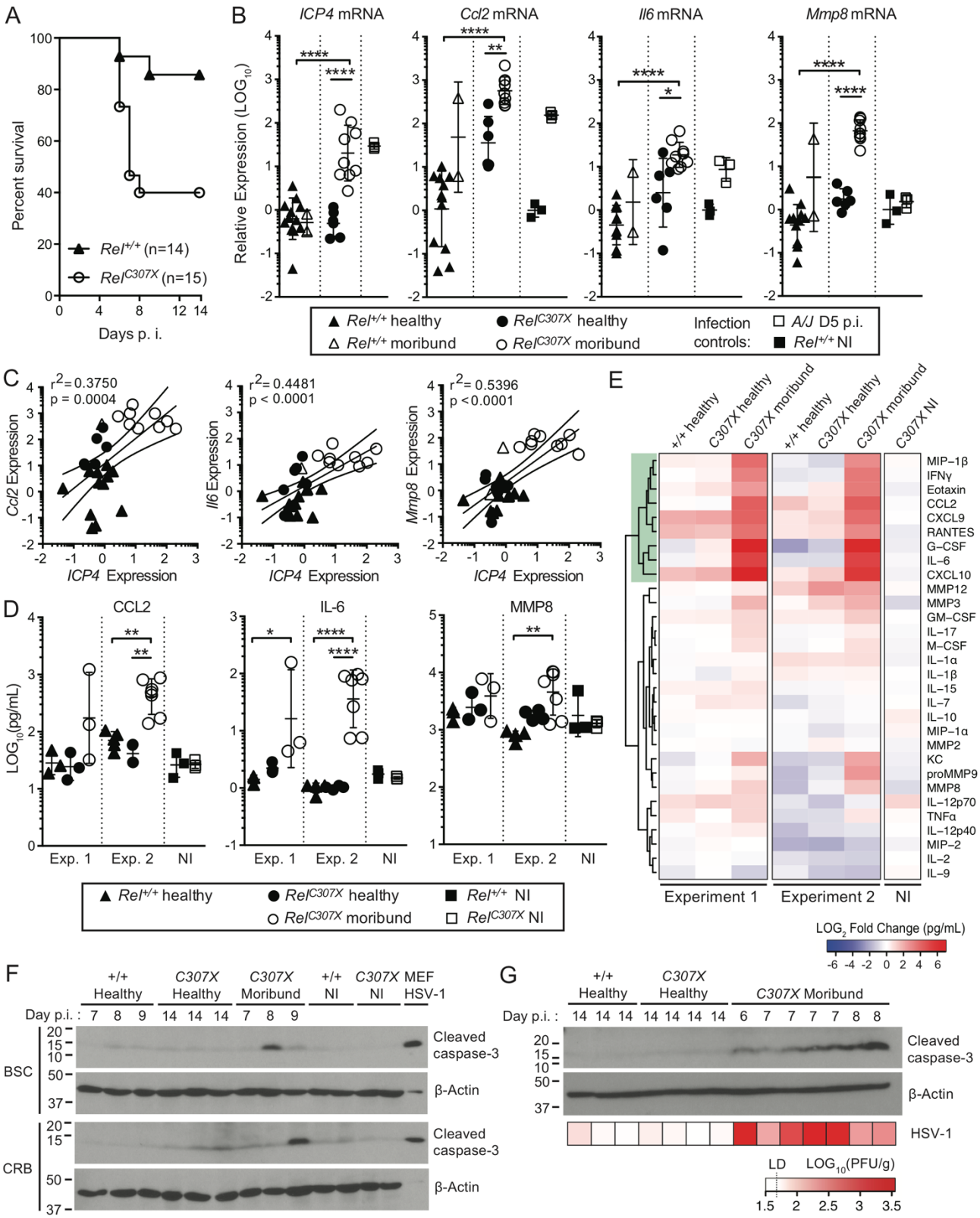

FIGURE 8. Elevated neuroinflammation and cell death in the CNS of moribund HSV-1 infected Rel^{C307X} mice.

FIGURE 8. Elevated neuroinflammation and cell death in the CNS of moribund HSV-1 infected Rel^{C307X} mice.

(A) Rel^{C307X} and $Rel^{+/+}$ mice were infected i.n. with 5 x 10^4 PFU/20 g HSV-1, with 8 of 15 Rel^{C307X} mice reaching clinical end point between days 6 to 8 p.i. and 2 of 14 $Rel^{+/+}$ mice reaching end point at days 6 and 9 p.i. (B) *ICP4*, *Ccl2*, *Il6*, and *Mmp8* mRNA expression was measured in BSC collected from moribund mice at clinical end point or from healthy mice at day 14. Infected A/J mice at day 5 p.i. and noninfected (NI) $Rel^{+/+}$ mice were included as positive and negative controls for the response to infection. (C) Regression analysis showing *Ccl2*, *Il6*, and *Mmp8* expression each relative to *ICP4* viral mRNA expression. (D) Littermate Rel^{C307X} and $Rel^{+/+}$ mice (Experiment 1), and bone marrow chimeric Rel^{C307X}. Rel^{C307X} and $Rel^{+/+}$. $Rel^{+/+}$ mice (Experiment 2), were infected i.n. with 5 x 10^4 PFU/20 g HSV-1. BSC tissue was collected from moribund Rel^{C307X} mice (end points on days 6, 7, 8, or 9 p.i.), healthy Rel^{C307X} and $Rel^{+/+}$ mice (end points on days 7, 8, 9, or 14 p.i.), and from NI littermate controls (n = 3 per group, age and sex matched). CCL2, IL-6, and MMP8 protein expression was measured in BSC tissue homogenates. (E) The expression of 30 detectable proteins in BSC tissue homogenates is represented as the fold change of the average expression of each group over that of NI $Rel^{+/+}$ mice. Cytokines and chemokines highlighted in the green cluster were most highly expressed in moribund Rel^{C307X} mice. (F) BSC and cerebrum (CRB) tissue homogenates from littermates in Experiment 1 were probed for cleaved caspase-3 protein expression. A protein lysate from Rel^{C307X} MEF at 48 h p.i. (MEF HSV-1) was included as a positive control. (G) Cleaved caspase-3 expression, and viral titer in LOG10(PFU/g), was quantified in BSC tissue homogenates from chimeric mice from Experiment 2. Protein sizes are indicated in kilodaltons. Data represent mean ± SD, and error bars in (C) represent mean with 95% confidence intervals. Statistical tests: (B and D) one-way ANOVA with Tukey multiple correction test. *$p < 0.05$, **$p < 0.01$, ****$p < 0.0001$. LD, limit of detection of viral PFU.

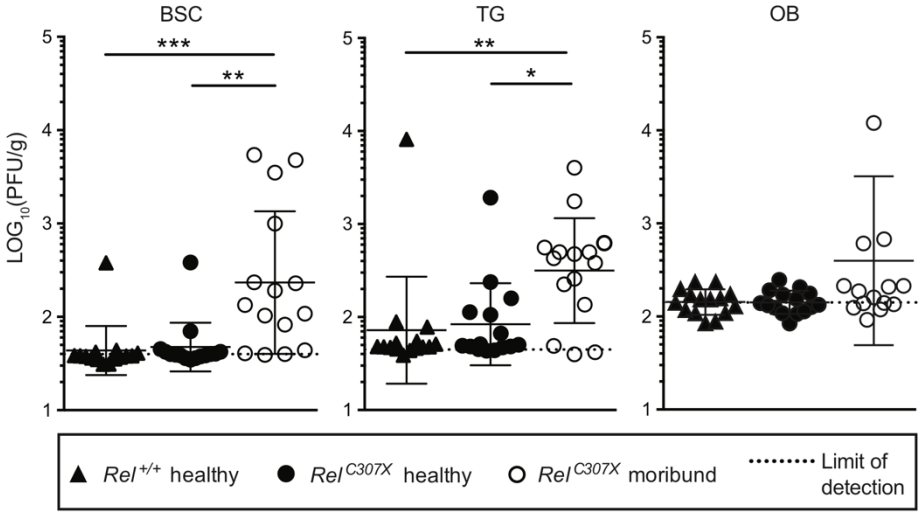

FIGURE 9. Moribund HSV-1 infected Rel^{C307X} mice have elevated viral load in the CNS.
Viral load was quantified by plaque assay in TG, BSC, and OB collected from mice infected i.n. with 5 x 10^4 PFU/20 g. Forty-five mice were infected and monitored for presentation of clinical HSE-like symptoms. Moribund *Rel*^{C307X} mice were paired at clinical end points with sex- and age-matched healthy *Rel*^{C307X} and healthy *Rel*$^{+/+}$ mice ($n = 15$ per group). The limit of detection denotes the viral titer corresponding to a single detectable PFU at the lowest sample dilution. Data represent mean ± SD. Statistical tests: one-way ANOVA with Tukey multiple correction test. *$p < 0.05$, **$p < 0.01$, ***$p < 0.001$.

2.8 SUPPLEMENTAL MATERIALS

SUPPLEMENTAL TABLE 1. Shared ENU-induced homozygous mutations in Coby pedigree mice.

Chromosome	Position	Gene	Codon change	Amino acid change	Mean coverage	V ariant allele frequency (%)			Impact	Effect
						#1	#2	#3		
11	23644438	*Rel*	tgT/tgA	C307X	153	100.0	38.8	100.0	High	Stop Gained
11	54723096	*Gpx3*	aAc/aTc	N206I	151	100.0	45.3	100.0	Moderate	Non-Synonymous Coding
17	34378129	*H2-Ob*	Cgc/Tgc	R19C	110	100.0	100.0	100.0	Moderate	Non-Synonymous Coding
18	20752738	*Dsg2*	Ggg/Agg	G614R	97	100.0	98.7	51.5	Moderate	Non-Synonymous Coding
18	22675566	*Asxl3*	Tcc/Ccc	S704P	167	99.4	100.0	47.1	Moderate	Non-Synonymous Coding
18	37495032	*Pcdhb6*	Acc/Tcc	T451S	804	99.9	100.0	50.1	Moderate	Non-Synonymous Coding
8	49075435	*Wwc2*	aTc/aAc	I39N	88	100.0	43.6	100.0	Moderate	Non-Synonymous Coding
8	64512226	*Ddx60*	Tac/Aac	Y1625N	106	100.0	100.0	100.0	Moderate	Non-Synonymous Coding
9	3001116	*Gm10722*	tTg/tCg	L64S	29	69.2	60.7	81.5	Moderate	Non-Synonymous Coding
9	3037857	*Gm10715*	cCt/cAt	P170H	13	90.0	100.0	100.0	Moderate	Non-Synonymous Coding
12	77026673	*Syne2*	ccA/ccG	P1065	95	100.0	45.6	100.0	Low	Synonymous Coding
17	26230600	*Nme4*	ccC/ccT	P133	89	42.7	97.3	100.0	Low	Synonymous Coding
17	29663445	*Tmem217*	taT/taC	Y85	179	100.0	100.0	100.0	Low	Synonymous Coding
18	35744403	*Matr3*	ggT/ggC	G671	41	100.0	100.0	54.9	Low	Synonymous Coding
9	3037858	*Gm10715*	ccT/ccC	P170	15	70.0	70.6	81.8	Low	Synonymous Coding
9	3038271	*Gm10715*	gtT/gtC	V210	16	100.0	85.7	90.9	Low	Synonymous Coding

Whole-exome sequencing of genomic DNA isolated from 3 HSV-1 susceptible mice (labeled #1, #2 and #3 above) was performed. The 16 variants described above were identified at a minimum coverage of 10 in all 3 samples, and were homozygous in at least 2 out of 3 mice. A variant with an alternate allele frequency above 70% was considered as homozygous for that sample.

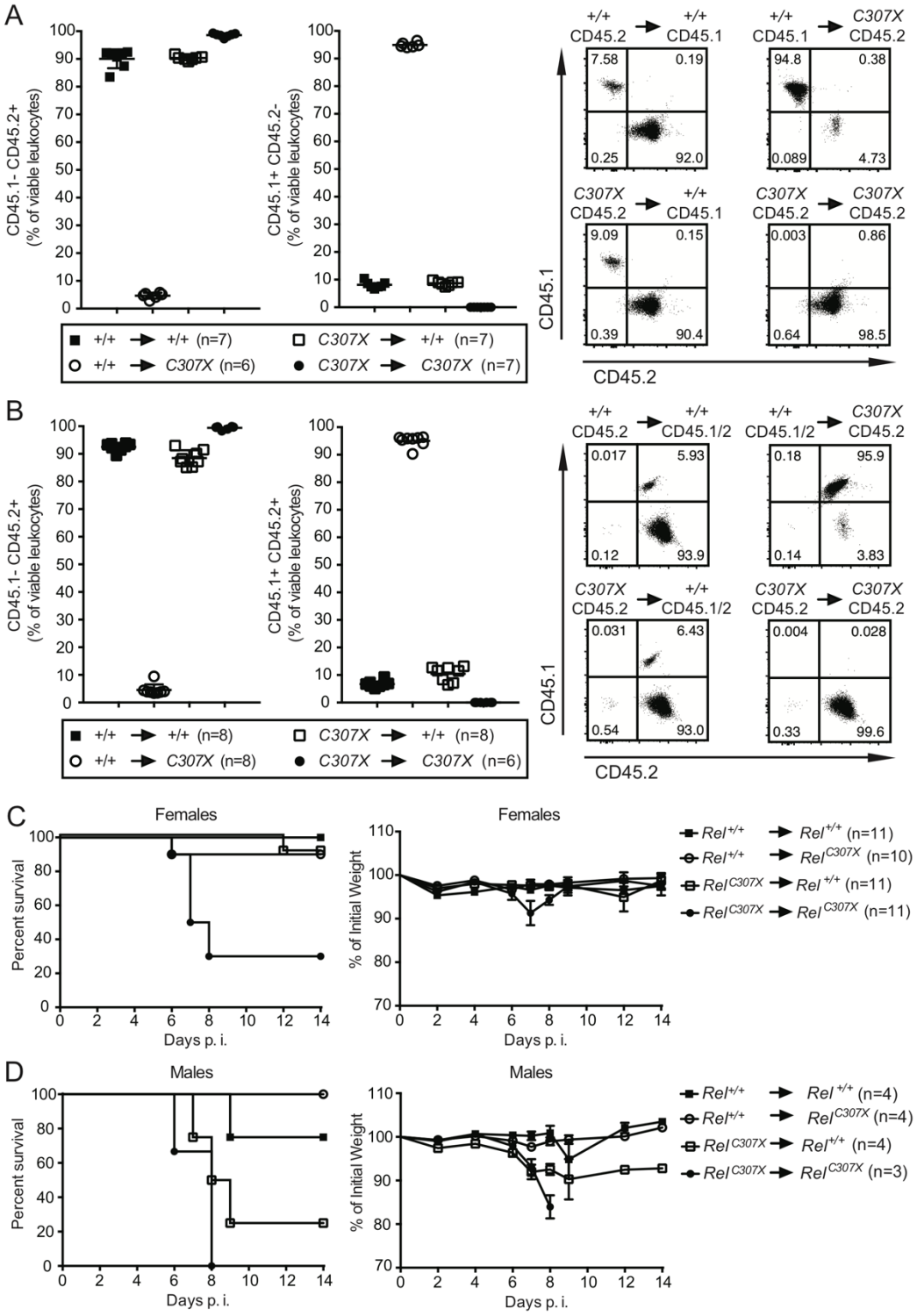

SUPPLEMENTAL FIGURE 1. Engraftment of donor cells and response to i.n. HSV-1 infection by sex in bone marrow chimera mice.

SUPPLEMENTAL FIGURE 1. Engraftment of donor cells and response to i.n. HSV-1 infection by sex in bone marrow chimera mice.

(A) Proportions of donor cells ($CD45.2^+$ into $CD45.1^+$ recipients) and of $CD45.1^+$ into $CD45.2^+$ recipients across chimeric animal groups, in percentages of total blood leukocytes at 6 weeks post-irradiation and transfer. (B) Proportions of donor cells ($CD45.2^+$ into $CD45.1^+CD45.2^+$ recipients) and of $CD45.1^+CD45.2^+$ into $CD45.2^+$ recipients across chimeric animal groups, in percentages of total blood leukocytes at 6 weeks post-irradiation and transfer. Survival and weight loss, expressed in percentage of initial pre-infection weight, were plotted for (C) female and (D) male chimeric mice issued from the i.n. HSV-1 infection of lethally- irradiated and reciprocal bone marrow transfer described in Fig 4. Data represents mean ± SD. Weight curves represent mean ± SEM.

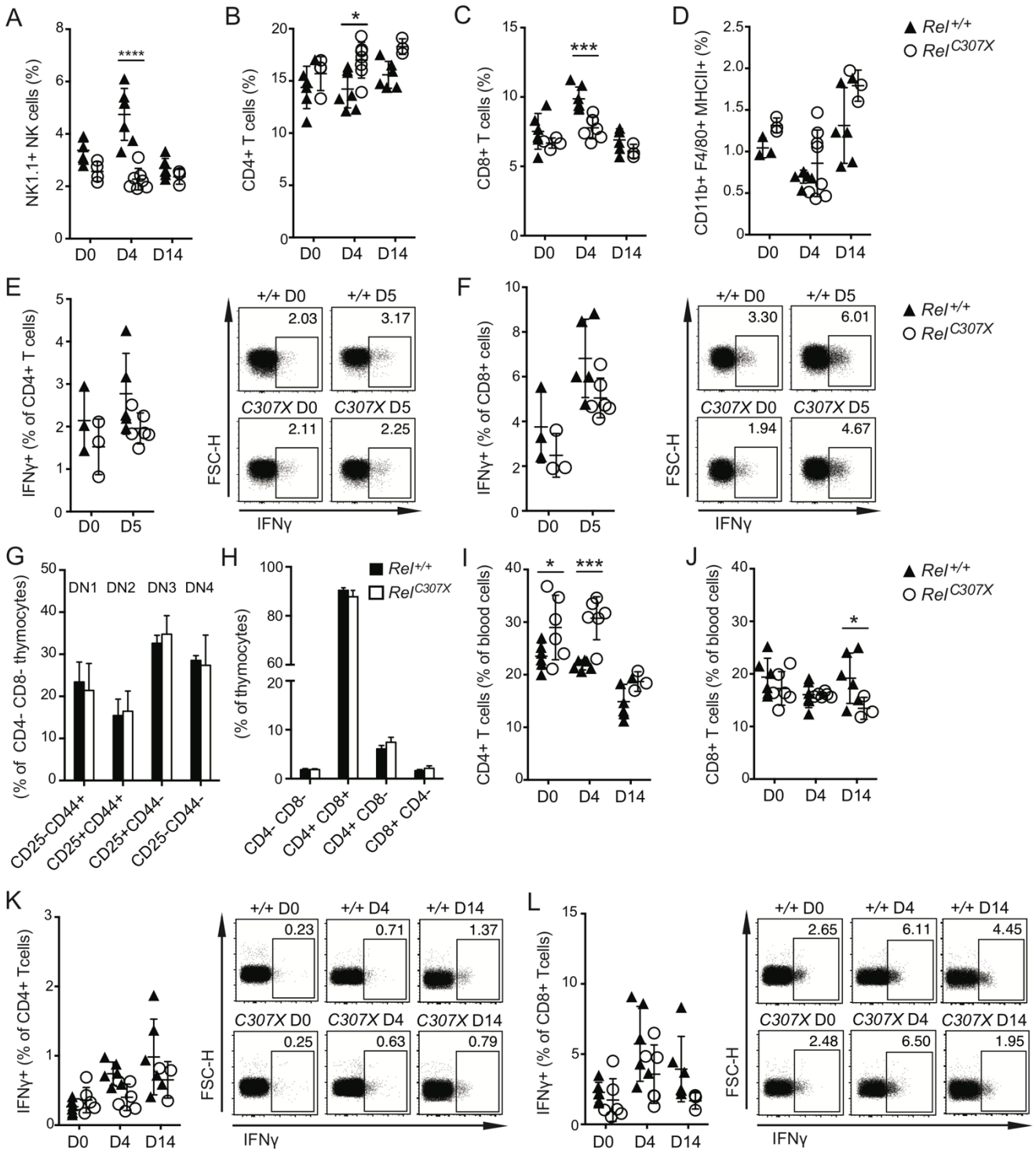

SUPPLEMENTAL FIGURE 2. Splenic, thymic and blood immune cell dynamics in Rel^{C307X} mice.

SUPPLEMENTAL FIGURE 2. Splenic, thymic and blood immune cell dynamics in Rel^{C307X} mice. Whole splenocytes were isolated from non-infected (D0) mice, and from mice infected i.n. with $5x10^4$ PFU/20g HSV-1 at D4 and D14 ($n \geq 3$ per group of Rel^{C307X} or $Rel^{+/+}$ mice). (A) $NK1.1^+$ NK cells, (B) $CD4^+$ T cells, (C) $CD8^+$ T cells, and (D) $CD11b^+F4/80^+MHCII^+$ macrophages are each shown as a percentage of total viable cells in the spleen. Whole splenocytes isolated from D0, D5 and D14 infected mice were stimulated *ex vivo* with PMA/ionomycin, and IFNγ production is shown as (E) a percentage of total $CD4^+$ T cells, and (F) a percentage of total $CD8^+$ T cells. Whole thymocytes were isolated from non-infected Rel^{C307X} and $Rel^{+/+}$ mice (n=3 per group). (G) Double negative thymocyte stages 1 through 4 (DN1, DN2, DN3, DN4) are shown as percentages of total $CD4^-CD8^-$ double negative thymocytes. (H) Double negative $CD4^-CD8^-$, double positive $CD4^+CD8^+$, and single positive $CD4^+$ or $CD8^+$ thymocytes are shown as percentages of total thymocytes. Rel^{C307X} and $Rel^{+/+}$ mice were infected i.n. with $5x10^4$ PFU/20g HSV-1, and blood was collected at D0, D4 and D14 post-infection (n=3 surviving Rel^{C307X} at D14, and n=6 for all other group). Blood leukocytes were stimulated *ex vivo* with anti-CD3/CD28 monoclonal antibodies. (I) $CD4^+$ and (J) $CD8^+$ T cell populations were measured in percentages of total viable leukocytes in the blood, and IFN-γ production is shown as (K) a percentage of total $CD4^+$ T cells, and (L) a percentage of total $CD8^+$ T cells. Data represents mean ±SD. Representative flow cytometry plots show IFN-γ^+ populations as percentages of parent $CD4^+$ or $CD8^+$ T cells. Statistical tests: Two-way ANOVA with Sidak's multiple correction test. *$p < 0.05$, ***$p < 0.001$, ****$p < 0.0001$.

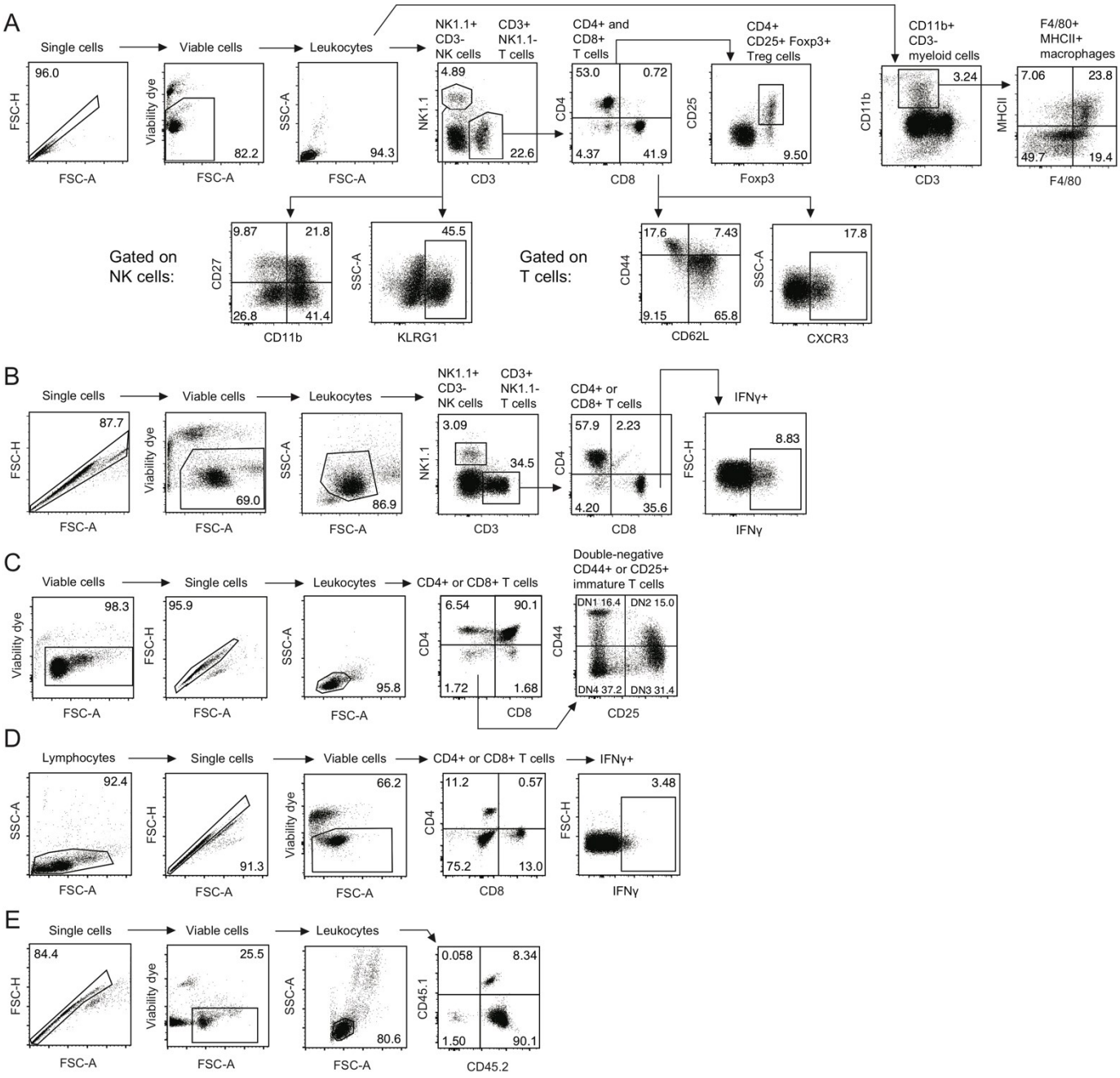

SUPPLEMENTAL FIGURE 3. Gating strategies for flow cytometry.

SUPPLEMENTAL FIGURE 3. Gating strategies for flow cytometry.

(A) Gating of whole splenocytes to identify viable NK1.1^{+}CD3^{-} NK cells, CD4^{+} and CD8^{+} T cells, CD4^{+}CD25^{+}Foxp3^{+} Tregs and CD11b^{+}F4/80^{+}MHCII^{+} macrophages. Additional markers for NK cells (bottom-left panels) indicate maturation (from least mature to most mature, CD11b^{-}CD27^{-}, CD11b^{-}CD27^{+}, CD27^{+}CD11b^{+}, CD27^{-}CD11b^{+}) and activation (KLRG1^{+}), and additional markers for T cells (bottom right panels) indicate activation (CD44^{+}CD62L^{-}, and CXCR3^{+}). (B) Gating of PMA/ionomycin *ex vivo* stimulated splenocytes. IFN-γ^{+} cells gated on CD8^{+} T cells are shown as an example in the right-most panel. (C) Gating of whole thymocytes to identify double negative CD4^{-}CD8^{-}, double positive CD4^{+}CD8^{+}, and single positive CD4^{+} or CD8^{+} thymocytes. Comparing CD44 and CD25 expression, all four stages of double negative thymocytes (DN1, DN2, DN3, DN4) are shown in the right-most panel. (D) Gating of anti-CD3/CD28 *ex vivo* stimulated whole blood leukocytes to identify CD4^{+} and CD8^{+} T cells. IFN-γ^{+} cells gated on CD8^{+} T cells are shown as an example in the right-most panel. (E) Gating of whole blood leukocytes to identify CD45.1^{+}, CD45.2^{+} and CD45.1^{+}CD45.2^{+} donor and host lymphocytes in *Rel*$^{+/+}$ into *Rel*$^{+/+}$ chimeras. Forward scatter-height: FSC-H, Forward scatter-area: FSC-A, side scatter-area: SSC-A.

2.9 REFERENCES

1. Petermann P, Thier K, Rahn E, Rixon FJ, Bloch W, Ozcelik S, Krummenacher C, Barron MJ, Dixon MJ, Scheu S, Pfeffer K, et al. 2015. Entry mechanisms of herpes simplex virus 1 into murine epidermis: involvement of nectin-1 and herpesvirus entry mediator as cellular receptors. *J Virol* 89: 262-74
2. Sayers CL, Elliott G. 2016. Herpes Simplex Virus 1 Enters Human Keratinocytes by a Nectin-1-Dependent, Rapid Plasma Membrane Fusion Pathway That Functions at Low Temperature. *J Virol* 90: 10379-89
3. Tsatsos M, MacGregor C, Athanasiadis I, Moschos MM, Hossain P, Anderson D. 2016. Herpes simplex virus keratitis: an update of the pathogenesis and current treatment with oral and topical antiviral agents. *Clin Exp Ophthalmol* 44: 824-37
4. Steiner I. 2011. Herpes simplex virus encephalitis: new infection or reactivation? *Curr Opin Neurol* 24: 268-74
5. Koskiniemi M, Piiparinen H, Mannonen L, Rantalaiho T, Vaheri A. 1996. Herpes encephalitis is a disease of middle aged and elderly people: polymerase chain reaction for detection of herpes simplex virus in the CSF of 516 patients with encephalitis. The Study Group. *J Neurol Neurosurg Psychiatry* 60: 174-8
6. Gnann JW, Jr., Whitley RJ. 2017. Herpes Simplex Encephalitis: an Update. *Curr Infect Dis Rep* 19: 13
7. Casanova JL. 2015. Severe infectious diseases of childhood as monogenic inborn errors of immunity. *Proc Natl Acad Sci U S A* 112: E7128-37
8. Jiang Z, Mak TW, Sen G, Li X. 2004. Toll-like receptor 3-mediated activation of NF-kappaB and IRF3 diverges at Toll-IL-1 receptor domain-containing adapter inducing IFN-beta. *Proc Natl Acad Sci U S A* 101: 3533-8
9. Blank T, Prinz M. 2017. Type I interferon pathway in CNS homeostasis and neurological disorders. *Glia*
10. Casrouge A, Zhang SY, Eidenschenk C, Jouanguy E, Puel A, Yang K, Alcais A, Picard C, Mahfoufi N, Nicolas N, Lorenzo L, et al. 2006. Herpes simplex virus encephalitis in human UNC-93B deficiency. *Science* 314: 308-12

11. Zhang SY, Jouanguy E, Ugolini S, Smahi A, Elain G, Romero P, Segal D, Sancho-Shimizu V, Lorenzo L, Puel A, Picard C, et al. 2007. TLR3 deficiency in patients with herpes simplex encephalitis. *Science* 317: 1522-7
12. Sancho-Shimizu V, Perez de Diego R, Lorenzo L, Halwani R, Alangari A, Israelsson E, Fabrega S, Cardon A, Maluenda J, Tatematsu M, Mahvelati F, et al. 2011. Herpes simplex encephalitis in children with autosomal recessive and dominant TRIF deficiency. *J Clin Invest* 121: 4889-902
13. Perez de Diego R, Sancho-Shimizu V, Lorenzo L, Puel A, Plancoulaine S, Picard C, Herman M, Cardon A, Durandy A, Bustamante J, Vallabhapurapu S, et al. 2010. Human TRAF3 adaptor molecule deficiency leads to impaired Toll-like receptor 3 response and susceptibility to herpes simplex encephalitis. *Immunity* 33: 400-11
14. Herman M, Ciancanelli M, Ou YH, Lorenzo L, Klaudel-Dreszler M, Pauwels E, Sancho-Shimizu V, Perez de Diego R, Abhyankar A, Israelsson E, Guo Y, et al. 2012. Heterozygous TBK1 mutations impair TLR3 immunity and underlie herpes simplex encephalitis of childhood. *J Exp Med* 209: 1567-82
15. Dupuis S, Jouanguy E, Al-Hajjar S, Fieschi C, Al-Mohsen IZ, Al-Jumaah S, Yang K, Chapgier A, Eidenschenk C, Eid P, Al Ghonaium A, et al. 2003. Impaired response to interferon-alpha/beta and lethal viral disease in human STAT1 deficiency. *Nat Genet* 33: 388-91
16. Andersen LL, Mork N, Reinert LS, Kofod-Olsen E, Narita R, Jorgensen SE, Skipper KA, Honing K, Gad HH, Ostergaard L, Orntoft TF, et al. 2015. Functional IRF3 deficiency in a patient with herpes simplex encephalitis. *J Exp Med* 212: 1371-9
17. Audry M, Ciancanelli M, Yang K, Cobat A, Chang HH, Sancho-Shimizu V, Lorenzo L, Niehues T, Reichenbach J, Li XX, Israel A, et al. 2011. NEMO is a key component of NF-kappaB- and IRF-3-dependent TLR3-mediated immunity to herpes simplex virus. *J Allergy Clin Immunol* 128: 610-7.e1-4
18. Laukoter S, Rauschka H, Troscher AR, Kock U, Saji E, Jellinger K, Lassmann H, Bauer J. 2017. Differences in T cell cytotoxicity and cell death mechanisms between progressive multifocal leukoencephalopathy, herpes simplex virus encephalitis and cytomegalovirus encephalitis. *Acta Neuropathol* 133: 613-27

19. Singh TD, Fugate JE, Hocker S, Wijdicks EF, Aksamit AJ, Jr., Rabinstein AA. 2016. Predictors of outcome in HSV encephalitis. *J Neurol* 263: 277-89
20. Lellouch-Tubiana A, Fohlen M, Robain O, Rozenberg F. 2000. Immunocytochemical characterization of long-term persistent immune activation in human brain after herpes simplex encephalitis. *Neuropathol Appl Neurobiol* 26: 285-94
21. Pasieka TJ, Cilloniz C, Carter VS, Rosato P, Katze MG, Leib DA. 2011. Functional genomics reveals an essential and specific role for Stat1 in protection of the central nervous system following herpes simplex virus corneal infection. *J Virol* 85: 12972-81
22. Wang JP, Bowen GN, Zhou S, Cerny A, Zacharia A, Knipe DM, Finberg RW, Kurt-Jones EA. 2012. Role of specific innate immune responses in herpes simplex virus infection of the central nervous system. *J Virol* 86: 2273-81
23. Mansur DS, Kroon EG, Nogueira ML, Arantes RM, Rodrigues SC, Akira S, Gazzinelli RT, Campos MA. 2005. Lethal encephalitis in myeloid differentiation factor 88-deficient mice infected with herpes simplex virus 1. *Am J Pathol* 166: 1419-26
24. Murphy AA, Rosato PC, Parker ZM, Khalenkov A, Leib DA. 2013. Synergistic control of herpes simplex virus pathogenesis by IRF-3, and IRF-7 revealed through non-invasive bioluminescence imaging. *Virology* 444: 71-9
25. Caignard G, Leiva-Torres GA, Leney-Greene M, Charbonneau B, Dumaine A, Fodil-Cornu N, Pyzik M, Cingolani P, Schwartzentruber J, Dupaul-Chicoine J, Guo H, et al. 2013. Genome-wide mouse mutagenesis reveals CD45-mediated T cell function as critical in protective immunity to HSV-1. *PLoS Pathog* 9: e1003637
26. Kastrukoff LF, Lau AS, Takei F, Carbone FR, Scalzo AA. 2015. A NK complex-linked locus restricts the spread of herpes simplex virus type 1 in the brains of C57BL/6 mice. *Immunol Cell Biol* 93: 877-84
27. Menasria R, Canivet C, Piret J, Gosselin J, Boivin G. 2017. Protective role of CX3CR1 signalling in resident cells of the central nervous system during experimental herpes simplex virus encephalitis. *J Gen Virol* 98: 447-60
28. Zimmermann J, Hafezi W, Dockhorn A, Lorentzen EU, Krauthausen M, Getts DR, Muller M, Kuhn JE, King NJC. 2017. Enhanced viral clearance and reduced leukocyte infiltration in experimental herpes encephalitis after intranasal infection of CXCR3-deficient mice. *J Neurovirol* 23: 394-403

29. Menasria R, Canivet C, Piret J, Boivin G. 2015. Infiltration Pattern of Blood Monocytes into the Central Nervous System during Experimental Herpes Simplex Virus Encephalitis. *PLoS One* 10: e0145773
30. Caignard G, Eva MM, van Bruggen R, Eveleigh R, Bourque G, Malo D, Gros P, Vidal SM. 2014. Mouse ENU Mutagenesis to Understand Immunity to Infection: Methods, Selected Examples, and Perspectives. *Genes (Basel)* 5: 887-925
31. Beutler B. 2016. Innate immunity and the new forward genetics. *Best Pract Res Clin Haematol* 29: 379-87
32. Andrews TD, Whittle B, Field MA, Balakishnan B, Zhang Y, Shao Y, Cho V, Kirk M, Singh M, Xia Y, Hager J, et al. 2012. Massively parallel sequencing of the mouse exome to accurately identify rare, induced mutations: an immediate source for thousands of new mouse models. *Open Biol* 2: 120061
33. Lymberopoulos MH, Pearson A. 2007. Involvement of UL24 in herpes-simplex-virus-1-induced dispersal of nucleolin. *Virology* 363: 397-409
34. Kontgen F, Grumont RJ, Strasser A, Metcalf D, Li R, Tarlinton D, Gerondakis S. 1995. Mice lacking the c-rel proto-oncogene exhibit defects in lymphocyte proliferation, humoral immunity, and interleukin-2 expression. *Genes Dev* 9: 1965-77
35. Lafferty EI, Flaczyk A, Angers I, Homer R, d'Hennezel E, Malo D, Piccirillo CA, Vidal SM, Qureshi ST. 2014. An ENU-induced splicing mutation reveals a role for Unc93b1 in early immune cell activation following influenza A H1N1 infection. *Genes Immun* 15: 320-32
36. Bolger AM, Lohse M, Usadel B. 2014. Trimmomatic: a flexible trimmer for Illumina sequence data. *Bioinformatics* 30: 2114-20
37. Li H, Durbin R. 2010. Fast and accurate long-read alignment with Burrows-Wheeler transform. *Bioinformatics* 26: 589-95
38. McKenna A, Hanna M, Banks E, Sivachenko A, Cibulskis K, Kernytsky A, Garimella K, Altshuler D, Gabriel S, Daly M, DePristo MA. 2010. The Genome Analysis Toolkit: a MapReduce framework for analyzing next-generation DNA sequencing data. *Genome Res* 20: 1297-303
39. Cingolani P, Platts A, Wang le L, Coon M, Nguyen T, Wang L, Land SJ, Lu X, Ruden DM. 2012. A program for annotating and predicting the effects of single nucleotide

polymorphisms, SnpEff: SNPs in the genome of Drosophila melanogaster strain w1118; iso-2; iso-3. *Fly (Austin)* 6: 80-92

40. Desrosiers MP, Kielczewska A, Loredo-Osti JC, Adam SG, Makrigiannis AP, Lemieux S, Pham T, Lodoen MB, Morgan K, Lanier LL, Vidal SM. 2005. Epistasis between mouse Klra and major histocompatibility complex class I loci is associated with a new mechanism of natural killer cell-mediated innate resistance to cytomegalovirus infection. *Nat Genet* 37: 593-9
41. Suzuki K, Bose P, Leong-Quong RY, Fujita DJ, Riabowol K. 2010. REAP: A two minute cell fractionation method. *BMC Res Notes* 3: 294
42. Gilmore TD, Gerondakis S. 2011. The c-Rel Transcription Factor in Development and Disease. *Genes Cancer* 2: 695-711
43. Gilmore TD. 1990. NF-kappa B, KBF1, dorsal, and related matters. *Cell* 62: 841-3
44. Sedarati F, Stevens JG. 1987. Biological basis for virulence of three strains of herpes simplex virus type 1. *J Gen Virol* 68 (Pt 9): 2389-95
45. Ramakrishna C, Newo AN, Shen YW, Cantin E. 2011. Passively administered pooled human immunoglobulins exert IL-10 dependent anti-inflammatory effects that protect against fatal HSV encephalitis. *PLoS Pathog* 7: e1002071
46. Bhela S, Varanasi SK, Jaggi U, Sloan SS, Rajasagi NK, Rouse BT. 2017. The Plasticity and Stability of Regulatory T Cells during Viral-Induced Inflammatory Lesions. *J Immunol* 199: 1342-52
47. Isomura I, Palmer S, Grumont RJ, Bunting K, Hoyne G, Wilkinson N, Banerjee A, Proietto A, Gugasyan R, Wu L, McNally A, et al. 2009. c-Rel is required for the development of thymic Foxp3+ CD4 regulatory T cells. *J Exp Med* 206: 3001-14
48. Aravalli RN, Hu S, Rowen TN, Gekker G, Lokensgard JR. 2006. Differential apoptotic signaling in primary glial cells infected with herpes simplex virus 1. *J Neurovirol* 12: 501-10
49. Balachandran S, Beg AA. 2011. Defining emerging roles for NF-kappaB in antivirus responses: revisiting the interferon-beta enhanceosome paradigm. *PLoS Pathog* 7: e1002165

50. Pizzi M, Goffi F, Boroni F, Benarese M, Perkins SE, Liou HC, Spano P. 2002. Opposing roles for NF-kappa B/Rel factors p65 and c-Rel in the modulation of neuron survival elicited by glutamate and interleukin-1beta. *J Biol Chem* 277: 20717-23
51. Cook ML, Stevens JG. 1973. Pathogenesis of herpetic neuritis and ganglionitis in mice: evidence for intra-axonal transport of infection. *Infect Immun* 7: 272-88
52. Menendez CM, Carr DJJ. 2017. Defining nervous system susceptibility during acute and latent herpes simplex virus-1 infection. *J Neuroimmunol* 308: 43-49
53. Shivkumar M, Milho R, May JS, Nicoll MP, Efstathiou S, Stevenson PG. 2013. Herpes simplex virus 1 targets the murine olfactory neuroepithelium for host entry. *J Virol* 87: 10477-88
54. Reinert LS, Harder L, Holm CK, Iversen MB, Horan KA, Dagnaes-Hansen F, Ulhoi BP, Holm TH, Mogensen TH, Owens T, Nyengaard JR, et al. 2012. TLR3 deficiency renders astrocytes permissive to herpes simplex virus infection and facilitates establishment of CNS infection in mice. *J Clin Invest* 122: 1368-76
55. Reinert LS, Lopusna K, Winther H, Sun C, Thomsen MK, Nandakumar R, Mogensen TH, Meyer M, Vaegter C, Nyengaard JR, Fitzgerald KA, et al. 2016. Sensing of HSV-1 by the cGAS-STING pathway in microglia orchestrates antiviral defence in the CNS. *Nat Commun* 7: 13348
56. Lafaille FG, Pessach IM, Zhang SY, Ciancanelli MJ, Herman M, Abhyankar A, Ying SW, Keros S, Goldstein PA, Mostoslavsky G, Ordovas-Montanes J, et al. 2012. Impaired intrinsic immunity to HSV-1 in human iPSC-derived TLR3-deficient CNS cells. *Nature* 491: 769-73
57. DeBiasi RL, Kleinschmidt-DeMasters BK, Richardson-Burns S, Tyler KL. 2002. Central nervous system apoptosis in human herpes simplex virus and cytomegalovirus encephalitis. *J Infect Dis* 186: 1547-57
58. Sarnico I, Lanzillotta A, Boroni F, Benarese M, Alghisi M, Schwaninger M, Inta I, Battistin L, Spano P, Pizzi M. 2009. NF-kappaB p50/RelA and c-Rel-containing dimers: opposite regulators of neuron vulnerability to ischaemia. *J Neurochem* 108: 475-85
59. Chen C, Edelstein LC, Gelinas C. 2000. The Rel/NF-kappaB family directly activates expression of the apoptosis inhibitor Bcl-x(L). *Mol Cell Biol* 20: 2687-95

60. Bernard D, Quatannens B, Begue A, Vandenbunder B, Abbadie C. 2001. Antiproliferative and antiapoptotic effects of crel may occur within the same cells via the up-regulation of manganese superoxide dismutase. *Cancer Res* 61: 2656-64

61. Ashkar AA, Rosenthal KL. 2003. Interleukin-15 and natural killer and NKT cells play a critical role in innate protection against genital herpes simplex virus type 2 infection. *J Virol* 77: 10168-71

62. Daniels BP, Jujjavarapu H, Durrant DM, Williams JL, Green RR, White JP, Lazear HM, Gale M, Jr., Diamond MS, Klein RS. 2017. Regional astrocyte IFN signaling restricts pathogenesis during neurotropic viral infection. *J Clin Invest* 127: 843-56

63. Butchi N, Kapil P, Puntambekar S, Stohlman SA, Hinton DR, Bergmann CC. 2015. Myd88 Initiates Early Innate Immune Responses and Promotes CD4 T Cells during Coronavirus Encephalomyelitis. *J Virol* 89: 9299-312

64. Li F, Wang Y, Yu L, Cao S, Wang K, Yuan J, Wang C, Wang K, Cui M, Fu ZF. 2015. Viral Infection of the Central Nervous System and Neuroinflammation Precede Blood-Brain Barrier Disruption during Japanese Encephalitis Virus Infection. *J Virol* 89: 5602-14

65. Ashley SL, Pretto CD, Stier MT, Kadiyala P, Castro-Jorge L, Hsu TH, Doherty R, Carnahan KE, Castro MG, Lowenstein PR, Spindler KR. 2017. Matrix Metalloproteinase Activity in Infections by an Encephalitic Virus, Mouse Adenovirus Type 1. *J Virol* 91

66. Rochfort KD, Collins LE, McLoughlin A, Cummins PM. 2016. Tumour necrosis factor-alpha-mediated disruption of cerebrovascular endothelial barrier integrity in vitro involves the production of proinflammatory interleukin-6. *J Neurochem* 136: 564-72

67. Stamatovic SM, Keep RF, Kunkel SL, Andjelkovic AV. 2003. Potential role of MCP-1 in endothelial cell tight junction 'opening': signaling via Rho and Rho kinase. *J Cell Sci* 116: 4615-28

68. Ruan Q, Kameswaran V, Tone Y, Li L, Liou HC, Greene MI, Tone M, Chen YH. 2009. Development of Foxp3(+) regulatory t cells is driven by the c-Rel enhanceosome. *Immunity* 31: 932-40

69. Varanasi SK, Reddy PB, Bhela S, Jaggi U, Gimenez F, Rouse BT. 2017. Azacytidine Treatment Inhibits the Progression of Herpes Stromal Keratitis by Enhancing Regulatory T Cell Function. *J Virol* 91

70. Harling-McNabb L, Deliyannis G, Jackson DC, Gerondakis S, Grigoriadis G, Brown LE. 1999. Mice lacking the transcription factor subunit Rel can clear an influenza infection and have functional anti-viral cytotoxic T cells but do not develop an optimal antibody response. *Int Immunol* 11: 1431-9

71. Mason NJ, Liou HC, Hunter CA. 2004. T cell-intrinsic expression of c-Rel regulates Th1 cell responses essential for resistance to Toxoplasma gondii. *J Immunol* 172: 3704-11

72. Reinhard K, Huber M, Wostl C, Hellhund A, Toboldt A, Abass E, Casper B, Joeris T, Herr C, Bals R, Steinhoff U, et al. 2011. c-Rel promotes type 1 and type 17 immune responses during Leishmania major infection. *Eur J Immunol* 41: 1388-98

73. Ott M, Jing L, Lorenzo L, Casanova JL, Zhang SY, Koelle DM. 2017. T-Cell Responses to HSV-1 in Persons Who Have Survived Childhood Herpes Simplex Encephalitis. *Pediatr Infect Dis J*

74. Zhernakova A, Festen EM, Franke L, Trynka G, van Diemen CC, Monsuur AJ, Bevova M, Nijmeijer RM, van 't Slot R, Heijmans R, Boezen HM, et al. 2008. Genetic analysis of innate immunity in Crohn's disease and ulcerative colitis identifies two susceptibility loci harboring CARD9 and IL18RAP. *Am J Hum Genet* 82: 1202-10

75. Ellinghaus E, Stuart PE, Ellinghaus D, Nair RP, Debrus S, Raelson JV, Belouchi M, Tejasvi T, Li Y, Tsoi LC, Onken AT, et al. 2012. Genome-wide meta-analysis of psoriatic arthritis identifies susceptibility locus at REL. *J Invest Dermatol* 132: 1133-40

76. Gregersen PK, Amos CI, Lee AT, Lu Y, Remmers EF, Kastner DL, Seldin MF, Criswell LA, Plenge RM, Holers VM, Mikuls TR, et al. 2009. REL, encoding a member of the NF-kappaB family of transcription factors, is a newly defined risk locus for rheumatoid arthritis. *Nat Genet* 41: 820-3

77. Consortium IMSG. 2013. Network-based multiple sclerosis pathway analysis with GWAS data from 15,000 cases and 30,000 controls. *Am J Hum Genet* 92: 854-65

BRIDGING STATEMENT TO CHAPTER THREE

In anticipating future experiments that would further define the mechanisms by which the *Rel*^{C307X} mutation had directly initiated a wide cascade of HSE-related phenotypes, we kept three major previous findings in mind above all else. First, that IFN signaling or innate host responses were not adversely affected in *Rel*^{C307X} mice, unlike TLR3/IFN axis mutations and deficiencies described in several human HSE cases. Second, that the cellular response was an important driver of HSE pathology and susceptibility, rooted in our bone marrow chimera experiment where HSE only occurred if both brain-resident and infiltrating cells expressed the homozygous mutation. Third, that HSE phenotypes and clinical symptoms were only detected in moribund *Rel*^{C307X} mice between days 7 – 9 p.i., exhibiting abundant cytokine and chemokine production, caspase-3 expression, and elevated viral loads. Thus, we reasoned that early *Rel*^{C307X}-driven defects in resident cells (i.e. cell death) or in hematopoietic cells (i.e. altered T cell dynamics) resulted in failure to control viral replication, which in turn triggered the late and excessive neuroinflammatory and apoptotic responses that characterize moribund animals.

To expand the scope of this first study, we shifted our focus exclusively on the brain, and hypothesized that early defects or changes in the host response would be causal and lead to dysregulation in mutant animals. We considered that day 7 – 9 p.i. timepoints, with overwhelming HSE and consequent pathological inflammation, would be too late to observe early or causal differences. Instead we chose day 5 p.i., at least one to two days prior to the *Rel*^{C307X} mice developing HSE. We opted for a combinatorial approach, where dual RNA sequencing would reveal host and viral gene expression profiles sampled across all cells present in the tissue, and flow cytometry to allow for the precise identification and quantification of infiltrating and resident cells. Together, the cellular profile can inform the transcriptome, and vice-versa, to capture all facets of the diverse c-Rel regulatory response, and perhaps prioritize cell types that can be further probed for mechanisms that lead to HSE susceptibility. Finally, the inclusion of non-infected animals, representing the brainstem at steady-state, has also proved invaluable to explore the regulatory effect of c-Rel on homeostasis, and how these effects might later interact with HSV-1 infection to favour HSE development.

CHAPTER THREE: c-REL-REGULATED PATHWAYS PROTECT MICE FROM HERPES SIMPLEX ENCEPHALITIS BY LIMITING PATHOLOGICAL INTERFERON RESPONSES AND NEUROINFLAMMATION

Mathieu Mancini,[*,†] Benoît Charbonneau,[*,†] David Langlais,[*,†,‡] and Silvia M. Vidal[*, †,§,¶]

∗ Department of Human Genetics, McGill University, Montréal, Québec, Canada

† McGill University Research Centre on Complex Traits, McGill University, Montréal, Québec, Canada

‡ McGill University Genome Centre, Montréal, Québec, Canada

§ Department of Medicine, McGill University, Montréal, Québec, Canada

¶ Corresponding author: Silvia M. Vidal, Tel. (514) 398-2362, Fax (514) 398-2603, Email silvia.vidal@mcgill.ca

3.1 ABSTRACT

Herpes simplex virus type 1 (HSV-1) is the predominant cause of herpes simplex encephalitis (HSE), characterized by acute neuroinflammation and viral replication in the brain. There is an important contribution of host genetics to HSE onset, where several studies have identified monogenic defects in components of TLR3/type I IFN cascade in cases of childhood HSE. Mouse models of experimental HSE have revealed a further contribution of immune cell-mediated inflammation to HSE pathogenesis. We have previously described a homozygous recessive truncating mutation in the c-Rel transcription factor (Rel^{C307X}). Following intranasal HSV-1 infection, lethal HSE was observed in 50% of Rel^{C307X} mice compared to resistant $Rel^{+/+}$ mice, due to defects in resident cell- and immune cell-mediated immunity. In this study, we have applied dual host-virus RNA sequencing in non-infected and day 5-infected brainstem tissue, coupled with flow cytometry in the brain at various timepoints, to explore the cells and pathways that are involved in the Rel^{C307X} HSE phenotype. At steady-state, the Rel^{C307X} brainstem was enriched for apoptosis and cell turnover-related gene expression compared to $Rel^{+/+}$, suggesting that c-Rel regulated tissue maintenance is disrupted prior to infection. By day 5 postinfection, HSV-1 transcripts were detected at higher levels in the brainstems of 3/6 Rel^{C307X} high-responding mice compared to low-responders or $Rel^{+/+}$ mice. These high-responding Rel^{C307X} brainstems were associated with augmented and excessive host IFN-stimulated and inflammatory gene expression (including *Mx1*, *Usp18, Ccl2*, *Cxcl10*, *Il1rn*), predictive of later HSE development. By day 7 p.i., Rel^{C307X} mice exhibited increased pathological infiltration of $Ly6C^+$ monocytes and of $CD4^+$ and $CD8^+$ T cells, and contributing to viral escape. These findings establish c-Rel as regulator of cell-mediated responses that, in the brainstem, is essential to achieving a protective response against mouse HSE.

3.2 INTRODUCTION

Herpes simplex encephalitis (HSE) is primarily caused by infection of the central nervous system (CNS) with herpes simplex virus 1 (HSV-1). With an estimated incidence of 2 to 4 per 100,000 individuals per year, HSE is the most common form of sporadic viral encephalitis (1). Approximately one third of HSE cases occur in children, while the average age of onset for adult HSE is 60 years of age (2). HSE typically involves focal inflammatory lesions in the frontal or

temporal lobes, or rarely, inflammation of the brainstem (3, 4). Genetic factors are known to contribute to HSE onset and severity in children, namely, single gene defects in the Toll-like receptor 3 (TLR3) cascade including *TLR3*, *UNC93B1*, *TRIF*, *TRAF3*, *TBK1* and *IRF3* (5-10). These mutations result in defective type I interferon (IFN) production, where for example *TLR3* deficient patient-derived neurons and oligodendrocytes exhibit compromised cell-intrinsic control of HSV-1 infection (11). However, these TLR3/type I IFN-related variants only explain a minority of childhood HSE cases. To date, the contribution of two gene etiologies (*DBR1*, *SNORA31*) independent of the TLR3 axis have been identified in childhood cases, and a further defect linked to an adult HSE patient has been reported in the *MASP2* gene involved in the innate immune complement system (12-14).

Single gene knockout studies in mouse models of HSV-1 infection have confirmed that type I IFN and IFN-stimulated gene (ISG) expression downstream of pathogen sensing is protective in the brain, but have also defined the role of the inflammatory cell-mediated response during HSE (15). Resident CX3CR1^{+} microglia, involved in tissue maintenance, proinflammatory cytokine secretion, and expression of chemokines, are protective during mouse HSE (16-18). The cytotoxic and IFN-γ secreting functions of invading NK cells, CD4^{+}, and CD8^{+} T cells are also essential to controlling HSV-1 viral replication in the CNS (19, 20). However, chemokine receptor deficient *Cxcr3*$^{-/-}$ and *Ccr5*$^{-/-}$ mice are resistant to HSE, suggesting that lymphocyte and myeloid infiltration may contribute to pathological neuroinflammation (21-23). Recently, invading Ly6C^{+} monocytes and Ly6G^{+} neutrophils have also been shown to exacerbate lethal HSE in mice (24, 25). Thus, the genetic regulation of inflammation, like type I IFN, is an important determinant of HSE in mice.

In a previous study, we identified a novel mutation in the reticuloendotheliosis oncogene *Rel*, encoding the NF-κB family transcription factor subunit c-Rel, that caused HSE susceptibility (26). Homozygous *Rel*^{C307X} mice express a truncated c-Rel product deprived of its transactivation domains, which upon intranasal (i.n.) HSV-1 infection results in a 50% decrease in survival between days 6 to 9 postinfection (p.i.) compared to wild-type *Rel*$^{+/+}$ mice. Interestingly, *Rel*^{C307X} mice were not deficient in their cell-intrinsic type I IFN response to infection. Rather, HSE susceptibility in mutant animals was cell-mediated, and required the expression of the *Rel*^{C307X} variant in both hematopoietic and non-hematopoietic cells. Thus, defects in c-Rel-dependent

regulation of infiltrating immune cells and of brain-resident cells, together, lead to increased viral load, neuroinflammation, and caspase-3-dependent cell death in moribund *Rel*^{C307X} mice.

In the present study, to determine the pathways and cell types that drive HSE susceptibility in the *Rel*^{C307X} CNS, we performed dual virus and host gene expression profiling in the brainstem of HSV-1 infected *Rel*^{C307X} and *Rel*$^{+/+}$ mice. Elevated viral gene transcription was detected as early as day 5 p.i. in 3/6 *Rel*^{C307X} brainstems, together with elevated interferon-related inflammatory gene expression that contributed to pathological T cell and Ly6C^{+} monocytes recruitment by day 7. Thus, c-Rel-dependent regulation is protective during HSV-1 infection of the brainstem.

3.3 MATERIALS AND METHODS

Ethics statement

All animals used in this study were housed and maintained at McGill University. All experiments were performed under the guidelines and recommendations of the Canadian Council on Animal Care (CCAC) and in accordance with protocol number #2001-4792 approved by the McGill University Animal Care Committee.

Mice and virus infection

Rel^{C307X} mice (MGI:6287253 or Rel^{Coby} allele on the Mouse Genome Informatics (MGI) database, http://www.informatics.jax.org/) were discovered in an *N*-ethyl-*N*-nitrosourea mutagenesis screen as previously described (26). Inbred *Rel*^{C307X} mice were backcrossed at least 4 times to the C57BL/6 background (The Jackson Laboratory), and are maintained in a breeding colony including littermate homozygous mutant *Rel*^{C307X} and homozygous wild-type *Rel*$^{+/+}$ mice at McGill University. For HSV-1 infections, as previously described in (26), seven to nine-week old mice were first anaesthetized via intraperitoneal (i.p.) ketamine and xylazine injection, and infected with 5 x 10^4 PFU of HSV-1 strain 17 per 20 g body weight via intranasal (i.n.) inoculation. The inoculum was delivered in 10 µl of sterile PBS per 20 g body weight in the left nostril with a micropipette and allowed to be completely inhaled. Infected animals were weighed daily, monitored at least daily, and up to three times a day during the peak of infection (days 6 – 10 p.i.). Mice were euthanized upon demonstration of HSE-like symptoms (hunched posture, reduced

mobility, neurologic symptoms) or of 15% loss of initial pre-infection body weight, or upon reaching experimental endpoints at day 5 or 7 p.i.

CNS tissue collection and RNA preparation

At clinical or experimental endpoint, mice were euthanized and quickly perfused transcardially through the left ventricle with 10 ml cold PBS. As specified in each figure legend, either the brainstem, both TG (as described in (27)), or the whole brain (including the olfactory bulbs, cerebrum, cerebellum and brainstem) were excised and collected in either 5 ml Hibernate-A medium (ThermoFisher Scientific) at 4^{o}C for downstream flow cytometry, or snap-frozen in liquid nitrogen and conserved at -80^{o}C for downstream RNA extraction. Snap-frozen brainstem or TG samples were transferred to 1 ml TRIzol reagent (Invitrogen) and homogenized at speed 6000 for 30 seconds with a MagNA Lyser Instrument (Roche). Total RNA was extracted as per the manufacturer's standard protocol. RNA samples were further cleaned up using the RNeasy Mini Kit (Qiagen #74104) and following DNase I treatment, as per the manufacturer's standard protocol. Purified RNA was reverse transcribed into cDNA and real-time quantitative PCR was performed as previously described (26), using the following primer pairs: *ICP4* (*RS1*) (forward 5' CGACACGGATCCACGACCC 3', reverse 5' GATCCCCCTCCCGCGCTTCGTCCG 3') and *Hprt* (forward 5' CAGGCCAG-ACTTTGTTGGAT 3', reverse 5' TGGCGCTCATCTTAGGC TTT 3').

Dual RNA sequencing and differential gene expression analysis

RNA sequencing was performed as previously described (28). Briefly, total RNA was purified from whole brainstem samples and assayed for RNA integrity using a Bioanalyzer RNA Pico kit (Agilent). cDNA libraries were generated after rRNA depletion with the KAPA Stranded RNA-Seq kit (Roche). Paired-end 50 bp read sequencing was performed using an Illumina HiSeq 2500 sequencer. Low-quality bases (Phred < 33) and adaptor sequences were removed with the Trimmomatic v.0.36 tool (29) using the following arguments: ILLUMINACLIP:TruSeq3-PE.fa:2:30:10 HEADCROP:4 LEADING:5 TRAILING:3 SLIDINGWINDOW:4:20 MINLEN:36. All trimmed reads were first aligned to the mouse GRCm38 (mm10) reference genome using TopHat2 v2.1.1 with Bowtie2 v2.3.1 algorithms (30, 31), and were quantified per gene by counting the number of strand-specific reads aligning to gene exon features using the

featureCounts tool (Subread package v1.5.2 (32)). In parallel, using HISAT2 v2.1.0 (33), all trimmed reads were also aligned to an indexed HSV-1 strain 17 reference genome (34) (GenBank: JN555585.1). Viral reads were quantified per viral gene by counting the number of strand-specific reads aligning to gene and/or exon features using featureCounts. Here, in addition to default arguments, the "M" and "primary" arguments were used to only count multiple-mapping reads once at their primary alignment site, and avoid to counting twice over genes that are naturally duplicated in the HSV-1 genome (*RS1*, *RL1*, *RL2*, *LAT*).

Raw read counts libraries for host gene were first filtered to remove residual rRNA reads, and to only keep genes expressed above 3 counts per million host reads (CPM) in at least 3 samples, for a total of 16,279 expressed host genes. For viral reads, all expressed viral genes were retained and were similarly normalized per million host reads. Filtered host count libraries were normalized with the TMM method and differential host gene expression was assessed pairwise between sample groups using the edgeR Bioconductor package (35). Genes whose expression was $> \pm 1.5$ fold change between groups, and that met a threshold of $q < 0.05$ (Benjamini-Hochberg (BH)-adjusted p-value), were considered statistically significant. Gene expression heatmaps of CPM values per sample, normalized to the average CPM values across a control group specified in each figure, were generated using the "gplots" package in R and clustered gene-wise using a Euclidean distance measure.

Gene ontology term and gene set enrichment analyses

Gene ontology (GO) term enrichment analysis for biological processes (BP4) was performed on differentially expressed genes identified by RNA sequencing between $Rel^{+/+}$ and Rel^{C307X} groups at select time points of infection using the DAVID v.6.8 online database (36). Enriched GO terms that met a nominal *p*-value cut-off of 0.05 were considered significant. To identify cellular or immune pathways that were present in either $Rel^{+/+}$ and Rel^{C307X} mice gene expression profiles (including all 16,279 expressed genes), gene set enrichment analysis was performed using GSEA (37) to detect enrichment of gene sets publicly listed in the MSigDB v6.2 collection, specifically among $N = 3406$ Curated Gene Sets (C2, including chemical and genetic perturbations, canonical pathways (BIOCARTA, KEGG, PID or REACTOME) or $N = 4872$ Immunological Signatures (C7). Gene sets that met a Benjamini-Hochberg (BH)-adjusted *p*-value cut-off of at least $q < 0.05$ were considered significantly enriched in each condition. Furthermore,

enriched gene sets were clustered according to shared leading edge genes (using Manhattan distance) to group similar or redundant signatures together, and better resolve general themes specific to Rel^{C307X} or $Rel^{+/+}$ mice. For these leading edge analyses, only those genes that were ranked prior or at the position of the gene with the maximum enrichment score in any given gene set (the leading edge), and that were represented in at least 5% of all enriched gene sets, were included for hierarchical clustering.

Flow cytometry on CNS tissue

Adapted from (38) with modifications, freshly excised HSV-1 infected whole brain, brainstem or TG tissue were collected in 5 ml Hibernate A medium at 4°C and were processed into single cell suspensions and stained for flow cytometry. Briefly, tissues were minced and digested in 1 ml 1X HBSS containing 510 U/ml collagenase II (Worthington Biochemical Corp.) and 28 U/ml DNase1 (Roche) for 15 minutes at 37°C. 9 ml 1X HBSS 2 mmol EDTA were added to digested samples, and the remaining tissue was gently homogenized through a 100 μm mesh in a cell dissociation sieve (Sigma #CD1) to generate a single cell suspension. Cells were pelleted, resuspended in a 37% Percoll™ solution, and centrifuged at 500 x g for 20 minutes with no break. The top-floating myelin/debris layer and the supernatant was removed by aspiration, and the cell pellet (containing hematopoietic immune cells, neurons, oligodendrocytes, microglia, and any remaining red blood cells or debris) was washed twice and resuspended in 1X PBS 2% FBS 2 mmol to accommodate two antibody staining panels. Cells were treated with anti-CD16/CD32 to block non-specific binding to Fc receptors (eBioscience #16-0161), and were stained with extracellular antibodies overnight at 4°C. The following fluorochrome-conjugated antibodies (clone, working dilution) were used from eBioscience (Invitrogen): B220 APC (RA3-6B2, 1:100), CD11b eFluor450 (M1/70, 1:50), CD44 FITC or PE (IM7, 1:100), CD45 PerCP-cy5.5 (30-F11, 1:200), CD62L FITC or PE (MEL-14, 1:100), CXCR3 PE-cy7 (CXCR3-173, 1:100), NK1.1 PE-cy7 (PK136, 1:100); from BioLegend: CD3 Brilliant Violet 605 (17A2, 1:100), CD4 Brilliant Violet 510 (GK1.5, 1:100), CD8a eFluor450 or Brilliant Violet 785 (53-6.7, 1:100), I-A/I-E (MHC-II) AlexaFluor700 (M5/114.15.2, 1:300), Ly6G Brilliant Violet 711 (1A8, 1:500), Ly6C Brilliant Violet 785 (HK1.4, 1:2000); and from Miltenyi Biotec: O4 APC (O4, 1:50). Cells were later stained with Fixable Viability Dye (eFluor780-conjugated or eFluor506-conjugated, eBioscience #65-0865 or #65-0866) to mark dead cells. Next, cells were fixed and permeabilized

with the Foxp3/Transcription Factor Staining Buffer Kit (eBioscience #00-5523-00) as per the manufacturer's instructions, and stained with the following intracellular antibodies (clone, working dilution, supplier): c-Rel PE (1RELAH5, 1:100, eBioscience) and NeuN AlexaFluor488 (EPR12763, 1:25, Abcam). 5000 counting beads (Spherotech #ACBP-50-10) were added to each sample prior to acquisition on a BD LSRFortessa cytometer. Total cell counts for each cell population were normalized to the total number of beads per sample and to the total number of singlet viable cells acquired in both staining panels. Cell populations were gated as described in Supplementary Figure 3.4 using FlowJo v. 10.1 software.

Statistics

Statistical tests were performed using the statistical package of GraphPad Prism v. 6 software, as detailed in each figure legend. Two-way ANOVA were performed with Tukey's multiple correction test between pairwise groups, where adjusted p values < 0.05 were considered significant (*p<0.05, **p<0.01, ***p<0.001, ****p<0.0001).

3.4 RESULTS

Rel^{C307X} mice exhibit differential viral and host responses as early as day 5 in HSV-1-infected brainstems

We have previously demonstrated that Rel^{C307X} mutant mice are susceptible to HSE, where typically 50% of Rel^{C307X} mice exhibit high elevated viral titer and reach clinical endpoint between days 6 to 9 post-HSV-1 infection, compared to resistant $Rel^{+/+}$ littermates (26). Here, dual RNA sequencing was performed in female $Rel^{+/+}$ and Rel^{C307X} littermate mice to measure differences in viral and host gene expression across the diverse resident and hematopoietic cells that populate the HSV-1-infected brainstem. Specifically, this analysis was focused on the brainstem, a well-characterized site of viral access to the CNS and of acute neuroinflammatory responses in mouse models of HSE (26, 39). We sought to detect early Rel^{C307X}-dependent effects on host gene expression before the onset of fulminant HSE response, which had the potential to mask any causal effects of the mutation. Therefore, day 5 p.i. was selected as an optimal timepoint, at least one day prior to the rapid onset of HSE clinical symptom and of pathological cell death in susceptible Rel^{C307X} mice.

At day 5 p.i., sequences derived from HSV-1-encoded viral mRNA were strongly detected in 3 of 6 Rel^{C307X} brainstems, and to a lesser degree in 3 of 5 $Rel^{+/+}$ brainstems, each annotated as high-responders to infection (denoted HSV^{HI} in Fig. 1A). In the remaining low-responding mice (3 of 6 Rel^{C307X} and 2 of 5 $Rel^{+/+}$, denoted HSV^{LO} in Fig. 1B) 16 or fewer paired read fragments were detected across the entire HSV-1 genome, and fewer than 3 in non-infected mice. Viral gene expression at 75 major open reading frames was also more elevated in high-responding Rel^{C307X} mice, and comparable across known immediate-early, early or late phases of expression (40) (Fig. 1B). Furthermore, all three high-responding Rel^{C307X} mice were clearly segregated together following a principal component analysis across expressed HSV-1 genes (Supplemental Fig. 1A, B). Overall, in high-responding groups at day 5 p.i., the total number of coding region-aligned viral reads was more elevated in Rel^{C307X} mice compared to $Rel^{+/+}$ mice (Fig. 1C). Thus, Rel^{C307X}-driven differences in HSV-1 viral RNA transcription were successfully detected and quantified by day 5 p.i. in the brainstem, earlier than a viral plaque assay would otherwise reveal at HSE-symptom onset (26).

To better determine if this early and greater detection of HSV-1-derived sequences could predict disease outcome and help refine downstream analyses, the expression of host-derived genes was also subjected to a principal component analysis (Supplemental Fig.1D, E). To best define clusters of similarly-responding mice, the first host principal component was plotted against the first viral principal component (Fig. 1D), or against the relative expression of the *RS1 (ICP4)* viral gene measured by RT-qPCR (Fig. 1E), confirming the presence of three distinct response groups (non-infected mice, low-responders at day 5 p.i., and high-responders at day 5 p.i.) in our dataset. Therefore, those animals with the most replicating virus also demonstrated the most polarized host responses in the brainstem, suggesting that high-responders, and especially those harbouring the Rel^{C307X} mutation, may go on to develop more severe HSE disease.

Altered cell survival and homeostatic responses in non-infected Rel^{C307X} brainstems

To establish how the Rel^{C307X} mutation might disrupt gene expression in the brainstem at steady-state, non-infected $Rel^{+/+}$ and Rel^{C307X} mice were directly compared to identify 45 differentially-expressed genes (DEG) (Fig. 2A, Supplemental Fig. 2A). Of note, *Rel* is expressed in the brainstem, and is marginally downregulated in Rel^{C307X} mice at steady state ($q = 0.0564$, fold-change = -1.44), and significantly downregulated later during infection ($q < 0.05$, fold-change

< -1.5), compared to wild-type mice (Fig. 2B). Other genes that were downregulated in Rel^{C307X} mice include *Prune2*, a tumour-suppressor gene with pro-apoptotic function (41). On the other hand, *Gabra2*, involved in neural development and signaling (42), and eukaryotic initiation factor *Eif1* were examples of upregulated genes in Rel^{C307X} brainstems (Fig. 2C). For a wider look at dysregulated pathways and functions, gen set enrichment analysis (GSEA) was performed across all brainstem-expressed genes, and enriched gene sets were grouped according to common leading-edge genes to better define overall up- or down-regulated signatures in Rel^{C307X} mice (Fig. 2D-F).

First, 66 curated gene sets were enriched at a threshold of $q < 0.05$ in Rel^{C307X} mice (Fig. 2D-F, upper panels). In particular, those gene sets (Clusters 1 and 2) related to hypoxia, to the AP-1 transcription factor pathway, and to TRAIL- or UV-dependent apoptotic responses indicate that cell survival may be adversely impacted in Rel^{C307X} brainstems. Furthermore, other signatures related to cell growth and proliferation (Clusters 3 and 4) were over-represented in mutant samples, namely the phosphoinositide 3-kinase (PI3K) pathway, modulation of circadian rhythm (*Clock*, *Npas1*) and the G1 phase of cell division (*Rb1, Ccnd2, Cdk6, Bcl6*).

Second, among 80 enriched gene sets in $Rel^{+/+}$ brainstems (Fig. 2D-F, lower panels), a distinct group of genes, including *Rel* and other NF-κB-family genes, underscored later stages of the cell cycle and the proteasome pathway (Clusters 5 and 6). Wild-type-enriched signatures also evoked mitochondrial function and cellular respiration, in addition to active transcription of ribosomal protein genes and heightened protein translation (Clusters 7 and 8). Altogether, these steady-state differences between $Rel^{+/+}$ and Rel^{C307X} mice support a role for c-Rel in regulating cellular proliferation, maintenance, and survival pathways in the brainstem.

Finally, we evaluated if any DEG were consistently disrupted in Rel^{C307X} mice at different stages of infection. Briefly, two parallel analyses were performed: first, high-responding HSV-1 infected Rel^{C307X} and $Rel^{+/+}$ mice were compared directly, and second, all high-responding HSV-1 infected mice were compared to non-infected mice irrespective of genotype group. Only those genes that varied exclusively as function of genotype group (analysis 1), and not driven by HSV-1 infection (analysis 2), were retained (Supplemental Fig. 2B). Only 13 Rel^{C307X}-dependent genes were found to be up or downregulated in Rel^{C307X} brainstems (Supplemental Fig. 2C), including galectin-family member *Lgals3* involved in innate and cellular immunity, CNS-tropic *Pgbd1,* and Serum/Glucocorticoid Regulated Kinase 1 (*Sgk1)* involved in cell survival (43). Five long non-coding RNAs were also identified as Rel^{C307X}-specific DEG that varied independently of the virus.

While these factors may further contribute to altered homeostasis in non-infected brainstems, most DEG that define the *Rel*^{C307X} transcriptional landscape are triggered at least in part by infection in this HSE model.

High-responding Rel^{C307X} *mice generate stronger IFN-stimulated and cell-mediated inflammatory responses to HSV-1 infection in the brainstem*

The impact of infection on gene expression at day 5 p.i. was first evaluated by independently comparing high-responding *Rel*$^{+/+}$ and *Rel*^{C307X} groups separately to non-infected *Rel*$^{+/+}$ controls. Here, 159 genes for *Rel*$^{+/+}$ and 249 genes for *Rel*^{C307X} were upregulated by each group in response to infection (Fig. 3A, B). However, while many of these upregulated genes overlapped across both conditions—like ISGs *Usp18* and *Mx1*, and secreted factors including *Cxcl10* and *Ccl2* chemokine genes and IL-1 receptor agonist *Il1rn*—their expression was significantly higher in *Rel*^{C307X} mice (Fig. 3 C). In addition to classical ISGs, many other genes involved in IFN-I or IFN-II signaling were also generally upregulated in *Rel*^{C307X} mice, while IFN receptors were steadily expressed at all timepoints in the brainstem (Supplemental Fig. 3A, B). To confirm that the defence response as a whole was heightened in mutant animals, fold-wise gene expression was compared between respective low- and high-responding groups (Fig. 3D, E). First, for either genotype group, genes expressed in high- and low-responders were plotted against each other, and standard residuals to the identity line ($y = x$ line) were calculated. By considering only genes whose expression skewed at greater than 1 standard deviation towards high-responders (with standard residuals > 1), *Rel*^{C307X} brainstems were found to be more enriched for functional GO terms related to innate immune, cytokine (IFN-1 and IFN-II) and virus responses (Fig. 3F). Thus, *Rel*^{C307X} mice respond to HSV-1 infection by expressing host defence and IFN-related genes at a much higher magnitude as early as day 5 p.i.

In an alternate DEG analysis, 51 DEG were identified by directly comparing high-responding groups (Fig. 4A) and were similarly enriched in *Rel*^{C307X} brainstems for IFN signaling, lymphoid and myeloid cell chemotaxis, and programmed cell death (Fig. 4B). Expanding beyond these 51 DEG using GSEA, *Rel*^{C307X}-enriched gene sets were related to type 1 helper CD4^{+} T cells, Tregs, IgG-stimulated B cells, and Fc receptor-stimulated monocytes, in addition to various TLR-stimulations in DCs (Fig. 4C, D). The high-responding *Rel*^{C307X} gene expression landscape further overlapped with inflammatory gene sets derived from IFN-I-stimulated microglia, peripheral

blood mononuclear cells and $CD8^+$ T cells. Together, these signatures not only underscore a stronger Rel^{C307X}-dependent IFN response, but also reveal an increased contribution of T cells, myeloid cells and other inflammatory cell-mediated pathways to the Rel^{C307X} response to HSV-1 infection.

HSE onset is associated with elevated pathological infiltration of myeloid and T cells in the Rel^{C307X} CNS

To confirm which resident or infiltrating cell types were populating the CNS during HSV-1 infection, and therefore which cells were concurrent with altered gene expression, neuronal, glial and hematopoietic cells were quantified at various timepoints leading up to HSE symptom onset in Rel^{C307X} mice. As HSV-1 typically accedes to the hindbrain via the trigeminal ganglia (TG) in i.n. models of infection, we first examine the TG at day 4 p.i. (Supplemental Fig. 5A-E) and the brainstem at day 5 p.i, (Supplemental Fig. 5F-J) and found no major differences in the number of myeloid, $CD4^+$ or $CD8^+$ T cells between $Rel^{+/+}$ and Rel^{C307X} groups. To better capture the global encephalitis response, whole brain tissue was processed at day 5 and later at day 7, near peak onset of symptoms in susceptible mutant mice. Here, at discrete timepoints, brain-resident neurons, oligodendrocytes and microglia, as well as infiltrating NK cells and neutrophils, remained unchanged in number across infection (Supplemental Fig. 5K-M). However, infiltrating $CD45^{HI}CD11b^+Ly6G^-Ly6C^+$ monocytes and $CD4^+$ T cells were slightly augmented in Rel^{C307X} compared to $Rel^{+/+}$ mice as early as D5 p.i., whereas B cells were generally decreased (Supplemental Fig. 5L, M).

By day 7 p.i., three major infiltrating populations were augmented in the Rel^{C307X} brain. First, increased $CD45^{HI}CD11b^+$ activated myeloid cells (Figure 5A, B) had accumulated in that numbers correlated with *ICP4* viral gene expression in TG collected from those same Rel^{C307X} mice at day 7 p.i. (Figure 5C). Among these myeloid cells, the $Ly6C^+$ monocyte subset was more elevated in Rel^{C307X} mice, and were also positive for CXCR3 expression, the cognate homing receptor for Rel^{C307X}-upregulate chemokine CXCL10 (Fig. 5D). Second and third respectively, $CD4^+$ and $CD8^+$ T cells were also more numerous in Rel^{C307X} mice (Fig. 5E, F, I), and again in step with levels of HSV-1 replication (Fig. 5G, J). These T cells all expressed CXCR3 as the infection progressed, and exhibited an activated $CD44^+CD62L^-$ profile by day 7 p.i. (Fig. 5H, K). Overall, these associations between activated myeloid and T cell subsets with HSV-1 replication support a

pathological role for these infiltrating cells in the development of HSE. Thus, these data suggest a model where high-responding *Rel*^{C307X} mice, having exhibited increased viral mRNA transcription and IFN-stimulated/inflammatory gene expression at day 5 p.i., may go on to attract a greater number of pathogenic monocytes and T cells brain, leading to viral escape and lethal HSE onset.

Finally, it was also observed in wild-type mice at day 5 p.i. that c-Rel protein expression was upregulated from steady-state levels predominantly in these activated myeloid cell, monocyte and T cell subsets, as well as in B cells (Supplemental Fig. 6F, D, H-K). c-Rel was also expressed in resident microglia and neurons, and further upregulated by infection in neurons (Supplemental Fig. 6A, B), where c-Rel dependent regulation of cell survival has previously been demonstrated (44). While expression of the truncated C307X c-Rel protein could not be reliably measured here, the response of the wild-type protein to HSV-1 infection in the brain, and specifically in the context of key dysregulated immune cell populations in *Rel*^{C307X} mice, may further point to a key role for c-Rel in the regulation of protective host responses to HSE.

3.5 DISCUSSION

To our knowledge, this study is the first to employ gene expression profiling dual RNA sequencing in an *in vivo* mouse model of HSE. Specifically, we have combined transcriptome profiling of HSV-1 infected brainstems together with flow cytometry of infiltrating and brain-resident cells to better understand the effect of the *Rel*^{C307X} mutation and contribution to HSE susceptibility. These strategies allowed for the detection of increased host responses and viral replication as early as day 5 p.i., at least one full day before typical HSE symptom onset and of excess production of cytokines, chemokines, and of caspase-3-dependent apoptosis in the brainstem and cerebellum previously reported in (26). In the present study, high-responding *Rel*^{C307X} mice were also distinguished by elevated infiltration of myeloid and T cell subsets to the brain, involving these cells directly in the pathological inflammatory response and failure to control viral replication during HSE.

Prior to infection, c-Rel is involved in maintenance and homeostasis in the brainstem in adult mice. Considering the diverse neuronal and glial cells that populate the brainstem, and prior to any infection-triggered inflammation or cellular infiltration, it was interesting to find that the *Rel*^{C307X} mutation had a measurable effect on gene expression related to basal cell division and

proliferation. The enrichment of these functional signatures was not only led by genes directly involved in cell cycle initiation, but more indirectly to the circadian clock, cyclic adenosine monophosphate/cAMP response element-binding (CREB) pathways, and PI3K/TRK pathways. In the brain, these processes are involved in neuronal and glial maintenance, survival and development (45-47), while *Crebbp* and *Creb1* are also prominent negative regulators of microglia and astrocyte inflammation via NF-κB (48, 49). Yet, Rel^{C307X} mice offered no evidence of differential basal inflammation compared to $Rel^{+/+}$ animals, which instead prioritized respiration, mitochondrial function, translation, and NF-κB signaling. Microglia and neurons were not detected in higher numbers in Rel^{C307X} brains, and while NF-κB is essential for basal homeostatic proliferation of naïve T cells (50), T cells numbers were also equivalent in the brainstem, TG and brain at steady-state. Thus, in the absence of hematopoietic infiltration or proliferation prior to infection, the Rel^{C307X} transcriptional profile has more likely captured a disruption of cell maintenance and turnover in the brainstem at steady-state.

In this regard, the Rel^{C307X}-specific enrichment of hypoxic and apoptotic responses is especially telling. *Prune2*, a pro-apoptotic tumour suppressor gene (51), stands out as one of the most extreme DEG in our dataset. c-Rel has been implicated in pro-survival responses in neurons (44, 52), and as we have previously shown, Rel^{C307X} fibroblasts are more susceptible to caspase-3-dependent cell death following *ex vivo* HSV-1 infection (26). Supporting a wider role for c-Rel in neuronal survival, $Rel^{-/-}$ mice have been found to exhibit Parkinson's disease-like symptoms and neurodegeneration at 18 months of age (53). In the case of the Rel^{C307X} brainstem, characterized by increased expression of genes involved in hypoxia, apoptosis and cell turnover by early adulthood at 8 weeks of age, it is tempting to speculate how subtle defects in c-Rel-dependent regulation of cell survival and homeostasis may be further exacerbated by age, injury or infection. Being that one of the final outcomes of HSE in susceptible Rel^{C307X} mice is elevated *in vivo* detection of cleaved caspase-3 in the infected brain, these early basal differences in the Rel^{C307X} transcriptome warrant further investigation, and may reflect an important contribution of the cell-resident compartment to HSV-1 susceptibility in our model.

In HSV-1 infected brainstems at day 5, the global capture of viral mRNA sequences was pivotal to the identification of early high- and low-responding mice to infection, ensuring that HSE-susceptible Rel^{C307X} mice could be analyzed together, and apart from the other (~40%) Rel^{C307X} mice that are expected to survive past the 14 day mark, and where the mutation is typically

nonpenetrant (26). As a result, high-responding *Rel*^{C307X} mice were found to have significantly more replicating virus compared to any other response or genotype group as early as day 5 p.i., and were also associated with striking IFN-stimulated and neuroinflammatory responses that would be likely to progress to lethal HSE by later timepoints. In particular, this heightened ISG response distinguished HSV-1-susceptible *Rel*^{C307X} mice from other HSE models, where type I IFN receptor *Ifnar*$^{-/-}$ and *Stat1*$^{-/-}$ knockout mice succumb early to HSV-1-induced neuroinflammation in the absence of IFN-stimulated responses (39, 54), and TLR3- and NF-κB (NEMO)-related inborn defects in IFN are also well established as causes of HSE in humans (11, 55, 56). Rather, the *Rel*^{C307X} IFN transcriptional response is evocative of excess type I IFN reactions in Aicardi-Goutières inflammatory syndrome, often caused by mutations of variable penetrance in IFN pathway genes (57). Pathological levels of type I IFN are also detected in human cases of ISG15 deficiency (58), of inflammatory diseases like systemic lupus erythematosus (SLE) and rheumatoid arthritis (RA), and during infectious tuberculosis (TB) and murine cerebral malaria (59-61). IFN itself can also be toxic to neurons and exacerbate neurodegeneration following tissue injury (62, 63). With the wide effect of the *Rel*^{C307X} mutation on upregulation of ISG gene expression, these excess and unchecked IFN responses may contribute to brain immunopathology and failure to contain viral replication.

A further subset of inflammatory genes that are highly induced beyond wild-type levels were interleukin-1 receptor antagonist-encoding *Il1rn*, and chemokine-encoding genes *Ccl2* and *Cxcl10*. Polymorphisms in human *IL1RN* have been associated with *in vivo* control of Epstein-Barr viral load, and with inflammatory bowel and skin disorders that have also been associated with the *REL* locus (64-66). On the other hand, *Cxcl10* is notable for being induced and regulated by c-Rel in T cells (67). While *Cxcl10* has been shown to be protective on its own against ocular HSV-1 infection (17), the expression of its cognate receptor *Cxcr3* is detrimental to the host following i.n. infection (21, 23). Here, infiltrating CXCR3^{+} T cells are pathological in the brain and auxiliary to viral replication during HSE, as are CCR2^{+} and CXCR3^{+} blood monocytes attracted by CCL2 and CXCL10 production (24). In *Rel*^{C307X} mice, these inflammatory factors are expressed at day 5 p.i., likely by resident microglia (16, 68), prior to the observed recruitment of peripheral immune cells to the brain at day 7 p.i. Here, the late and excessive infiltration of activated myeloid cells (CD45^{HI} and in majority Ly6C^{+}), and of CD4^{+} and CD8^{+} T cells (in majority CXCR3^{+} and CD44^{+}), was associated with augmented viral replication in paired TG, and

concurrent with previously characterized production of T helper type 1 (Th1) cytokines in the brainstem and cerebellum (26), suggesting that these cells also play a pathological role in *Rel*^{C307X}-triggered HSE.

Interestingly, these later increases in leukocyte trafficking to the *Rel*^{C307X} brain were preceded at day 5 p.i. by enrichment of IFN-stimulated and activated T cell and myeloid cell gene signatures. Moreover, inflammatory gene profiles similar to CD4^{+} T cells and peripheral blood mononuclear cells (PBMCs) respectively isolated from SLE and multiple sclerosis patients were overrepresented in *Rel*^{C307X} mice, as opposed to cytotoxic or antigen-dependent antiviral programs. Overall, our RNA sequencing dataset did not support a role for *Rel*^{C307X}-dependent defects in the classical cellular antiviral response, echoing normal antiviral T cell responses observed in *Rel*$^{-/-}$ mice during influenza infection (69). With peripheral CD4^{+} T cell numbers being augmented in the blood and spleen at day 4 post-infection but producing normal levels of IFN-γ at day 5 (26), the *Rel*^{C307X} mutation instead appears to affect the regulation of T cells in their capacity to mediate inflammation, in their recruitment to the brain, and their misplaced role as pathological effectors in the infected *Rel*^{C307X} CNS. Furthermore, intracellular staining indicated that wild-type c-Rel protein is highly expressed and notably upregulated by HSV-1 infection in Ly6C^{+} infiltrating myeloid cells and T cells in the brain, in contrast to resident microglia that express c-Rel well, but do not upregulate it during following infection. Thus, infiltrating T and myeloid cells and resident myeloid cells would be worth examining at the single cell level, collected from the *in vivo* HSV-1-infected CNS, to determine if *Rel*^{C307X}-driven dysregulation in homeostatic, IFN-related or inflammatory responses is occurring in distinct or multiple cell populations. Further investigation by immunohistochemistry would clarify how astrocytes, that do not survive tissue digestion and mincing, behave and contribute to our model. Brain-infiltrating regulatory T cells (Tregs) and other T cell subsets, that were too few to reliably quantify in our flow cytometry experiments, may be more easily detectable using magnetic pre-enrichment of T cells.

Thus, the *Rel*^{C307X} HSV-1 infection model captured an altogether different aspect of HSE disease compared to cases of inherited type I IFN/TLR axis deficiencies. *Rel*^{C307X} mice were instead defined by excess IFN-stimulated and neuroinflammatory responses, in turn attracting pathological T and myeloid cells to the brainstem whose resident cells, showing early signs of dysregulated cell cycle and survival, ultimately failed to tolerate inflammation and to control viral replication. In the wider context of c-Rel-dependent regulation of host responses, the association

between the *Rel*^{C307X} mutation and susceptibility to HSE, an acute viral infection, was notable, compared to *Rel*$^{-/-}$ animals that are generally resistant to acute influenza infection, to experimental autoimmune encephalomyelitis (EAE) and to anti-CD40-induced colitis (69-71), and only susceptible to long-term parasitic (*Toxoplasma*, *Leishmania*) or bacterial (*Citrobacter rodentium*) infections and colitis-associated cancer (72-75). Beyond the known contribution of the human *REL* locus to a wide range of human inflammatory diseases, *REL* has also recently been implicated in broad susceptibility to chronic human herpesvirus-5, *Salmonella* and *Cryptosporidium* infections in a c-Rel-deficient patient (76). The involvement of c-Rel in these diseases, in its capacity as a regulator of inflammation, supports our findings that the truncated C307X c-Rel protein disrupts the regulation of cell-mediated host defence to HSV-1 infection. The *Rel*^{C307X} model also highlights the detrimental effect of cellular infiltration and pathological inflammation in HSE and in virus control, where c-Rel or upstream regulators of the c-Rel pathway may potentially be targeted to reduce inflammation and long-term sequelae in the HSV-1 infected brain.

3.6 ACKNOWLEDGMENTS

We would like to acknowledge the technical expertise and support of Patricia D'Arcy. We also thank the Cell Vision Core Facility at McGill University and the Plateau de biologie moléculaire of the Institut de recherches cliniques de Montréal (IRCM) for their technical assistance. M.M. was supported by the Fonds de recherche du Québec – Santé. S.M.V. was supported by the Canada Research Chair Program. This project was conducted with the support of Canadian Institutes for Health Research Grants CTP-87520 and MOP-238757. The authors declare no financial conflicts of interest.

3.7 FIGURES AND LEGENDS

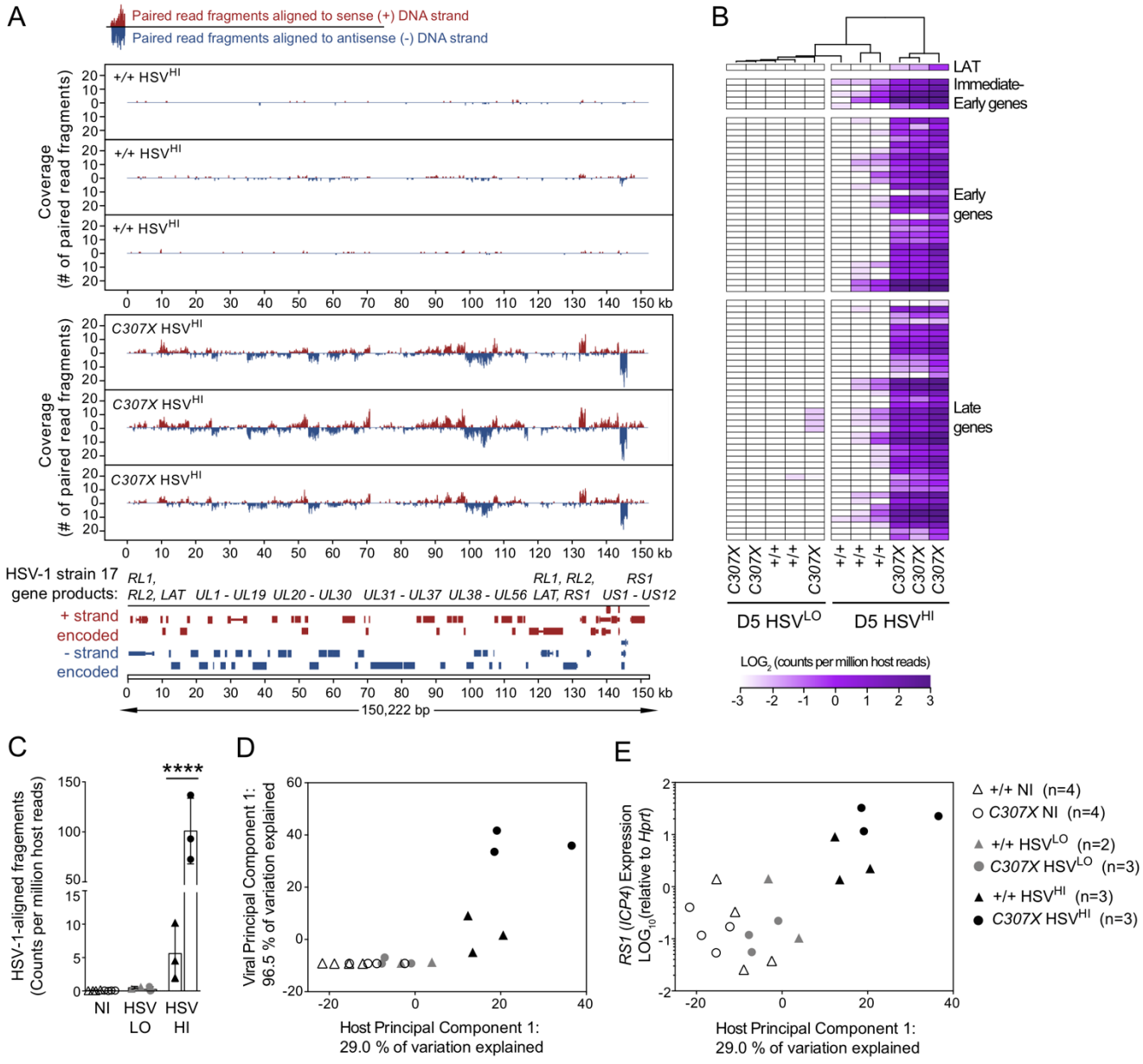

FIGURE 1. Global transcriptional changes in HSV-1-infected brainstems define high and low response groups among Rel$^{+/+}$ and Rel^{C307X} mice.

FIGURE 1. Global transcriptional changes in HSV-1-infected brainstems define high and low response groups among $Rel^{+/+}$ and Rel^{C307X} mice.

Dual RNA sequencing was performed on brainstems collected from HSV-1-infected $Rel^{+/+}$ (n = 5) and Rel^{C307X} (n = 6) female mice at day 5 p.i., along with corresponding and non-infected controls (NI; n = 4 per genotype). (A) Coverage of viral transcript reads mapping to the sense or anti-sense strands of the HSV-1 strain 17 genome. 3 of 5 $Rel^{+/+}$ and 3 of 6 Rel^{C307X} HSV-1-infected samples that demonstrated the highest coverage are denoted (+/+ HSV^{HI}) and (*C307X* HSV^{HI}). (B) Hierarchical clustering of HSV-1-infected samples into high- and low-responding groups [HSV^{HI} or HSV^{LO}] based on the detection of 75 viral open reading frames. These 75 viral transcripts are grouped by their known expression kinetics, namely the immediate-early, early, and late gene phases, and the latency-associated transcript (LAT). (C) Total paired sequence fragments aligning to the HSV-1 genome per group, expressed as counts normalized per million host reads. (D, E) Separate principal component analyses (PCA) for all 19 samples were performed across all 75 viral transcripts, and across 16,303 host genes expressed at > 3 CPM in at least 3 samples. In (D) viral PC1 is shown against host PC1, and in (E) *RS1 (ICP4)* relative expression is shown against host PC1. (C) Data represent mean ± SD. Statistical tests: (C) Two-way ANOVA with Tukey's multiple correction test. **** $p < 0.0001$

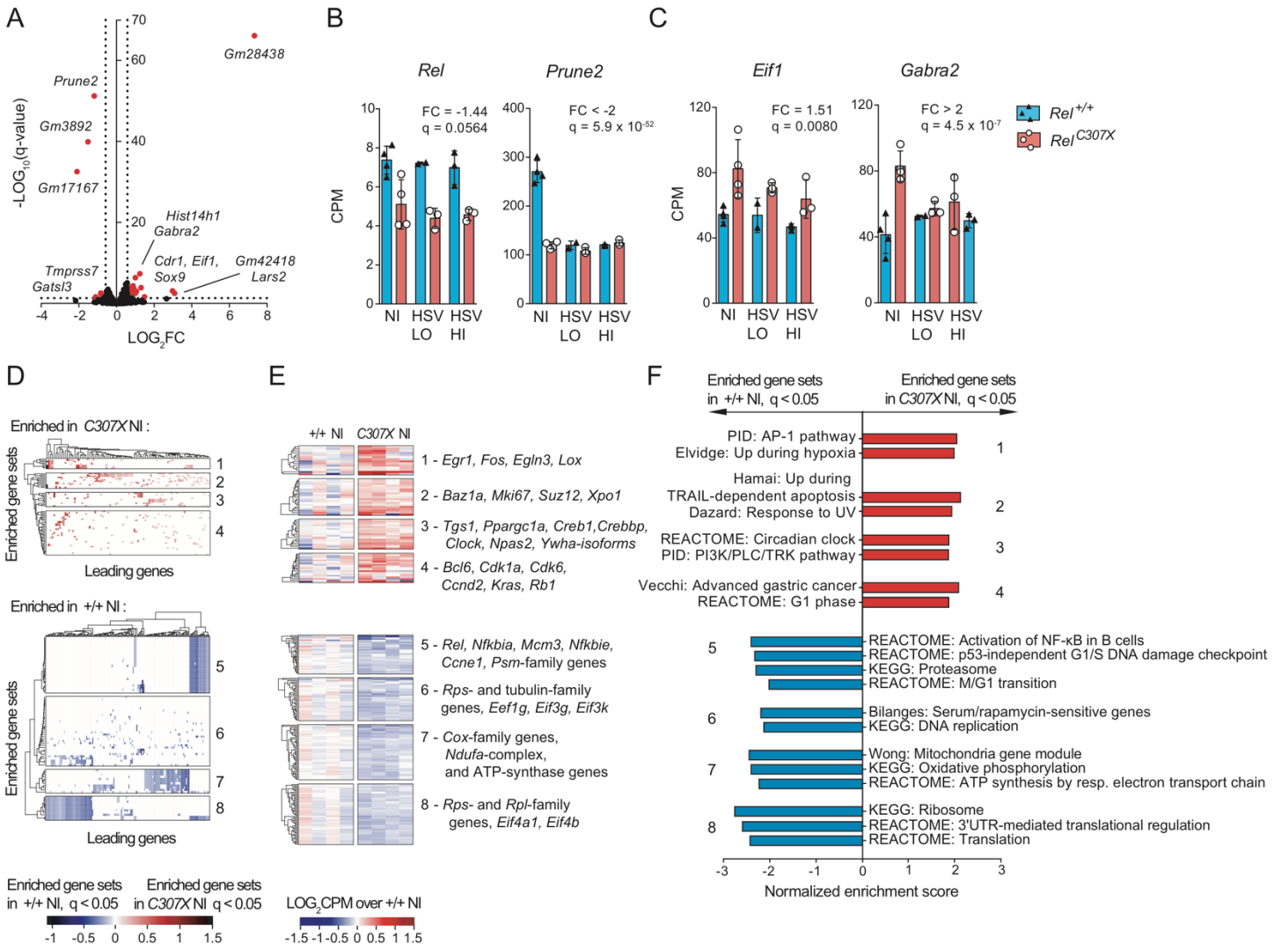

FIGURE 2. Differentially expressed gene networks in non-infected Rel^{C307X} brainstems.

FIGURE 2. Differentially expressed gene networks in non-infected Rel^{C307X} brainstems.
(A) Volcano plot of gene expression differences at steady-state in *C307X* NI compared directly to +/+ NI (n = 4 mice per group). Coloured points indicate differentially expressed genes (36 DEG upregulated, 9 DEG downregulated) with ≥1.5-fold change in expression and that met a threshold of $q < 0.05$ (BH-adjusted). (B, C) Expression of select Rel^{C307X}-downregulated (B) and Rel^{C307X}-upregulated (C) genes identified in A across all sample groups. (D) Hierarchical clustering of leading genes that drive the enrichment ($q < 0.05$) of curated gene sets in *C307X* NI mice (red, N=66) and in +/+ NI mice (blue, N=80) using GSEA. (E) Normalized expression of leading genes common to at least 10% of the enriched gene sets in each cluster defined in D, with select genes highlighted for each cluster. (F) Representative enriched gene sets representative of *C307X* NI (red) and of +/+ NI (blue) enrichment clusters defined in D. (B, C) Data represent mean ± SD; FC and q-values (BH-adjusted) were assessed between NI groups using edgeR. (D and F) q-values (BH-adjusted) and normalized enrichment scores were assessed using GSEA, as further described in Materials and Methods.

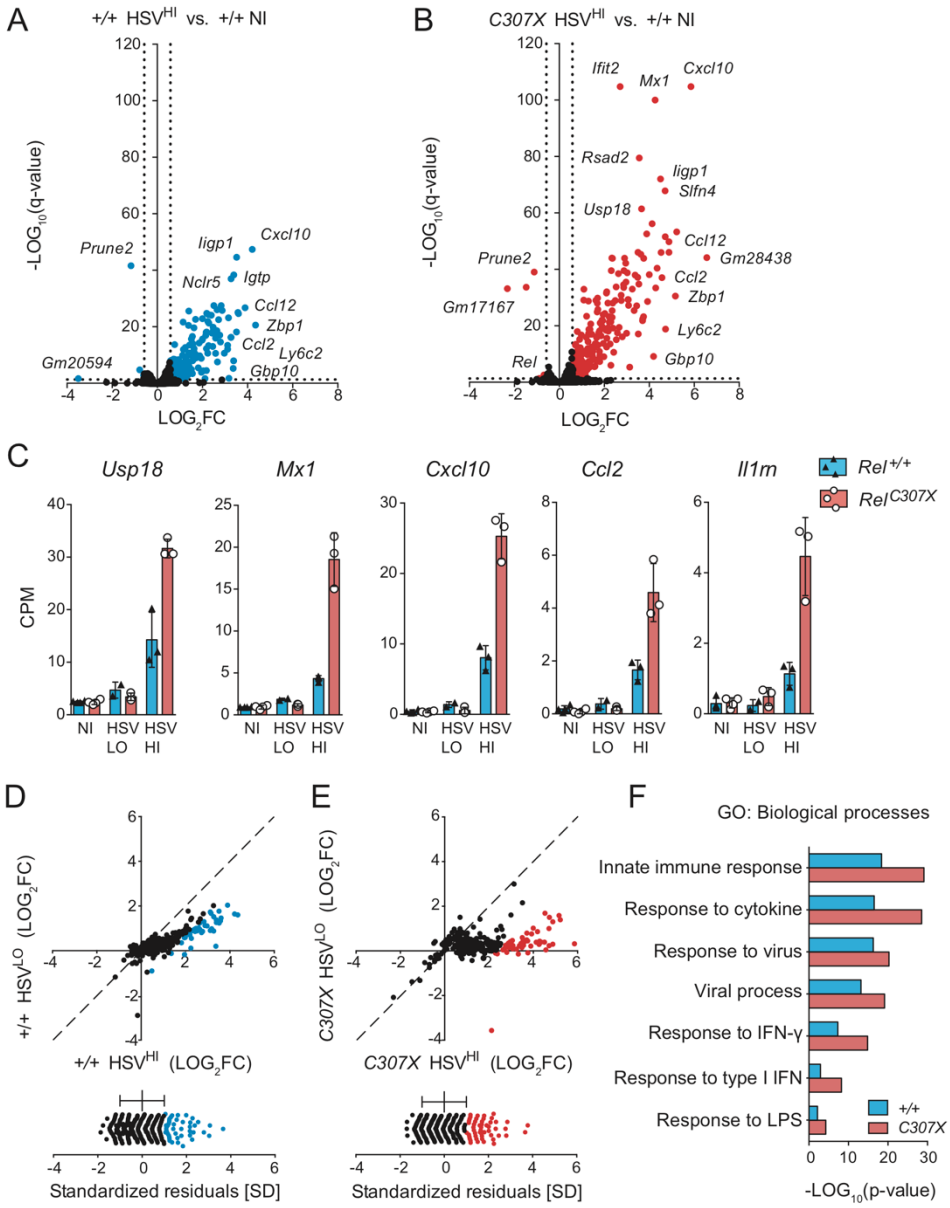

FIGURE 3. Elevated expression of defence response genes in high-responding Rel^{C307X} brainstems at day 5 post HSV-1 infection.

FIGURE 3. Elevated expression of defence response genes in high-responding Rel^{C307X} brainstems at day 5 post HSV-1 infection.

Volcano plots of gene expression changes in (A) +/+ HSV^{HI} brainstems and (B) *C307X* HSV^{HI} brainstems compared to the +/+ NI group. Coloured points indicate differentially expressed genes at a threshold of $q < 0.05$ (B-H-adjusted) and of greater than 1.5-fold change in expression. (C) Expression of select differentially expressed genes (DEG) identified in A and B across all sample groups. (D, E) DEG for both +/+ HSV^{HI} and *C307X* HSV^{HI} high-responders are plotted against their corresponding fold-change in each respective low-responding groups (upper panels). Upregulated genes for which standard residuals > 1 standard deviation from the mean are indicated in blue for +/+ groups, and in red for *C307X* groups (lower panels). (F) Representative gene ontology (GO) terms enriched ($p < 0.05$) in both +/+ and *C307X* gene groups whose standard residuals ≥1 as defined in E and F. (B, C) Data represent mean ± SD. (F) Nominal *p*-values for enriched GO terms were assessed using DAVID, as further described in Materials and Methods.

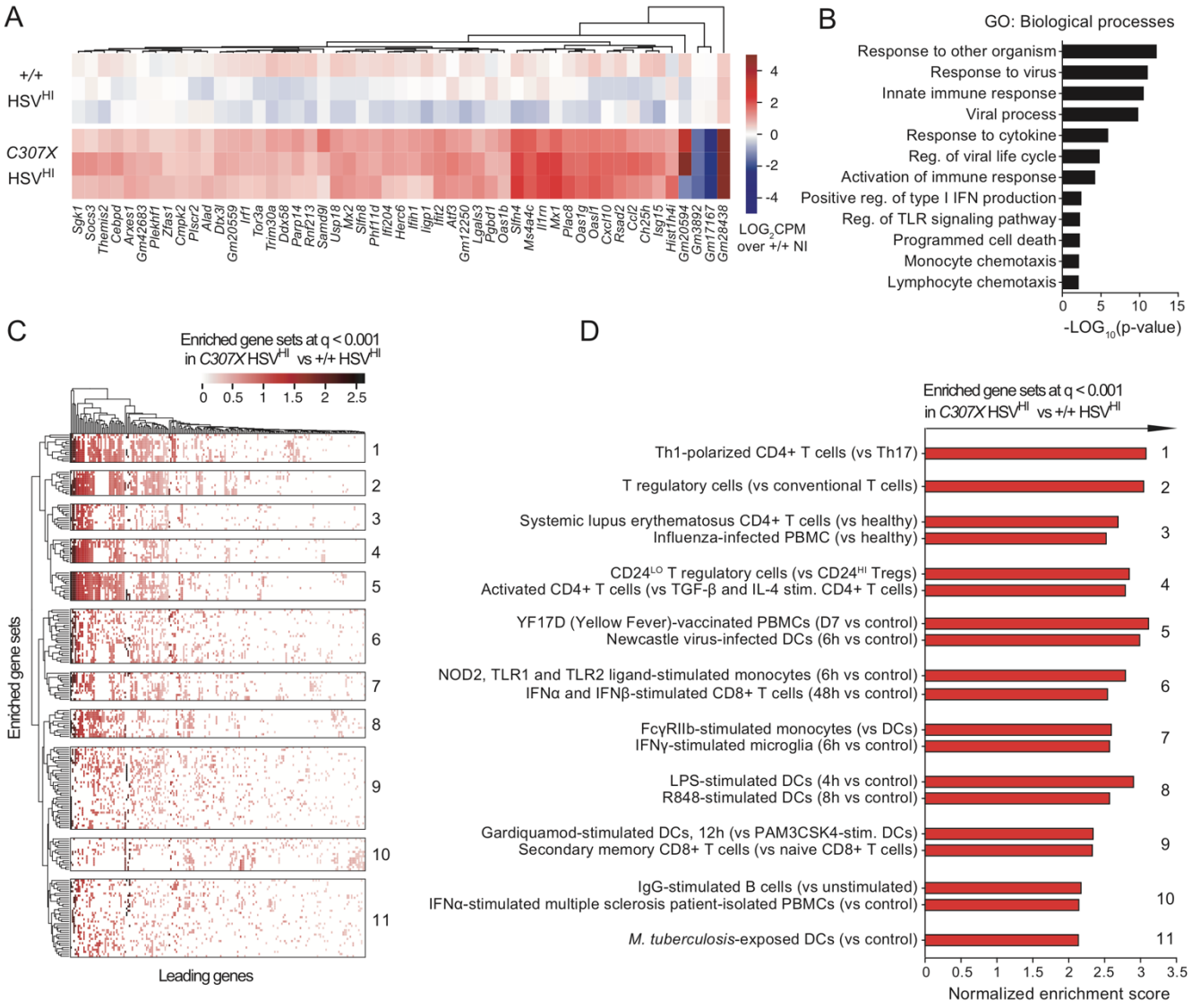

FIGURE 4. Dysregulated IFN and inflammatory pathways in high-responding HSV-1-infected Rel^{C307X} brainstems.

FIGURE 4. Dysregulated IFN and inflammatory pathways in high-responding HSV-1-infected Rel^{C307X} brainstems.

(A) Heatmap of normalized gene expression of 51 DEG [≥ 1.5-fold change in expression, and $q <$ 0.05 (BH-adjusted)] in *C307X* HSV^{HI} compared directly to +/+ HSV^{HI} (n=3 mice per group) in the brainstem at day 5 post HSV-1 infection. (B) Gene ontology (GO) terms enriched ($p < 0.05$) across the 51 *C307X* HSV^{HI} DEG defined in A. (C) Hierarchical clustering of leading genes that drive the enrichment of curated gene sets in *C307X* HSV^{HI} mice compared to +/+ HSV^{HI} mice using GSEA (at least $q < 0.001$, top N=200 gene sets). (D) Normalized enrichment scores for select gene sets enriched in *C307X* HSV^{HI} mice ($q < 0.001$), representative of the 11 clusters defined in C. (B) Nominal p-values for enriched GO terms were assessed as using DAVID, and (C and D) q-values (BH-adjusted) and normalized enrichment scores were assessed using GSEA, as further described in Materials and Methods.

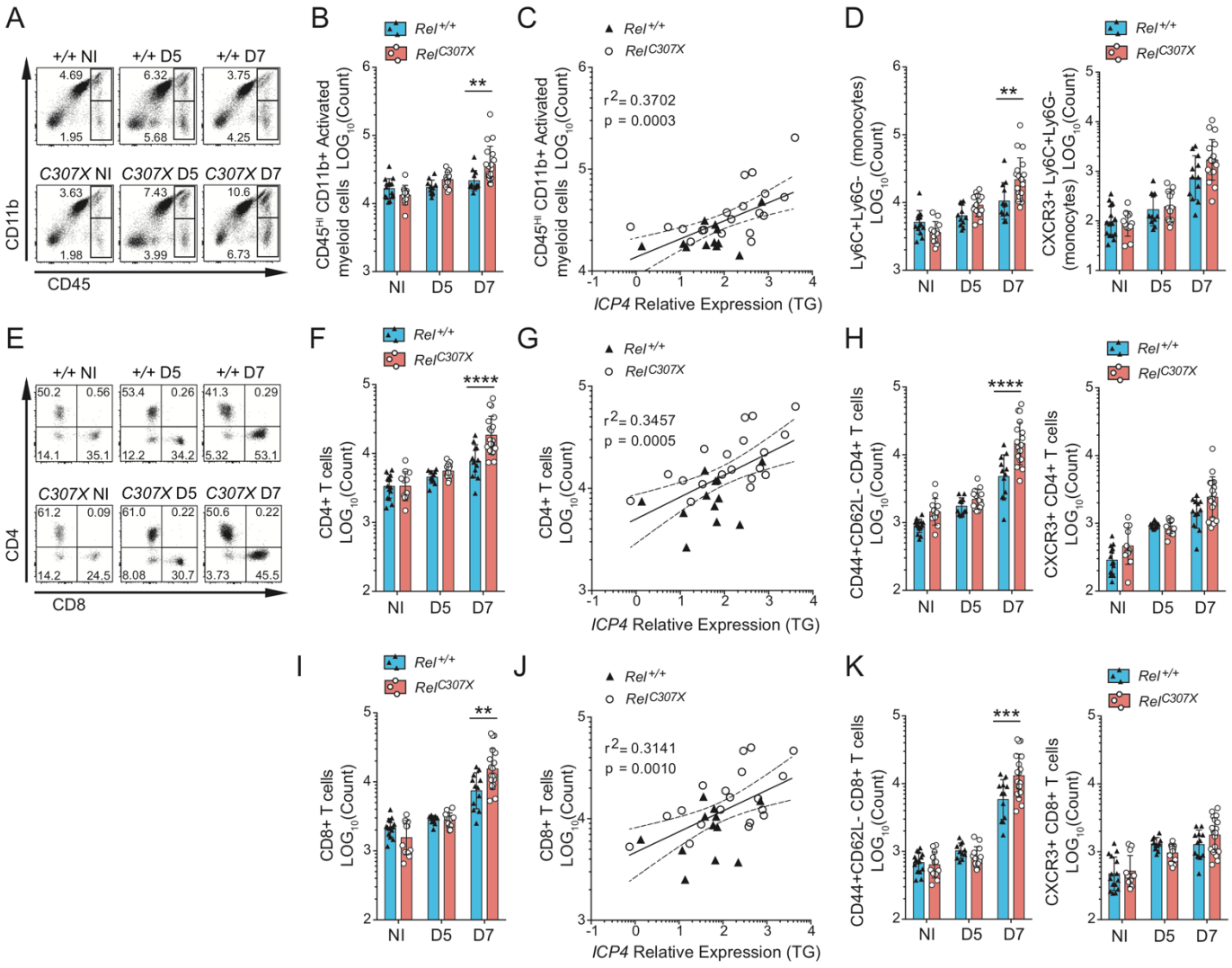

FIGURE 5. Myeloid and T cell infiltrations in the brain of high-responding Rel^{C307X} mice.

FIGURE 5. Myeloid and T cell infiltrations in the brain of high-responding Rel^{C307X} mice.
Whole brain tissue was collected from HSV-1-infected $Rel^{+/+}$ and Rel^{C307X} mice at day 5 (D5) and day 7 (D7) p.i., along with corresponding and non-infected controls (NI) ($n \geq 11$ per group). (A) Flow cytometry plots of representative myeloid ($CD45^{HI}$ $CD11b^{+}$) and lymphoid ($CD45^{HI}$ $CD11b^{-}$) cell populations at NI, D5 and D7 timepoints, and indicating percentages of singlet and viable brain-isolated cells. (B) $CD45^{HI}$ $CD11b^{+}$ activated myeloid cells were enumerated, with (C) D7 cell counts plotted against viral *ICP4* relative expression in corresponding trigeminal ganglia (TG). (D) $Ly6C^{+}Ly6G^{-}$ (monocyte-like) activated myeloid cells were also quantified, as well as $CXCR3^{+}Ly6C^{+}Ly6G^{-}$cells. (E) Flow cytometry plots of representative $CD4^{+}$ and $CD8^{+}$ T cell populations at NI, D5 and D7 timepoints, and indicating percentages of singlet and viable $CD45^{HI}CD11b^{-}CD3^{+}NK1.1^{-}$ T cells. (F) $CD4^{+}$ T cells were enumerated, and (G) D7 cell counts plotted against viral *ICP4* relative expression in corresponding TG. (H) $CD44^{+}CD62L^{-}$ and $CXCR3^{+}$ $CD4^{+}$ T cells were also quantified. (I) $CD8^{+}$ T cells were enumerated, and (J) D7 cell counts plotted against viral *ICP4* relative expression in corresponding TG. (K) $CD44^{+}CD62L^{-}$ and $CXCR3^{+}$ $CD8^{+}$ T cells were also quantified. Full gating strategies are detailed in Supplementary Fig. S3.4C. Experiments include male and female mice, and data represent mean ± SD. Statistical tests: (B, D, F, H, I, K) Two-way ANOVA with Tukey's multiple correction test. (C, G, J) For linear regressions, 95% confidence intervals (dotted lines), r^2, and *p*-values are included to evaluate goodness-of-fit. ** $p < 0.01$, *** $p < 0.001$, **** $p < 0.0001$

3.8 SUPPLEMENTAL MATERIALS

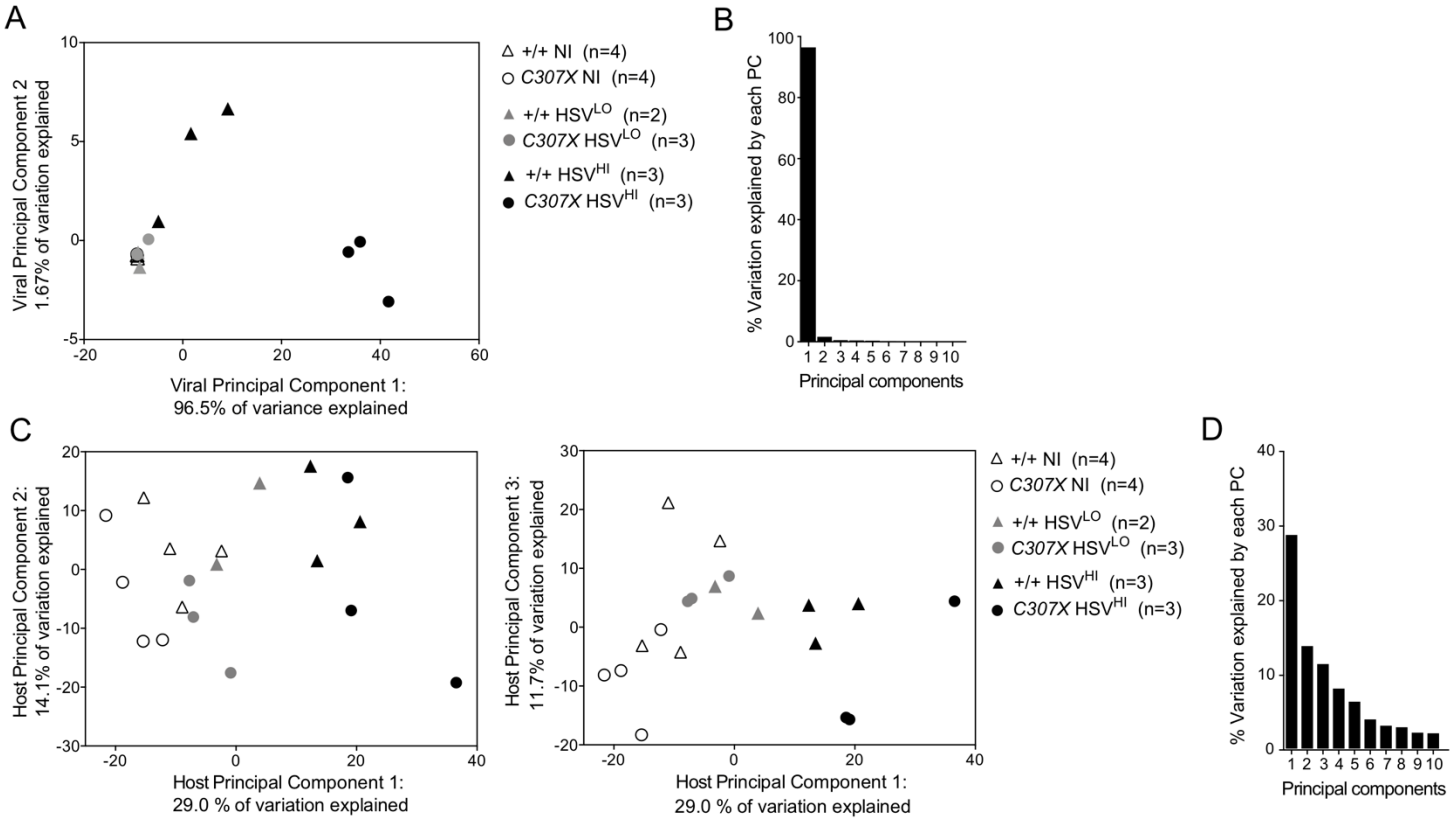

SUPPLEMENTAL FIGURE 1. Dimension reduction analyses of viral and host gene expression. Dual RNA sequencing was performed on brainstems collected from 19 HSV-1-infected mice, here labeled and divided into 6 groups as defined in Figure 1, first by genotype, and further by either non-infected (NI) mice, or low-responders at day 5 p.i. with HSV-1 (HSV^{LO}), or high-responders at day 5 p.i. with HSV-1 (HSV^{HI}). (A) Principal component analysis (PCA) performed for all 19 samples across all 75 viral transcripts, with PC1 plotted against PC2. (B) Percentage of total variation explained by the first viral 10 PC in A. (C) PCA performed for all 19 samples across all 16,303 host genes expressed at ≥ 3 CPM in at least 3 samples, with PC1 plotted against PC2 (left panel), and with PC1 plotted against PC3 (right panel). (D) Percentage of total variation explained by the first 10 host PC in C.

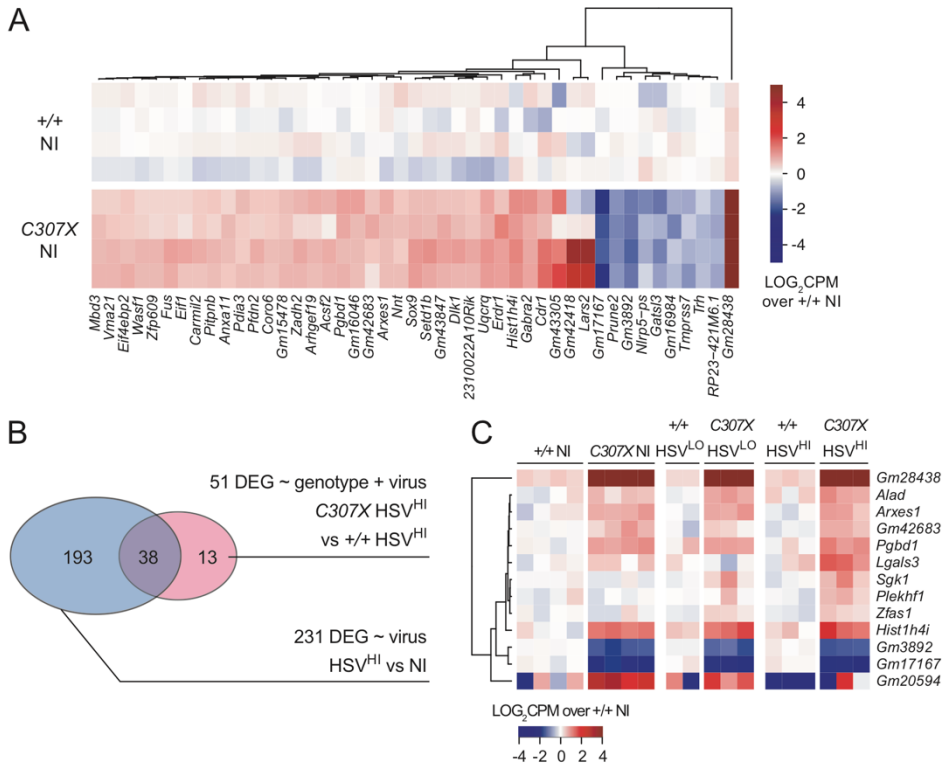

SUPPLEMENTAL FIGURE 2. Non-infected and Rel^{C307X} genotype-dependent gene expression profiles.

(A) Heatmap of normalized gene expression of 45 DEG [≥1.5-fold change in expression, and $q <$ 0.05 (BH-adjusted)] in *C307X* NI compared directly to +/+ NI (n = 4 mice per group). (B) 231 total virus-driven DEG [≥1.5-fold change in expression, and $q <$ 0.05 (BH-adjusted)] were identified by comparing all high-responding HSV^{HI} mice (n = 6) against all NI mice (n = 8), irrespective of genotype. Of the 51 DEG identified between *C307X* HSV^{HI} and +/+ HSV^{HI} mice in Figure 3.4A, 13 DEG varied only due to the contribution of the *Rel*^{C307X} genotype. (C) Heatmap of normalized expression of these 13 *Rel*^{C307X}-specific DEG across all sample groups.

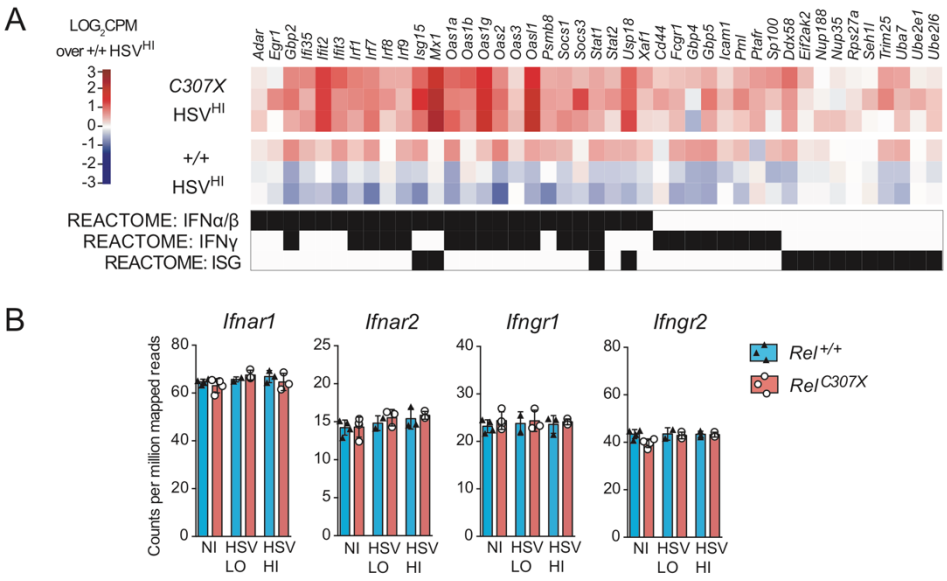

SUPPLEMENTAL FIGURE 3. Expression of IFN-related genes in HSV-1-infected brainstems. (A) Heatmap of normalized expression of select IFN-related genes defined in the REACTOME pathways "Interferon alpha/beta signaling", "Interferon gamma signaling", and "Antiviral mechanism by IFN-stimulated genes" in *C307X* HSV^{HI} brainstems compared to +/+ HSV^{HI} brainstems. (B) Expression of IFN-I and IFN-II receptor genes in the brainstem across all sample groups.

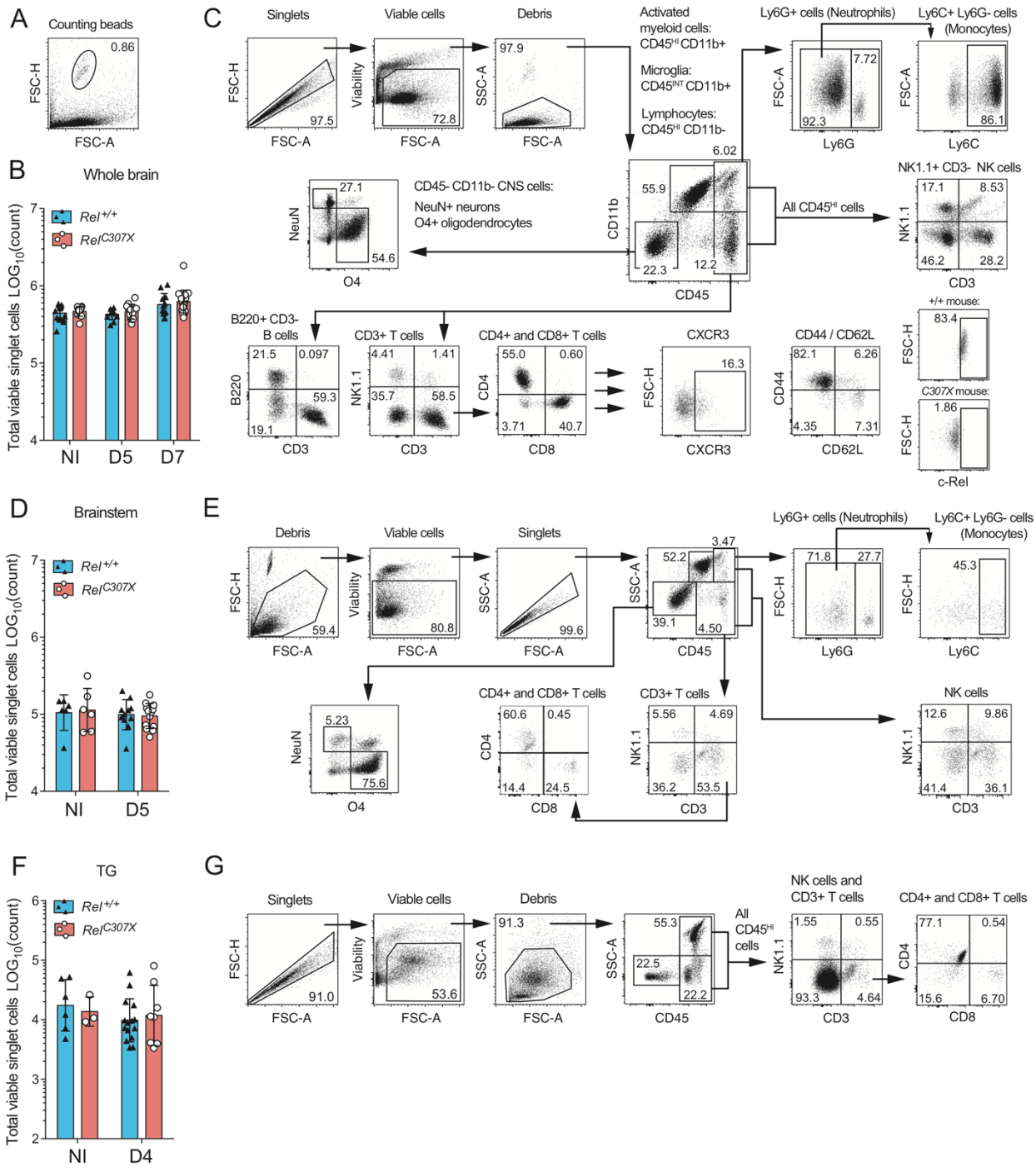

SUPPLEMENTAL FIGURE 4. Gating strategies for flow cytometry in the brain.

SUPPLEMENTAL FIGURE 4. Gating strategies for flow cytometry in the brain.

Whole brain, brainstem and trigeminal ganglia (TG) tissues were processed and single cell suspensions isolated and stained for flow cytometry. (A) Counting beads (5000 per sample) added to each sample immediately prior to acquisition. (B) Total singlet, viable, and debris-excluded cells quantified per sample in the whole brain. (C) Representative gating strategy for cells acquired in day 7 HSV-infected whole brain samples. Cells are first gated on singlet and viable populations, and debris gated out, followed by the separation of key brain-resident and infiltrating populations using CD11b and CD45 markers. From $CD45^{-}CD11b^{-}$ resident cells, neurons ($NeuN^{+}$) and oligodendrocytes ($O4^{+}$) are identified, while resident microglia are $CD45^{INT}CD11b^{+}$. Activated myeloid cells ($CD45^{HI}CD11b^{+}$) may include both inflammatory infiltrating myeloid cells or activated microglia, and are further separated into $Ly6G^{+}$ (neutrophil-like) or $Ly6G^{-}Ly6C^{+}$ (monocyte-like). $NK1.1^{+}CD3^{-}$ NK cells, which may temporarily express $CD11b^{+}$ in their penultimate stage of development, are gated from all $CD45^{HI}$ cells. Lymphocytes ($CD45^{HI}$ $CD11b^{-}$) are gated into $B220^{+}CD3^{-}$ B cells and $CD3^{+}NK1.1^{-}$ T cells, and these T cells further by $CD4^{+}$ and $CD8^{+}$ expression. Further endophenotypes included $CXCR3^{+}$, $CD44^{+}$ or $CD62^{+}$ expressing subsets. Finally, c-Rel expression was quantified in wild-type $Rel^{+/+}$ mice, with Rel^{C307X} mice serving as a biological negative control to set the c-Rel positive gate, owing to the C-terminal-specific anti-c-Rel antibody not recognizing the truncated C307X c-Rel protein. (D) Total debris-gated, viable, and singlet cells quantified per sample in the brainstem. (E) Representative gating strategy for cells acquired in day 5 HSV-infected brainstems, following a similar strategy as described in C. (F) Total singlet, viable and debris-gated cells quantified per sample in the TG. (G) Representative gating strategy for cells acquired in day 4 HSV-infected TG, following a similar strategy as described in C. In the absence of microglia and with fewer total cells, all $CD45^{HI}$ cells were used to better gate NK cells and T cells.

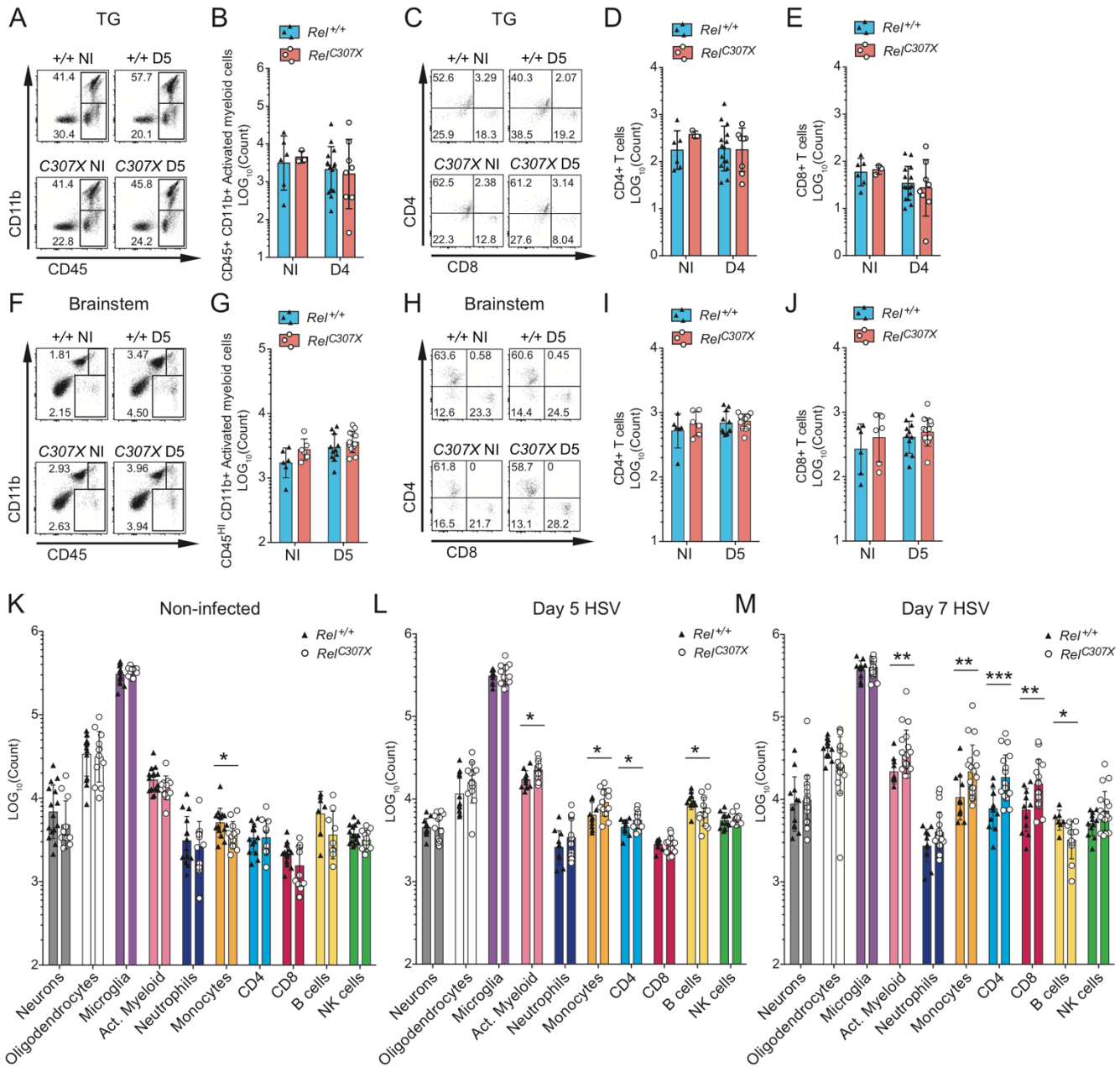

SUPPLEMENTAL FIGURE 5. Flow cytometry analysis of CNS-resident and infiltrating cells.

SUPPLEMENTAL FIGURE 5. Flow cytometry analysis of CNS-resident and infiltrating cells. (A) TG were collected from HSV-1-infected *Rel*$^{+/+}$ and *Rel*^{C307X} mice at day 4 (D4) along with corresponding and non-infected controls (NI) ($n \geq 3$ per group). Flow cytometry plots of representative myeloid ($CD45^+CD11b^+$) and lymphoid ($CD45^+CD11b^-$) cell populations indicate percentages of singlet and viable TG-isolated cells, and $CD45^+CD11b^+$ activated myeloid cells are quantified in (B). (C) In the TG, flow cytometry plots of representative $CD4^+$ and $CD8^+$ T cell populations indicate percentages of $CD45^+CD11b^-CD3^+NK1.1^-$ T cells, and (D) $CD4^+$ and (E) $CD8^+$ T cells are quantified. (F) Brainstems were collected from HSV-1-infected *Rel*$^{+/+}$ and *Rel*^{C307X} mice at day 5 (D5) along with corresponding and non-infected controls (NI) ($n \geq 6$ per group). Flow cytometry plots of representative myeloid ($CD45^{HI}CD11b^+$) and lymphoid ($CD45^+CD11b^-$) cell populations indicate percentages of singlet and viable brainstem-isolated cells, and $CD45^{HI}CD11b^+$ activated myeloid cells are quantified in (G). (H) In the brainstem, flow cytometry plots of representative $CD4^+$ and $CD8^+$ T cell populations indicate percentages of $CD45^+CD11b^-CD3^+NK1.1^-$ T cells, and (I) $CD4^+$ and (J) $CD8^+$ T cells are quantified. In whole brain samples corresponding with Figure 3.5, all myeloid, lymphoid and brain-resident cell populations are enumerated in *Rel*$^{+/+}$ and *Rel*^{C307X} mice by timepoint, namely (K) NI, (L) day 5 post-HSV-1 infection, and (M) day 7 post-HSV-1 infection. Full gating strategies are detailed in Supplementary Fig. S3.4C. Experiments include male and female mice, and data represent mean ± SD. Statistical tests: (B, D, E, G, I, J) Two-way ANOVA with Tukey's multiple correction test. (K-M) Student's T test comparing both genotype groups per cell type. $*p < 0.05$, $**p < 0.01$, $***p < 0.001$, $****p < 0.0001$

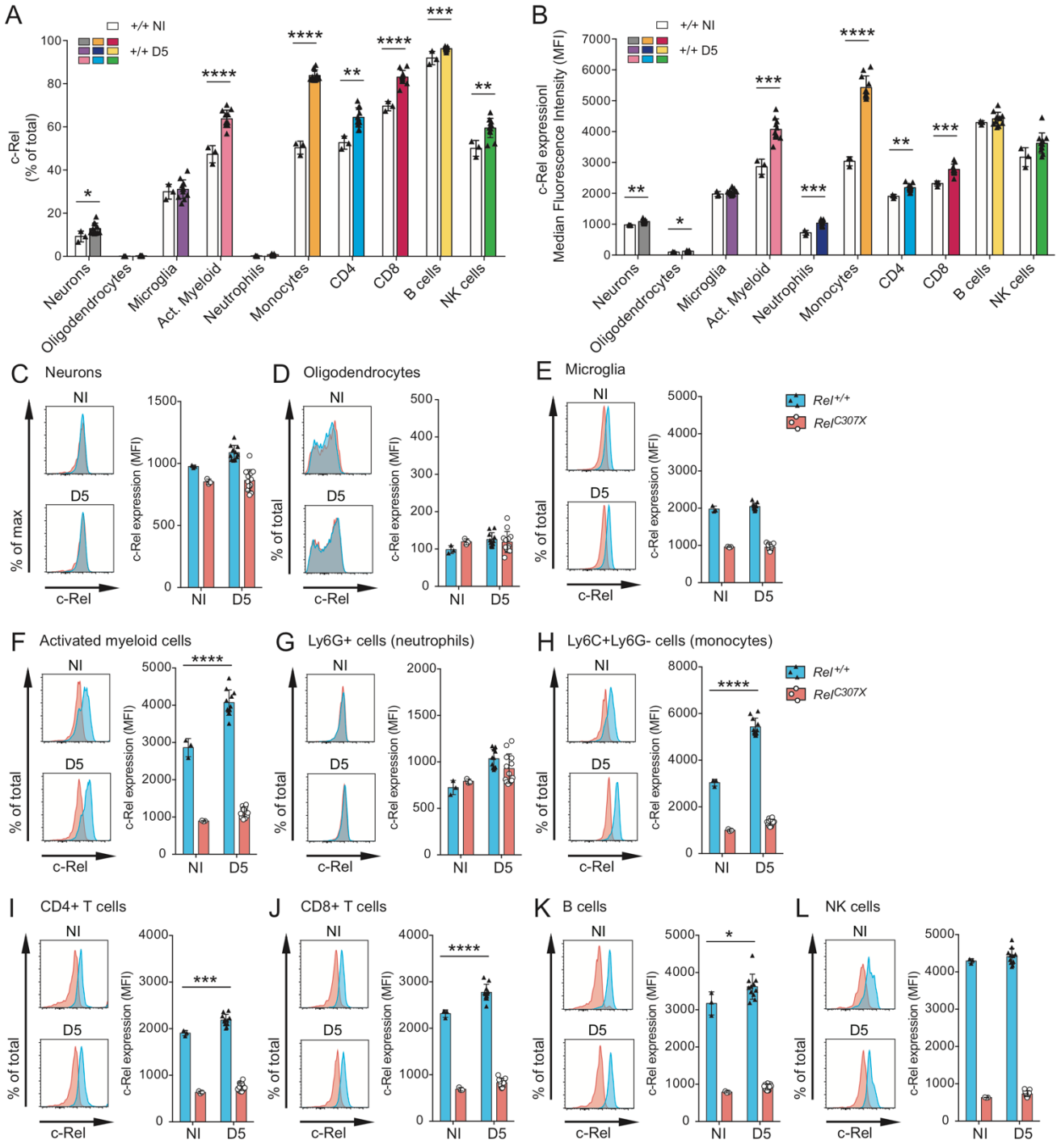

SUPPLEMENTAL FIGURE 6. c-Rel expression in resident and infiltrating cells of the brain.

SUPPLEMENTAL FIGURE 6. c-Rel expression in resident and infiltrating cells of the brain. Expression of c-Rel as a (A) percent of total cells and (B) median fluorescence intensity (MFI) for major resident and infiltrating cell populations in the wild-type $Rel^{+/+}$ whole brain at steady-state (NI in white; n = 3 mice) or at day 5 post HSV-1 infection (D5 in colour; n = 11 mice). Representative histograms depicting c-Rel expression as fluorescence intensity or quantified by MFI for NI and D5-infected $Rel^{+/+}$ and Rel^{C307X} groups in (C) neurons, (D) oligodendrocytes, (E) microglia, (F) Activated myeloid cells, (G) $Ly6G^+$ neutrophil-like and (H) $Ly6C^+Ly6G^-$ monocyte-like activated myeloid cells, (I) $CD4^+$ T cells, (J) $CD8^+$ T cells, (K) B cells, and finally (L) NK cells. Full gating strategies are detailed in Supplementary Fig. S3.4C. Experiments include male and female mice, and data represent mean ± SD. Statistical tests: (A-C) Student's T test comparing both timepoint groups per cell type. (E-L) Two-way ANOVA with Tukey's multiple correction test. $*p < 0.05$, $**p < 0.01$, $***p < 0.001$, $****p < 0.0001$

3.9 REFERENCES

1. Jorgensen LK, Dalgaard LS, Ostergaard LJ, Norgaard M, Mogensen TH. 2017. Incidence and mortality of herpes simplex encephalitis in Denmark: A nationwide registry-based cohort study. *J Infect* 74: 42-49
2. Steiner I. 2011. Herpes simplex virus encephalitis: new infection or reactivation? *Curr Opin Neurol* 24: 268-74
3. Kaewpoowat Q, Salazar L, Aguilera E, Wootton SH, Hasbun R. 2016. Herpes simplex and varicella zoster CNS infections: clinical presentations, treatments and outcomes. *Infection* 44: 337-45
4. Livorsi D, Anderson E, Qureshi S, Howard M, Wang YF, Franco-Paredes C. 2010. Brainstem encephalitis: an unusual presentation of herpes simplex virus infection. *J Neurol* 257: 1432-7
5. Casrouge A, Zhang SY, Eidenschenk C, Jouanguy E, Puel A, Yang K, Alcais A, Picard C, Mahfoufi N, Nicolas N, Lorenzo L, et al. 2006. Herpes simplex virus encephalitis in human UNC-93B deficiency. *Science* 314: 308-12
6. Herman M, Ciancanelli M, Ou YH, Lorenzo L, Klaudel-Dreszler M, Pauwels E, Sancho-Shimizu V, Perez de Diego R, Abhyankar A, Israelsson E, Guo Y, et al. 2012. Heterozygous TBK1 mutations impair TLR3 immunity and underlie herpes simplex encephalitis of childhood. *J Exp Med* 209: 1567-82
7. Perez de Diego R, Sancho-Shimizu V, Lorenzo L, Puel A, Plancoulaine S, Picard C, Herman M, Cardon A, Durandy A, Bustamante J, Vallabhapurapu S, et al. 2010. Human TRAF3 adaptor molecule deficiency leads to impaired Toll-like receptor 3 response and susceptibility to herpes simplex encephalitis. *Immunity* 33: 400-11
8. Sancho-Shimizu V, Perez de Diego R, Lorenzo L, Halwani R, Alangari A, Israelsson E, Fabrega S, Cardon A, Maluenda J, Tatematsu M, Mahvelati F, et al. 2011. Herpes simplex encephalitis in children with autosomal recessive and dominant TRIF deficiency. *J Clin Invest* 121: 4889-902
9. Zhang SY, Jouanguy E, Ugolini S, Smahi A, Elain G, Romero P, Segal D, Sancho-Shimizu V, Lorenzo L, Puel A, Picard C, et al. 2007. TLR3 deficiency in patients with herpes simplex encephalitis. *Science* 317: 1522-7

10. Andersen LL, Mork N, Reinert LS, Kofod-Olsen E, Narita R, Jorgensen SE, Skipper KA, Honing K, Gad HH, Ostergaard L, Orntoft TF, et al. 2015. Functional IRF3 deficiency in a patient with herpes simplex encephalitis. *J Exp Med* 212: 1371-9
11. Lafaille FG, Pessach IM, Zhang SY, Ciancanelli MJ, Herman M, Abhyankar A, Ying SW, Keros S, Goldstein PA, Mostoslavsky G, Ordovas-Montanes J, et al. 2012. Impaired intrinsic immunity to HSV-1 in human iPSC-derived TLR3-deficient CNS cells. *Nature* 491: 769-73
12. Lafaille FG, Harschnitz O, Lee YS, Zhang P, Hasek ML, Kerner G, Itan Y, Ewaleifoh O, Rapaport F, Carlile TM, Carter-Timofte ME, et al. 2019. Human SNORA31 variations impair cortical neuron-intrinsic immunity to HSV-1 and underlie herpes simplex encephalitis. *Nat Med* 25: 1873-84
13. Zhang SY, Clark NE, Freije CA, Pauwels E, Taggart AJ, Okada S, Mandel H, Garcia P, Ciancanelli MJ, Biran A, Lafaille FG, et al. 2018. Inborn Errors of RNA Lariat Metabolism in Humans with Brainstem Viral Infection. *Cell* 172: 952-65.e18
14. Bibert S, Piret J, Quinodoz M, Collinet E, Zoete V, Michielin O, Menasria R, Meylan P, Bihl T, Erard V, Fellmann F, et al. 2019. Herpes simplex encephalitis in adult patients with MASP-2 deficiency. *PLoS Pathog* 15: e1008168
15. Mancini M, Vidal SM. 2018. Insights into the pathogenesis of herpes simplex encephalitis from mouse models. *Mamm Genome* 29: 425-45
16. Lokensgard JR, Hu S, Sheng W, vanOijen M, Cox D, Cheeran MC, Peterson PK. 2001. Robust expression of TNF-alpha, IL-1beta, RANTES, and IP-10 by human microglial cells during nonproductive infection with herpes simplex virus. *J Neurovirol* 7: 208-19
17. Wuest TR, Carr DJ. 2008. Dysregulation of CXCR3 signaling due to CXCL10 deficiency impairs the antiviral response to herpes simplex virus 1 infection. *J Immunol* 181: 7985-93
18. Menasria R, Canivet C, Piret J, Gosselin J, Boivin G. 2017. Protective role of CX3CR1 signalling in resident cells of the central nervous system during experimental herpes simplex virus encephalitis. *J Gen Virol* 98: 447-60
19. Kastrukoff LF, Lau AS, Takei F, Carbone FR, Scalzo AA. 2015. A NK complex-linked locus restricts the spread of herpes simplex virus type 1 in the brains of C57BL/6 mice. *Immunol Cell Biol* 93: 877-84

20. Caignard G, Leiva-Torres GA, Leney-Greene M, Charbonneau B, Dumaine A, Fodil-Cornu N, Pyzik M, Cingolani P, Schwartzentruber J, Dupaul-Chicoine J, Guo H, et al. 2013. Genome-wide mouse mutagenesis reveals CD45-mediated T cell function as critical in protective immunity to HSV-1. *PLoS Pathog* 9: e1003637
21. Zimmermann J, Hafezi W, Dockhorn A, Lorentzen EU, Krauthausen M, Getts DR, Muller M, Kuhn JE, King NJC. 2017. Enhanced viral clearance and reduced leukocyte infiltration in experimental herpes encephalitis after intranasal infection of CXCR3-deficient mice. *J Neurovirol* 23: 394-403
22. Vilela MC, Lima GK, Rodrigues DH, Lacerda-Queiroz N, Pedroso VS, Miranda AS, Rachid MA, Kroon EG, Campos MA, Teixeira MM, Sellner J, et al. 2013. Absence of CCR5 increases neutrophil recruitment in severe herpetic encephalitis. *BMC Neurosci* 14: 19
23. Wickham S, Lu B, Ash J, Carr DJ. 2005. Chemokine receptor deficiency is associated with increased chemokine expression in the peripheral and central nervous systems and increased resistance to herpetic encephalitis. *J Neuroimmunol* 162: 51-9
24. Menasria R, Canivet C, Piret J, Boivin G. 2015. Infiltration Pattern of Blood Monocytes into the Central Nervous System during Experimental Herpes Simplex Virus Encephalitis. *PLoS One* 10: e0145773
25. Ramakrishna C, Cantin EM. 2018. IFNgamma inhibits G-CSF induced neutrophil expansion and invasion of the CNS to prevent viral encephalitis. *PLoS Pathog* 14: e1006822
26. Mancini M, Caignard G, Charbonneau B, Dumaine A, Wu N, Leiva-Torres GA, Gerondakis S, Pearson A, Qureshi ST, Sladek R, Vidal SM. 2019. Rel-Dependent Immune and Central Nervous System Mechanisms Control Viral Replication and Inflammation during Mouse Herpes Simplex Encephalitis. *J Immunol* 202: 1479-93
27. Katzenell S, Cabrera JR, North BJ, Leib DA. 2017. Isolation, Purification, and Culture of Primary Murine Sensory Neurons. *Methods Mol Biol* 1656: 229-51
28. Langlais D, Barreiro LB, Gros P. 2016. The macrophage IRF8/IRF1 regulome is required for protection against infections and is associated with chronic inflammation. *J Exp Med* 213: 585-603

29. Bolger AM, Lohse M, Usadel B. 2014. Trimmomatic: a flexible trimmer for Illumina sequence data. *Bioinformatics* 30: 2114-20
30. Kim D, Pertea G, Trapnell C, Pimentel H, Kelley R, Salzberg SL. 2013. TopHat2: accurate alignment of transcriptomes in the presence of insertions, deletions and gene fusions. *Genome Biol* 14: R36
31. Langmead B, Salzberg SL. 2012. Fast gapped-read alignment with Bowtie 2. *Nat Methods* 9: 357-9
32. Liao Y, Smyth GK, Shi W. 2014. featureCounts: an efficient general purpose program for assigning sequence reads to genomic features. *Bioinformatics* 30: 923-30
33. Kim D, Paggi JM, Park C, Bennett C, Salzberg SL. 2019. Graph-based genome alignment and genotyping with HISAT2 and HISAT-genotype. *Nat Biotechnol* 37: 907-15
34. Davison AJ. 2011. Evolution of sexually transmitted and sexually transmissible human herpesviruses. *Ann N Y Acad Sci* 1230: E37-49
35. Robinson MD, Oshlack A. 2010. A scaling normalization method for differential expression analysis of RNA-seq data. *Genome Biol* 11: R25
36. Huang da W, Sherman BT, Lempicki RA. 2009. Systematic and integrative analysis of large gene lists using DAVID bioinformatics resources. *Nat Protoc* 4: 44-57
37. Subramanian A, Tamayo P, Mootha VK, Mukherjee S, Ebert BL, Gillette MA, Paulovich A, Pomeroy SL, Golub TR, Lander ES, Mesirov JP. 2005. Gene set enrichment analysis: a knowledge-based approach for interpreting genome-wide expression profiles. *Proc Natl Acad Sci U S A* 102: 15545-50
38. Legroux L, Pittet CL, Beauseigle D, Deblois G, Prat A, Arbour N. 2015. An optimized method to process mouse CNS to simultaneously analyze neural cells and leukocytes by flow cytometry. *J Neurosci Methods* 247: 23-31
39. Pasieka TJ, Cilloniz C, Carter VS, Rosato P, Katze MG, Leib DA. 2011. Functional genomics reveals an essential and specific role for Stat1 in protection of the central nervous system following herpes simplex virus corneal infection. *J Virol* 85: 12972-81
40. Stingley SW, Ramirez JJ, Aguilar SA, Simmen K, Sandri-Goldin RM, Ghazal P, Wagner EK. 2000. Global analysis of herpes simplex virus type 1 transcription using an oligonucleotide-based DNA microarray. *J Virol* 74: 9916-27

41. Islam MS, Takano R, Yokochi T, Akter J, Nakamura Y, Nakagawara A, Tatsumi Y. 2019. Programmed expression of pro-apoptotic BMCC1 during apoptosis, triggered by DNA damage in neuroblastoma cells. *BMC Cancer* 19: 542
42. Gonzalez-Nunez V. 2015. Role of gabra2, GABA(A) receptor alpha-2 subunit, in CNS development. *Biochem Biophys Rep* 3: 190-201
43. Inoue K, Sakuma E, Morimoto H, Asai H, Koide Y, Leng T, Wada I, Xiong ZG, Ueki T. 2016. Serum- and glucocorticoid-inducible kinases in microglia. *Biochem Biophys Res Commun* 478: 53-59
44. Pizzi M, Goffi F, Boroni F, Benarese M, Perkins SE, Liou HC, Spano P. 2002. Opposing roles for NF-kappa B/Rel factors p65 and c-Rel in the modulation of neuron survival elicited by glutamate and interleukin-1beta. *J Biol Chem* 277: 20717-23
45. Musiek ES, Lim MM, Yang G, Bauer AQ, Qi L, Lee Y, Roh JH, Ortiz-Gonzalez X, Dearborn JT, Culver JP, Herzog ED, et al. 2013. Circadian clock proteins regulate neuronal redox homeostasis and neurodegeneration. *J Clin Invest* 123: 5389-400
46. Atkins CM, Oliva AA, Jr., Alonso OF, Pearse DD, Bramlett HM, Dietrich WD. 2007. Modulation of the cAMP signaling pathway after traumatic brain injury. *Exp Neurol* 208: 145-58
47. Volosin M, Song W, Almeida RD, Kaplan DR, Hempstead BL, Friedman WJ. 2006. Interaction of survival and death signaling in basal forebrain neurons: roles of neurotrophins and proneurotrophins. *J Neurosci* 26: 7756-66
48. Rehman SU, Ikram M, Ullah N, Alam SI, Park HY, Badshah H, Choe K, Kim MO. 2019. Neurological Enhancement Effects of Melatonin against Brain Injury-Induced Oxidative Stress, Neuroinflammation, and Neurodegeneration via AMPK/CREB Signaling. *Cells* 8
49. Zhou Z, Ikegaya Y, Koyama R. 2019. The Astrocytic cAMP Pathway in Health and Disease. *Int J Mol Sci* 20
50. Mold JE, Réu P, Olin A, Bernard S, Michaëlsson J, Rane S, Yates A, Khosravi A, Salehpour M, Possnert G, Brodin P, et al. 2019. Cell generation dynamics underlying naive T-cell homeostasis in adult humans. *PLoS Biol* 17: e3000383
51. Tatsumi Y, Takano R, Islam MS, Yokochi T, Itami M, Nakamura Y, Nakagawara A. 2015. BMCC1, which is an interacting partner of BCL2, attenuates AKT activity, accompanied by apoptosis. *Cell Death Dis* 6: e1607

52. Wang Z, Dong H, Wang J, Huang Y, Zhang X, Tang Y, Li Q, Liu Z, Ma Y, Tong J, Huang L, et al. 2020. Pro-survival and anti-inflammatory roles of NF-κB c-Rel in the Parkinson's disease models. *Redox Biol* 30: 101427
53. Parrella E, Bellucci A, Porrini V, Benarese M, Lanzillotta A, Faustini G, Longhena F, Abate G, Uberti D, Pizzi M. 2019. NF-κB/c-Rel deficiency causes Parkinson's disease-like prodromal symptoms and progressive pathology in mice. *Transl Neurodegener* 8: 16
54. Wang JP, Bowen GN, Zhou S, Cerny A, Zacharia A, Knipe DM, Finberg RW, Kurt-Jones EA. 2012. Role of specific innate immune responses in herpes simplex virus infection of the central nervous system. *J Virol* 86: 2273-81
55. Casanova JL. 2015. Severe infectious diseases of childhood as monogenic inborn errors of immunity. *Proc Natl Acad Sci U S A* 112: E7128-37
56. Zhao T, Yang L, Sun Q, Arguello M, Ballard DW, Hiscott J, Lin R. 2007. The NEMO adaptor bridges the nuclear factor-kappaB and interferon regulatory factor signaling pathways. *Nat Immunol* 8: 592-600
57. Crow YJ. 2013. Aicardi-Goutières syndrome. *Handb Clin Neurol* 113: 1629-35
58. Zhang X, Bogunovic D, Payelle-Brogard B, Francois-Newton V, Speer SD, Yuan C, Volpi S, Li Z, Sanal O, Mansouri D, Tezcan I, et al. 2015. Human intracellular ISG15 prevents interferon-α/β over-amplification and auto-inflammation. *Nature* 517: 89-93
59. Jiang J, Zhao M, Chang C, Wu H, Lu Q. 2020. Type I Interferons in the Pathogenesis and Treatment of Autoimmune Diseases. *Clin Rev Allergy Immunol*
60. Singhania A, Verma R, Graham CM, Lee J, Tran T, Richardson M, Lecine P, Leissner P, Berry MPR, Wilkinson RJ, Kaiser K, et al. 2018. A modular transcriptional signature identifies phenotypic heterogeneity of human tuberculosis infection. *Nat Commun* 9: 2308
61. Torre S, Polyak MJ, Langlais D, Fodil N, Kennedy JM, Radovanovic I, Berghout J, Leiva-Torres GA, Krawczyk CM, Ilangumaran S, Mossman K, et al. 2017. USP15 regulates type I interferon response and is required for pathogenesis of neuroinflammation. *Nat Immunol* 18: 54-63
62. Barrett JP, Henry RJ, Shirey KA, Doran SJ, Makarevich OD, Ritzel RM, Meadows VA, Vogel SN, Faden AI, Stoica BA, Loane DJ. 2020. Interferon-β Plays a Detrimental Role in Experimental Traumatic Brain Injury by Enhancing Neuroinflammation That Drives Chronic Neurodegeneration. *J Neurosci* 40: 2357-70

63. Abdullah A, Zhang M, Frugier T, Bedoui S, Taylor JM, Crack PJ. 2018. STING-mediated type-I interferons contribute to the neuroinflammatory process and detrimental effects following traumatic brain injury. *J Neuroinflammation* 15: 323

64. Kasztelewicz B, Jankowska I, Pawłowska J, Teisseyre J, Dzierżanowska-Fangrat K. 2012. The impact of cytokine gene polymorphisms on Epstein-Barr virus infection outcome in pediatric liver transplant recipients. *J Clin Virol* 55: 226-32

65. Bank S, Julsgaard M, Abed OK, Burisch J, Broder Brodersen J, Pedersen NK, Gouliaev A, Ajan R, Nytoft Rasmussen D, Honore Grauslund C, Roug S, et al. 2019. Polymorphisms in the NFkB, TNF-alpha, IL-1beta, and IL-18 pathways are associated with response to anti-TNF therapy in Danish patients with inflammatory bowel disease. *Aliment Pharmacol Ther* 49: 890-903

66. Oudot T, Lesueur F, Guedj M, de Cid R, McGinn S, Heath S, Foglio M, Prum B, Lathrop M, Prud'homme JF, Fischer J. 2009. An association study of 22 candidate genes in psoriasis families reveals shared genetic factors with other autoimmune and skin disorders. *J Invest Dermatol* 129: 2637-45

67. Bunting K, Rao S, Hardy K, Woltring D, Denyer GS, Wang J, Gerondakis S, Shannon MF. 2007. Genome-wide analysis of gene expression in T cells to identify targets of the NF-kappa B transcription factor c-Rel. *J Immunol* 178: 7097-109

68. Marques CP, Cheeran MC, Palmquist JM, Hu S, Urban SL, Lokensgard JR. 2008. Prolonged microglial cell activation and lymphocyte infiltration following experimental herpes encephalitis. *J Immunol* 181: 6417-26

69. Harling-McNabb L, Deliyannis G, Jackson DC, Gerondakis S, Grigoriadis G, Brown LE. 1999. Mice lacking the transcription factor subunit Rel can clear an influenza infection and have functional anti-viral cytotoxic T cells but do not develop an optimal antibody response. *Int Immunol* 11: 1431-9

70. Chen G, Hardy K, Pagler E, Ma L, Lee S, Gerondakis S, Daley S, Shannon MF. 2011. The NF-κB transcription factor c-Rel is required for Th17 effector cell development in experimental autoimmune encephalomyelitis. *J Immunol* 187: 4483-91

71. Visekruna A, Linnerz T, Martinic V, Vachharajani N, Hartmann S, Harb H, Joeris T, Pfefferle PI, Hofer MJ, Steinhoff U. 2015. Transcription factor c-Rel plays a crucial role in driving anti-CD40-mediated innate colitis. *Mucosal Immunol* 8: 307-15

72. Mason NJ, Liou HC, Hunter CA. 2004. T cell-intrinsic expression of c-Rel regulates Th1 cell responses essential for resistance to Toxoplasma gondii. *J Immunol* 172: 3704-11
73. Reinhard K, Huber M, Wostl C, Hellhund A, Toboldt A, Abass E, Casper B, Joeris T, Herr C, Bals R, Steinhoff U, et al. 2011. c-Rel promotes type 1 and type 17 immune responses during Leishmania major infection. *Eur J Immunol* 41: 1388-98
74. Luu M, Romero R, Bazant J, Abass E, Hartmann S, Leister H, Fischer F, Mahdavi R, Plaza-Sirvent C, Schmitz I, Steinhoff U, et al. 2020. The NF-κB transcription factor c-Rel controls host defense against Citrobacter rodentium. *Eur J Immunol* 50: 292-94
75. Burkitt MD, Hanedi AF, Duckworth CA, Williams JM, Tang JM, O'Reilly LA, Putoczki TL, Gerondakis S, Dimaline R, Caamano JH, Pritchard DM. 2015. NF-κB1, NF-κB2 and c-Rel differentially regulate susceptibility to colitis-associated adenoma development in C57BL/6 mice. *J Pathol* 236: 326-36
76. Beaussant-Cohen S, Jaber F, Massaad MJ, Weeks S, Jones J, Alosaimi MF, Wallace J, Al-Herz W, Geha RS, Chou J. 2019. Combined immunodeficiency in a patient with c-Rel deficiency. *J Allergy Clin Immunol* 144: 606-08.e4

BRIDGING STATEMENT TO CHAPTER FOUR

The previous two chapters provide an in-depth characterization of a novel chemically-induced *Rel*^{C307X} mutation and its associated phenotypes as they relate to HSE disease. Interestingly, HSE susceptibility relied on *Rel*^{C307X}-dependent defects in both brain resident and infiltrating hematopoietic cell compartments, and on dysregulated and augmented type I IFN-related responses in the brain. As a novel HSE etiology in mice, *Rel* is distinct from the type I IFN deficiencies that account for a majority of childhood HSE cases for which a genetic cause has been reported, and instead emphasizes the contribution of cell-mediated pathological inflammation and cell death to HSE. Specifically, our studies have helped to define CD4^{+} T cells and infiltrating activated myeloid cells as linchpins of these adverse responses, and likely to be most affected by defective regulation by the truncated C307X c-Rel transcription factor.

The susceptible *Rel*^{C307X} HSE model also stood out among other disease models that we routinely employ in our laboratory, where preliminary investigations showed that *Rel*^{C307X} mice were resistant to influenza infection and to experimental autoimmune encephalomyelitis (EAE), a model of multiple sclerosis-like disease. Considering that immune responses to viruses must often balance antiviral immunity against excess damage to the host, we questioned if *Rel*^{C307X}-dependent defects or mechanisms that were detrimental in HSE, would be otherwise beneficial in another infection. We selected coxsackievirus B3 (CVB3), an RNA enterovirus known to induce viral myocarditis in the hearts of genetically susceptible mice, as the focus of the following chapter. From the literature, studies have suggested that NF-κB responses may be detrimental to CVB3 myocarditis in mice, with upstream adaptor *Myd88*$^{-/-}$ mice being resistant to infection compared to susceptible wild-type mice. As our group and others have shown, *Myd88*$^{-/-}$ mice are susceptible to HSE. Thus, we hypothesized that *Rel*^{C307X} mice would be resistant to CVB3 infection. The following chapter will examine the effect of the mutation in an opposite model; CVB3 is an RNA virus, cardiotropic, and resident cardiomyocytes may have a different tolerance to inflammation. Yet, both the heart and the brain are essential organs, with high energy requirements, and likely to attract a similar profile of infiltrating c-Rel-expressing immune cells in response to viral infection. The CVB3 model would also provide a further opportunity to refine our two-pronged RNA sequencing/flow cytometry approach to understand regulatory disruptions in the *Rel*^{C307X} transcriptional landscape.

CHAPTER FOUR: A TRUNCATING MUTATION IN THE c-REL TRANSCRIPTION FACTOR PROTECTS MICE FROM LETHAL COXSACKIEVIRAL MYOCARDITIS

Mathieu Mancini,[*,†] Benoît Charbonneau,[*,†] Jennifer Marton,[*,†] Steve Gerondakis,[‡,§] David Langlais[*,†,¶] and Silvia M. Vidal[*, †, | |,#]

∗ Department of Human Genetics, McGill University, Montréal, Québec, Canada

† McGill University Research Centre on Complex Traits, McGill University, Montréal, Québec, Canada

‡ Biomedicine Discovery Institute, Monash University, Clayton, Victoria, Australia

§ Department of Biochemistry and Molecular Biology, Monash University, Clayton, Victoria, Australia

¶ McGill University Genome Centre, Montréal, Québec, Canada

| | Department of Medicine, McGill University, Montréal, Québec, Canada

Corresponding author: Silvia M. Vidal, Tel. (514) 398-2362, Fax (514) 398-2603, Email silvia.vidal@mcgill.ca

4.1 ABSTRACT

Coxsackievirus B3 (CVB3) is the predominant cause of viral myocarditis in humans. Experimental mouse models of CVB3 infection have underscored the important contribution of host genetics to viral myocarditis onset and severity. Cell-intrinsic type I interferon production is an essential component of the protective host response to CVB3. On the other hand, cell-mediated inflammation and T cell infiltration can be pathological in the CVB3-infected heart. We have previously reported that mice carrying a homozygous Rel^{C307X} mutation, resulting in a premature truncation of the NF-κB family transcription factor c-Rel, succumb to lethal herpes simplex encephalitis due to excessive viral replication and neuroinflammation. In the present study, we sought to evaluate the role of c-Rel-dependent regulation in the inflamed heart. Following intraperitoneal infection with 30 PFU/g CVB3, Rel^{C307X} mice were more resistant to lethal myocarditis ($p = 0.0026$) compared to wild-type $Rel^{+/+}$ littermates, of which half developed lethal myocarditis by day 8 postinfection. Using dual RNA sequencing in the heart, we found that Rel^{C307X} hearts exhibited lower CVB3 viral transcript expression by day 4 and reduced viral titers by day 8 compared to $Rel^{+/+}$ hearts. The host gene expression landscape in Rel^{C307X} hearts was characterized by dampened basal inflammation and interferon (IFN)-dependent signaling at steady-state. At the day 4 peak of viral infection, Rel^{C307X} mice produced an IFN-dependent response that was equivalent to $Rel^{+/+}$ mice. Importantly, upon lymphocyte infiltration of the heart at day 8 postinfection, the Rel^{C307X} mutation resulted in the downregulation of several genes involved in cell-mediated inflammation and activation (including *Igkc*, *H2-Aa*, *Cd2*, *Sla*, *Gzma*), and upregulation of genes involved in normal heart function and metabolism (*Herpud1, Ucp3, Pdk4*) compared to $Rel^{+/+}$ mice. In sum, this dual transcriptome profiling of CVB3-infected Rel^{C307X} mice establishes c-Rel as a key regulator of pathological cell-mediated cardiac inflammation during CVB3 infection.

4.2 INTRODUCTION

Viral myocarditis, and its possible complication of dilated cardiomyopathy (DCM), account for 4 to 20% of sudden heart failure in young adults (1). The most common etiology of viral myocarditis is infection with strains of coxsackievirus B3 (CVB3) that explain an estimated 25 to 40% of childhood and young adult cases, followed by adenovirus, cytomegalovirus, or

parvovirus infections (1, 2). CVB3 is a single-stranded RNA enterovirus of the *Picornaviridae* family transmitted by the fecal-oral route, and can infect cardiomyocytes via host coxsackievirus and adenovirus receptor CAR and decay-accelerating factor DAF (3). Acute viral replication in the heart triggers lymphocyte infiltration and tissue necrosis, and eventually tissue remodeling upon viral clearance (4). In some cases, fibrosis and hypertrophic remodeling will lead to ventricular dilation, and subsequent heart failure (2). Thus, CVB3 myocarditis is a heterogeneous disease, and severity is not always correlated with the virulence of the causal CVB3 strain, suggesting that host genetics may play a role in disease onset and pathogenesis.

In cardiac resident cells and infiltrating hematopoietic cells, cell-intrinsic pathogen sensing through Toll-like receptors (TLRs) and RIG-I-like receptors (RLRs) activate transcription factors IRF3, IRF7 and NF-κB, which in turn induce expression of antiviral type I interferon (IFN) and of proinflammatory cytokines. The protective role of the TLR/type I IFN axis been confirmed in mouse models of CVB3 myocarditis. Mice deficient in *Tlr3*, *Unc93b1*, *Ticam1* (TRIF) and *Ifnb*, as well as cytoplasmic RLR sensor *Ifih1* (MDA5) and adaptor *Mavs*, exhibit elevated viral replication and cardiac inflammation (5-8). On the other hand, myeloid differentiation primary response 88 (MYD88) and interleukin-1 receptor associated kinase 4 (IRAK4), respectively an adapter and a kinase involved in TLR2, TLR4, TLR7, TLR8 and TLR9 signaling upstream of NF-κB, contribute to lethal myocarditis and CVB3 viral escape in mice (9, 10). In particular, CVB3-resistant *Myd88*$^{-/-}$ mice produce augmented IRF3-dependent IFN-β, and exhibit reduced leukocyte infiltration and lowered expression of p56lck, a tyrosine kinase essential for T cell signaling and activation (9). Regarding the antigen-specific T cell-mediated response to CVB3 infection, the resistance of *p56lck*$^{-/-}$, *Cd4*$^{-/-}$*Cd8*$^{-/-}$, and *Tcrb*$^{-/-}$ mice all indicate that cardiac T cell infiltration is detrimental to the host (11, 12). Additionally, from resistant *Irak4*$^{-/-}$ mice that featured increased recruitment of protective CCR5^{+} myeloid cells to the heart, it is clear that the regulation of infiltrating immune can affect the outcome of cardiac infection (10).

An effective cell-mediated antiviral response must balance the need for protective inflammation against the risk of causing pathological damage to the host, as is the case for neurotropic herpes simplex virus 1 infection in the brain. Childhood cases of herpes simplex encephalitis (HSE), resulting from infection with HSV-1, have been linked to inborn genetic mutations in several genes of the TLR3/type I IFN axis, including *TLR3*, *UNC93B1*, and *TRIF* (13-16). In mice, our group has previously identified an *N*-ethyl-*N*-nitrosourea (ENU)-induced

nonsense mutation in the reticuloendotheliosis oncogene *Rel*, encoding the NF-κB family c-Rel transcription factor (17). Homozygous Rel^{C307X} mice express a truncated c-Rel product, and are susceptible to lethal HSE, exhibiting elevated viral titers, excessive neuroinflammation, and cell death in the brain. Notably, Rel^{C307X} mice are not deficient in type I IFN signaling or in cytotoxic antigen-specific T cell function. They are instead compromised in their ability to regulate cell-mediated responses, and are characterized by augmented $CD4^+$ effector T cells and depleted $CD4^+CD25^+Foxp3^+$ regulatory T cells (Tregs) in the periphery during HSV-1 infection. Thus, c-Rel is protective during HSE.

Given that MYD88 and IRAK4 contribute to the pathological cell-mediated response during CVB3 myocarditis (9, 10), and that these factors lie upstream of NF-κB and c-Rel, here we employed host-virus RNA sequencing and flow cytometry to determine how CVB3-infected Rel^{C307X} mice regulate cellular responses and control virus in the inflamed heart. Where half of wild-type $Rel^{+/+}$ mice succumbed to lethal CVB3 myocarditis by day 8 postinfection (p.i.), Rel^{C307X} were resistant, reducing CVB3 viral transcription at day 4 and viral titer by day 8. Gene expression profiling further revealed that the Rel^{C307X} hearts dampened basal IFN and inflammation in the heart at homeostasis, mounted effective IFN-dependent responses at day 4, and significantly reduced inflammatory and pathological gene expression at day 8 at the height of cardiac T cell infiltration. Overall, these data indicate that c-Rel-dependent regulation plays a pathological role in CVB3 myocarditis.

4.3 MATERIALS AND METHODS

Ethics statement

All experiments in this study were performed following the guidelines and recommendations of the Canadian Council on Animal Care (CCAC) and in compliance with protocol number #2001-4792 approved by the McGill University Animal Care Committee.

Mice and virus

Rel^{C307X} mice were first generated in-house in an *N*-ethyl-*N*-nitrosourea (ENU) mutagenesis screen as previously described in (17), and at the Mouse Genome Informatics (MGI) database (MGI:6287253 or Rel^{Coby} allele, http://www.informatics.jax.org/). Inbred Rel^{C307X} mice

were backcrossed at least 4 times to the C57BL/6 background (The Jackson Laboratory), and were maintained in a breeding colony at McGill University. *Rel*$^{-/-}$ knockout mice were a kind gift from Dr. S. Gerondakis (18). CVB3 H3 strain was amplified as previously described (19). For CVB3 infections, eight-week old mice were infected with 30 PFU of CVB3 per g body weight via intraperitoneal (i.p.) injection, delivered in 200 ml sterile PBS. Infected animals were weighed and monitored daily, and further monitored up to three times a day during the peak of infection (days 5 - 8 p.i.). Mice were euthanized upon observation of 20% loss of initial pre-infection body weight and of lethargy, reduced mobility, piloerection or dehydration, or, in absence of clinical signs, at experimental endpoint at day 2, 4 or 8 p.i. Following euthanasia at clinical or experimental endpoint, mice were transcardially perfused with 10 ml cold PBS thorough the left ventricle. Excised hearts were weighed, and for each mouse, a heart index was calculated relative to the average tibia length (of both tibias) as described in (20), where heart index = (heart weight [mg] / average tibia length^3 [mm^3]), and further normalized to the average *Rel*$^{+/+}$ heart index for each sample group. Excised hearts were either collected in 5 ml PBS at 4ºC for downstream flow cytometry, or snap-frozen in liquid nitrogen for downstream viral plaque assay or RNA extraction.

CVB3 viral plaque assay

Snap-frozen infected heart tissue samples were homogenized in 1 ml DMEM using a MagNA Lyser Instrument (Roche) at speed 6000 for 40 s. Confluent HeLa cell (ATCC CCL-2) monolayers in 12-well plates were inoculated in duplicate with 10-fold serially diluted homogenate samples, in supplement-free DMEM. After a 1 h incubation at 37ºC with 5% CO_2, cells were covered with DMEM containing 2% FBS, 1% penicillin/streptomycin, and 0.5 % agarose. Following a 3-day incubation at 37ºC with 5% CO_2, cells were fixed with 10% phosphate-buffered saline, and stained with 0.5% crystal violet in 70% ethanol to visualize viral plaque formation. PFU were calculated by averaging counts between two duplicate wells. The limit of detection indicated in each figure represent the viral titer corresponding to a single detectable PFU at the lowest sample dilution.

Flow cytometry of heart-infiltrating immune cells

Adapted from (21) with modifications, freshly excised hearts were minced and digested in 1 ml 1X HBSS containing 675 U/ml collagenase I (Sigma), 187.5 U/ml collagenase XI (Sigma),

and 9 U/ml hyaluronidase (Sigma) for 40 min at 37ºC. Digested tissue was further triturated with a micropipette, resuspended in a 40% Percoll™ solution laid over an 80% Percoll™ layer, and centrifuged at 500 x g for 15 min with no break. Single cells were collected at the gradient interphase, washed twice and resuspended in 1X PBS 2% FBS 2 mmol EDTA pending surface staining. Cells were first blocked with anti-CD16/CD32 (eBioscience #16-0161) for 10 min at 4ºC, and were stained extracellularly for 20 min at 4ºC with the following fluorochrome-conjugated antibodies (clone, working dilution) from eBioscience (Invitrogen): B220 APC (RA3-6B2, 1:300), CD11b eFluor450 (M1/70, 1:300), CD11c APC-eFluor780 (N418, 1:200), CD25 PerCP-cy5.5 (PC61.5, 1:500), CD44 PE or APC (IM7, 1:200), CD45 PerCP-cy5.5 (30-F11, 1:200), CD62L FITC (MEL-14, 1:200), CD69 FITC (H1.2F3, 1:200), CXCR3 PE-cy7 (CXCR3-173, 1:200), F4/80 PE (V3NTY24, 1:250), NK1.1 PE-cy7 or eFluor450 (PK136, 1:200); and from BioLegend: CD3 Brilliant Violet 605 (17A2, 1:200), CD4 Brilliant Violet 510 (GK1.5, 1:200), CD8a eFluor450 or Brilliant Violet 785 (53-6.7, 1:200), CD45 Brilliant Violet 785 (30-F11, 1:200), Ly6G Brilliant Violet 711 (1A8, 1:500), Ly6C Brilliant Violet 785 (HK1.4, 1:2000) and I-A/I-E (MHC-II) AlexaFluor700 (M5/114.15.2, 1:1000). Cells were next stained with Fixable Viability Dye (eFluor780-conjugated or eFluor506-conjugated, eBioscience #65-0865 or #65-0866) to label dead cells. Finally, cells were fixed and permeabilized according to the manufacturer's protocol using the Foxp3/Transcription Factor Staining Buffer Kit (eBioscience #00-5523-00), and counterstained intracellularly for 20 min at 4ºC with the following antibodies (clone, working dilution) from eBioscience (Invitrogen): Foxp3 APC (FJK-16s, 1:100) and RORγt PE-eFluor610 (B2D, 1:100). Prior to acquisition, 5000 counting beads (Spherotech #ACBP-50-10) were added per sample. Cells were acquired on a BD LSRFortessa cytometer, and populations were gated using FlowJo v. 10.1 software, as described in Supplementary Figure S4.2. Total cell counts for each population were normalized to the total number of beads per sample and to the total number of singlet and viable $CD45^+$ cells acquired in both staining panels.

RNA extraction and dual RNA sequencing

Total RNA was purified from excised heart tissue (corresponding to tissue surrounding the left ventricle), and RNA sequencing was performed as previously described (22). Briefly, snap-frozen samples were transferred to 1 ml TRIzol reagent (Invitrogen) and homogenized at speed 6000 for 40 seconds with a MagNA Lyser Instrument (Roche). Total RNA was extracted as per

the manufacturer's standard protocol. RNA samples were further cleaned up using the RNeasy Mini Kit (Qiagen #74104) and following a DNase1 treatment, as per the manufacturer's standard protocol. RNA integrity and purity was evaluated using a Bioanalyzer RNA Pico kit (Agilent), and rRNA-depleted RNA samples were converted to cDNA libraries using the KAPA Stranded RNA-Seq kit (Roche). Libraries were sequenced with an Illumina NovaSeq 6000 instrument to generate 50 bp paired-end reads. Low-quality reads (Phred score < 33) and leftover adaptor sequences were removed with the Trimmomatic v.0.36 tool (23) using the following arguments: ILLUMINACLIP:TruSeq3-PE.fa:2:30:10 HEADCROP:4 LEADING:5 TRAILING:3 SLIDINGWINDOW:4:20 MINLEN:36. All trimmed reads were first mapped using the HISAT2 v2.1.0 alignment tool (24) to an indexed mouse genome (GRCm38/mm10) using default arguments. Mouse (host) gene expression was quantified by counting the number of strand-specific reads aligning to exon features using the featureCounts tool (Subread package v1.5.2) (25). In parallel, remaining unmapped trimmed reads were instead aligned to an indexed CVB3 Woodruff variant ((26), GenBank: U57056.1) reference genome using HISAT2 with default arguments. Each CVB3-aligned read pair was considered to be the product of an independent viral transcript, and total CVB3 transcripts were counted over the 7,400 bp viral genome using featureCounts with the default arguments.

Variant calling in the CVB3 viral population

In the scope of the following analysis, each pair of CVB3-aligned reads was considered to belong to a distinct viral particle. First, sequencing depth was measured at all nucleotide positions using samtools function "depth" function in the samtools v1.4.1 package (27). Available in the bcftools v1.9 package (28), the "mpileup" and "call" functions were used to identify the occurrence of A, C, T, G or N bases at each genomic position at a maximum depth of 10,000 reads, and to call variants at every position compared to the Woodruff CVB3 H3 reference genome, using the default calling method and assuming a ploidy level of 1. For each position with a minimum depth of 10 and where a variant occurred at a frequency > 1% of the viral sequence population, a mutation rate was calculated (variants per kb), in addition to Shannon's entropy as a second measure of nucleotide variation as described (29). To determine the variability across specific regions of the CVB3 genome, the average entropy value was calculated across all variant positions in the entire genome, or within the P1, P2 or P3 proto-peptide regions of the CVB3 genome.

Differential host gene expression analysis

From raw host gene read counts, residual rRNA reads were discarded, and only host gene that were expressed above 5 counts per million host reads (CPM) in at least 2 samples were retained for downstream analysis, for a total of 13,610 expressed host genes. Using the edgeR Bioconductor package, filtered count libraries were normalized with the TMM method (30), and differentially expressed host genes were considered statistically significant if they demonstrated $> \pm 1.5$ fold change between pairwise groups, with $q < 0.05$ (Benjamini-Hochberg (BH)-adjusted *p*-value). Heatmaps were generated with CPM expression values per sample, normalized to the average CPM values of a specified control group, using the "gplots" package in R and clustered gene-wise using a Manhattan distance measure.

Functional enrichment analyses

Differentially expressed gene lists identified by RNA sequencing were queried using the DAVID v.6.8 online database (31) for enriched gene ontology (GO) terms. Enriched GO terms in the biological processes (BP4) category that met a nominal *p*-value cut-off of 0.05 were considered significant. Additionally, gene set enrichment analysis was performed using GSEA (32) to detect enrichment of previously published gene sets among all 13,610 expressed genes in our RNA sequencing dataset between experimental groups. Our dataset was queried against gene sets listed in the MSigDB v6.2 collection, available under the Curated Gene Sets (C2, $N = 3406$ sets, including chemical and genetic perturbations, canonical pathways BIOCARTA, KEGG, PID and REACTOME) or Immunological Signatures (C7, $N = 4872$ sets) category. Gene sets that met a BH-adjusted *p*-value cut-off of at least $q < 0.05$ were considered significantly enriched in each condition. Finally, similar or redundant gene sets were grouped together to identify main immune or cellular pathways that were dysregulated in Rel^{C307X} or $Rel^{+/+}$ mice using a leading edge analysis. Briefly, genes that led the enrichment for each gene set (genes whose rank fell before or at the rank of the gene with the highest enrichment score), and that were represented in at least 5% of all enriched gene sets, were retained to hierarchically cluster gene sets using Manhattan distance as a measure.

Statistical tests

Specified in each Figure legend, statistical tests were performed using GraphPad Prism v. 6 software. Survival curves were evaluated with a log-rank (Mantel-Cox) test. Unpaired parametric Student's T tests were performed in experiments involving only two experimental groups. Otherwise, Two-way ANOVA were performed with Tukey's multiple correction test between pairwise groups. A threshold of $p < 0.05$ was considered significant (*$p < 0.05$, **$p < 0.01$, ***$p < 0.001$, ****$p < 0.0001$).

4.4 RESULTS

Rel^{C307X} mice are more resistant to CVB3-induced myocarditis and better control viral replication by day 8 post-infection

Originally identified in an ENU mutagenesis screen, mutant Rel^{C307X} mice have previously been shown to express a truncated c-Rel protein (17). Following i.p. infection with 30 PFU/g CVB3, male mice that were homozygous for the Rel^{C307X} allele exhibited increased survival by day 8 p.i. compared to wild-type $Rel^{+/+}$ littermates (Fig. 1A), at which both groups had lost an equal amount of body weight (Fig. 1B). As a gross measure of cellular infiltration, heart weights and normalized heart indices were also comparable by day 8 (Fig. 1C, D). While viral titers were equivalent between groups at day 2 and at the day 4 peak of viremia, Rel^{C307X} males saw reduced viral replication by day 8 (Fig. 1E), providing further evidence of their CVB3 infection-resistant phenotype. On the other hand, where approximately 50% of $Rel^{+/+}$ mice survived the infection, CVB3 viral loads remained high by day 8 p.i. Of note, female mice of either genotype did not succumb to CVB3 infection a 30 PFU/g CVB3 dose (Supplemental Fig. 1A), and while they lost weight and harboured productive viral replication in the heart, no differential phenotypes were recorded between genotype groups (Supplemental Fig. 1B-E). Thus, male mice were used in all subsequent analyses.

Interestingly, full $Rel^{-/-}$ knockout mice, as well as compound heterozygotes ($Rel^{+/-}$, $Rel^{C307X/-}$or $Rel^{C307X/+}$), were susceptible to CVB3 infection at a similar proportion to $Rel^{+/+}$ mice, and none of these group successfully controlled viral replication better than another (Supplemental Fig. 1F-J). Thus, two copies of the Rel^{C307X} allele are required to confer resistance to CVB3 infection.

T cell infiltration and activation occur by day 8 post-CVB3 infection in the heart

To explore how the protective effect of the *Rel*^{C307X} mutation might involve the cell-mediated response to CVB3 infection, hematopoietic cell populations were quantified at days 2, 4 and 8 p.i. in the heart as absolute counts (Fig. 2) or in proportion to the total number of infiltrating CD45$^+$ cells (Supplemental Fig. 3). Most lymphocytes, including NK cells, B cells, CD4$^+$ and CD8$^+$ T cells, invaded the infected heart at D8 p.i., compared to day 4 (Fig. 2A, C, E, G, K). Macrophages, classical dendritic cells (DC) and monocytes were also detected among day 8 infiltrating myeloid cells, with monocytes numbers increasing as early as day 4 p.i. (Fig. 2O). Cell counts for all populations were similar between *Rel*$^{+/+}$ and *Rel*^{C307X} mice at day 8. Only CD4$^+$ T cells, and their parent CD3$^+$ T cell population, constituted slightly larger proportions of total CD45$^+$ cells in *Rel*^{C307X} mice by day 8 p.i. (Supplemental Fig. 3). No further differences were observed in the CD4$^+$ to CD8$^+$ T cell ratio across infection (Fig. 2F, Supplemental Fig. 3N). Finally, while specialized CD4$^+$ T cell subsets, including CD4$^+$RORγt$^+$ Th17 cells and CD4$^+$Foxp3$^+$ regulatory T cells (Treg), were detected in the heart at steady-state and at D8 p.i., their numbers (Fig. 2J, N) or proportions (Fig. 3I, J) were not otherwise affected by the mutation. Together, these data suggest that in general, CVB3 infection does not trigger large-scale defects in cellular responses that could explain differential viral titer control by day 8 p.i.

Lymphocyte populations were further examined to determine if the *Rel*^{C307X} mutation had any influence on their activation. Activated CD69$^+$ NK cells gradually increased in number as the infection progressed (Fig. 2B), and upregulated CD69 as early as day 2 p.i. (Supplemental Fig. 3B). CD69$^+$CD3+ T cells were only detected in high numbers at day 8 p.i. (Fig. 2D, Supplemental Fig. 3D). By day 8, most CD4$^+$ and CD8$^+$ T cells expressed the chemokine receptor CXCR3 (Fig. 2H, L), Supplemental Fig. 3G, L), and had mostly shifted towards an activated CD44$^+$CD62L$^-$ profile (Fig. 2I, M, Supplemental Fig. 3H, M). Overall, *Rel*^{C307X} lymphocytes expressed similar levels of these activation markers at all timepoints compared to susceptible *Rel*$^{+/+}$ mice. Together, these data suggest that in general, CVB3 infection does not trigger large-scale defects in cellular responses that could explain differential viral titer control by day 8 p.i. in *Rel*^{C307X} mice.

Expression of CVB3 viral mRNA is limited by day 4 post-infection in Rel^{C307X} mice

Using a dual RNA sequencing approach, we measured the expression of virus- and host-derived mRNA in heart tissue collected from non-infected mice, and from day 4 and day 8 CVB3-infected mice. As early as day 4 p.i., $Rel^{+/+}$ hearts harboured at least two-fold higher levels of CVB3-derived sequences compared to resistant Rel^{C307X} mice (Fig. 3A, 3B). By day 8, levels of actively transcribed CVB3 mRNA products were similar and had decreased in both groups, in strong contrast to the marked difference in productive, mature virus particles previously noted at day 8 (Fig. 1E). Furthermore, in comparing discrete viral populations replicating in each mouse, all groups exhibited a similar number of viral single nucleotide variants detected at a frequency of greater than 1% of the entire virus sequence pool across all samples (Supplemental Table 1). Synonymous and non-synonymous mutations were spread equally across the CVB3 genome (Supplemental Fig. 4A-D). Mutations that were common to all mice, with an elevated 70 to 100% penetrance in each host-isolated virus population, likely reflected variants that were already present in the original CVB3 stock. Emerging variants (below 30% penetrance) were usually unique to one sample and not to an entire group, suggesting that these mutations had emerged independently of c-Rel-dependent host pressure. Finally, no differences in mutation rate, quantified in variants per kb (Supplementary Fig. 4E) or by Shannon's entropy (Supplementary Fig. 4F), were observed between groups over the entire genome, or across sections corresponding to the three major processed polyproteins of CVB3. Together, these data support a model where the Rel^{C307X} mutation is associated with decreased viral transcription at day 4, and later translating to a lower level of infectious virus at day 8, without affecting the diversity or fitness of the viral populations in either host group.

Finally, a principal component analysis on our dataset to determine if host gene expression was affected by active viral mRNA replication, absolute viral titers, or genotype. Non-infected, day 4-infected and day 8-infected mice formed distinct clusters that were spaced apart from each other, confirming that all three timepoints had captured a different aspect of the host response (Fig. 3C). However, where both genotype groups behaved very similarly at steady-state and at day 4 p.i., $Rel^{+/+}$ mice only diverged from Rel^{C307X} mice at day 8 p.i. In other words, any variation in viral mRNA transcription at day 4 appeared to have had little effect on the host transcriptome, which was more closely associated with viral titers detected in corresponding samples at day 8

(Fig. 1D). Thus, in this CVB3 infection model, differential host gene expression in the heart may be driven in part by genotype and by infectious viral load.

The Rel^{C307X} mutation dampens basal inflammatory gene expression in non-infected hearts

Early steady-state alterations in c-Rel-driven regulation of gene expression can inform survival outcome at later timepoints of infection. 10 differentially expressed genes (DEG) were identified between non-infected $Rel^{+/+}$ and Rel^{C307X} mice (Fig. 4A). In addition to *Rel*, well-expressed in the heart but downregulated in mutant mice at all timepoints, the immunoglobulin-family *Igha* gene was another prominently Rel^{C307X}-downregulated gene at steady-state and later at D8 p.i. (Fig. 4B). Otherwise, Rel^{C307X} mice had higher expression of the long non-coding RNA *H19*, a negative regulator of cell division notably induced in ischemic heart tissue (33), of the regulator of lipid metabolism and apoptosis *G0s2*, and of molecular chaperone *Hspa2*. These genes were foremost among leading-edge genes that drove the enrichment of ribosomal, translational, and hypoxia pathways in Rel^{C307X} mice (Fig. 4C-E, upper panels). On the other hand, the $Rel^{+/+}$ steady-state was enriched for signatures related to cell division (driven by genes including *Mcm3*, *Ccnb1*, *Cdk1*, *Cdca3*, and *Cenpe*), collagen-family genes, and surprisingly, IFN and myeloid cell responses (driven in part by *Stat1*, *Oasl1*, *Ifit3*, *Rsad2*, *Ccr2*, *Fcer1g*, *Fcr2b*, *Cd14*, and various complement genes) (Fig. 4C-E, lower panels). These gene sets suggest that cell division, basal IFN signaling and some innate immune responses are dampened in the Rel^{C307X} heart even prior to stimulation or infection. Thus, alternative regulation by the truncated C307X c-Rel protein in homeostatic conditions may leave the heart poised to develop a protective immune response to CVB3 infection that will be less damaging to the Rel^{C307X} host.

Rel^{C307X} mice mount a normal IFN-stimulated defence response by the peak of CVB3 infection at day 4

To further expand on the early effects of the Rel^{C307X} mutation on a protective outcome to CVB3 infection, gene expression profiles were compared at the day 4 peak of viral replication, immediately prior to the onset of lethal disease and pathology in $Rel^{+/+}$ mice. An additional 10 DEG were discovered at day 4 p.i. (Fig. 5A), including Rel^{C307X}-downregulated cardiac α-actin and contactin-2 (*Actc1, Cntn2*) implicated in dilated cardiomyopathy and arrythmia (34, 35), and

the eukaryotic elongation factor 2 kinase-encoding *Eef2k* gene, whose induction can modulate CVB3 replication (36). Genes that were upregulated in Rel^{C307X} mice included chemokine-encoding *Cxcl12*, protocadherin-family member *Pcdh12,* and the *Hey1* transcription factor involved in heart and vascular development (37-39) (Fig. 5B). However, while these select DEG are involved in different aspects of heart function and development, they do not capture the full impact of CVB3 infection at day 4 on the host transcriptome. Rather, both $Rel^{+/+}$ and Rel^{C307X} mice mounted a strong and equivalent innate response to infection, where the expression of 3353 genes is either induced or repressed at a similar level in both groups compared to non-infected controls (Fig. 5C). These comparable responses involve leukocyte migration, inflammation, cell death, and cardiovascular development (Fig. 5D), with type I and type II IFN responses being largely equal in both $Rel^{+/+}$ and Rel^{C307X} mice (Fig. 5E). Considering the above 10 DEG together with other infection-responding genes, only a handful of enriched gene sets were identified in Rel^{C307X} mice, related to cell division, NK cell activation, and *Bcl6*-dependent transcriptional regulation (Fig. 5F). Contrarily, $Rel^{+/+}$ mice were defined by signatures that included ventricular heart failure (Fig. 5G). In sum, both genotype groups at day 4 p.i. had similar gene expression profiles and appeared to respond efficiently to infection, despite emerging signs of altered heart function. In particular, the non-infected $Rel^{+/+}$ or Rel^{C307X} milieu, respectively characterized by augmented or reduced inflammation at steady-state, may exert differential pressure on the heart by day 4 p.i., and later influence leukocytes as they prepare to expand, invade and respond to CVB3 infection by day 8.

Dysregulated inflammatory, metabolic and adaptive immune pathways underlie the protective Rel^{C307X} host response in CVB3-infected hearts at day 8

Accompanying CVB3 escape or control in the heart, the greatest disruption of gene expression occurred at day 8 p.i. In Rel^{C307X} mice, 1769 repressed (blue) and 880 induced (red) DEG were separated into 12 gene clusters, and were further grouped together by their kinetic expression in $Rel^{+/+}$ and Rel^{C307X} mice across all timepoints (Fig. 6A, B). Among Rel^{C307X}-downregulated genes, the lymphocyte-specific markers *Lsp1* and *Cd2*, immunoglobulin chain- and H2-family genes, and pro-apoptotic *Bak1* all belonged to clusters 1 to 3 (Fig. 6C, D), where lymphocyte activation and motility, and antigen presentation via MHC-II had gradually increased over infection in $Rel^{+/+}$ hearts, but to a lesser extent in Rel^{C307X} hearts (Supplemental Fig. 5A-B). Expression of C-C-motif- and C-X-C-motif-family chemokines was similarly augmented in wild-

type animals (Supplemental Fig. 6A, B). *Rel*$^{+/+}$ mice also upregulated mitotic cell division genes that comprised clusters 4 to 6 (Fig. 6E, Supplemental Fig. 5C), while cluster 12 genes confirmed that innate cytokine (IFN-γ) responses and antigen presentation via MHC-I dominated the wild-type host response (Fig. 6H, Supplemental Fig. 5F). Also, the expression of IFN receptor genes was higher in *Rel*$^{+/+}$ mice by day 8 p.i., as well as *Casp3*, *Bok*, *Bcl2a1b* regulating cell survival (Supplemental Fig. 6E, F). Contrary to these wild-type-enriched inflammatory pathways, genes that were upregulated in mutant animals were grouped in Clusters 7-11 and belonged to pathways related to metabolism, cellular respiration and lipid oxidation (*Ucp3, Pdk4, Egln1*) (Fig. 6F, G, Supplemental Fig. 5D, E). Together with elevated expression of markers (*Cxcl12*, *Ctf1*, *Kitl* and *Vegfb*) involved in heart development, remodeling and wound healing (Supplemental Fig. 6B-D), these data indicate that normal heart tissue function is resuming in resistant *Rel*^{C307X} mice by day 8 p.i.

Additionally, a global look at genes that were uniquely dysregulated in either *Rel*$^{+/+}$ or *Rel*^{C307X} hearts revealed that their transcriptional profiles completely diverged between inflammatory immune cell activation or metabolic processes in the heart at day 8 p.i., directly reflecting susceptible or resistant outcomes (Fig. 6I-K). These opposite and wide-ranging responses were further captured by GSEA, where susceptible *Rel*$^{+/+}$ mice were enriched for activated and proliferating cellular immune responses, and resistant *Rel*^{C307X} mice for mitochondrial, metabolic and ventricular functions (Supplemental Fig. 7A, B). Therefore, altered c-Rel-dependent regulation restricts myocarditis in CVB3-infected *Rel*^{C307X} mice.

Finally, to better define genes that were directly or indirectly regulated by c-Rel by day 8 p.i., DEG that varied as a function of the virus were excluded from our dataset, leaving 406 DEG uniquely driven by the *Rel*^{C307X} genotype, of which a majority were variable at day 8, but not yet induced at day 4 (Fig. 7A, B). Here, *Rel*^{C307X}-upregulated genes belonged to hormone, metabolic and heart development pathways, and included *Herpud1*, involved in maintenance of basal cardiac homeostasis (40), and translation initiation factor *Eif1* (Fig. 7C, D). Disrupted expression of the *Tgfbr3* receptor-encoding and *Tgfb3* ligand-encoding genes in *Rel*^{C307X} mice also suggest that c-Rel may play a more direct role in regulating heart function (41). In contrast, cytoskeleton, organelle, and cellular processes were hampered in mutant animals, along with *Rel*^{C307X}-depleted immune-related genes like *Ctla4* and *Traf3*. Altogether, these data further reinforce a model where the *Rel*^{C307X} mutation, encoding a truncated c-Rel transcription factor, differentially regulates gene

expression and shifts the cellular immune response to one that limits cardiac pathological inflammation and promotes CVB3 resistance.

4.5 DISCUSSION

By revealing the full extent to which the host and virus transcriptomes diverged in $Rel^{+/+}$ and Rel^{C307X} heart tissue, dual RNA sequencing has provided a framework to understand how c-Rel regulation impacts heart function at steady-state and upon CVB3 infection. In particular, early differences in homeostatic, inflammatory, and viral gene expression may grow to influence immune cell responses, as immune cells infiltrate the heart by day 8 p.i. and allow Rel^{C307X} mice to better control virus-induced pathology, rather than exacerbate it.

A key finding of this study was that Rel^{C307X} mice were more resistant to CVB3 infection compared to wild-type mice. This phenotype was only observed in male mice; in the context of C57BL/6 background mice, males are more susceptible to CVB3-induced myocarditis compared to females, in part due to dimorphic heightened TLR4 expression over TLR2, augmented T cell responses, and endocrine differences (42, 43). Where c-Rel has also been associated in cardiac hypertrophy in mice (44), heart weight and indices were similar between genotype groups upon infection. Also notable was the relative susceptibility of $Rel^{-/-}$ mice to CVB3 infection compared to resistant Rel^{C307X} mice, suggesting that mechanisms uniquely altered by the truncated C307X c-Rel protein may underlie CVB3 resistance.

Empirically, increased survival of Rel^{C307X} mice was associated with an important reduction in infectious CVB3 viral load by day 8 p.i., as measured by plaque assay. Interestingly, at peak CVB3 titers at day 4, transcription of CVB3-derived mRNA was significantly dampened in Rel^{C307X} mice, suggesting that the host milieu had an early limiting effect on viral replication, that would later translate to a decrease in mature virus particles by day 8. These effects were not associated with variable expression of CVB3 entry receptors (coxsackievirus and adenovirus receptor *Cxadr* or decay-accelerating factor *Cd55*) between the $Rel^{+/+}$ and Rel^{C307X} heart muscle. Nor were differences in viral replication driven by virus-specific factors. Where other studies have reported multiple clonal populations of enterovirus sequences emerging in an infected host and affecting viral pathogenesis (45), CVB3 sequences in $Rel^{+/+}$ and Rel^{C307X} hearts accrued a similar number of variants at day 4 or day 8 p.i., and overall had deviated very little from the original

infectious stock. Thus, *Rel*^{C307X}-dependent viral control was likely the result of an effective early innate host response, in a tissue environment that proved unfavourable to the CVB3 replication.

Among the major disruptions of the *Rel*^{C307X} heart at steady-state were decreased inflammatory and basal IFN-stimulated responses. Relative to non-infected *Rel*^{C307X} mice, *Rel*$^{+/+}$ hearts were enriched in STAT1-dependent IFN signaling at homeostasis, itself predictive of pathology in models of heart failure (46, 47). With many ISGs also doubling as inflammatory mediators, and together with heightened expression genes encoding of Fc-family receptors, cell cycle proteins, myeloid CCR2 and CD14 markers, and especially IgA heavy chain, wild-type heart tissue was more prone to basal cardiac inflammation compared to *Rel*^{C307X} mice. Together, steady-state inflammation and IFN signaling could impact patrolling myeloid and naïve T cells as they transit the heart, and prime them towards a later pathological response to viral infection (48). Furthermore, NF-κB activation and chronic inflammation are known to be detrimental to heart function and to protective anti-CVB3 responses (49, 50), and could therefore explain how the C307X truncated product acted as a dampener on these responses to promote resistance to an eventual CVB3 challenge. However, while type I IFN can be damaging to the heart at homeostasis, it is absolutely essential for control of CVB3 infection (8); *Tlr3*$^{-/-}$, *Ifih1*$^{-/-}$ and *Mavs*$^{-/-}$ mice are also critically susceptible to CVB3 myocarditis (5, 51). Yet in this respect, both *Rel*$^{+/+}$ and *Rel*^{C307X} IFN responses are strong and equal by day 4 p.i., suggesting that the innate anti-CVB3 response was effective at the height of viral replication, but that an earlier dampening of basal inflammation by the *Rel*^{C307X} mutation may have a protracted and protective effect against myocarditis.

With the innate host response being largely normal at day 4 p.i., only a handful of genes were differentially expressed in the *Rel*^{C307X} heart. These DEG did, however, demonstrate that the condition of the heart tissue was in accord with infection outcome. For one, the CVB3-susceptible *Rel*$^{+/+}$ transcriptional landscape at day 4 is characteristic of early heart failure. Specifically, *Cntn2* expression is typical in Purkinje fiber cardiomyocytes and can be a marker of arrythmia (35), human *ACTC1* mutations have been identified in inherited dilated cardiomyopathies (34), and *Eef2k* can be induced during the host response to reduce EEF2 activity and attenuate translation of the CVB3 polyprotein (36). Otherwise, the response to CVB3 replication in the *Rel*^{C307X} heart is distinguished by genes involved in heart or vascular development, notably by *Cxcl12* (39). While CXCL12 may also play a role in recruiting lymphocytes (52), expression of its cognate receptors (*Cxcr4* and *Ackr3*/CXCR7) were equivalent in *Rel*$^{+/+}$ and *Rel*^{C307X} hearts, and T or B lymphocytes

had not yet infiltrated by day 4 p.i. in either genotype group. Rather, genes related to cytokine-stimulated NK cells were enriched in *Rel*^{C307X} hearts, suggesting that an effective innate antiviral response occurred in *Rel*^{C307X} tissue. Further investigation into earlier gene expression profiles of *Rel*$^{+/+}$ and *Rel*^{C307X} mice at day 2 p.i. may reveal additional disruptions with far-reaching influence on the pathological or protective host response by day 8.

However, by day 8 post-CVB3 infection, the host response in *Rel*$^{+/+}$ and *Rel*^{C307X} mice was deeply polarized. *Rel*$^{+/+}$ mice were highly enriched for T cell and myeloid-dependent genes, for antigen-specific responses, and for cell death mediators, diverging completely from resistant *Rel*^{C307X} mice that instead benefited from improved metabolic and heart specific processes. However, heart-infiltrating cell populations were similar across both groups, with no significant differences in CD4$^+$ or CD8$^+$ T cell numbers or ratio; only CD4$^+$ T cells comprised a slightly higher proportion of total infiltrating cells in resistant *Rel*^{C307X} mice compared to *Rel*$^{+/+}$ mice. Rather, the downregulation of genes related to the leukocyte response is a driver of CVB3 myocarditis resistance in *Rel*^{C307X} hearts. Crucially, similar to other c-Rel models of viral infection (17, 53), these *Rel*^{C307X}-dependent defects did not compromise the antigen-specific cytotoxic cell response, as mutant animals successfully cleared the infection. Much like CVB3 resistant *Cd4*$^{-/-}$*Cd8*$^{-/-}$, *Myd88*$^{-/-}$ or NF-κB inhibitor-treated mice and their associated reductions in cytokine- and chemokine-mediated inflammation (9, 11, 49), *Rel*^{C307X} mice were able to limit inflammation and pathological T cell responses to CVB3. Other CD4$^+$ T cell subsets, including Foxp3$^+$ Tregs and RORγt$^+$ Th17 cells, have been reported to play a role in murine myocarditis models, with RORγt$^+$ Th17 cells generally exacerbating pathology, and the impact of Foxp3$^+$ Tregs proving more controversial (54). While *Rel*^{C307X} have fewer peripheral Tregs (17), and both Tregs and Th17 cells require c-Rel for their development (55), no significant differences were found between groups in the relatively few heart-infiltrating Tregs and Th17 cells quantified in *Rel*$^{+/+}$ and *Rel*^{C307X} mice at day 8. Bone marrow chimeras would be especially useful to determine the relative contribution of hematopoietic or resident cells to CVB3 resistance in our model, and prompt more focused examination of key immune cell subsets or of c-Rel-expressing cardiomyocytes (44) and their role in pathological inflammation or cell death.

Overall, this first dual transcriptome profiling of CVB3 myocarditis in *Rel*^{C307X} mice establishes c-Rel as a necessary regulator of the pathological cellular immune response during CVB3-induced myocarditis. Further dysregulation by *Rel*^{C307X} mutation of basal interferon and

inflammatory responses, and its early dampening effect on CVB3 viral replication defect in regulation, also stand out as key findings. Interestingly, the CVB3 resistance phenotype of *Rel*^{C307X} mice does not align with their susceptibility to HSV-1 encephalitis; the *Rel*^{C307X} mutation drives higher chemokine and IFN-related gene expression the brain, with pathological immune cell recruitment resulting in viral escape and lethal encephalitis. Therefore, depending on the tissue context, the RNA or DNA nature of a virus, or on the tissue-specific impacts of the host genetic background, the same *Rel*^{C307X} mutation can affect different cell-mediated pathways in its capacity as a regulator of inflammation. With human *REL* also involved as a risk factor associated with several inflammatory diseases (56-58), the c-Rel cascade and its effectors may prove to be effective targets to help modulate inflammation.

4.6 ACKNOWLEDGMENTS

We are grateful to Patricia D'Arcy for expert technical support. We also thank the Cell Vision Core Facility at McGill University and the Plateau de biologie moléculaire of the Institut de recherches cliniques de Montréal (IRCM) for their assistance. M.M. was supported by the Fonds de recherche du Québec – Santé. S.M.V. was supported by the Canada Research Chair Program. This project was conducted with the support of Canadian Institutes for Health Research Grants CTP-87520 and MOP-238757. The authors declare no financial conflicts of interest.

4.7 FIGURES AND LEGENDS

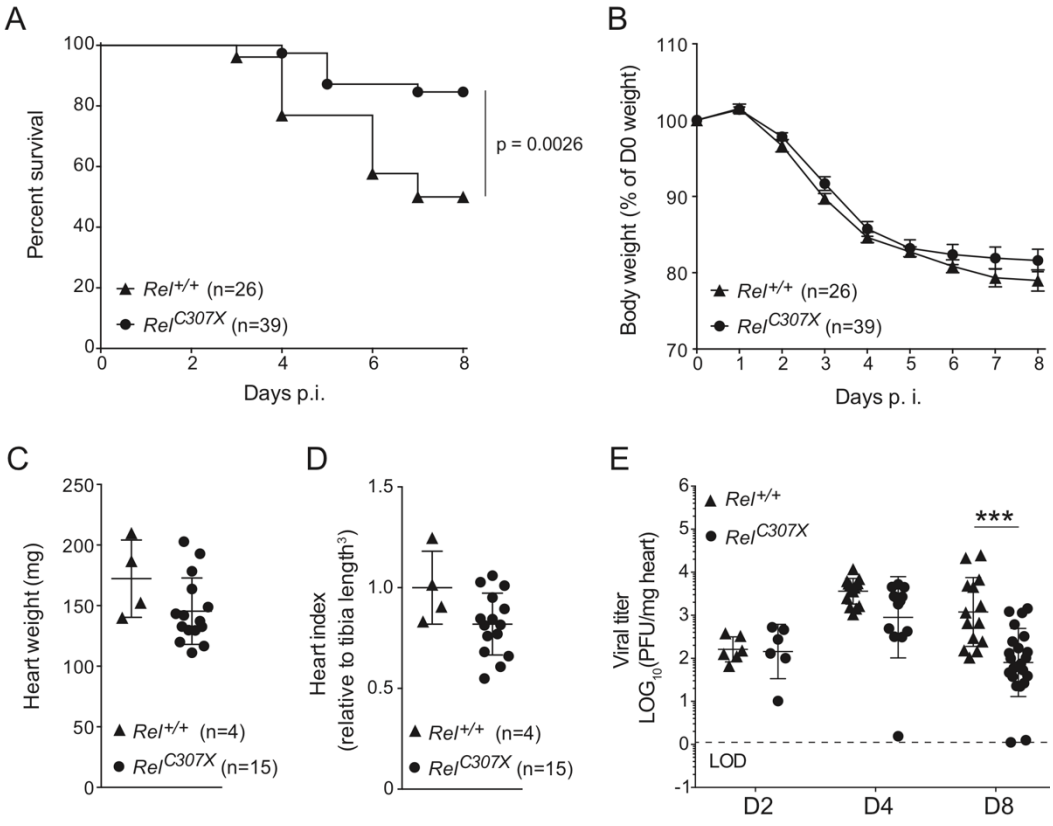

FIGURE 1. Survival outcome and control of viral replication in CVB3-infected Rel^{C307X} mice.
(A) Survival and (B) weight loss of male littermate $Rel^{+/+}$ and Rel^{C307X} mice following i.p. infection with 30 PFU/g CVB3. (C) Heart weight and (D) heart index normalized to the average tibia length^3 per mouse were measured at D8 post-CVB3 infection in male littermate $Rel^{+/+}$ and Rel^{C307X} mice. (E) CVB3 viral titer was measured by viral plaque assay at days 2, 4 and 8 p.i. in male littermate $Rel^{+/+}$ and Rel^{C307X} mice; LOD indicates the limit of detection. (B) Data represent mean ± SEM, and (C, D, E) mean ± SD. Statistical tests: (A) log-rank (Mantel-Cox) test, (C, D) Student's T-test and (E) Two-way ANOVA. $^{**}p < 0.01$, $^{***}p < 0.001$.

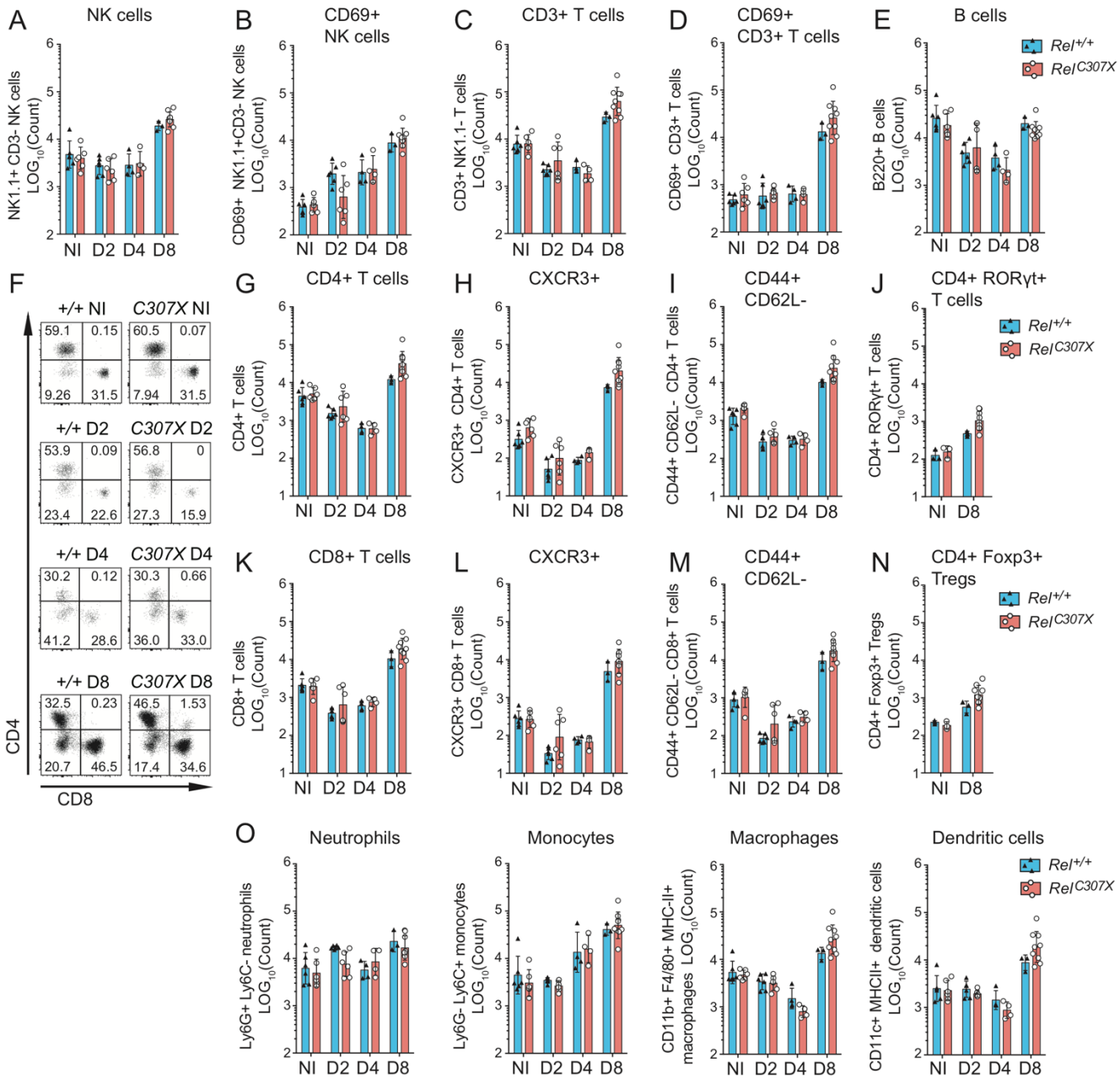

FIGURE 2. Infiltrating immune cell dynamics in Rel^{C307X} hearts following CVB3 infection.

FIGURE 2. Infiltrating immune cell dynamics in Rel^{C307X} hearts following CVB3 infection. Hematopoietic cells were isolated from whole hearts collected from CVB3-infected *Rel*$^{+/+}$ and *Rel*^{C307X} male littermate mice at days 2, 4 and 8 p.i., or non-infected (NI) controls ($n \geq 3$ per group), and enumerated by flow cytometry according to the gating strategy described in Supplementary Figure 4.2. General lymphocyte populations include (A) NK cells (NK1.1^{+}CD3^{-}), (B) CD69^{+} activated NK cells, (C) CD3^{+} T cells (CD3^{+}NK1.1^{-}), (D) CD69^{+} activated CD3^{+} T cells and (E) B lymphocytes (B220^{+}CD3^{-}). (F) Representative plots show CD4^{+} and CD8^{+} T cell populations, with proportions indicated as percentage of total CD3^{+} T cells, and further quantified in (G) CD4^{+} T cells, (H) CXCR3^{+} or (I) CD44^{+}CD62L^{-} activated CD4^{+} T cells, in (K) CD8^{+} T cells, (L) CXCR3^{+} or (M) CD44^{+}CD62L^{-} activated CD8^{+} T cells, and finally in (J) CD4^{+} RORγt^{+} T cells and (N) CD4^{+}Foxp3^{+} Tregs. (O) General myeloid and dendritic cell population counts, including neutrophils (CD11b^{+}Ly6G^{+}Ly6C^{-}), monocytes (CD11b^{+}Ly6C^{+}Ly6G^{-}), macrophages (CD11b^{+}F4/80^{+}MHC-II^{+}), and dendritic cells (CD11c^{+}MHC-II^{+}). Data represent mean ± SD. Statistical tests: Two-way ANOVA.

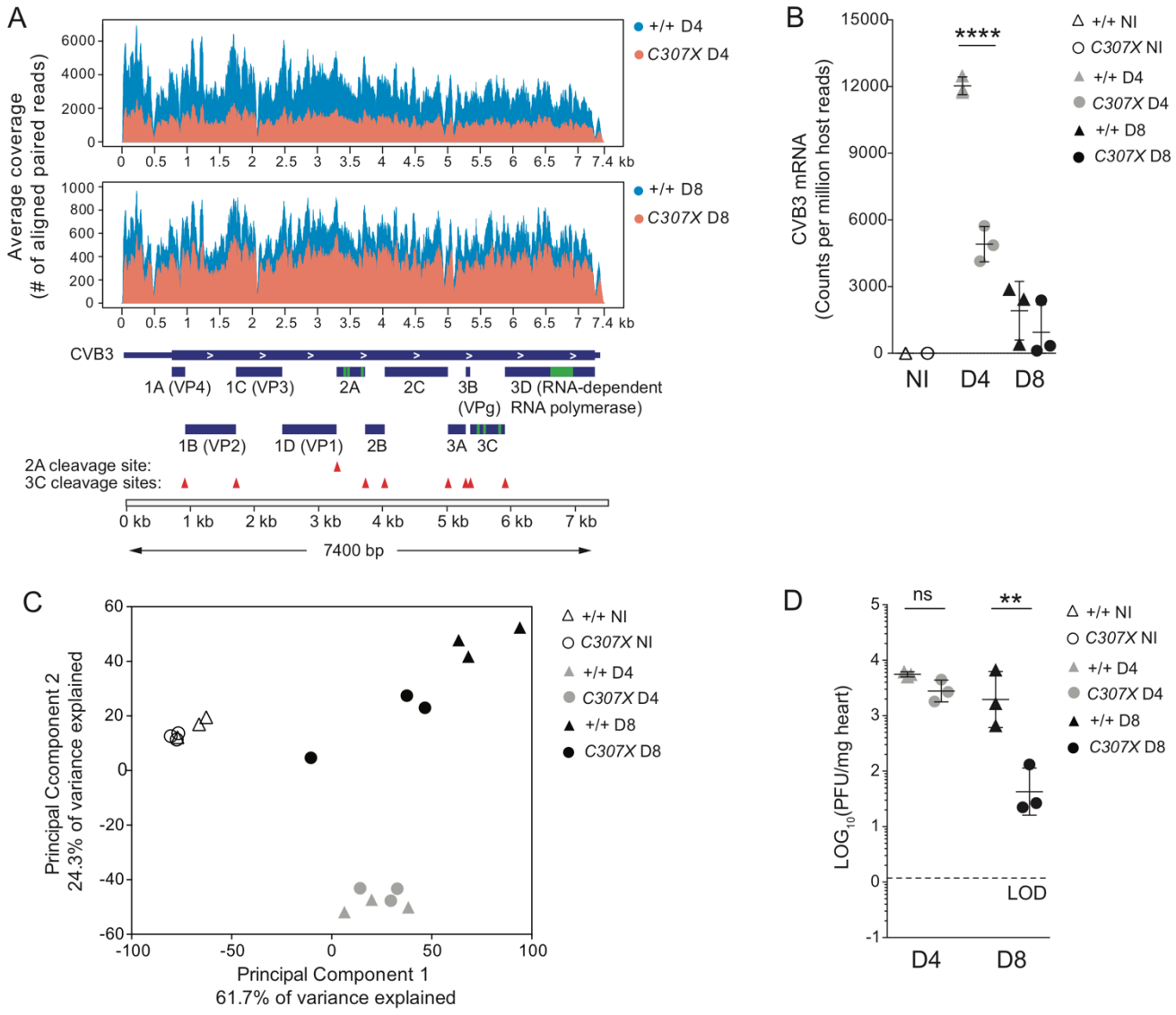

FIGURE 3. Dual RNA sequencing of viral and host mRNA in CVB3-infected heart tissue.

FIGURE 3. Dual RNA sequencing of viral and host mRNA in CVB3-infected heart tissue.

Dual RNA sequencing was performed on hearts (left ventricle) collected from CVB3-infected $Rel^{+/+}$ and Rel^{C307X} male littermate mice at day 4 and day 8 p.i., along with corresponding and non-infected controls (NI) (n=3 mice per group). (A) Coverage of paired reads aligning to the CVB3 strain H3 (Woodruff) genome, averaged over three mice in both +/+ and *C307X* genotype groups at days 4 and 8 p.i. CVB3 final protein products, active sites (green), and cleavage sites by viral proteases (red arrows) are indicated below. (B) Total CVB3 mRNA copies detected in each group, expressed as CVB3-aligning counts normalized per million host reads. (C) Principal component analysis was performed for all 18 samples across 13,620 genes expressed above a > 5 CPM cut-off in at least 2 samples. (D) CVB3 viral titers are depicted for corresponding infected samples; LOD indicates the limit of detection. (B, D) Data represent mean ± SD. Statistical tests: (B, D) Two-way ANOVA. $^{**}p < 0.01$, $^{****}p < 0.0001$, ns=non-significant.

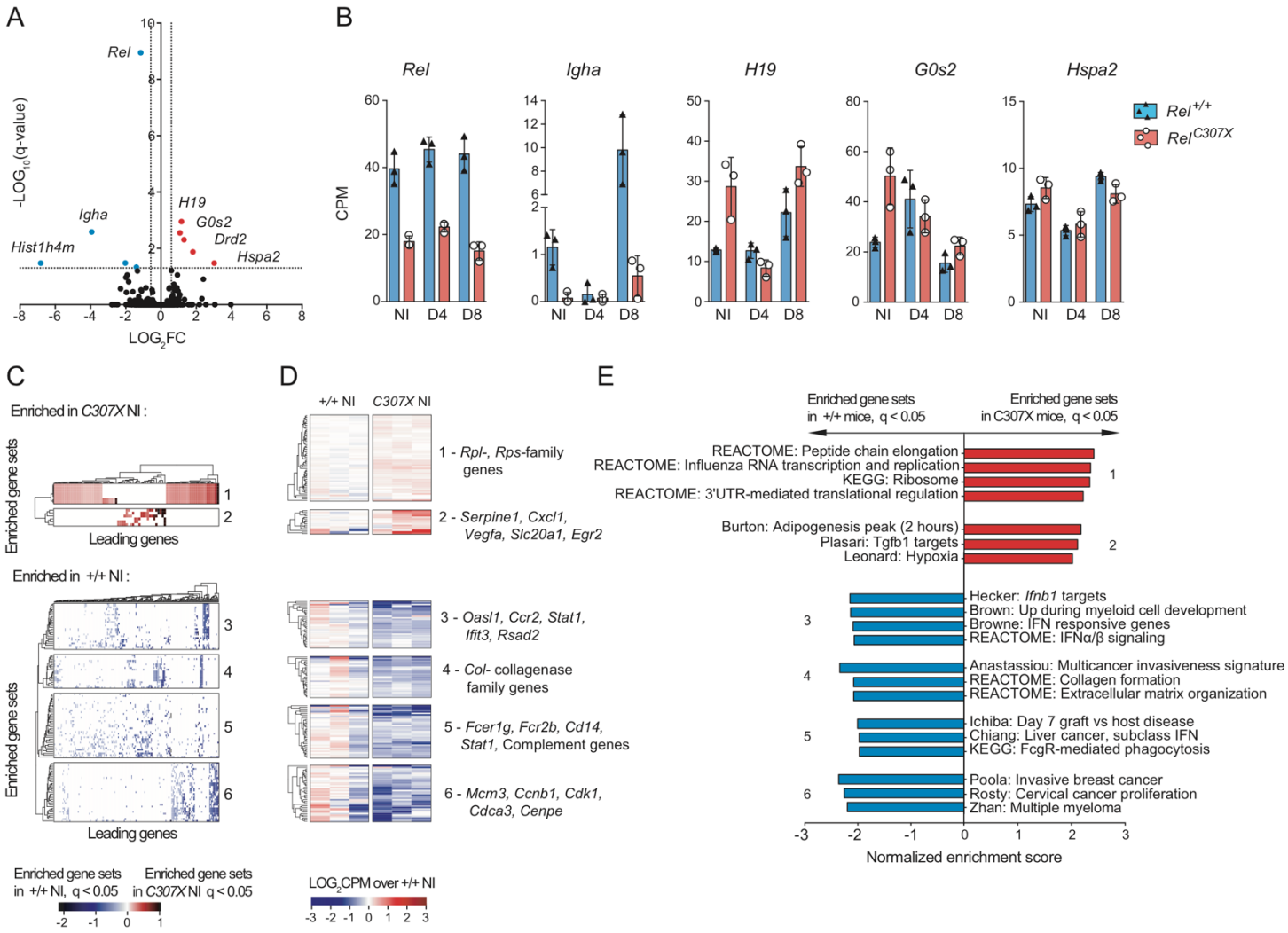

FIGURE 4. Host gene expression profile in Rel^{C307X} hearts at steady-state.

FIGURE 4. Host gene expression profile in Rel^{C307X} hearts at steady-state.

(A) Volcano plot of 10 differentially expressed genes (DEG) in *C307X* NI mice (directly compared to +/+ NI mice) that met a fold-change threshold of ± 1.5 and a BH-adjusted *q*-value < 0.05. DEG that are upregulated or downregulated in C307X NI mice relative to +/+ NI mice are coloured in red or blue, respectively. (B) Expression of select DEG in non-infected mice, including +/+ NI-upregulated *Rel* and *Igha*, and *C307X* NI-upregulated *H19*, *G0s2* and *Hspa2*. (C) GSEA analysis was performed to identify enriched ($q < 0.05$) curated gene sets in *C307X* NI mice (red) or in +/+ NI mice (blue), with gene sets in each group clustered by common leading genes that drive their enrichment. (D) Normalized expression of leading genes that are present in at least 10% of the enriched gene sets in each cluster defined in C, with select genes highlighted for each cluster. (E) Select enriched gene sets that are representative of *C307X* NI (red) and of +/+ NI (blue) enrichment clusters defined in C. (B) Data represent mean ± SD. Statistical tests: (B) FC and *q*-values (BH-adjusted) were assessed between NI groups using edgeR. (C and E) *q*-values (BH-adjusted) and normalized enrichment scores were assessed using GSEA, as further described in Materials and Methods.

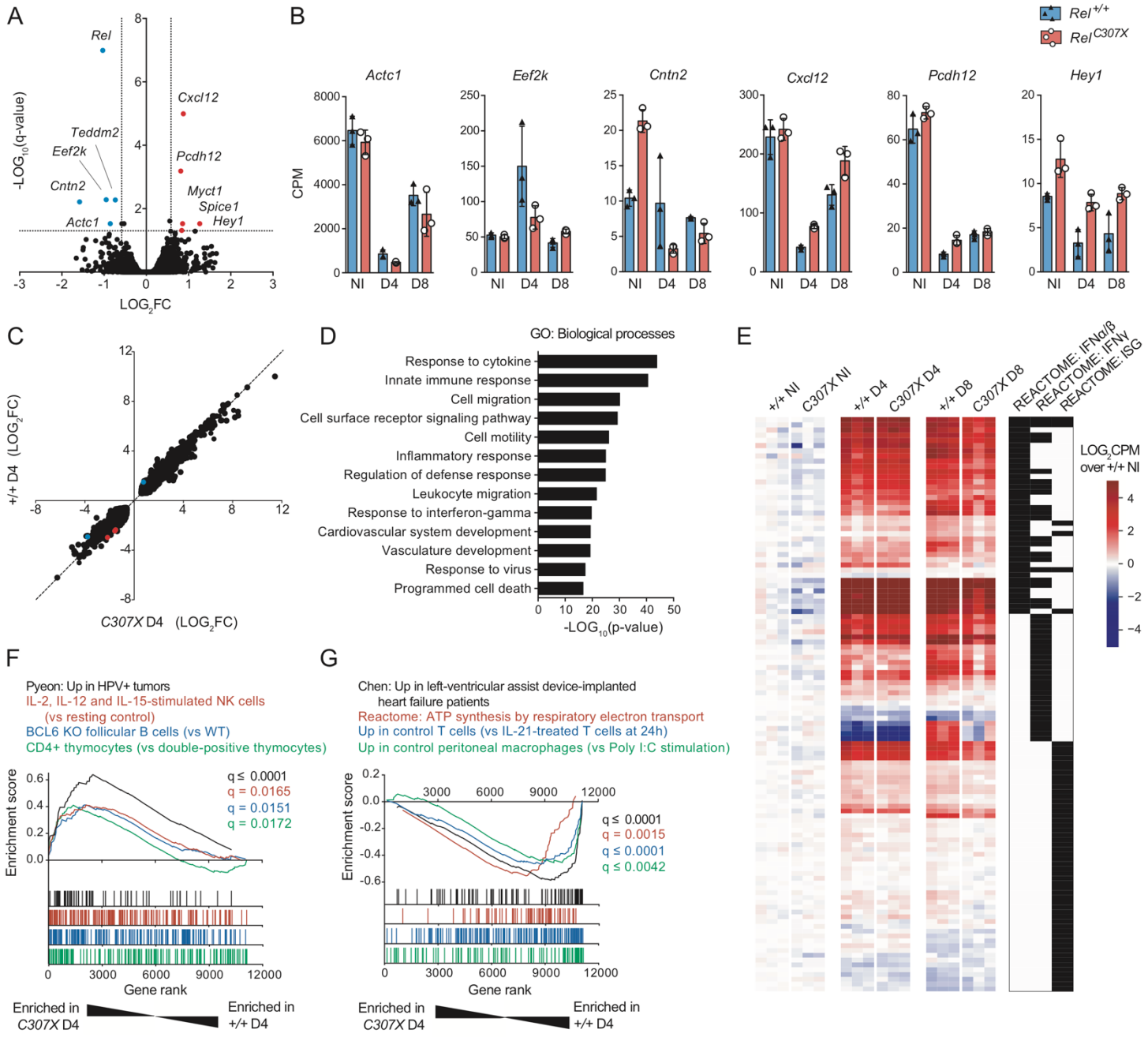

FIGURE 5. Equivalent IFN-stimulated responses in Rel$^{+/+}$ and Rel^{C307X} hearts at day 4 post-CVB3 infection.

FIGURE 5. Equivalent IFN-stimulated responses in $Rel^{+/+}$ and Rel^{C307X} hearts at day 4 post-CVB3 infection.

(A) Volcano plot of 10 DEG in *C307X* D4 mice that met a fold-change threshold of ± 1.5 and a *q*-value < 0.05 (BH-adjusted) compared to +/+ D4 mice. DEG that are upregulated or downregulated in C307X D4 mice relative to +/+ D4 mice are coloured in red or blue, respectively. (B) Expression of select DEG at D4 p.i., including +/+ D4-upregulated *Actc1, Eefk2* and *Cntn2*, and *C307X* D4-upregulated *Cxcl12*, *Pcdh12* and *Hey1*. (C) DEG for C307X D4 or +/+ D4 mice, each compared to +/+ NI controls, are plotted by fold-change. DEG that are common in both *C307X* D4 and +/+ D4 groups are depicted in black, while DEG that are unique to *C307X* D4 or to +/+ D4 are coloured red or blue, respectively. (D) Enriched gene ontology (GO) terms for 3353 DEG common to both *C307X* D4 and +/+ D4 mice. (E) Heatmap of normalized expression of select IFN-related genes defined in the REACTOME pathways "Interferon alpha/beta signaling", "Interferon gamma signaling", and "Antiviral mechanism by IFN-stimulated genes" for all sample groups. (F, G) GSEA analysis was performed to identify enriched ($q < 0.05$) curated gene sets in *C307X* D4 mice (F) or in +/+ D4 mice (G), with enrichment curves shown for select immune or curated gene sets. (B) Data represent mean ± SD. Statistical tests: (B) FC and *q*-values (BH-adjusted) were assessed between D4 groups using edgeR. (D) Nominal p-values for enriched GO terms were assessed using DAVID. (F, G) *q*-values (BH-adjusted) and normalized enrichment scores were assessed using GSEA, as further described in Materials and Methods.

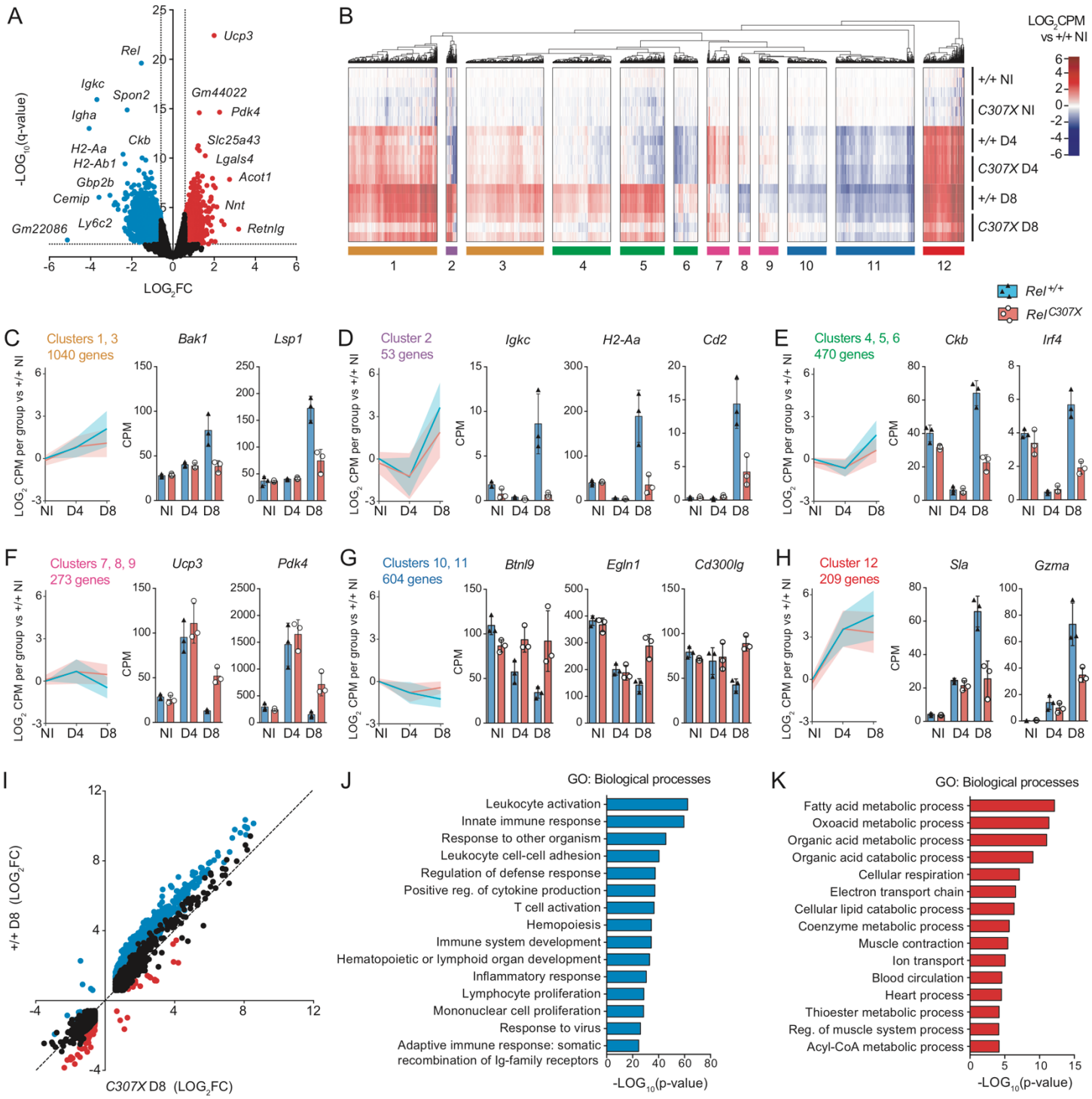

FIGURE 6. Altered expression of hematopoietic and heart-associated genes in Rel^{C307X} hearts at day 8 post-CVB3 infection.

FIGURE 6. Altered expression of hematopoietic and heart-associated genes in Rel^{C307X} hearts at day 8 post-CVB3 infection.

(A) Volcano plot of 2649 DEG in *C307X* D8 mice that met a fold-change threshold of ± 1.5 and a *q*-value <0.05 (BH-adjusted) compared to +/+ D8 mice. DEG that are upregulated or downregulated in *C307X* D8 mice relative to +/+ D8 mice are coloured in red or blue, respectively. (B) Hierarchical clustering of DEG at D8 p.i. into 12 clusters, and further grouped by colour based on their similar expression profiles across all time points. (C-H) Average gene expression (solid lines) across $n = 3$ mice per group and across all genes grouped in (C) clusters 1 and 3, (D) cluster 2, (E) clusters 4, 5 and 6, (F) clusters 7, 8, and 9, (G) clusters 10 and 11, and (H) cluster 12; shaded areas represent the standard deviation for each group and time point. Representative DEG and their expression are also shown in CPM. (I) DEG for *C307X* D8 or +/+ D8 mice, each compared to +/+ NI controls, are plotted by fold-change. DEG that are common in both *C307X* D8 and +/+ D8 groups are depicted in black, while DEG that are unique to *C307X* D8 or to +/+ D8 are coloured red or blue, respectively. (J) Enriched GO terms for 1107 DEG unique to +/+ D4 mice (blue), or (K) for 215 DEG unique to *C307X* D8 mice (red). (C-H) Data represent mean ± SD. Statistical tests: (C-H) FC and *q*-values (BH-adjusted) were assessed between D8 groups using edgeR. (J-K) Nominal *p*-values for enriched GO terms were assessed using DAVID, as further described in Materials and Methods.

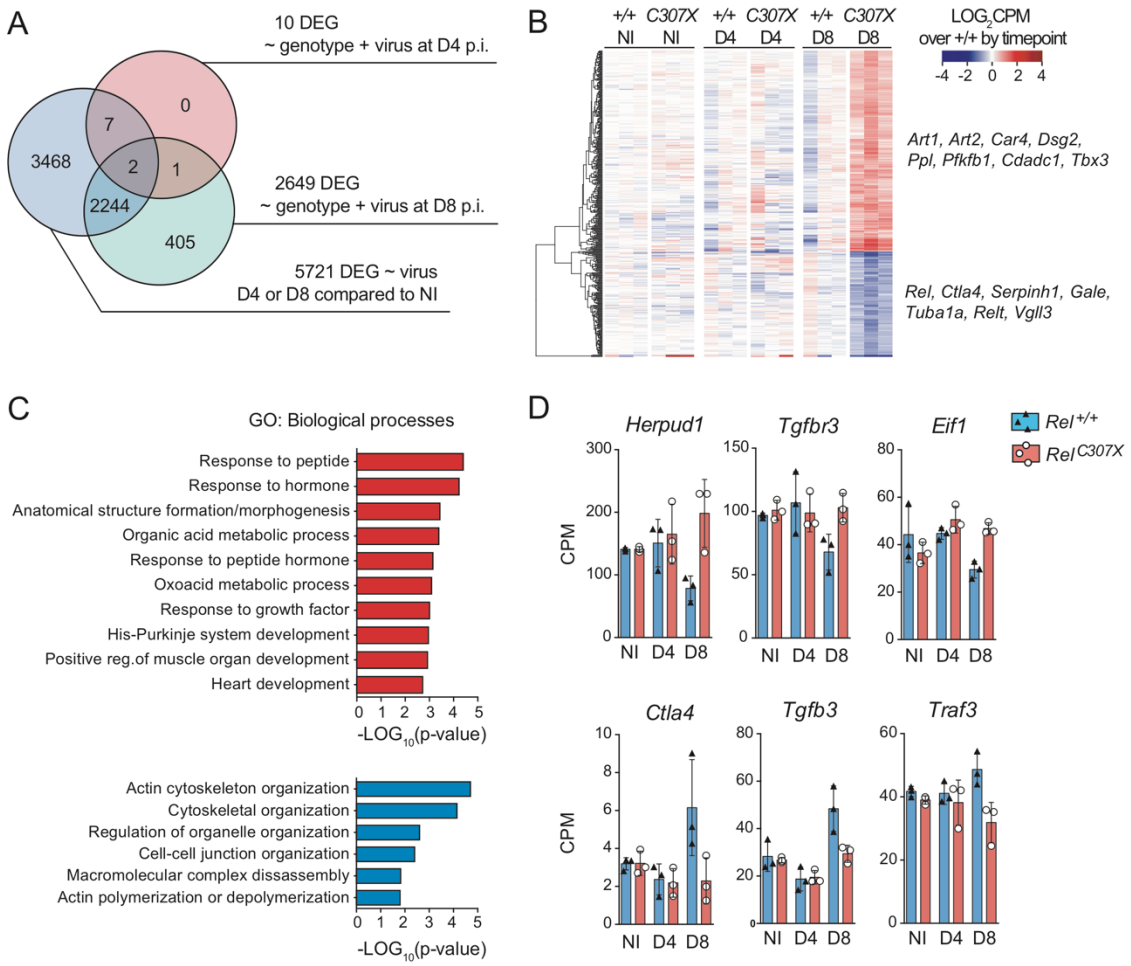

FIGURE 7. c-Rel-dependent changes in gene expression at day 8 post-CVB3 infection.

(A) 5721 total virus-driven DEG [≥1.5-fold change in expression, and $q < 0.05$ (BH-adjusted)] were identified by comparing all mice at D4 or D8 p.i. ($n = 12$) against all NI mice ($n = 6$), irrespective of genotype. Of the 2649 DEG identified between *C307X* D8 and +/+ D8 mice in Figure 3.4A, 406 DEG varied only due to the contribution of the Rel^{C307X} genotype. (B) Heatmap of normalized expression of these 406 Rel^{C307X}-specific DEG across all sample groups. (C) Enriched GO terms for 406 genotype-dependent DEG, with the upper panel (red) drawn from Rel^{C307X}-upregulated genes, and the lower panel (blue) drawn from Rel^{C307X}-downregulated genes. (D) Expression of select DEG in CPM, including *C307X* D8-upregulated genes *Herpud1*, *Tgfbr3* and *Eif1*, and +/+ D8-upregulated genes *Ctla4*, *Tgfb3*, and *Traf3*. (D) Data represent mean ± SD. Statistical tests: (C) Nominal *p*-values for enriched GO terms were assessed using DAVID, as further described in Materials and Methods.

4.8 SUPPLEMENTAL MATERIALS

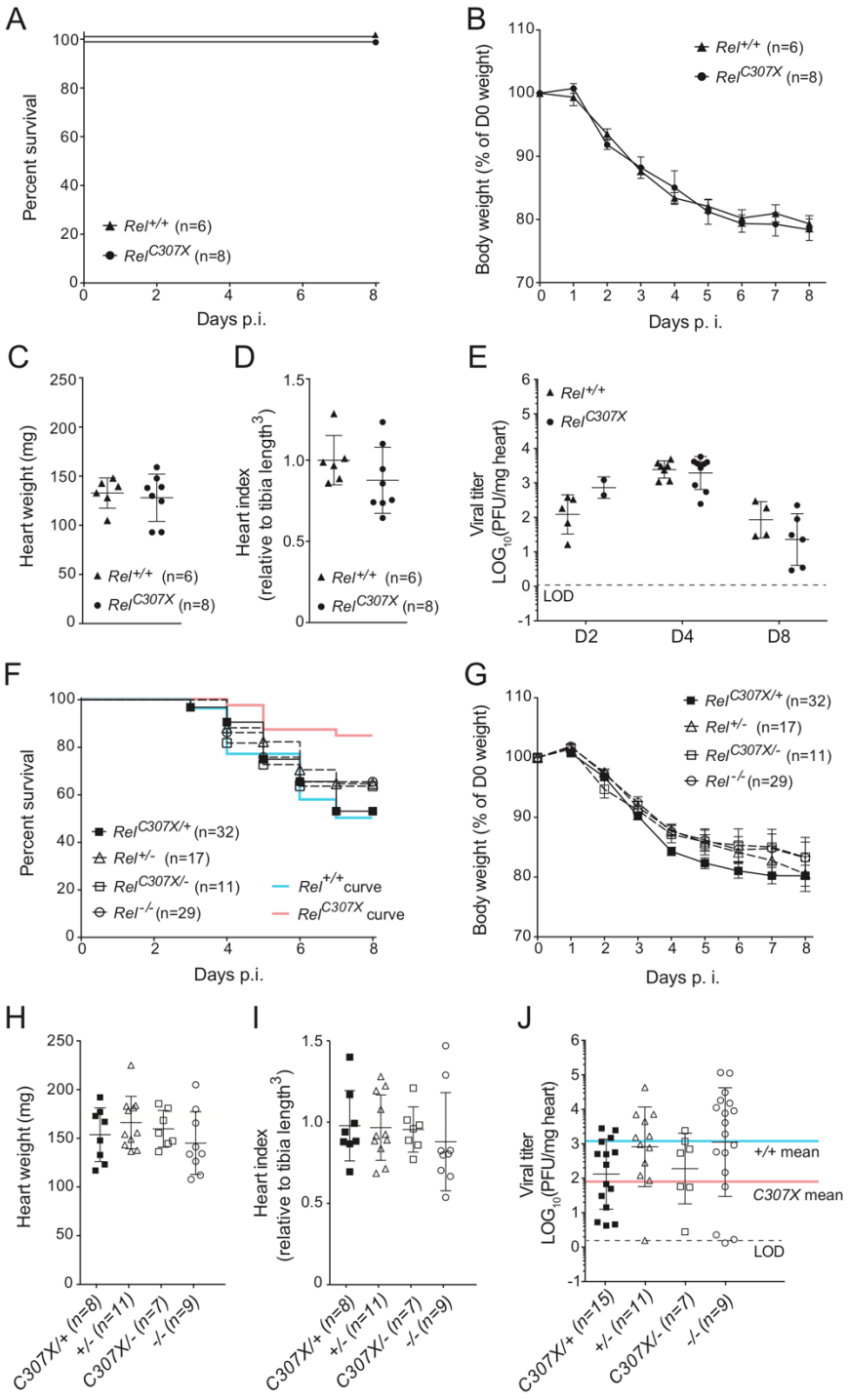

SUPPLEMENTAL FIGURE 1. CVB3 infection in female Rel^{C307X} mice, in Rel$^{-/-}$ males, and in compound heterozygous males.

SUPPLEMENTAL FIGURE 1. CVB3 infection in female Rel^{C307X} mice, in $Rel^{-/-}$ males, and in compound heterozygous males.

(A) Survival (B) weight loss, C) heart weight and (D) heart index normalized to the average tibia length^3 per mouse, for female littermate $Rel^{+/+}$ and Rel^{C307X} mice following i.p. infection with 30 PFU/g CVB3. (E) CVB3 viral titer was measured by viral plaque assay at days 2, 4 and 8 p.i. in female littermate $Rel^{+/+}$ and Rel^{C307X} mice. (F) Survival, (G) weight loss, (H) heart weight, (I) heart index, and (J) CVB3 viral titer for male $Rel^{-/-}$, $Rel^{+/-}$, $Rel^{C307X/-}$, and $Rel^{C307X/+}$ mice following i.p. infection with 30 PFU/g CVB3. (B, G) Data represent mean ± SEM, and (C-E, H-J) mean ± SD. LOD represents the limit of detection for each plaque assay, while blue or red dotted lines represent the average viral titer for male $Rel^{+/+}$ or Rel^{C307X} mice presented in Figure 4.1E, respectively.

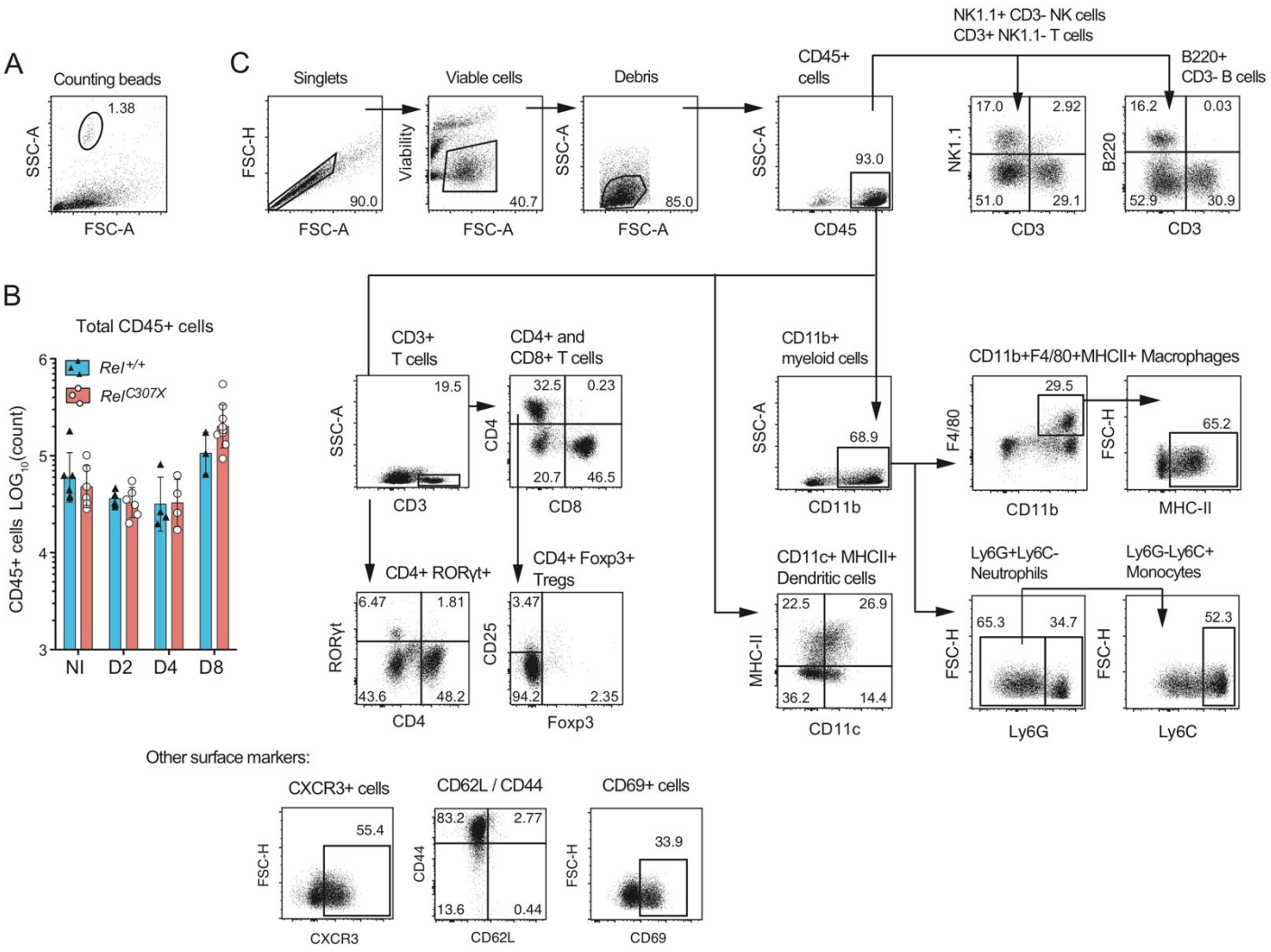

SUPPLEMENTAL FIGURE 2. Gating strategies for flow cytometry in the heart.

SUPPLEMENTAL FIGURE 2. Gating strategies for flow cytometry in the heart.

Single cell suspensions isolated from whole heart tissue were stained for flow cytometry as described in Materials and Methods. (A) Counting beads (5000 per sample) added to each sample immediately prior to acquisition. (B) Total singlet, viable, and debris-gated cells quantified per sample in the whole heart. (C) Representative gating strategy for cells acquired in day 8 CVB3-infected whole heart samples. Cells are first gated on singlet and viable populations, and debris gated out, followed by the separation of key infiltrating $CD45^+$ immune cell populations. $CD45^+$ cells are gated into $NK1.1^+CD3^-$ NK cells, $CD3^+NK1.1^-$ T cells and $B220^+CD3^-$ B cells, and $CD3^+$ T cells are further separated by $CD4^+$, $CD8^+$, $CD4^+ROR\gamma t^+$ or $CD4^+Foxp3^+$ expression. Further endophenotypes included CXCR3, CD44/CD62 or CD69-expressing subsets. Finally, $CD45^+$ cells are further gated into myeloid and dendritic cell populations, including $CD11b^+F4/80^+MHC\text{-}II^+$ macrophages, $CD11b^+Ly6G^+Ly6C^-$ neutrophils, $CD11b^+Ly6G^-Ly6C^+$ monocytes, and $CD11c^+$ $MHC\text{-}II^+$ dendritic cells.

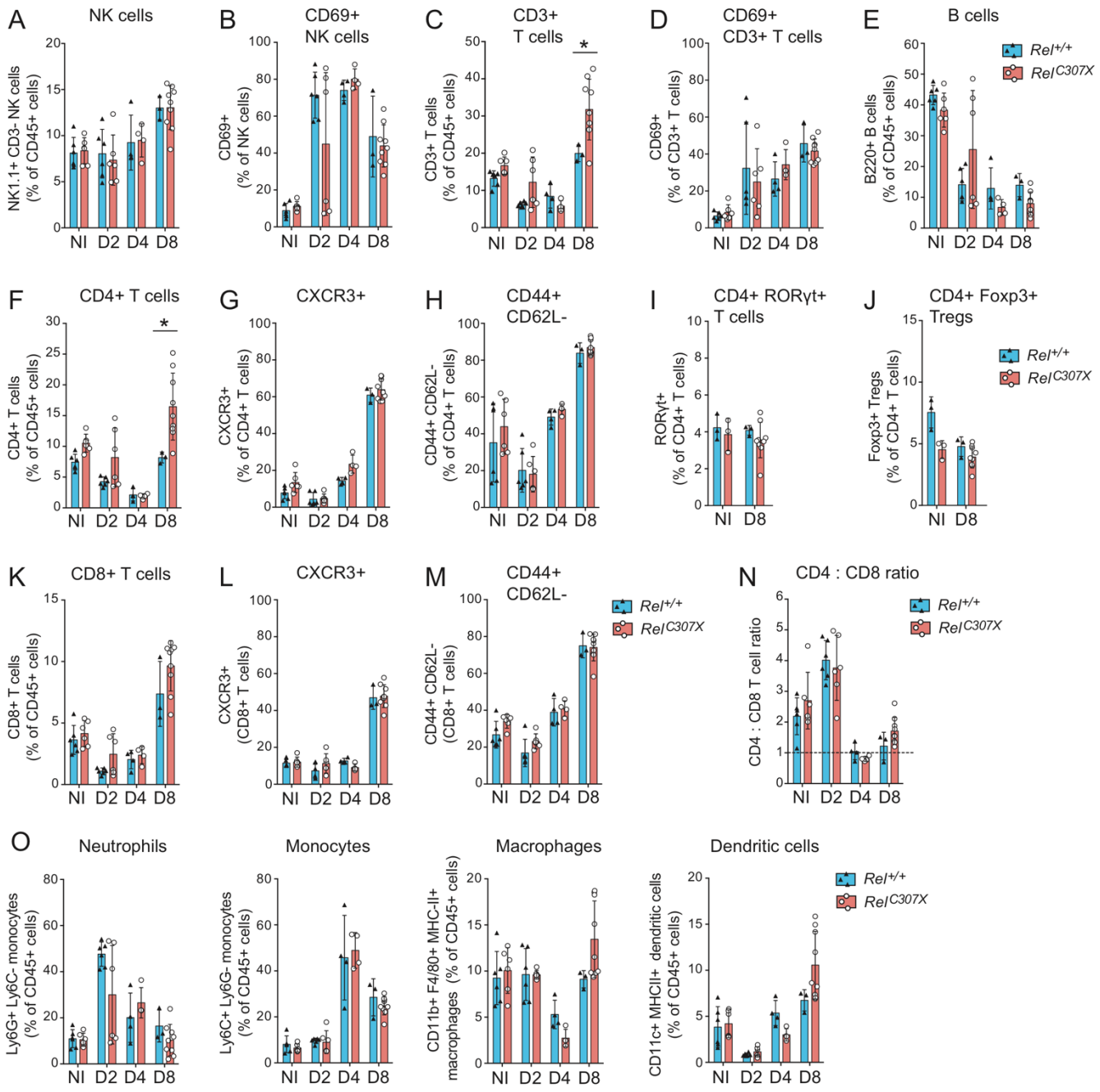

SUPPLEMENTAL FIGURE 3. Proportions of infiltrating immune cell populations in Rel^{C307X} hearts following CVB3 infection.

SUPPLEMENTAL FIGURE 3. Proportions of infiltrating immune cell populations in Rel^{C307X} hearts following CVB3 infection.

Hematopoietic cells were isolated from whole hearts collected from CVB3-infected *Rel*$^{+/+}$ and *Rel*^{C307X} male littermate mice at days 2, 4 and 8 p.i., or non-infected (NI) controls ($n \geq 3$ per group). Lymphocyte populations are expressed as a percentage of total CD45$^+$ cells, and include (A) NK cells (NK1.1$^+$CD3$^-$), (B) CD69$^+$ activated NK cells, (C) CD3$^+$ T cells (CD3$^+$NK1.1$^-$), (D) CD69$^+$ activated CD3$^+$ T cells, (E) B lymphocytes (B220$^+$CD3$^-$), (F) CD4$^+$ T cells, and (K) CD8$^+$ T cells. (G, L) CXCR3$^+$, (H, M) CD44$^+$CD62L$^-$, (I) RORγt$^+$ or (J) Foxp3$^+$ subsets are shown as a percentage of CD4$^+$ or CD8$^+$ T cells. (N) CD4$^+$ to CD8$^+$ T cell ratio is shown for groups across infection. (O) General myeloid and dendritic cell populations are shown as a percentage of total CD45$^+$ cells. Data represent mean ± SD. Statistical tests: Two-way ANOVA. *$p < 0.05$

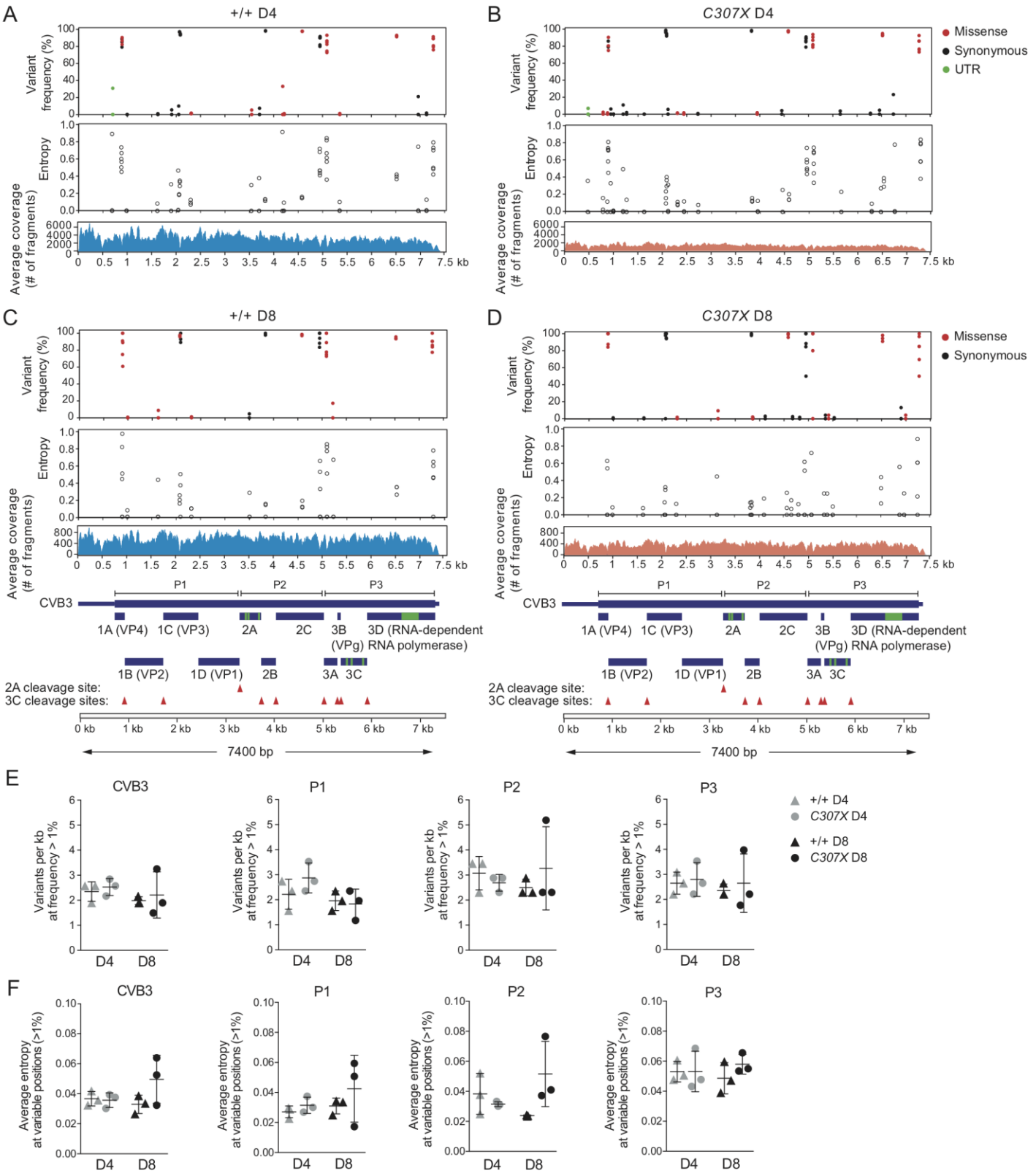

SUPPLEMENTAL FIGURE 4. Single nucleotide variants identified in infected host-isolated CVB3 viral genomes.

SUPPLEMENTAL FIGURE 4. Single nucleotide variants identified in infected host-isolated CVB3 viral genomes.

Following dual RNA sequencing of infected left ventricle tissue of $Rel^{+/+}$ and Rel^{C307X} male littermate mice at day 4 and day 8 p.i., viral mRNA reads were aligned to the CVB3 genome. In the following analysis, each CVB3-aligning read counted toward an independent viral particle, adding up to a population of CVB3 genomes found in each host sample. For (A) +/+ D4, (B) *C307X* D4, (C) +/+ D8, and (D) *C307X* D8 ($n = 3$ mice per group), the average frequency (above) and the Shannon's entropy value (middle) for each variant appearing at < 1% frequency in the virus population are shown in relation to the CVB3 genome. The average coverage of paired reads is also indicated (below), along with pro-polyprotein regions P1, P2 and P3, final protein products, active sites (green), and cleavage sites by viral proteases (red arrows). (E) Number of variants at < 1% frequency in the virus population per kilobase, and (F) Average Shannon's entropy across all variants <1 % frequency, for the entire CVB3 genome, and for P1, P2 and P3 pro-polyprotein regions. (E, F) Data represent mean ± SD. Statistical tests: (E, F) Two-way ANOVA.

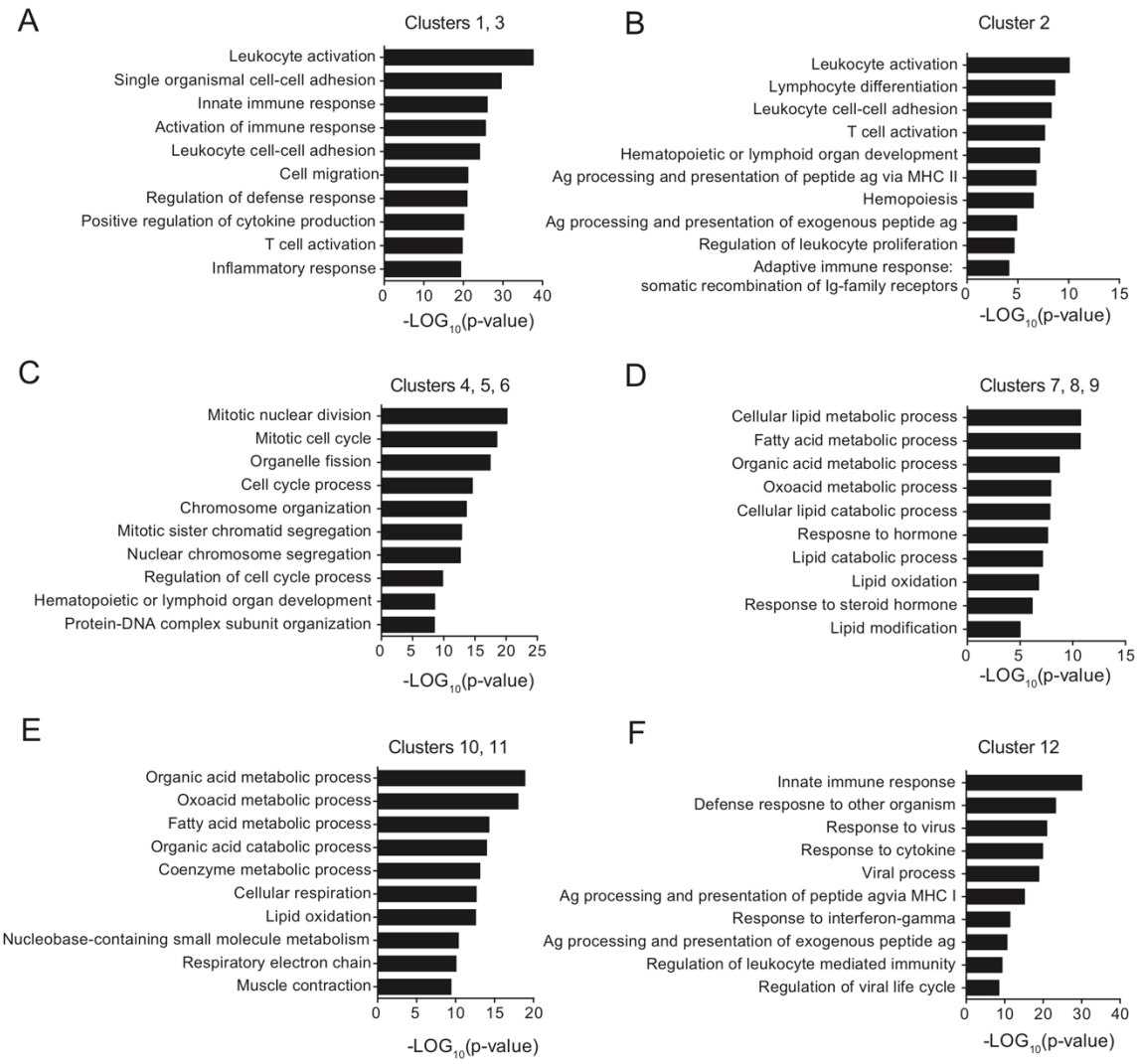

SUPPLEMENTAL FIGURE 5. Functional processes associated with clusters of DEG in Rel^{C307X} hearts at day 8 post-CVB3 infection.

2649 DEG between *C307X* D8 and +/+ D8 mice were identified and clustered according to their expression levels across infection, as shown in Figure 4.6B. Enriched GO terms for the DEG in each cluster are shown for (A) clusters 1 and 3, (B) cluster 2, (C) clusters 4, 5 and 6, (D) clusters 7, 8, and 9, (E) clusters 10 and 11, and (F) cluster 12. Statistical tests: (A-F) Nominal *p*-values for enriched GO terms were assessed using DAVID, as further described in Materials and Methods.

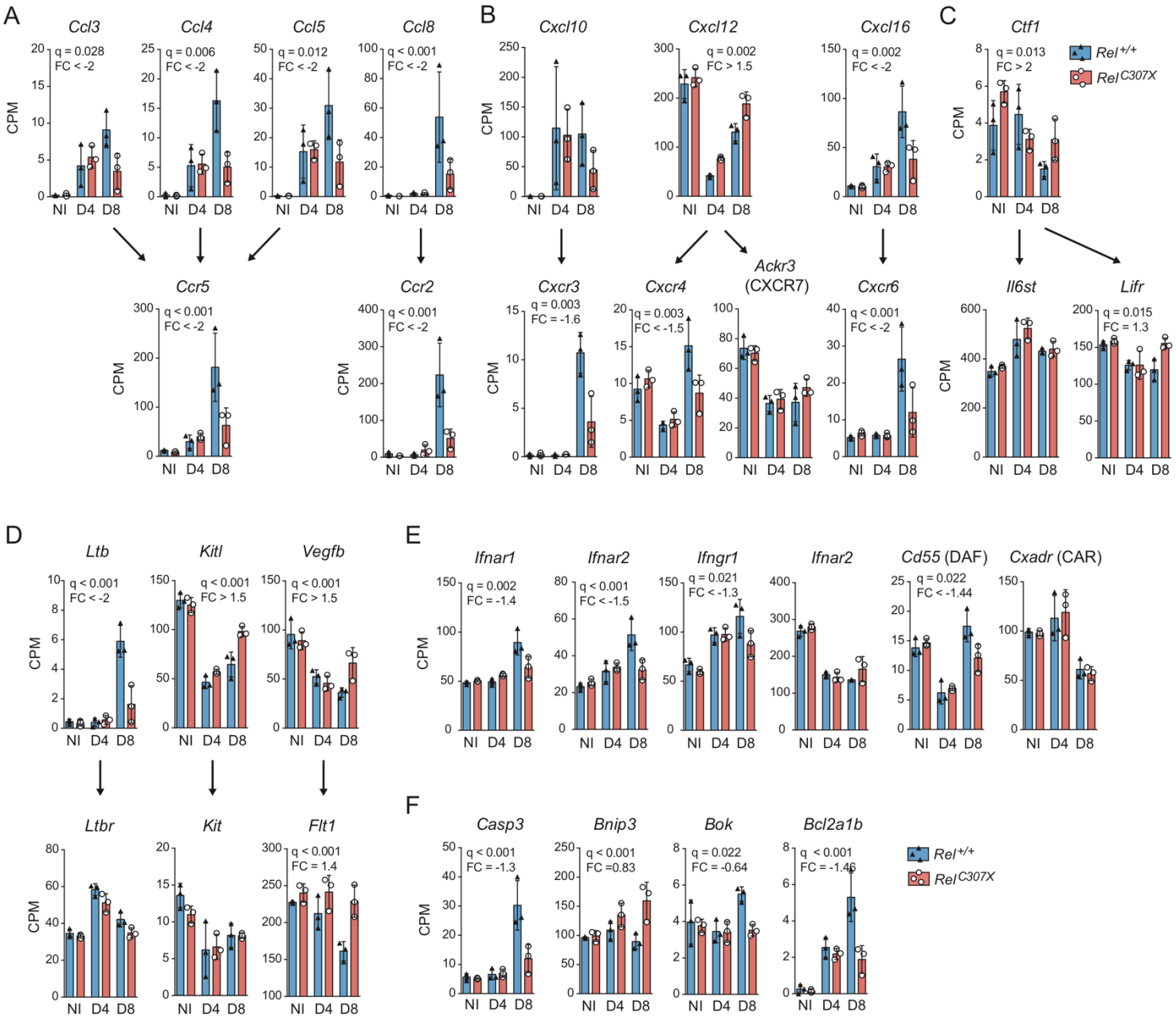

SUPPLEMENTAL FIGURE 6. Expression of cytokine, chemokine, their receptors, and cell survival genes during CVB3 infection in Rel$^{+/+}$ and Rel^{C307X} hearts.

SUPPLEMENTAL FIGURE 6. Expression of cytokine, chemokine, their receptors, and cell survival genes during CVB3 infection in $Rel^{+/+}$ and Rel^{C307X} hearts.

(A) Gene expression of select CC-family chemokines that signal through CCR5 and CCR2, and (B) CXC-family chemokines and their receptors across infection. (C) Gene expression of cardiotrophin (*Ctf1*) and its receptors (*Il6st*, *Lifr*), and of (D) ligand-receptor pairs including *Ltb*, *Kitl* and *Vegfb*. (E) Expression of IFN receptor genes, CAR and DAF entry receptor genes, and of (F) cell survival-associated genes, including *Casp3*, *Bnip3*, *Bok*, *Bcl2a1b*. Data represent mean ± SD. (A-F) FC and *q*-values (BH-adjusted) were assessed between D8 groups using edgeR, as further described in Materials and Methods.

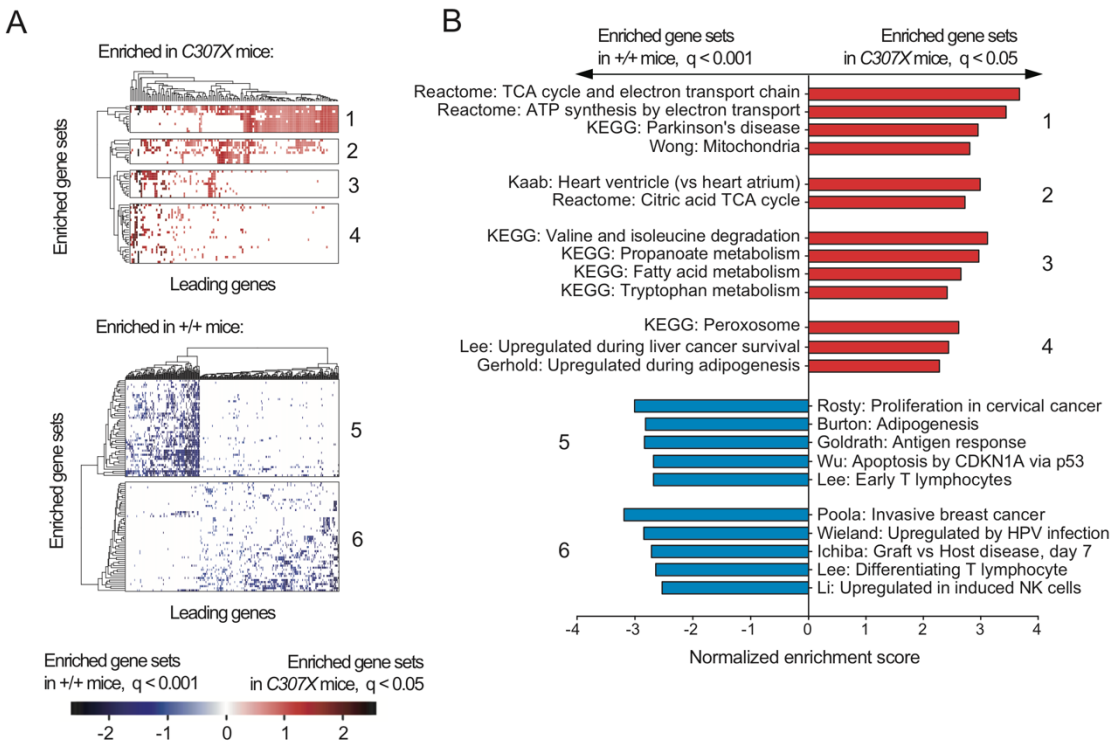

SUPPLEMENTAL FIGURE 7. Enriched immune and pathway signatures in CVB3-infected Rel$^{+/+}$ and Rel^{C307X} hearts at day 8 p.i.

(A) GSEA analysis was performed to identify enriched curated gene sets in *C307X* D8 mice (red, $q < 0.05$) or in +/+ D4 mice (blue, $q < 0.001$), with gene sets in each group clustered by common leading genes that drive their enrichment. Select (B) enriched curated gene sets that are representative of *C307X* D8 (red) and of +/+ D8 (blue) clusters defined in A. (B) Data represent mean ± SD. Statistical tests: *q*-values (BH-adjusted) and normalized enrichment scores were assessed using GSEA, as further described in Materials and Methods.

SUPPLEMENTAL TABLE 1. Single nucleotide variants in host-isolated CVB3 viral transcripts.

Variant (nucleotide)	Variant (amino acid)	CVB3 feature	Mutation type	Frequency (%)	Coverage*	Host**
Common variants identified in > 1 mouse across multiple groups						
c.889T>C	p.Asp49	1A (VP4)	Synonymous	87.4	49.6	All groups
c.893A>G	p.Ser51Gly	1A (VP4)	Missense	86.9	48.7	All groups
c.2071G>A	p.Ser443	1C (VP3)	Synonymous	89.4	194.7	All groups
c.2086C>T	p.Leu448	1C (VP3)	Synonymous	94.4	192.3	All groups
c.2309A>G	p.Thr523Ala	1C (VP3)	Missense	1.0	994.8	All groups
c.3832G>A	p.Lys1030	2B	Synonymous	98.5	1168.8	All groups
c.4585A>C	p.Lys1281Asn	2C	Missense	97.9	524.2	All groups
c.4948T>C	p.Ser1402	2C	Synonymous	88.2	26.4	All groups
c.4951A>C	p.Leu1403	2C	Synonymous	89.5	26.4	All groups
c.5090C>G	p.Arg1450Ala	3A	Missense	73.5	19.7	All groups
c.5091G>C	p.Arg1450Ala	3A	Missense	85.0	18.1	All groups
c.6521G>A	p.Val1927Ile	3D	Missense	93.6	1080.8	All groups
c.7271A>T	p.Ile2177Leu	3D	Missense	86.2	84.8	All groups
c.7273T>A	p.Ile2177Leu	3D	Missense	81.4	84.8	All groups
Unique variants						
c.702G>C	N/A	5’ UTR	N/A	31.0	1331	+/+ D4 #3
c.1627C>T	p.Ile295	1B (VP2)	Synonymous	1.1	4405	+/+ D4 #3
c.1909T>C	p.Asn389	1B (VP2)	Synonymous	5.5	5041	+/+ D4 #3
c.2053C>T	p.Asn437	1C (VP3)	Synonymous	10.0	3192	+/+ D4 #2
c.3549A>G	p.Gln936Arg	2A	Missense	5.3	2634	+/+ D4 #3
c.3709T>C	p.Arg989	2A	Synonymous	7.4	3626	+/+ D4 #2
c.4185A>C	p.Asn1148Ser	2C	Missense	33.2	3970	+/+ D4 #3
c.4215G>A	p.Ser1158Asn	2C	Missense	1.2	4275	+/+ D4 #2
c.5355A>T	p.Lys1538Ile	3B	Missense	1.4	2282	+/+ D4 #2
c.6964T>C	p.Tyr2074	3D	Synonymous	21.2	2837	+/+ D4 #1
c.7132T>C	p.Asp2130	3D	Synonymous	1.8	2055	+/+ D4 #2
c.475T>C	N/A	5’ UTR	N/A	6.9	452	*C307X* D4 #1
c.784G>C	p.Glu14Asp	1A (VP4)	Missense	2.4	1316	*C307X* D4 #1
c.874G>T	p.Gln44His	1A (VP4)	Missense	1.6	622	*C307X* D4 #2
c.943T>C	p.Ala67	1A (VP4)	Synonymous	6.1	1078	*C307X* D4 #2
c.1195G>A	p.Leu151	1B (VP2)	Synonymous	10.9	1075	*C307X* D4 #1
c.1267T>C	p.Tyr175	1B (VP2)	Synonymous	2.0	1104	*C307X* D4 #1
c.2116C>T	p.Ala458	1C (VP3)	Synonymous	5.7	1091	*C307X* D4 #3
c.2442A>G	p.Asn567Ser	1C (VP3)	Missense	1.7	1445	*C307X* D4 #1
c.2731A>G	p.Thr663	1D (VP1)	Synonymous	1.0	1586	*C307X* D4 #3
c.3947G>A	p.Ala1069Thr	2B	Missense	1.8	1368	*C307X* D4 #2
c.4453T>C	p.Val1237	2C	Synonymous	4.3	912	*C307X* D4 #1
c.5653C>T	p.Val1637	3C	Synonymous	3.8	1210	*C307X* D4 #1
c.6274C>T	p.Val1844	3D	Synonymous	1.2	822	*C307X* D4 #1
c.6460C>T	p.Asp1906	3D	Synonymous	4.7	1018	*C307X* D4 #2
c.6745C>T	p.Asp2001	3D	Synonymous	23.1	752	*C307X* D4 #2
c.3502C>T	p.Asn920	2A	Synonymous	4.8	493	+/+ D8 #2
c.5222T>C	p.Leu1494Ser	3A	Missense	17.3	81	+/+ D8 #3

SUPPLEMENTAL TABLE 1 (continued)

Variant (nucleotide)	Variant (amino acid)	CVB3 feature	Mutation type	Frequency (%)	Coverage*	Host*
c.997C>T	p.Ile85	1B (VP2)	Synonymous	1.1	1002	*C307X* D8 #1
c.3147C>T	p.Thr802Ile	1D (VP1)	Missense	9.4	139	*C307X* D8 #3
c.3857A>G	p.Ile1039Val	2B	Missense	2.1	1130	*C307X* D8 #1
c.3860T>C	p.Leu1040	2B	Synonymous	1.4	1128	*C307X* D8 #1
c.4114G>A	p.Lys1124	2C	Synonymous	2.9	1055	*C307X* D8 #1
c.4676T>C	p.Leu1312	2C	Synonymous	2.5	907	*C307X* D8 #1
c.4822A>C	p.Ile1360	2C	Synonymous	1.7	1054	*C307X* D8 #1
c.5350A>G	p.Gln1536	3B	Synonymous	4.1	723	*C307X* D8 #1
c.5415T>C	p.Val1558Ala	3C	Missense	4.1	943	*C307X* D8 #1
c.5530G>A	p.Val1596	3C	Synonymous	1.3	800	*C307X* D8 #1
c.6901T>C	p.Asp2053	3D	Synonymous	13.1	1018	*C307X* D8 #1
c.6996A>G	p.Glu2085Gly	3D	Missense	4.2	24	*C307X* D8 #2

* For common variants, this reflects the average sequencing coverage over all host samples. For unique variants, this value reflects the coverage in the specified host sample.

** Host samples (n = 3 mice per groups) are individually denoted #1, #2, or #3.

4.9 REFERENCES

1. Fairweather D, Stafford KA, Sung YK. 2012. Update on coxsackievirus B3 myocarditis. *Curr Opin Rheumatol* 24: 401-7
2. Gupta S, Markham DW, Drazner MH, Mammen PP. 2008. Fulminant myocarditis. *Nat Clin Pract Cardiovasc Med* 5: 693-706
3. Wells AI, Coyne CB. 2019. Enteroviruses: A Gut-Wrenching Game of Entry, Detection, and Evasion. *Viruses* 11
4. Cooper LT, Jr. 2009. Myocarditis. *N Engl J Med* 360: 1526-38
5. Negishi H, Osawa T, Ogami K, Ouyang X, Sakaguchi S, Koshiba R, Yanai H, Seko Y, Shitara H, Bishop K, Yonekawa H, et al. 2008. A critical link between Toll-like receptor 3 and type II interferon signaling pathways in antiviral innate immunity. *Proc Natl Acad Sci U S A* 105: 20446-51
6. Lafferty EI, Wiltshire SA, Angers I, Vidal SM, Qureshi ST. 2015. Unc93b1 -Dependent Endosomal Toll-Like Receptor Signaling Regulates Inflammation and Mortality during Coxsackievirus B3 Infection. *J Innate Immun* 7: 315-30
7. Riad A, Westermann D, Zietsch C, Savvatis K, Becher PM, Bereswill S, Heimesaat MM, Lettau O, Lassner D, Dörner A, Poller W, et al. 2011. TRIF is a critical survival factor in viral cardiomyopathy. *J Immunol* 186: 2561-70
8. Deonarain R, Cerullo D, Fuse K, Liu PP, Fish EN. 2004. Protective role for interferon-beta in coxsackievirus B3 infection. *Circulation* 110: 3540-3
9. Fuse K, Chan G, Liu Y, Gudgeon P, Husain M, Chen M, Yeh WC, Akira S, Liu PP. 2005. Myeloid differentiation factor-88 plays a crucial role in the pathogenesis of Coxsackievirus B3-induced myocarditis and influences type I interferon production. *Circulation* 112: 2276-85
10. Valaperti A, Nishii M, Liu Y, Naito K, Chan M, Zhang L, Skurk C, Schultheiss HP, Wells GA, Eriksson U, Liu PP. 2013. Innate immune interleukin-1 receptor-associated kinase 4 exacerbates viral myocarditis by reducing CCR5(+) CD11b(+) monocyte migration and impairing interferon production. *Circulation* 128: 1542-54
11. Opavsky MA, Penninger J, Aitken K, Wen WH, Dawood F, Mak T, Liu P. 1999. Susceptibility to myocarditis is dependent on the response of alphabeta T lymphocytes to coxsackieviral infection. *Circ Res* 85: 551-8

12. Liu P, Aitken K, Kong YY, Opavsky MA, Martino T, Dawood F, Wen WH, Kozieradzki I, Bachmaier K, Straus D, Mak TW, et al. 2000. The tyrosine kinase p56lck is essential in coxsackievirus B3-mediated heart disease. *Nat Med* 6: 429-34
13. Dupuis S, Jouanguy E, Al-Hajjar S, Fieschi C, Al-Mohsen IZ, Al-Jumaah S, Yang K, Chapgier A, Eidenschenk C, Eid P, Al Ghonaium A, et al. 2003. Impaired response to interferon-alpha/beta and lethal viral disease in human STAT1 deficiency. *Nat Genet* 33: 388-91
14. Casrouge A, Zhang SY, Eidenschenk C, Jouanguy E, Puel A, Yang K, Alcais A, Picard C, Mahfoufi N, Nicolas N, Lorenzo L, et al. 2006. Herpes simplex virus encephalitis in human UNC-93B deficiency. *Science* 314: 308-12
15. Sancho-Shimizu V, Perez de Diego R, Lorenzo L, Halwani R, Alangari A, Israelsson E, Fabrega S, Cardon A, Maluenda J, Tatematsu M, Mahvelati F, et al. 2011. Herpes simplex encephalitis in children with autosomal recessive and dominant TRIF deficiency. *J Clin Invest* 121: 4889-902
16. Casanova JL. 2015. Severe infectious diseases of childhood as monogenic inborn errors of immunity. *Proc Natl Acad Sci U S A* 112: E7128-37
17. Mancini M, Caignard G, Charbonneau B, Dumaine A, Wu N, Leiva-Torres GA, Gerondakis S, Pearson A, Qureshi ST, Sladek R, Vidal SM. 2019. Rel-Dependent Immune and Central Nervous System Mechanisms Control Viral Replication and Inflammation during Mouse Herpes Simplex Encephalitis. *J Immunol* 202: 1479-93
18. Kontgen F, Grumont RJ, Strasser A, Metcalf D, Li R, Tarlinton D, Gerondakis S. 1995. Mice lacking the c-rel proto-oncogene exhibit defects in lymphocyte proliferation, humoral immunity, and interleukin-2 expression. *Genes Dev* 9: 1965-77
19. Marton J, Albert D, Wiltshire SA, Park R, Bergen A, Qureshi S, Malo D, Burelle Y, Vidal SM. 2015. Cyclosporine A Treatment Inhibits Abcc6-Dependent Cardiac Necrosis and Calcification following Coxsackievirus B3 Infection in Mice. *PLoS One* 10: e0138222
20. Hagdorn QAJ, Bossers GPL, Koop AC, Piek A, Eijgenraam TR, van der Feen DE, Silljé HHW, de Boer RA, Berger RMF. 2019. A novel method optimizing the normalization of cardiac parameters in small animal models: the importance of dimensional indexing. *Am J Physiol Heart Circ Physiol* 316: H1552-h57

21. Choi JH, Cheong C, Dandamudi DB, Park CG, Rodriguez A, Mehandru S, Velinzon K, Jung IH, Yoo JY, Oh GT, Steinman RM. 2011. Flt3 signaling-dependent dendritic cells protect against atherosclerosis. *Immunity* 35: 819-31
22. Langlais D, Barreiro LB, Gros P. 2016. The macrophage IRF8/IRF1 regulome is required for protection against infections and is associated with chronic inflammation. *J Exp Med* 213: 585-603
23. Bolger AM, Lohse M, Usadel B. 2014. Trimmomatic: a flexible trimmer for Illumina sequence data. *Bioinformatics* 30: 2114-20
24. Kim D, Paggi JM, Park C, Bennett C, Salzberg SL. 2019. Graph-based genome alignment and genotyping with HISAT2 and HISAT-genotype. *Nat Biotechnol* 37: 907-15
25. Liao Y, Smyth GK, Shi W. 2014. featureCounts: an efficient general purpose program for assigning sequence reads to genomic features. *Bioinformatics* 30: 923-30
26. Knowlton KU, Jeon ES, Berkley N, Wessely R, Huber S. 1996. A mutation in the puff region of VP2 attenuates the myocarditic phenotype of an infectious cDNA of the Woodruff variant of coxsackievirus B3. *J Virol* 70: 7811-8
27. Li H, Handsaker B, Wysoker A, Fennell T, Ruan J, Homer N, Marth G, Abecasis G, Durbin R. 2009. The Sequence Alignment/Map format and SAMtools. *Bioinformatics* 25: 2078-9
28. Li H. 2011. A statistical framework for SNP calling, mutation discovery, association mapping and population genetical parameter estimation from sequencing data. *Bioinformatics* 27: 2987-93
29. Ghasemzadeh A, Ter Haar MM, Shams-Bakhsh M, Pirovano W, Pantaleo V. 2018. Shannon Entropy to Evaluate Substitution Rate Variation Among Viral Nucleotide Positions in Datasets of Viral siRNAs. *Methods Mol Biol* 1746: 187-95
30. Robinson MD, Oshlack A. 2010. A scaling normalization method for differential expression analysis of RNA-seq data. *Genome Biol* 11: R25
31. Huang da W, Sherman BT, Lempicki RA. 2009. Systematic and integrative analysis of large gene lists using DAVID bioinformatics resources. *Nat Protoc* 4: 44-57
32. Subramanian A, Tamayo P, Mootha VK, Mukherjee S, Ebert BL, Gillette MA, Paulovich A, Pomeroy SL, Golub TR, Lander ES, Mesirov JP. 2005. Gene set enrichment analysis: a knowledge-based approach for interpreting genome-wide expression profiles. *Proc Natl Acad Sci U S A* 102: 15545-50

33. Hobuss L, Foinquinos A, Jung M, Kenneweg F, Xiao K, Wang Y, Zimmer K, Remke J, Just A, Nowak J, Schmidt A, et al. 2020. Pleiotropic cardiac functions controlled by ischemia-induced lncRNA H19. *J Mol Cell Cardiol* 146: 43-59
34. Olson TM, Michels VV, Thibodeau SN, Tai YS, Keating MT. 1998. Actin mutations in dilated cardiomyopathy, a heritable form of heart failure. *Science* 280: 750-2
35. Pallante BA, Giovannone S, Fang-Yu L, Zhang J, Liu N, Kang G, Dun W, Boyden PA, Fishman GI. 2010. Contactin-2 expression in the cardiac Purkinje fiber network. *Circ Arrhythm Electrophysiol* 3: 186-94
36. Zhang HM, Wang F, Qiu Y, Ye X, Hanson P, Shen H, Yang D. 2016. Emodin inhibits coxsackievirus B3 replication via multiple signalling cascades leading to suppression of translation. *Biochem J* 473: 473-85
37. Kostina A, Shishkova A, Ignatieva E, Irtyuga O, Bogdanova M, Levchuk K, Golovkin A, Zhiduleva E, Uspenskiy V, Moiseeva O, Faggian G, et al. 2018. Different Notch signaling in cells from calcified bicuspid and tricuspid aortic valves. *J Mol Cell Cardiol* 114: 211-19
38. Ninh VK, El Hajj EC, Mouton AJ, Gardner JD. 2019. Prenatal Alcohol Exposure Causes Adverse Cardiac Extracellular Matrix Changes and Dysfunction in Neonatal Mice. *Cardiovasc Toxicol* 19: 389-400
39. Cavallero S, Shen H, Yi C, Lien CL, Kumar SR, Sucov HM. 2015. CXCL12 Signaling Is Essential for Maturation of the Ventricular Coronary Endothelial Plexus and Establishment of Functional Coronary Circulation. *Dev Cell* 33: 469-77
40. Torrealba N, Navarro-Marquez M, Garrido V, Pedrozo Z, Romero D, Eura Y, Villalobos E, Roa JC, Chiong M, Kokame K, Lavandero S. 2017. Herpud1 negatively regulates pathological cardiac hypertrophy by inducing IP3 receptor degradation. *Sci Rep* 7: 13402
41. Sun F, Li X, Duan WQ, Tian W, Gao M, Yang J, Wu XY, Huang D, Xia W, Han YN, Wang JX, et al. 2017. Transforming Growth Factor-β Receptor III is a Potential Regulator of Ischemia-Induced Cardiomyocyte Apoptosis. *J Am Heart Assoc* 6
42. Roberts BJ, Dragon JA, Moussawi M, Huber SA. 2012. Sex-specific signaling through Toll-Like Receptors 2 and 4 contributes to survival outcome of Coxsackievirus B3 infection in C57Bl/6 mice. *Biol Sex Differ* 3: 25

43. Fairweather D, Cooper LT, Jr., Blauwet LA. 2013. Sex and gender differences in myocarditis and dilated cardiomyopathy. *Curr Probl Cardiol* 38: 7-46
44. Gaspar-Pereira S, Fullard N, Townsend PA, Banks PS, Ellis EL, Fox C, Maxwell AG, Murphy LB, Kirk A, Bauer R, Caamaño JH, et al. 2012. The NF-κB subunit c-Rel stimulates cardiac hypertrophy and fibrosis. *Am J Pathol* 180: 929-39
45. Xiao Y, Rouzine IM, Bianco S, Acevedo A, Goldstein EF, Farkov M, Brodsky L, Andino R. 2016. RNA Recombination Enhances Adaptability and Is Required for Virus Spread and Virulence. *Cell Host Microbe* 19: 493-503
46. Becher PM, Hinrichs S, Fluschnik N, Hennigs JK, Klingel K, Blankenberg S, Westermann D, Lindner D. 2018. Role of Toll-like receptors and interferon regulatory factors in different experimental heart failure models of diverse etiology: IRF7 as novel cardiovascular stress-inducible factor. *PLoS One* 13: e0193844
47. Rivera-Serrano EE, DeAngelis N, Sherry B. 2017. Spontaneous activation of a MAVS-dependent antiviral signaling pathway determines high basal interferon-β expression in cardiac myocytes. *J Mol Cell Cardiol* 111: 102-13
48. Robbins SH, Bessou G, Cornillon A, Zucchini N, Rupp B, Ruzsics Z, Sacher T, Tomasello E, Vivier E, Koszinowski UH, Dalod M. 2007. Natural killer cells promote early CD8 T cell responses against cytomegalovirus. *PLoS Pathog* 3: e123
49. Gui J, Yue Y, Chen R, Xu W, Xiong S. 2012. A20 (TNFAIP3) alleviates CVB3-induced myocarditis via inhibiting NF-κB signaling. *PLoS One* 7: e46515
50. Zhazykbayeva S, Pabel S, Mügge A, Sossalla S, Hamdani N. 2020. The molecular mechanisms associated with the physiological responses to inflammation and oxidative stress in cardiovascular diseases. *Biophys Rev*
51. Wang JP, Cerny A, Asher DR, Kurt-Jones EA, Bronson RT, Finberg RW. 2010. MDA5 and MAVS mediate type I interferon responses to coxsackie B virus. *J Virol* 84: 254-60
52. Levoye A, Balabanian K, Baleux F, Bachelerie F, Lagane B. 2009. CXCR7 heterodimerizes with CXCR4 and regulates CXCL12-mediated G protein signaling. *Blood* 113: 6085-93
53. Harling-McNabb L, Deliyannis G, Jackson DC, Gerondakis S, Grigoriadis G, Brown LE. 1999. Mice lacking the transcription factor subunit Rel can clear an influenza infection and

have functional anti-viral cytotoxic T cells but do not develop an optimal antibody response. *Int Immunol* 11: 1431-9

54. Vdovenko D, Eriksson U. 2018. Regulatory Role of CD4(+) T Cells in Myocarditis. *J Immunol Res* 2018: 4396351
55. Ruan Q, Chen YH. 2012. Nuclear factor-kappaB in immunity and inflammation: the Treg and Th17 connection. *Adv Exp Med Biol* 946: 207-21
56. Consortium IMSG. 2013. Network-based multiple sclerosis pathway analysis with GWAS data from 15,000 cases and 30,000 controls. *Am J Hum Genet* 92: 854-65
57. Gregersen PK, Amos CI, Lee AT, Lu Y, Remmers EF, Kastner DL, Seldin MF, Criswell LA, Plenge RM, Holers VM, Mikuls TR, et al. 2009. REL, encoding a member of the NF-kappaB family of transcription factors, is a newly defined risk locus for rheumatoid arthritis. *Nat Genet* 41: 820-3
58. Zhernakova A, Festen EM, Franke L, Trynka G, van Diemen CC, Monsuur AJ, Bevova M, Nijmeijer RM, van 't Slot R, Heijmans R, Boezen HM, et al. 2008. Genetic analysis of innate immunity in Crohn's disease and ulcerative colitis identifies two susceptibility loci harboring CARD9 and IL18RAP. *Am J Hum Genet* 82: 1202-10

CHAPTER FIVE: GENERAL DISCUSSION

Together, the three previous chapters of this thesis comprise an in-depth characterization of various phenotypes associated with a novel ENU-induced mutation in the mouse *Rel* gene. This Rel^{C307X} mutation resulted in the expression of a truncated c-Rel product that was expected to impact a multitude of pathways that signal through NF-κB. Since *Rel* is expressed constitutively across many different cell types, and notably in hematopoietic cells, we hypothesized that the c-Rel transcription factor had an determining role in the regulation of the inflammatory response to viral infection. Thus, we focused our experimental design on neurotropic HSV-1 and cardiotropic CVB3 viruses, using flow cytometry and dual host-virus RNA sequencing to reveal how tissue resident and hematopoietic cells may affect the balance between beneficial and harmful inflammation.

In the model of mouse HSE presented in chapters 2 and 3 (Figure 5.1), the Rel^{C307X} mutation resulted in higher cell death in fibroblasts and in the steady-state brainstem, together with a congenital reduction in peripheral $Foxp3^+$ Tregs and increased peripheral $CD4^+$ T cells. Upon HSV-1 infection, early and elevated viral replication and inflammation were detected in high-responding Rel^{C307X} mice, attracting pathological infiltration of $CD4^+$ T cells and $Ly6C^+$ monocytes, triggering even higher viral loads and inflammatory Th1 cytokine production, and culminating in susceptibility to severe HSE.

In the model of CVB3-induced myocarditis presented in chapter 4 (Figure 5.2), the Rel^{C307X} mutation dampened basal IFN, inflammatory, and proliferative gene signatures in the homeostatic heart. Upon CVB3 infection, Rel^{C307X} mice controlled viral mRNA transcription by day 4 p.i., and viral loads by day 8 p.i., and developed an attenuated T cell and myeloid cell inflammatory response that limited damage to the heart muscle and promoted resistance to lethal myocarditis.

Where NF-κB-dependent regulation and upstream signaling are known to vary depending on the cell type, tissue, or trigger, these studies have narrowed the effect of the Rel^{C307X} mutation to a few key cell types ($CD4^+$ T cells and their subsets, inflammatory monocytes, microglia), within which to explore the biochemical impact of the mutation and its effect on disparate pathways. Our findings in the HSV-1-infected CNS and the CVB3-infected heart will be further discussed in parallel, and in the context of (1) intracellular viral infection and IFN responses, of (2) the cell-mediated leukocyte response, of (3) pathological damage to the infected tissue, and of (4) the molecular basis for alternative c-Rel transcriptional regulation.

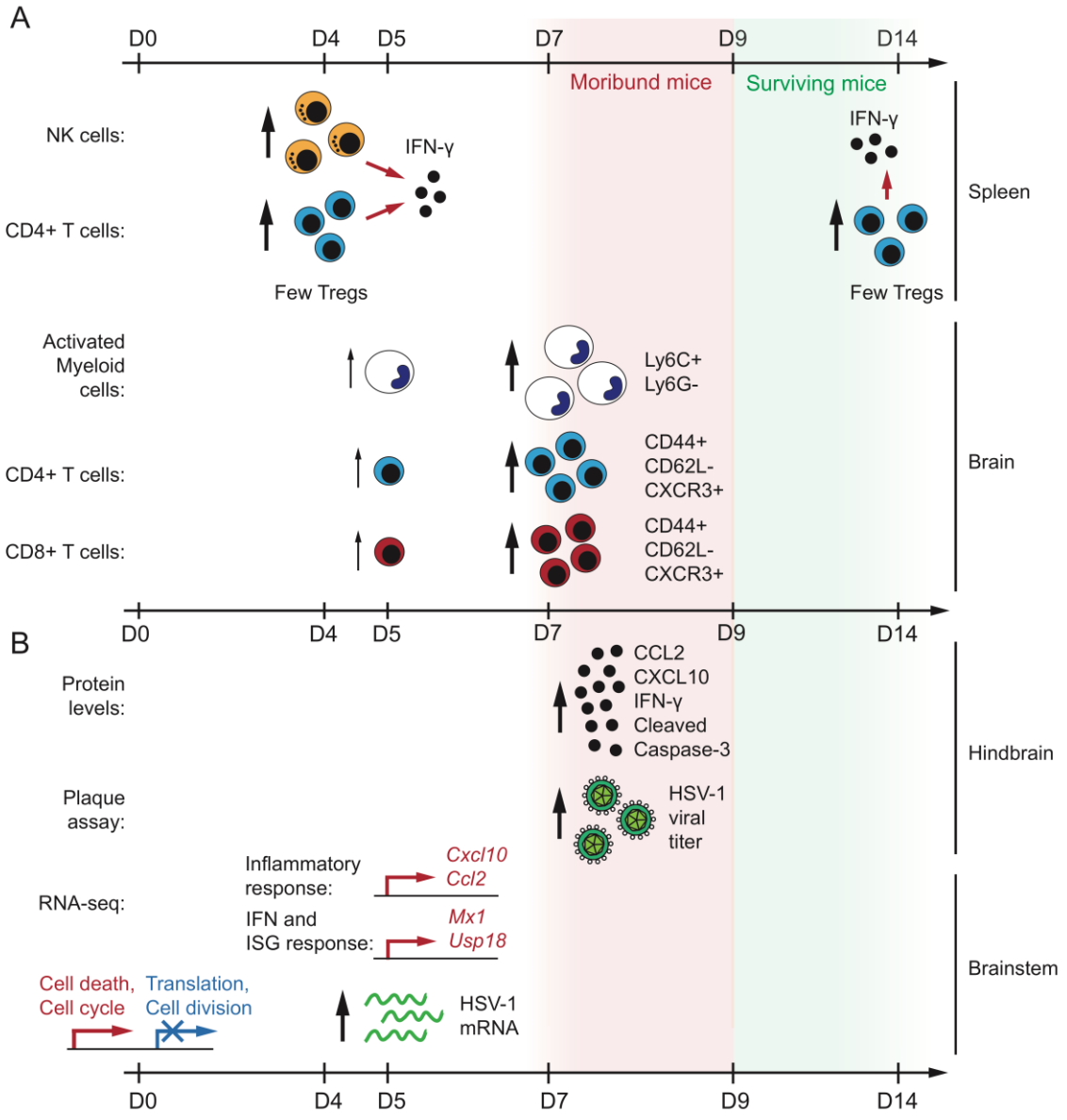

FIGURE 1. The Rel^{C307X} model of herpes simplex encephalitis.

(A) Changes in peripheral and brain-infiltrating cell populations by flow cytometry in *Rel*^{C307X} mice. (B) Changes in the transcriptional, protein and viral landscape in *Rel*^{C307X} hindbrains by RNA sequencing. All increases or decreases are relative to *Rel*$^{+/+}$ mice.

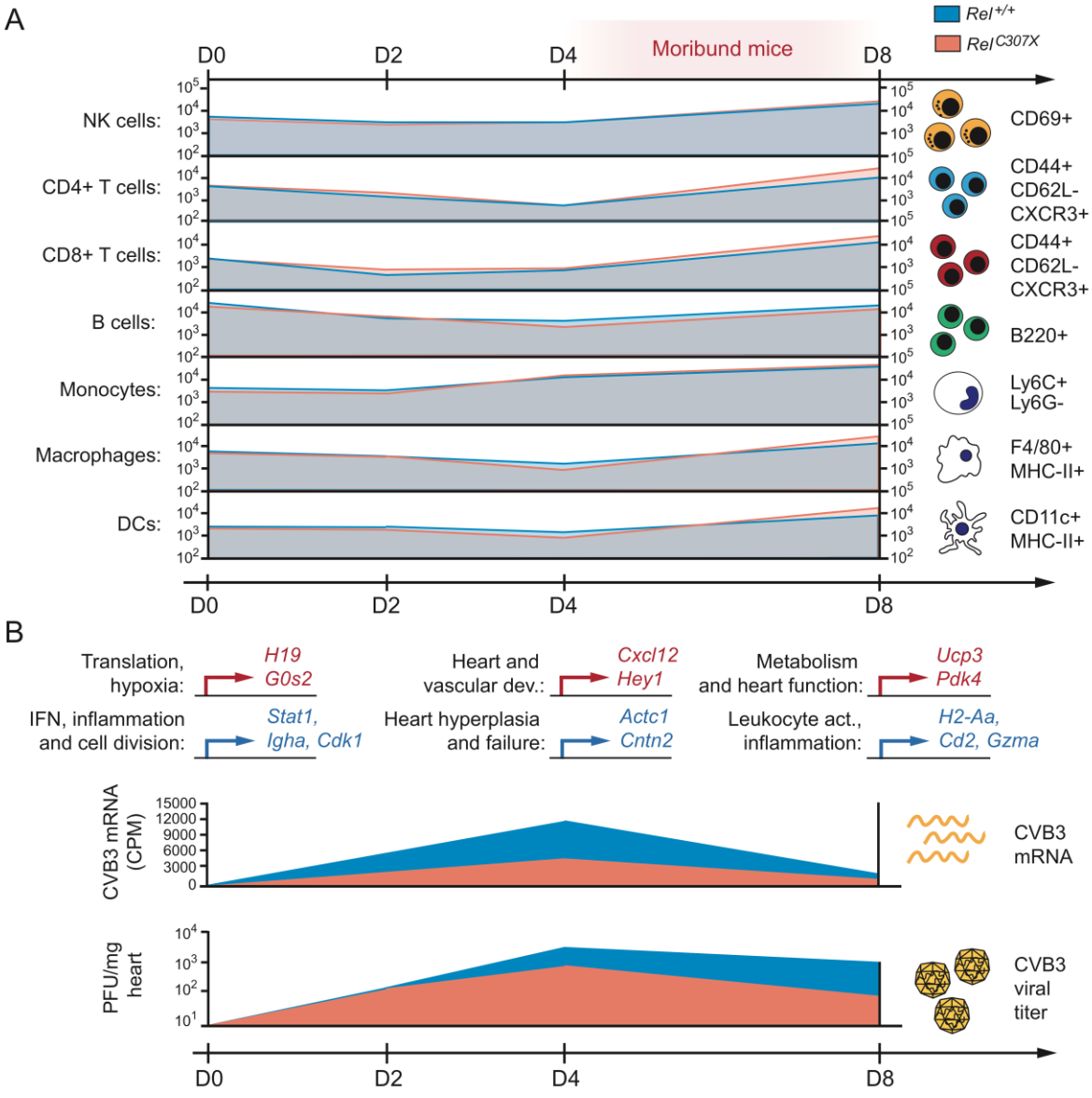

FIGURE 2. The Rel^{C307X} model of CVB3 myocarditis.

(A) Dynamics in heart-infiltrating cell populations by flow cytometry. (B) Changes in host and viral transcriptional landscapes in the heart *by RNA sequencing*, and of cardiac viral titers by plaque assay.

5.1 Viral replication and host type I IFN responses

Second only to survival proportions, divergent control of viral replication was the most striking effect of the mutation in both infection models. For HSV-1-infected *Rel*^{C307X} mice, that consistently yielded higher CNS viral loads compared to wild-types, our infection of mouse fibroblasts confirmed that intrinsic anti-HSV-1 control was not compromised in mutant animals—type I IFN-dependent responses were actually higher in infected brainstem. On the other hand, CVB3-infected *Rel*^{C307X} mice had normal ISG responses to infection, capable of reducing viral titers, and ensuring long-term survival. Overall, these findings suggest that the *Rel*^{C307X} mutation does not abrogate type I IFN signaling.

Other inborn genetic defects can result in differential outcomes to DNA or RNA viral infections. Where *Ticam1* (TRIF), *Ifnar* and *Ifng* are essential to the clearance of both HSV-1 and CVB3 (110, 123, 171, 174, 188, 194), *Rel*^{C307X} mice are most similar to *Myd88*$^{-/-}$ mice in their susceptibility to HSE but resistance to viral myocarditis (172, 175, 191). Even as we have confirmed that *Tlr3*$^{-/-}$, *Unc93b1*$^{-/-}$ and *Mavs*$^{-/-}$ mice were resistant to i.n. HSV-1 infection (172), but susceptible to CVB3 (110, 189, 192), c-Rel did not fit this pattern, and likely plays a redundant function in these primarily RNA-sensing cascades. While cGAS and STING, as cytoplasmic DNA sensors, have not been tested in the context of CVB3, they are required for protective responses against HSV-1 that may also involve c-Rel (177). Furthermore, with human *MYD88* mutations linked to pyogenic bacterial infections and not viral infections (245), and a newly-reported *REL*-deficient patient with wider ranging susceptibility to bacterial, viral and fungal infections (246), these models further confirm that a regulatory defect in *Rel*^{C307X} mice may fall beyond cell-intrinsic antiviral IFN signaling.

Rel^{C307X} did modulate IFN in other ways, first by dampening IFN-stimulated and inflammatory responses relative to wild-type mice in the adult heart at homeostasis. Both type I IFN and chronic inflammation are pathological in the non-infected heart (247-249), but may also have an effect in priming trafficking immune cells to respond more actively upon infection (77, 250). Notably, infected cardiomyocytes are not major producers of type I IFN, and benefit little from IFN responses during infection, suggesting that other cells modulate IFN via c-Rel in the heart (107). On the other hand, stronger type I IFN responses were detected in the HSV-1 infected *Rel*^{C307X} brainstem. In the CNS, previous studies have shown that TLR3-dependent type I IFN production by infected neurons, oligodendrocytes and astrocytes (87, 170), as well as

cGAS/STING-dependent type I IFN expression in microglia (177), are protective against HSE. Here, the *Rel*^{C307X} model deviates from TLR3/IFN deficiencies that underlie many childhood HSE cases, and instead recalls features of Aicardi-Goutières interferonopathies (251), and of IFN toxicity to neuronal cells (252). Of note, IFN-β production has been shown to be negatively regulated by the YingYang1 (YY1) transcription factor in a c-Rel-dependent manner, suggesting that in such cell-intrinsic contexts, a c-Rel deficiency could result in augmented type I IFN expression (253). Quantification of IFN production in the brain, and eventually in disparate primary cells in response to viral peptides or TLR agonists, may help to clarify potential mechanisms altered by the *Rel*^{C307X} mutation.

5.2 Cell-mediated immune responses

A definite advantage of *in vivo* mouse models of infection is that the system remains intact, and allows numerous interactions between cells, virus and secreted factors to be captured at once. Flow cytometry can further add to our understanding of these dynamics. For example, monocytes and CD69^{+} NK cells were present in the heart at day 4 post-CVB3 infection, and many chemokines expressed, before cardiac infiltration of T cells by day 8; only *Cxcl12* was specifically upregulated at day 4 and day 8 in *Rel*^{C307X} heart, hinting at a possible beneficial role for c-Rel/CXCL12 regulation in viral myocarditis (254). In the brain, *Cxcl10* (previously reported as a c-Rel target (235)) was upregulated in *Rel*^{C307X} mice at day 5 before symptom onset, and attracted CXCR3^{+} CD4^{+} T cells to the Th1-inflammed brain from day 7 onwards. On the myeloid side, *Ccl2* expression was also elevated in the early stages of infection, likely contributing with *Cxcl10* to the infiltration of activated CD45^{HI}CD11b^{+}Ly6C^{+} activated myeloid cells in the *Rel*^{C307X} brain—while a subset of these cells were CXCR3^{+}, their expression of CCR2 remains to be tested. Thus, the upregulation of certain chemokines beyond normal thresholds by C307X c-Rel merits further investigation, especially in our models where subsequent changes to the cellular landscape can determine infection outcome.

Cytotoxic T cell responses and IFN-γ are essential to manage viral replication during HSE (80, 88, 99, 194). Yet upon infection, HSE-susceptible *Rel*^{C307X} had significantly more circulating CD4^{+} T cells in the spleen and blood, and excess infiltration of CD4^{+} and CD8^{+} T cells in the brain. With *Rel*^{C307X} T cells expressing normal levels of CD44 and of IFN-γ, even elevated IFN-γ in the brainstem and cerebellum during HSE, and having detected no defects in the cytotoxic gene

module by RNA sequencing, we concluded that *Rel*^{C307X} mice did not succumb to HSE due to a defect in antigen-specific cytotoxic T cell responses. Neither were cellular cytotoxic responses compromised in CVB3-infected Rel^{C307X} mice that controlled and resolved infection in the heart better than wild-types.

Instead, *Rel*^{C307X}-dependent regulation of CD4^{+} T cell made an important contribution to HSE pathology, extending even into the *Rel*^{C307X} periphery, in both blood and spleen, where CD4^{+} T cell levels were augmented in at day 4 p.i. and remained elevated even in recovered *Rel*^{C307X} mice at day 14. While IL-2 was one of the first recognized c-Rel targets (226), defects in c-Rel-mediated IL-2 production had no effect on the proliferative capacity of T cells in other *in vivo* infection models (102, 255). In *Rel*^{C307X} mice, no defects in IL-2 production were detected in the brainstem and cerebellum during HSE, and T cell numbers were consistently elevated, suggesting that defective IL-2-depedent T cell proliferation did not account for viral escape. Rather, as in other models of CNS infection (81, 102, 103), excess Th1 CD4^{+} cells, in their role as mediators of neuroinflammation, were pathological in the HSV-1-infected *Rel*^{C307X} brain.

However, it was also clear from our studies that CVB3 cardiac infection captured a different facet of c-Rel regulation in T cells. Contrary to the brain, T cell infiltration in the heart is detrimental to the host and may help sustain lethal type I inflammation during acute infection (138, 139, 141, 142). Yet, heart-infiltrating *Rel*^{C307X} T cell genes related to migration, activation and cytokine production were reduced by day 8, once viral titers had been adequately suppressed. As proposed in Chapter 4, earlier *Rel*^{C307X}-dependent effects on heart homeostasis may allow the heart to better tolerate T cell-mediated inflammation. RNA sequencing did not reveal an imbalanced Th1 to Th2 response in *Rel*^{C307X} mice at the level of gene expression, thus further experiments to measure cytokine production in the heart at different stages of infection would be useful to assess the contribution of CD4^{+} T cell-mediated inflammation to pathology in *Rel*$^{+/+}$, or viral clearance in *Rel*^{C307X} mice.

Given the essential role of c-Rel in Treg and Th17 cell development, these T cell subsets may also play a role in either or both of these infection models. While few CD4^{+}Foxp3^{+} Tregs were detected in the brain overall, similar numbers were detected in the heart between *Rel*$^{+/+}$ and *Rel*^{C307X} mice. CD4^{+}CD25^{+}Foxp3^{+} were consistently lower in *Rel*^{C307X} the periphery. Past the intuitive notion that fewer Tregs would result in higher inflammation in *Rel*^{C307X} mice, our understanding of Treg contributions to HSE is limited (256, 257), and still controversial during

CVB3 myocarditis (148). As for the effect of the mutation on Th17 cells, that were poorly represented in the infected brain and heart, nor represented in the $Rel^{+/+}$ or Rel^{C307X} transcriptional profiles of these tissues, our preliminary unpublished work has shown that Rel^{C307X} mice are resistant to EAE induction (not shown), and thus may harbour a defect in pathological Th17 cells similar to $Rel^{-/-}$ mice (81). Future experiments will examine contributions by these subsets, but focus primarily on conventional T cells, particularly Th1 $CD4^+$ cells, whose dysregulation in Rel^{C307X} mice was common to both HSV-1 and CVB3 models.

5.3 Cell survival, metabolism and pathology

Global RNA sequencing is also useful for revealing the overall condition of an infected tissue. During infection, cell death markers correlated with pathology in HSV-1-susceptible Rel^{C307X} mice at day 5 (*Atf3, Sgk1, Plekhf1, Ifit2*) or in CVB3-susceptible $Rel^{+/+}$ mice (*Casp1, Casp3, Casp8, Bok, Bcl2a1b*) by day 8. However, the Rel^{C307X} mutation often resulted in earlier perturbations of cell survival pathways. Regarding HSV-1, Rel^{C307X} fibroblasts demonstrated elevated cleaved caspase-3 expression and cell death upon infection. Increased cell death was also detected in vivo at many different stages of HSV-1 infection: in non-infected brainstems (elevated *Prune2* expression, and signatures related to TRAIL- or UV-dependent apoptosis and hypoxia), at day 3 (decreased expression of anti-apoptotic *Sod2* and *Bcl2l1* by RT-qPCR*)*, at day 5 by RNA sequencing, and culminating at day 7 with high cleaved caspase-3 expression in the susceptible Rel^{C307X} brain. While cell death is often considered beneficial to reduce and abort viral replication, high Rel^{C307X} viral titers suggested that cell survival defects exacerbated pathology, as noted in other HSE models (258, 259). Cell death in Rel^{C307X} mice may specifically occur in infected neurons, given that c-Rel and c-Rel-dependent *Sod2* and *Bcl2l1* expression has been shown to play a pro-survival role in neurons (232, 260, 261), and that c-Rel-deficiency leads to long-term neurodegeneration in mice (262, 263). Microglia also undergo apoptosis after their activation in the inflamed CNS (264), and cAMP, PI3K and NF-κB inhibition also trigger astrocyte apoptosis (265, 266); these pathways were similarly dysregulated in the Rel^{C307X} brainstem at steady-state. Ultimately, the question of which CNS-resident cell types are preferentially infected by HSV-1 in Rel^{C307X} mice is yet to be determined; immunohistochemical staining of cleaved caspase-3 and HSV-1 glycoproteins to identify key cells, followed by *ex vivo* infection of primary neurons,

microglia or astrocytes (267) may help clarify the role of C307X c-Rel in cell survival or promotion of HSE disease.

In the homeostatic heart, cell survival gene signatures were not dysregulated in *Rel*^{C307X} mice. Still, the transcriptional profile of the heart was characteristic of hypoxia, like the *Rel*^{C307X} brainstem. However, ribosomal protein, mitochondrial, and oxidative respiration gene expression diverged completely between *Rel*^{C307X} brains and hearts—reduced in the HSV-1-susceptible brainstem or induced in the CVB3-resistant heart—and acted as indicators of healthy tissue and as predictors of an eventual protective response. Following through with CVB3 infection, mutant animals promoted vascular and heart development over heart failure at day 4, and metabolism over hyperinflammation at day 8. With such polarized effects on the condition of the infected heart, the *Rel*^{C307X} mutation may have a direct effect on resident cardiomyocytes. c-Rel has previously been implicated in cardiomyocyte function, where *Rel*$^{-/-}$ cardiomyocytes were smaller compared to wild-type cells (234); while infected *Rel*^{C307X} mice did not demonstrate cardiac hypertrophy, the cellular function and survival of these preferentially infected cells, and their contributions to CVB3 resistance in *Rel*^{C307X} mice, remain to be tested. Overall, RNA sequencing of these key energy-intensive tissues has revealed numerous effects of the *Rel*^{C307X} mutation on heart and brain function, whose impacts on the pathological host response to infection translated to increased caspase-3-dependent cell death in the brain, and remain to be ascertained in the heart.

5.4 Molecular impact of the Rel^{C307X} mutation on c-Rel transcriptional activity

The homozygous *Rel*^{C307X} mutation was first identified in a pedigree of HSV-1-susceptible mice issued from a founder ENU-treated male mouse (*Coby*). By introducing a premature stop codon in a gene previously implicated in hematopoietic cell responses, and given the susceptibility of *Rel*$^{-/-}$ mice to HSV-1 infection, the ENU-induced *Rel*^{C307X} mutation was singled-out as the causal mutation that explained HSE susceptibility in our initial phenotypic screen. However, following the wider characterization of *Rel*^{C307X} phenotypes presented in this thesis, the nature of the mutation remains unclear, or at least, it does not comfortably fit any one definite category. For one, *Rel*^{C307X} and *Rel*$^{-/-}$ mice were both susceptible to HSE, while heterozygous *Rel*$^{C307X/+}$ and wild-type *Rel*$^{+/+}$ mice were resistant, supporting a recessive loss-of-function mode of inheritance. However, *Rel*^{C307X} mice were uniquely resistant to CVB3 myocarditis compared to both wild-type *Rel*$^{+/+}$ and even *Rel*$^{-/-}$ mice. While a loss-of-function defect in pathological immune cells could also underlie

the protective host response to CVB3, it is also possible that the truncated c-Rel product possesses additional functionality (gain-of-function). Finally, as a transcription factor that can induce or repress many target genes, the loss of its transactivation domains and inhibitory domain may potentially cost the truncated C307X product some of its native activity (a hypermorphic effect) (268). Ultimately, as the behaviour of the mutation may vary across different phenotypes or read-outs, the only consistent findings were that the mutant allele does not behave in a dose-dependent manner or as a dominant negative allele, but that two copies of the Rel^{C307X} allele are required to mediate HSE susceptibility or CVB3 resistance. The Rel^{C307X} mutation therefore behaves as a fully recessive variant in these contexts.

Functionally, RNA sequencing confirmed that Rel^{C307X} transcripts were downregulated at all timepoints in the brain and heart, and therefore may be subject to some nonsense-mediated decay. Homozygous Rel^{C307X} mice have also been confirmed to exclusively express a truncated ~35 kDa c-Rel product in splenocytes, and that this product was capable of nuclear translocation. As for its effect on NF-κB activity and DNA binding, preliminary work has shown that TLR agonist-stimulated Rel^{C307X} BMDM yielded an altered pattern of nuclear proteins bound to NF-κB consensus sequences using band-shift assays (not shown). Chromatin immunoprecipitation-qPCR of key c-Rel targets would be a sensible first step to determining if the truncated factor, in homodimer or heterodimer configuration with another NF-κB subunit, can bind to promoter consensus sequences. Effectively, we have validated that expression of *Il12p40* and *Il23p19*, encoding subunits of mature IL-12p70 and IL-23 cytokines, is severely reduced in TLR agonist-treated Rel^{C307X} BMDM and BMDC, as in $Rel^{-/-}$ cells (not shown). These clear cell-intrinsic effects, however, did not translate to the HSV-1 infected Rel^{C307X} brainstem, which yielded normal levels of IL-12p70. Interestingly, like Rel^{C307X} mice, $Il12rb1^{-/-}$ mice are resistant to CVB3 infection, prompting further investigation into how c-Rel-dependent defects in IL-12 and IL-23 production may play a role in explaining the Rel^{C307X} phenotype in the heart (143).

Ultimately, the *in vivo* effect of the mutation, and its penetrance, is made more complex by the fact that c-Rel is a transcription factor. First, given how c-Rel-dependent gene induction or repression will reasonably occur in many hematopoietic and non-hematopoietic cell types where c-Rel is constitutively expressed, there is a random element to these diverse pathway and cellular interaction, as they navigate a specific tissue context among resident cells that are preferentially infected or vary in their viral phase of infection (269). During HSV-1 infection alone, recent single

cell RNA sequencing of *ex vivo* infected fibroblasts has revealed significant variability in the number of viral sequences captured per cell (270, 271) that, if extrapolated an *in vivo* system, would create variation in pathogenicity and in host responses. Second, protein structure and biochemical function can provide a molecular basis to explain a mutation's penetrance. For example, a Janus-associated kinase 3 $Jak3^{W81R}$ mutation was shown to have a negative dominant effect on *Plasmodium berghei* infection outcome, where homozygotes were fully resistant, and $Jak3^{W81R/+}$ heterozygotes ~50% resistant to experimental cerebral malaria; in cells where both wild-type and mutant Jak3 kinases are recruited as heterodimers to membrane-associated signaling receptors, Bongfen and colleagues proposed that mutant kinases may impede cross-phosphorylation events on neighbouring wild-type kinases and dampen proper signaling (272).

Therefore regarding the homozygous Rel^{C307X} mutation, which only drove an aberrant HSE response roughly 50% of the time, it is important to note that NF-κB subunit dynamics are complex, tightly regulated, and context-specific (218, 273). The formation and configuration of active NF-κB dimers, as the most proximal event to nuclear entry and DNA binding, is likely to influence the target gene expression. In theory, where C307X c-Rel homodimers cannot directly modulate transcription, heterodimeric association of C307X c-Rel with p65 or p50 subunits would be possible. Further investigation of the cells and contexts within which these heterodimers form, and how they might compete to effect transcription or complex stability, might clarify our understanding of the Re^{lC307X} mutation's penetrance. As a notable parallel, the transcription factor IRF3 can also homodimerize, or heterodimerize with IRF7 to modulate inflammatory gene transcription; the partial susceptibility of $Irf3^{-/-}$ mice to HSE, but complete susceptibility of $Irf3^{-/-}$ $Irf7^{-/-}$ double knockouts, supports the concept that heterodimer dynamics can influence HSE development in mice (172, 195).

As further examples of how NF-κB subunit interactions can be modified during infection or by cleavage events, polioviruses (of the same enterovirus family as CVB3) can cleave RelA/p65 via their encoded 3C viral protease, while host-mediated cleavage of RelA by host caspase-3 can reduce HIV-1 replication (274, 275). Furthermore, virulence factors gp63 (various *Leishmania* species) and NleC (enteropathogenic/hemorrhagic *Escherichia coli*) both cleave RelA to a respective 35 or 38 kDa product to alter NF-κB-mediated proinflammatory responses (276, 277). Given the similar size of this RelA product compared to our truncated C307X c-Rel product, *Leishmania* gp63 is of particularly interest, since the cleaved N-terminal $p35^{RelA}$ could recruit NF-

κB subunit p50, and together induce the expression of chemokines CCL2, CCL3, CCL4 and CXCL2 (276). Thus, it is conceivable that despite a lack of transactivation domains, the truncated C307X c-Rel product could theoretically bind both DNA and other NF-κB subunits to activate gene expression, a gained mechanism that could perhaps underlie augmentations of *Ccl2*, *Cxcl10* and *Cxcl12* in the infected brain and heart. While exact mechanisms of action have not yet been elucidated, we expect from the data presented in this thesis that such regulatory checkpoints may be lost in infected Rel^{C307X} cells, and modify the protective response in non-immune tissues that are sensitive to pathological cellular infiltration and hyperinflammation.

CHAPTER SIX: CONCLUSION AND FUTURE DIRECTIONS

In this work, we have identified and characterized the *Rel* gene as a novel genetic etiology of mouse HSE, and as a key regulator of the protection host response to CVB3 infection in mice. The first objective of this research project was met in the finding that defects in both hematopoietic and brain-resident cells, together, contributed to viral escape, hyperinflammation and cell death in HSE-susceptible Rel^{C307X} mice. Our second objective further developed this model, and established that pathological $CD4^+$ and $CD8^+$ T cells together with infiltrating $Ly6C^+$ monocytes were singularly augmented in the Rel^{C307X} brain at symptom onset, in response to early detection of elevated chemokine, IFN-related and viral gene expression by resident cells at least one day prior to typical onset of lethal HSE. Finally, our implementation of a second model of CVB3 infection fulfilled our third objective, revealing that Rel^{C307X} mice were in fact more resistant to CVB3 myocarditis, and confirming that c-Rel is a key regulator of cell-mediated inflammatory responses to viral infection. Overall, these divergent models demonstrate that the same Rel^{C307X} mutation can affect different pathways, and drive pathogenic or protective responses that vary in the brain or heart, by DNA or RNA virus, and in dysregulation of resident cell homeostasis.

Future directions for the Rel^{C307X} project will involve histological examination of infected brain tissue, followed by co-staining for cleaved caspase-3 and for HSV-1 surface glycoproteins to determine if both focalize together in lesioned areas, to map the distribution of infected in the hindbrain and beyond, and to define which resident cells exactly are hosting the most replicating virus. It will be interesting to identify the earliest timepoint at which inflammation or tissue damage is first detected, perhaps at day 5 p.i., along with how quickly breaches in the blood-brain barrier and leukocyte infiltration occur, to predict which Rel^{C307X} mice will go on to develop lethal HSE. Based on these experiments, primary neuronal or glial cell cultures could be infected *ex vivo* to confirm how Rel^{C307X} affects cell survival to expand upon our original findings in primary fibroblasts.

With regards to pathology in the CVB3-infected heart, we are planning to examine histological $Rel^{+/+}$ and Rel^{C307X} heart sections using hematoxylin and eosin staining, but also upon *in vivo* injection of Evan's blue dye to determine if, as in other genetic models of CVB3 myocarditis, heart calcification occurs or is affected by the Rel^{C307X} mutation (118). In addition to examining hearts at steady-state for signs of hypertrophy, we also hope to perform dual RNA sequencing at day 2 to capture any variation in innate or inflammatory gene expression as the early

host response is still developing, prior to its saturation at the day 4 peak of infection. A day 2 timepoint may also bring additional context to the observed day 4 reduction in CVB3 viral transcripts in resistant *Rel*^{C307X} hearts—how early can a dampening effect of CVB3 transcription be detected *in vivo*? Finally, to fully complement the sequencing and flow cytometric experiments already performed in this model, we aim to evaluate the immune cell composition of the periphery, first in the spleen where little CVB3 replication occurs, and in a second organ that hosts elevated CVB3 replication, such as the liver or pancreas. Bone marrow transfers may also prove effective to evaluate the relative contributions of hematopoietic cells and of resident cardiomyocytes to CVB3 resistance in *Rel*^{C307X} mice, as we have previously applied to the HSV-1 model.

With the emergence of CD4^{+} T cells, monocytes and inflammatory microglia as cells that rely on c-Rel during infection, we would favour the use of conditional c-Rel knockout mice to further narrow down cell types in which c-Rel regulation is absolutely required for HSE protection. These key cell types, sorted from *in vivo* infected animals, may form the basis of future single cell RNA sequencing or chromatin immunoprecipitation sequencing experiments to better resolved c-Rel targets and promoter activity in induced or repressed genes. Such experiments may also bring further context to several uncharacterized long non-coding RNA transcripts detected in our brain or heart *Rel*^{C307X} datasets, in how they are regulated, but particularly if they derive from the tissue context, or from infiltrating immune cells. In response to infection or to TLR stimulation, a BioID proteomic screen could help to define interacting protein partners to the C307X truncated c-Rel product, and provide an ensemble view of which molecular functions may be lost, retained or gained in *Rel*^{C307X} cells (278).

Altogether, the success of our experimental approach involved the use of host and viral gene expression profiling at the site of infection, informed by an understanding of how immune cell dynamics evolved from the periphery to the infected tissue. Dual RNA sequencing in whole tissues also allowed for sufficient viral sequences to be perceived in pre-symptomatic mice, together with the developing host inflammatory response, to predict if a mouse would go on to succumb to or clear the infection. In the HSE model especially, where peripheral CD4^{+} T cells, viral transcription, and genes like *Cxcl10* and *Ccl2* were augmented early at day 5 p.i. in high-responding *Rel*^{C307X} mice, the implication that early detection of certain factors or signatures could predict disease onset is worth testing at the protein level in various tissues including serum.

These *Rel*^{C307X} models also have implications for human disease. In contrast to childhood HSE cases involving TLR3/IFN axis defects, the *Rel*^{C307X} model highlights the contributions of infiltrating immune cells and of cell death to HSE pathology, as others have proposed (100, 101, 178), and evoking cases of adult HSE (155). Where acyclovir is the principal recourse to treat HSE and reduce fulminant viral replication, it does not prevent necrosis or inflammatory pathology that may result in life-long sequelae, suggesting that treatment to reduce inflammation should also be considered. Furthermore, in our finding that the same mutation had detrimental or protective outcomes in the brain or heart, these studies demonstrate that c-Rel-dependent regulation of inflammation can affect different cell-mediated pathways, and may be tolerated differently depending on the tissue context. The contribution of c-Rel to various other mouse models of infectious or inflammatory disease also appears to be polarized, where c-Rel is either protective (102, 279, 280) or detrimental (81, 243, 244). In light of human genome-wide association studies that have implicated the *REL* locus in inflammatory diseases (236, 237, 239), it is clear that the c-Rel transcription factor is a far-ranging regulator of inflammation, and plays a non-redundant and essential role in many pathways that can result in penetrant *in vivo* phenotype. Thus, the *Rel*^{C307X} mouse offers an interesting opportunity to further explore the c-Rel regulatory axis or its upstream modulators, and to determine whether their successful targeting could dampen pathological inflammation and lead to novel treatment strategies for infectious or inflammatory diseases.

CHAPTER SEVEN: MASTER REFERENCE LIST

1. Belshaw R, Pereira V, Katzourakis A, Talbot G, Paces J, Burt A, Tristem M. 2004. Long-term reinfection of the human genome by endogenous retroviruses. *Proc Natl Acad Sci U S A* 101: 4894-9
2. Mancini M, Vidal SM. 2020. Mechanisms of Natural Killer Cell Evasion Through Viral Adaptation. *Annu Rev Immunol* 38: 511-39
3. Wertheim JO, Smith MD, Smith DM, Scheffler K, Kosakovsky Pond SL. 2014. Evolutionary origins of human herpes simplex viruses 1 and 2. *Mol Biol Evol* 31: 2356-64
4. Smith MG, Lennette EH, Reames HR. 1941. Isolation of the virus of herpes simplex and the demonstration of intranuclear inclusions in a case of acute encephalitis. *Am J Pathol* 17: 55-68.1
5. White JG. 1963. Fulminating infection with herpes-simplex virus in premature and newborn infants. *N Engl J Med* 269: 455-60
6. Smith MG. 1956. Propagation in tissue cultures of a cytopathogenic virus from human salivary gland virus (SGV) disease. *Proc Soc Exp Biol Med* 92: 424-30
7. Henle W, Diehl V, Kohn G, Zur Hausen H, Henle G. 1967. Herpes-type virus and chromosome marker in normal leukocytes after growth with irradiated Burkitt cells. *Science* 157: 1064-5
8. Smith KO. 1964. RELATIONSHIP BETWEEN THE ENVELOPE AND THE INFECTIVITY OF HERPES SIMPLEX VIRUS. *Proc Soc Exp Biol Med* 115: 814-6
9. Williams LE, Nesburn AB, Kaufman HE. 1965. EXPERIMENTAL INDUCTION OF DISCIFORM KERATITIS. *Arch Ophthalmol* 73: 112-4
10. Subak-Sharpe JH. 1973. The genetics of herpesvirus. *Cancer Res* 33: 1385-92
11. Thompson RL, Cook ML, Devi-Rao GB, Wagner EK, Stevens JG. 1986. Functional and molecular analyses of the avirulent wild-type herpes simplex virus type 1 strain KOS. *J Virol* 58: 203-11
12. Sedarati F, Stevens JG. 1987. Biological basis for virulence of three strains of herpes simplex virus type 1. *J Gen Virol* 68 (Pt 9): 2389-95
13. Wang H, Davido DJ, Morrison LA. 2013. HSV-1 strain McKrae is more neuroinvasive than HSV-1 KOS after corneal or vaginal inoculation in mice. *Virus Res* 173: 436-40

14. McGeoch DJ, Dalrymple MA, Davison AJ, Dolan A, Frame MC, McNab D, Perry LJ, Scott JE, Taylor P. 1988. The complete DNA sequence of the long unique region in the genome of herpes simplex virus type 1. *J Gen Virol* 69 (Pt 7): 1531-74
15. Stingley SW, Ramirez JJ, Aguilar SA, Simmen K, Sandri-Goldin RM, Ghazal P, Wagner EK. 2000. Global analysis of herpes simplex virus type 1 transcription using an oligonucleotide-based DNA microarray. *J Virol* 74: 9916-27
16. Davison AJ. 2011. Evolution of sexually transmitted and sexually transmissible human herpesviruses. *Ann N Y Acad Sci* 1230: E37-49
17. McGeoch DJ. 1987. The genome of herpes simplex virus: structure, replication and evolution. *J Cell Sci Suppl* 7: 67-94
18. Petermann P, Thier K, Rahn E, Rixon FJ, Bloch W, Ozcelik S, Krummenacher C, Barron MJ, Dixon MJ, Scheu S, Pfeffer K, et al. 2015. Entry mechanisms of herpes simplex virus 1 into murine epidermis: involvement of nectin-1 and herpesvirus entry mediator as cellular receptors. *J Virol* 89: 262-74
19. Suk H, Knipe DM. 2015. Proteomic analysis of the herpes simplex virus 1 virion protein 16 transactivator protein in infected cells. *Proteomics* 15: 1957-67
20. Kolb AW, Ané C, Brandt CR. 2013. Using HSV-1 genome phylogenetics to track past human migrations. *PLoS One* 8: e76267
21. Simpson SA, Manchak MD, Hager EJ, Krummenacher C, Whitbeck JC, Levin MJ, Freed CR, Wilcox CL, Cohen GH, Eisenberg RJ, Pizer LI. 2005. Nectin-1/HveC Mediates herpes simplex virus type 1 entry into primary human sensory neurons and fibroblasts. *J Neurovirol* 11: 208-18
22. Zhang Y, Xin Q, Zhang JY, Wang YY, Cheng JT, Cai WQ, Han ZW, Zhou Y, Cui SZ, Peng XC, Wang XW, et al. 2020. Transcriptional Regulation of Latency-Associated Transcripts (LATs) of Herpes Simplex Viruses. *J Cancer* 11: 3387-99
23. Bolovan CA, Sawtell NM, Thompson RL. 1994. ICP34.5 mutants of herpes simplex virus type 1 strain 17syn+ are attenuated for neurovirulence in mice and for replication in confluent primary mouse embryo cell cultures. *J Virol* 68: 48-55
24. Ahmed M, Lock M, Miller CG, Fraser NW. 2002. Regions of the herpes simplex virus type 1 latency-associated transcript that protect cells from apoptosis in vitro and protect neuronal cells in vivo. *J Virol* 76: 717-29

25. Orvedahl A, Alexander D, Talloczy Z, Sun Q, Wei Y, Zhang W, Burns D, Leib DA, Levine B. 2007. HSV-1 ICP34.5 confers neurovirulence by targeting the Beclin 1 autophagy protein. *Cell Host Microbe* 1: 23-35
26. Pan S, Liu X, Ma Y, Cao Y, He B. 2018. Herpes Simplex Virus 1 γ(1)34.5 Protein Inhibits STING Activation That Restricts Viral Replication. *J Virol* 92
27. Lin R, Noyce RS, Collins SE, Everett RD, Mossman KL. 2004. The herpes simplex virus ICP0 RING finger domain inhibits IRF3- and IRF7-mediated activation of interferon-stimulated genes. *J Virol* 78: 1675-84
28. Galocha B, Hill A, Barnett BC, Dolan A, Raimondi A, Cook RF, Brunner J, McGeoch DJ, Ploegh HL. 1997. The active site of ICP47, a herpes simplex virus-encoded inhibitor of the major histocompatibility complex (MHC)-encoded peptide transporter associated with antigen processing (TAP), maps to the NH2-terminal 35 residues. *J Exp Med* 185: 1565-72
29. Looker KJ, Magaret AS, May MT, Turner KM, Vickerman P, Gottlieb SL, Newman LM. 2015. Global and Regional Estimates of Prevalent and Incident Herpes Simplex Virus Type 1 Infections in 2012. *PLoS One* 10: e0140765
30. Looker KJ, Magaret AS, Turner KM, Vickerman P, Gottlieb SL, Newman LM. 2015. Correction: Global estimates of prevalent and incident herpes simplex virus type 2 infections in 2012. *PLoS One* 10: e0128615
31. McQuillan G, Kruszon-Moran D, Flagg EW, Paulose-Ram R. 2018. Prevalence of Herpes Simplex Virus Type 1 and Type 2 in Persons Aged 14-49: United States, 2015-2016. *NCHS Data Brief*: 1-8
32. Steiner I. 2011. Herpes simplex virus encephalitis: new infection or reactivation? *Curr Opin Neurol* 24: 268-74
33. Long SS, Pool TE, Vodzak J, Daskalaki I, Gould JM. 2011. Herpes simplex virus infection in young infants during 2 decades of empiric acyclovir therapy. *Pediatr Infect Dis J* 30: 556-61
34. Dalldorf G, Sickles GM. 1948. An Unidentified, Filtrable Agent Isolated From the Feces of Children With Paralysis. *Science* 108: 61-2
35. Dalldorf G. 1955. The Coxsackie viruses. *Annu Rev Microbiol* 9: 277-96

36. Lugo D, Krogstad P. 2016. Enteroviruses in the early 21st century: new manifestations and challenges. *Curr Opin Pediatr* 28: 107-13
37. Van Houten N, Bouchard PE, Moraska A, Huber SA. 1991. Selection of an attenuated Coxsackievirus B3 variant, using a monoclonal antibody reactive to myocyte antigen. *J Virol* 65: 1286-90
38. Drake JW. 1993. Rates of spontaneous mutation among RNA viruses. *Proc Natl Acad Sci U S A* 90: 4171-5
39. Knowlton KU, Jeon ES, Berkley N, Wessely R, Huber S. 1996. A mutation in the puff region of VP2 attenuates the myocarditic phenotype of an infectious cDNA of the Woodruff variant of coxsackievirus B3. *J Virol* 70: 7811-8
40. Pelletier J, Sonenberg N. 1988. Internal initiation of translation of eukaryotic mRNA directed by a sequence derived from poliovirus RNA. *Nature* 334: 320-5
41. Wells AI, Coyne CB. 2019. Enteroviruses: A Gut-Wrenching Game of Entry, Detection, and Evasion. *Viruses* 11
42. Cohen CJ, Shieh JT, Pickles RJ, Okegawa T, Hsieh JT, Bergelson JM. 2001. The coxsackievirus and adenovirus receptor is a transmembrane component of the tight junction. *Proc Natl Acad Sci U S A* 98: 15191-6
43. Yanagawa B, Spiller OB, Proctor DG, Choy J, Luo H, Zhang HM, Suarez A, Yang D, McManus BM. 2004. Soluble recombinant coxsackievirus and adenovirus receptor abrogates coxsackievirus b3-mediated pancreatitis and myocarditis in mice. *J Infect Dis* 189: 1431-9
44. Shi Y, Chen C, Lisewski U, Wrackmeyer U, Radke M, Westermann D, Sauter M, Tschöpe C, Poller W, Klingel K, Gotthardt M. 2009. Cardiac deletion of the Coxsackievirus-adenovirus receptor abolishes Coxsackievirus B3 infection and prevents myocarditis in vivo. *J Am Coll Cardiol* 53: 1219-26
45. Feng Q, Langereis MA, Lork M, Nguyen M, Hato SV, Lanke K, Emdad L, Bhoopathi P, Fisher PB, Lloyd RE, van Kuppeveld FJ. 2014. Enterovirus 2Apro targets MDA5 and MAVS in infected cells. *J Virol* 88: 3369-78
46. Li Q, Zheng Z, Liu Y, Zhang Z, Liu Q, Meng J, Ke X, Hu Q, Wang H. 2016. 2C Proteins of Enteroviruses Suppress IKKβ Phosphorylation by Recruiting Protein Phosphatase 1. *J Virol* 90: 5141-51

47. Cornell CT, Kiosses WB, Harkins S, Whitton JL. 2007. Coxsackievirus B3 proteins directionally complement each other to downregulate surface major histocompatibility complex class I. *J Virol* 81: 6785-97
48. Baer CF, Miyamoto MM, Denver DR. 2007. Mutation rate variation in multicellular eukaryotes: causes and consequences. *Nat Rev Genet* 8: 619-31
49. Xiao Y, Rouzine IM, Bianco S, Acevedo A, Goldstein EF, Farkov M, Brodsky L, Andino R. 2016. RNA Recombination Enhances Adaptability and Is Required for Virus Spread and Virulence. *Cell Host Microbe* 19: 493-503
50. Kempf BJ, Watkins CL, Peersen OB, Barton DJ. 2019. Picornavirus RNA Recombination Counteracts Error Catastrophe. *J Virol* 93
51. Abedi GR, Watson JT, Nix WA, Oberste MS, Gerber SI. 2018. Enterovirus and Parechovirus Surveillance - United States, 2014-2016. *MMWR Morb Mortal Wkly Rep* 67: 515-18
52. Sciandra I, Falasca F, Maida P, Tranquilli G, Di Carlo D, Mazzuti L, Melengu T, Giannelli G, Antonelli G, Turriziani O. 2020. Seroprevalence of group B Coxsackieviruses: Retrospective study in an Italian population. *J Med Virol*
53. Gkrania-Klotsas E, Langenberg C, Tauriainen S, Sharp SJ, Luben R, Forouhi NG, Khaw KT, Hyöty H, Wareham NJ. 2012. The association between prior infection with five serotypes of Coxsackievirus B and incident type 2 diabetes mellitus in the EPIC-Norfolk study. *Diabetologia* 55: 967-70
54. Tao Z, Li B, Xu A, Liu Y, Song L, Wang S, Xiong P, Lin X, Song Y. 2013. Seroprevalence of coxsackievirus B3 in Yantai, China. *Jpn J Infect Dis* 66: 537-8
55. Liu X, He S, Peng J, Guo X, Tan W. 2019. Expression Profile Analysis of Selenium-Related Genes in Peripheral Blood Mononuclear Cells of Patients with Keshan Disease. *Biomed Res Int* 2019: 4352905
56. Jun EJ, Ye JS, Hwang IS, Kim YK, Lee H. 2011. Selenium deficiency contributes to the chronic myocarditis in coxsackievirus-infected mice. *Acta Virol* 55: 23-9
57. Beck MA, Esworthy RS, Ho YS, Chu FF. 1998. Glutathione peroxidase protects mice from viral-induced myocarditis. *Faseb j* 12: 1143-9
58. Akira S, Takeda K. 2004. Toll-like receptor signalling. *Nat Rev Immunol* 4: 499-511

59. Pichlmair A, Schulz O, Tan CP, Näslund TI, Liljeström P, Weber F, Reis e Sousa C. 2006. RIG-I-mediated antiviral responses to single-stranded RNA bearing 5'-phosphates. *Science* 314: 997-1001

60. Pichlmair A, Schulz O, Tan CP, Rehwinkel J, Kato H, Takeuchi O, Akira S, Way M, Schiavo G, Reis e Sousa C. 2009. Activation of MDA5 requires higher-order RNA structures generated during virus infection. *J Virol* 83: 10761-9

61. Kawai T, Takahashi K, Sato S, Coban C, Kumar H, Kato H, Ishii KJ, Takeuchi O, Akira S. 2005. IPS-1, an adaptor triggering RIG-I- and Mda5-mediated type I interferon induction. *Nat Immunol* 6: 981-8

62. Seth RB, Sun L, Ea CK, Chen ZJ. 2005. Identification and characterization of MAVS, a mitochondrial antiviral signaling protein that activates NF-kappaB and IRF 3. *Cell* 122: 669-82

63. Wu J, Sun L, Chen X, Du F, Shi H, Chen C, Chen ZJ. 2013. Cyclic GMP-AMP is an endogenous second messenger in innate immune signaling by cytosolic DNA. *Science* 339: 826-30

64. Ablasser A, Goldeck M, Cavlar T, Deimling T, Witte G, Röhl I, Hopfner KP, Ludwig J, Hornung V. 2013. cGAS produces a 2'-5'-linked cyclic dinucleotide second messenger that activates STING. *Nature* 498: 380-4

65. Li D, Wu R, Guo W, Xie L, Qiao Z, Chen S, Zhu J, Huang C, Huang J, Chen B, Qin Y, et al. 2019. STING-Mediated IFI16 Degradation Negatively Controls Type I Interferon Production. *Cell Rep* 29: 1249-60.e4

66. Chunfa L, Xin S, Qiang L, Sreevatsan S, Yang L, Zhao D, Zhou X. 2017. The Central Role of IFI204 in IFN-β Release and Autophagy Activation during Mycobacterium bovis Infection. *Front Cell Infect Microbiol* 7: 169

67. Ishikawa H, Ma Z, Barber GN. 2009. STING regulates intracellular DNA-mediated, type I interferon-dependent innate immunity. *Nature* 461: 788-92

68. Zhong B, Yang Y, Li S, Wang YY, Li Y, Diao F, Lei C, He X, Zhang L, Tien P, Shu HB. 2008. The adaptor protein MITA links virus-sensing receptors to IRF3 transcription factor activation. *Immunity* 29: 538-50

69. Unterholzner L, Keating SE, Baran M, Horan KA, Jensen SB, Sharma S, Sirois CM, Jin T, Latz E, Xiao TS, Fitzgerald KA, et al. 2010. IFI16 is an innate immune sensor for intracellular DNA. *Nat Immunol* 11: 997-1004
70. Pestka S, Krause CD, Walter MR. 2004. Interferons, interferon-like cytokines, and their receptors. *Immunol Rev* 202: 8-32
71. Blank T, Prinz M. 2017. Type I interferon pathway in CNS homeostasis and neurological disorders. *Glia*
72. Sadler AJ, Williams BR. 2008. Interferon-inducible antiviral effectors. *Nat Rev Immunol* 8: 559-68
73. Haller O, Staeheli P, Schwemmle M, Kochs G. 2015. Mx GTPases: dynamin-like antiviral machines of innate immunity. *Trends Microbiol* 23: 154-63
74. Lenschow DJ, Lai C, Frias-Staheli N, Giannakopoulos NV, Lutz A, Wolff T, Osiak A, Levine B, Schmidt RE, Garcia-Sastre A, Leib DA, et al. 2007. IFN-stimulated gene 15 functions as a critical antiviral molecule against influenza, herpes, and Sindbis viruses. *Proc Natl Acad Sci U S A* 104: 1371-6
75. Mancini M, Vidal SM. 2018. Insights into the pathogenesis of herpes simplex encephalitis from mouse models. *Mamm Genome* 29: 425-45
76. Stawowczyk M, Van Scoy S, Kumar KP, Reich NC. 2011. The interferon stimulated gene 54 promotes apoptosis. *J Biol Chem* 286: 7257-66
77. Baranek T, Manh TP, Alexandre Y, Maqbool MA, Cabeza JZ, Tomasello E, Crozat K, Bessou G, Zucchini N, Robbins SH, Vivier E, et al. 2012. Differential responses of immune cells to type I interferon contribute to host resistance to viral infection. *Cell Host Microbe* 12: 571-84
78. Ruterbusch M, Pruner KB, Shehata L, Pepper M. 2020. In Vivo CD4(+) T Cell Differentiation and Function: Revisiting the Th1/Th2 Paradigm. *Annu Rev Immunol* 38: 705-25
79. Blum JS, Wearsch PA, Cresswell P. 2013. Pathways of antigen processing. *Annu Rev Immunol* 31: 443-73
80. Caignard G, Leiva-Torres GA, Leney-Greene M, Charbonneau B, Dumaine A, Fodil-Cornu N, Pyzik M, Cingolani P, Schwartzentruber J, Dupaul-Chicoine J, Guo H, et al.

2013. Genome-wide mouse mutagenesis reveals CD45-mediated T cell function as critical in protective immunity to HSV-1. *PLoS Pathog* 9: e1003637

81. Chen G, Hardy K, Pagler E, Ma L, Lee S, Gerondakis S, Daley S, Shannon MF. 2011. The NF-κB transcription factor c-Rel is required for Th17 effector cell development in experimental autoimmune encephalomyelitis. *J Immunol* 187: 4483-91
82. Isomura I, Palmer S, Grumont RJ, Bunting K, Hoyne G, Wilkinson N, Banerjee A, Proietto A, Gugasyan R, Wu L, McNally A, et al. 2009. c-Rel is required for the development of thymic Foxp3+ CD4 regulatory T cells. *J Exp Med* 206: 3001-14
83. Dahm T, Rudolph H, Schwerk C, Schroten H, Tenenbaum T. 2016. Neuroinvasion and Inflammation in Viral Central Nervous System Infections. *Mediators Inflamm* 2016: 8562805
84. Cook ML, Stevens JG. 1973. Pathogenesis of herpetic neuritis and ganglionitis in mice: evidence for intra-axonal transport of infection. *Infect Immun* 7: 272-88
85. Holm TH, Draeby D, Owens T. 2012. Microglia are required for astroglial Toll-like receptor 4 response and for optimal TLR2 and TLR3 response. *Glia* 60: 630-8
86. Rosenberger K, Derkow K, Dembny P, Kruger C, Schott E, Lehnardt S. 2014. The impact of single and pairwise Toll-like receptor activation on neuroinflammation and neurodegeneration. *J Neuroinflammation* 11: 166
87. Lafaille FG, Pessach IM, Zhang SY, Ciancanelli MJ, Herman M, Abhyankar A, Ying SW, Keros S, Goldstein PA, Mostoslavsky G, Ordovas-Montanes J, et al. 2012. Impaired intrinsic immunity to HSV-1 in human iPSC-derived TLR3-deficient CNS cells. *Nature* 491: 769-73
88. Zolini GP, Lima GK, Lucinda N, Silva MA, Dias MF, Pessoa NL, Coura BP, Cartelle CT, Arantes RM, Kroon EG, Campos MA. 2014. Defense against HSV-1 in a murine model is mediated by iNOS and orchestrated by the activation of TLR2 and TLR9 in trigeminal ganglia. *J Neuroinflammation* 11: 20
89. Daniels BP, Jujjavarapu H, Durrant DM, Williams JL, Green RR, White JP, Lazear HM, Gale M, Jr., Diamond MS, Klein RS. 2017. Regional astrocyte IFN signaling restricts pathogenesis during neurotropic viral infection. *J Clin Invest* 127: 843-56

90. Butchi N, Kapil P, Puntambekar S, Stohlman SA, Hinton DR, Bergmann CC. 2015. Myd88 Initiates Early Innate Immune Responses and Promotes CD4 T Cells during Coronavirus Encephalomyelitis. *J Virol* 89: 9299-312
91. Aravalli RN, Hu S, Rowen TN, Gekker G, Lokensgard JR. 2006. Differential apoptotic signaling in primary glial cells infected with herpes simplex virus 1. *J Neurovirol* 12: 501-10
92. Yordy B, Iijima N, Huttner A, Leib D, Iwasaki A. 2012. A neuron-specific role for autophagy in antiviral defense against herpes simplex virus. *Cell Host Microbe* 12: 334-45
93. Rosato PC, Katzenell S, Pesola JM, North B, Coen DM, Leib DA. 2016. Neuronal IFN signaling is dispensable for the establishment of HSV-1 latency. *Virology* 497: 323-7
94. Katzenell S, Chen Y, Parker ZM, Leib DA. 2014. The differential interferon responses of two strains of Stat1-deficient mice do not alter susceptibility to HSV-1 and VSV in vivo. *Virology* 450-451: 350-4
95. Rochfort KD, Collins LE, McLoughlin A, Cummins PM. 2016. Tumour necrosis factor-alpha-mediated disruption of cerebrovascular endothelial barrier integrity in vitro involves the production of proinflammatory interleukin-6. *J Neurochem* 136: 564-72
96. Stamatovic SM, Keep RF, Kunkel SL, Andjelkovic AV. 2003. Potential role of MCP-1 in endothelial cell tight junction 'opening': signaling via Rho and Rho kinase. *J Cell Sci* 116: 4615-28
97. Ashley SL, Pretto CD, Stier MT, Kadiyala P, Castro-Jorge L, Hsu TH, Doherty R, Carnahan KE, Castro MG, Lowenstein PR, Spindler KR. 2017. Matrix Metalloproteinase Activity in Infections by an Encephalitic Virus, Mouse Adenovirus Type 1. *J Virol* 91
98. Kastrukoff LF, Lau AS, Takei F, Carbone FR, Scalzo AA. 2015. A NK complex-linked locus restricts the spread of herpes simplex virus type 1 in the brains of C57BL/6 mice. *Immunol Cell Biol* 93: 877-84
99. Manickan E, Rouse BT. 1995. Roles of different T-cell subsets in control of herpes simplex virus infection determined by using T-cell-deficient mouse-models. *J Virol* 69: 8178-9
100. Menasria R, Canivet C, Piret J, Boivin G. 2015. Infiltration Pattern of Blood Monocytes into the Central Nervous System during Experimental Herpes Simplex Virus Encephalitis. *PLoS One* 10: e0145773

101. Zimmermann J, Hafezi W, Dockhorn A, Lorentzen EU, Krauthausen M, Getts DR, Muller M, Kuhn JE, King NJC. 2017. Enhanced viral clearance and reduced leukocyte infiltration in experimental herpes encephalitis after intranasal infection of CXCR3-deficient mice. *J Neurovirol* 23: 394-403

102. Mason NJ, Liou HC, Hunter CA. 2004. T cell-intrinsic expression of c-Rel regulates Th1 cell responses essential for resistance to Toxoplasma gondii. *J Immunol* 172: 3704-11

103. Neal LM, Xing E, Xu J, Kolbe JL, Osterholzer JJ, Segal BM, Williamson PR, Olszewski MA. 2017. CD4(+) T Cells Orchestrate Lethal Immune Pathology despite Fungal Clearance during Cryptococcus neoformans Meningoencephalitis. *mBio* 8

104. Wickham S, Lu B, Ash J, Carr DJ. 2005. Chemokine receptor deficiency is associated with increased chemokine expression in the peripheral and central nervous systems and increased resistance to herpetic encephalitis. *J Neuroimmunol* 162: 51-9

105. Yajima T, Knowlton KU. 2009. Viral myocarditis: from the perspective of the virus. *Circulation* 119: 2615-24

106. Hong T, Shaw RM. 2017. Cardiac T-Tubule Microanatomy and Function. *Physiol Rev* 97: 227-52

107. Belkaya S, Kontorovich AR, Byun M, Mulero-Navarro S, Bajolle F, Cobat A, Josowitz R, Itan Y, Quint R, Lorenzo L, Boucherit S, et al. 2017. Autosomal Recessive Cardiomyopathy Presenting as Acute Myocarditis. *J Am Coll Cardiol* 69: 1653-65

108. Rivera-Serrano EE, DeAngelis N, Sherry B. 2017. Spontaneous activation of a MAVS-dependent antiviral signaling pathway determines high basal interferon-β expression in cardiac myocytes. *J Mol Cell Cardiol* 111: 102-13

109. Meneghin A, Hogaboam CM. 2007. Infectious disease, the innate immune response, and fibrosis. *J Clin Invest* 117: 530-8

110. Negishi H, Osawa T, Ogami K, Ouyang X, Sakaguchi S, Koshiba R, Yanai H, Seko Y, Shitara H, Bishop K, Yonekawa H, et al. 2008. A critical link between Toll-like receptor 3 and type II interferon signaling pathways in antiviral innate immunity. *Proc Natl Acad Sci U S A* 105: 20446-51

111. Deonarain R, Cerullo D, Fuse K, Liu PP, Fish EN. 2004. Protective role for interferon-beta in coxsackievirus B3 infection. *Circulation* 110: 3540-3

112. Song JH, Ahn JH, Kim SR, Cho S, Hong EH, Kwon BE, Kim DE, Choi M, Choi HJ, Cha Y, Chang SY, et al. 2019. Manassantin B shows antiviral activity against coxsackievirus B3 infection by activation of the STING/TBK-1/IRF3 signalling pathway. *Sci Rep* 9: 9413
113. Wallach D, Kang TB, Dillon CP, Green DR. 2016. Programmed necrosis in inflammation: Toward identification of the effector molecules. *Science* 352: aaf2154
114. Badorff C, Lee GH, Lamphear BJ, Martone ME, Campbell KP, Rhoads RE, Knowlton KU. 1999. Enteroviral protease 2A cleaves dystrophin: evidence of cytoskeletal disruption in an acquired cardiomyopathy. *Nat Med* 5: 320-6
115. Tschöpe C, Müller I, Xia Y, Savvatis K, Pappritz K, Pinkert S, Lassner D, Heimesaat MM, Spillmann F, Miteva K, Bereswill S, et al. 2017. NOD2 (Nucleotide-Binding Oligomerization Domain 2) Is a Major Pathogenic Mediator of Coxsackievirus B3-Induced Myocarditis. *Circ Heart Fail* 10
116. Wang Y, Jia L, Shen J, Wang Y, Fu Z, Su SA, Cai Z, Wang JA, Xiang M. 2018. Cathepsin B aggravates coxsackievirus B3-induced myocarditis through activating the inflammasome and promoting pyroptosis. *PLoS Pathog* 14: e1006872
117. Wang C, Fung G, Deng H, Jagdeo J, Mohamud Y, Xue YC, Jan E, Hirota JA, Luo H. 2019. NLRP3 deficiency exacerbates enterovirus infection in mice. *Faseb j* 33: 942-52
118. Marton J, Albert D, Wiltshire SA, Park R, Bergen A, Qureshi S, Malo D, Burelle Y, Vidal SM. 2015. Cyclosporine A Treatment Inhibits Abcc6-Dependent Cardiac Necrosis and Calcification following Coxsackievirus B3 Infection in Mice. *PLoS One* 10: e0138222
119. Saraste A, Arola A, Vuorinen T, Kytö V, Kallajoki M, Pulkki K, Voipio-Pulkki LM, Hyypiä T. 2003. Cardiomyocyte apoptosis in experimental coxsackievirus B3 myocarditis. *Cardiovasc Pathol* 12: 255-62
120. Barry WH. 1994. Mechanisms of immune-mediated myocyte injury. *Circulation* 89: 2421-32
121. Kania G, Blyszczuk P, Eriksson U. 2009. Mechanisms of cardiac fibrosis in inflammatory heart disease. *Trends Cardiovasc Med* 19: 247-52
122. Cheung C, Marchant D, Walker EK, Luo Z, Zhang J, Yanagawa B, Rahmani M, Cox J, Overall C, Senior RM, Luo H, et al. 2008. Ablation of matrix metalloproteinase-9 increases severity of viral myocarditis in mice. *Circulation* 117: 1574-82

123. Fairweather D, Yusung S, Frisancho S, Barrett M, Gatewood S, Steele R, Rose NR. 2003. IL-12 receptor beta 1 and Toll-like receptor 4 increase IL-1 beta- and IL-18-associated myocarditis and coxsackievirus replication. *J Immunol* 170: 4731-7

124. Yuan J, Liu Z, Lim T, Zhang H, He J, Walker E, Shier C, Wang Y, Su Y, Sall A, McManus B, et al. 2009. CXCL10 inhibits viral replication through recruitment of natural killer cells in coxsackievirus B3-induced myocarditis. *Circ Res* 104: 628-38

125. Klingel K, Fabritius C, Sauter M, Göldner K, Stauch D, Kandolf R, Ettischer N, Gahlen S, Schönberger T, Ebner S, Makrigiannis AP, et al. 2014. The activating receptor NKG2D of natural killer cells promotes resistance against enterovirus-mediated inflammatory cardiomyopathy. *J Pathol* 234: 164-77

126. Rivadeneyra L, Charó N, Kviatcovsky D, de la Barrera S, Gómez RM, Schattner M. 2018. Role of neutrophils in CVB3 infection and viral myocarditis. *J Mol Cell Cardiol* 125: 149-61

127. Cook DN, Beck MA, Coffman TM, Kirby SL, Sheridan JF, Pragnell IB, Smithies O. 1995. Requirement of MIP-1 alpha for an inflammatory response to viral infection. *Science* 269: 1583-5

128. Huber SA, Sartini D. 2005. Roles of tumor necrosis factor alpha (TNF-alpha) and the p55 TNF receptor in CD1d induction and coxsackievirus B3-induced myocarditis. *J Virol* 79: 2659-65

129. Poffenberger MC, Horwitz MS. 2009. IL-6 during viral-induced chronic autoimmune myocarditis. *Ann N Y Acad Sci* 1173: 318-25

130. Szalay G, Sauter M, Hald J, Weinzierl A, Kandolf R, Klingel K. 2006. Sustained nitric oxide synthesis contributes to immunopathology in ongoing myocarditis attributable to interleukin-10 disorders. *Am J Pathol* 169: 2085-93

131. Li Y, Huang Y, Wu W, Wei B, Qin L. 2019. B Cells Increase Myocardial Inflammation by Suppressing M2 Macrophage Polarization in Coxsackie Virus B3-Induced Acute Myocarditis. *Inflammation* 42: 953-60

132. Li K, Xu W, Guo Q, Jiang Z, Wang P, Yue Y, Xiong S. 2009. Differential macrophage polarization in male and female BALB/c mice infected with coxsackievirus B3 defines susceptibility to viral myocarditis. *Circ Res* 105: 353-64

133. Okuno M, Nakagawa M, Shimada M, Saito M, Hishinuma S, Yamauchi-Takihara K. 2000. Expressional patterns of cytokines in a murine model of acute myocarditis: early expression of cardiotrophin-1. *Lab Invest* 80: 433-40

134. Lindner D, Hilbrandt M, Marggraf K, Becher PM, Hilfiker-Kleiner D, Klingel K, Pauschinger M, Schultheiss HP, Tschöpe C, Westermann D. 2012. Protective Function of STAT3 in CVB3-Induced Myocarditis. *Cardiol Res Pract* 2012: 437623

135. Kurdi M, Zgheib C, Booz GW. 2018. Recent Developments on the Crosstalk Between STAT3 and Inflammation in Heart Function and Disease. *Front Immunol* 9: 3029

136. Valaperti A, Nishii M, Liu Y, Naito K, Chan M, Zhang L, Skurk C, Schultheiss HP, Wells GA, Eriksson U, Liu PP. 2013. Innate immune interleukin-1 receptor-associated kinase 4 exacerbates viral myocarditis by reducing CCR5(+) CD11b(+) monocyte migration and impairing interferon production. *Circulation* 128: 1542-54

137. Müller I, Pappritz K, Savvatis K, Puhl K, Dong F, El-Shafeey M, Hamdani N, Hamann I, Noutsias M, Infante-Duarte C, Linke WA, et al. 2017. CX3CR1 knockout aggravates Coxsackievirus B3-induced myocarditis. *PLoS One* 12: e0182643

138. Opavsky MA, Penninger J, Aitken K, Wen WH, Dawood F, Mak T, Liu P. 1999. Susceptibility to myocarditis is dependent on the response of alphabeta T lymphocytes to coxsackieviral infection. *Circ Res* 85: 551-8

139. Liu P, Aitken K, Kong YY, Opavsky MA, Martino T, Dawood F, Wen WH, Kozieradzki I, Bachmaier K, Straus D, Mak TW, et al. 2000. The tyrosine kinase p56lck is essential in coxsackievirus B3-mediated heart disease. *Nat Med* 6: 429-34

140. Irie-Sasaki J, Sasaki T, Matsumoto W, Opavsky A, Cheng M, Welstead G, Griffiths E, Krawczyk C, Richardson CD, Aitken K, Iscove N, et al. 2001. CD45 is a JAK phosphatase and negatively regulates cytokine receptor signalling. *Nature* 409: 349-54

141. Huber SA, Pfaeffle B. 1994. Differential Th1 and Th2 cell responses in male and female BALB/c mice infected with coxsackievirus group B type 3. *J Virol* 68: 5126-32

142. Huber SA, Sartini D, Exley M. 2002. Vgamma4(+) T cells promote autoimmune CD8(+) cytolytic T-lymphocyte activation in coxsackievirus B3-induced myocarditis in mice: role for CD4(+) Th1 cells. *J Virol* 76: 10785-90

143. Frisancho-Kiss S, Nyland JF, Davis SE, Frisancho JA, Barrett MA, Rose NR, Fairweather D. 2006. Sex differences in coxsackievirus B3-induced myocarditis: IL-12Rbeta1

signaling and IFN-gamma increase inflammation in males independent from STAT4. *Brain Res* 1126: 139-47

144. Fairweather D, Stafford KA, Sung YK. 2012. Update on coxsackievirus B3 myocarditis. *Curr Opin Rheumatol* 24: 401-7

145. Zhu H, Lou C, Liu P. 2015. Interleukin-27 ameliorates coxsackievirus-B3-induced viral myocarditis by inhibiting Th17 cells. *Virol J* 12: 189

146. Li Z, Yue Y, Xiong S. 2013. Distinct Th17 inductions contribute to the gender bias in CVB3-induced myocarditis. *Cardiovasc Pathol* 22: 373-82

147. Xie Y, Gong C, Bo L, Jiang S, Kan H, Song W, Zhao J, Li Y. 2015. Treg responses are associated with PM2.5-induced exacerbation of viral myocarditis. *Inhal Toxicol* 27: 281-6

148. Vdovenko D, Eriksson U. 2018. Regulatory Role of CD4(+) T Cells in Myocarditis. *J Immunol Res* 2018: 4396351

149. Mena I, Perry CM, Harkins S, Rodriguez F, Gebhard J, Whitton JL. 1999. The role of B lymphocytes in coxsackievirus B3 infection. *Am J Pathol* 155: 1205-15

150. Jorgensen LK, Dalgaard LS, Ostergaard LJ, Norgaard M, Mogensen TH. 2017. Incidence and mortality of herpes simplex encephalitis in Denmark: A nationwide registry-based cohort study. *J Infect* 74: 42-49

151. Solomon T, Michael BD, Smith PE, Sanderson F, Davies NW, Hart IJ, Holland M, Easton A, Buckley C, Kneen R, Beeching NJ. 2012. Management of suspected viral encephalitis in adults--Association of British Neurologists and British Infection Association National Guidelines. *J Infect* 64: 347-73

152. Kaewpoowat Q, Salazar L, Aguilera E, Wootton SH, Hasbun R. 2016. Herpes simplex and varicella zoster CNS infections: clinical presentations, treatments and outcomes. *Infection* 44: 337-45

153. Livorsi D, Anderson E, Qureshi S, Howard M, Wang YF, Franco-Paredes C. 2010. Brainstem encephalitis: an unusual presentation of herpes simplex virus infection. *J Neurol* 257: 1432-7

154. Rozenberg F. 2013. Acute viral encephalitis. *Handb Clin Neurol* 112: 1171-81

155. Armangue T, Spatola M, Vlagea A, Mattozzi S, Cárceles-Cordon M, Martinez-Heras E, Llufriu S, Muchart J, Erro ME, Abraira L, Moris G, et al. 2018. Frequency, symptoms, risk

factors, and outcomes of autoimmune encephalitis after herpes simplex encephalitis: a prospective observational study and retrospective analysis. *Lancet Neurol* 17: 760-72

156. Dupuis S, Jouanguy E, Al-Hajjar S, Fieschi C, Al-Mohsen IZ, Al-Jumaah S, Yang K, Chapgier A, Eidenschenk C, Eid P, Al Ghonaium A, et al. 2003. Impaired response to interferon-alpha/beta and lethal viral disease in human STAT1 deficiency. *Nat Genet* 33: 388-91

157. Niehues T, Reichenbach J, Neubert J, Gudowius S, Puel A, Horneff G, Lainka E, Dirksen U, Schroten H, Doffinger R, Casanova JL, et al. 2004. Nuclear factor kappaB essential modulator-deficient child with immunodeficiency yet without anhidrotic ectodermal dysplasia. *J Allergy Clin Immunol* 114: 1456-62

158. Casrouge A, Zhang SY, Eidenschenk C, Jouanguy E, Puel A, Yang K, Alcais A, Picard C, Mahfoufi N, Nicolas N, Lorenzo L, et al. 2006. Herpes simplex virus encephalitis in human UNC-93B deficiency. *Science* 314: 308-12

159. Zhang SY, Jouanguy E, Ugolini S, Smahi A, Elain G, Romero P, Segal D, Sancho-Shimizu V, Lorenzo L, Puel A, Picard C, et al. 2007. TLR3 deficiency in patients with herpes simplex encephalitis. *Science* 317: 1522-7

160. Sancho-Shimizu V, Perez de Diego R, Lorenzo L, Halwani R, Alangari A, Israelsson E, Fabrega S, Cardon A, Maluenda J, Tatematsu M, Mahvelati F, et al. 2011. Herpes simplex encephalitis in children with autosomal recessive and dominant TRIF deficiency. *J Clin Invest* 121: 4889-902

161. Perez de Diego R, Sancho-Shimizu V, Lorenzo L, Puel A, Plancoulaine S, Picard C, Herman M, Cardon A, Durandy A, Bustamante J, Vallabhapurapu S, et al. 2010. Human TRAF3 adaptor molecule deficiency leads to impaired Toll-like receptor 3 response and susceptibility to herpes simplex encephalitis. *Immunity* 33: 400-11

162. Herman M, Ciancanelli M, Ou YH, Lorenzo L, Klaudel-Dreszler M, Pauwels E, Sancho-Shimizu V, Perez de Diego R, Abhyankar A, Israelsson E, Guo Y, et al. 2012. Heterozygous TBK1 mutations impair TLR3 immunity and underlie herpes simplex encephalitis of childhood. *J Exp Med* 209: 1567-82

163. Andersen LL, Mork N, Reinert LS, Kofod-Olsen E, Narita R, Jorgensen SE, Skipper KA, Honing K, Gad HH, Ostergaard L, Orntoft TF, et al. 2015. Functional IRF3 deficiency in a patient with herpes simplex encephalitis. *J Exp Med* 212: 1371-9

164. Zhang SY. 2020. Herpes simplex virus encephalitis of childhood: inborn errors of central nervous system cell-intrinsic immunity. *Hum Genet* 139: 911-18

165. Lafaille FG, Harschnitz O, Lee YS, Zhang P, Hasek ML, Kerner G, Itan Y, Ewaleifoh O, Rapaport F, Carlile TM, Carter-Timofte ME, et al. 2019. Human SNORA31 variations impair cortical neuron-intrinsic immunity to HSV-1 and underlie herpes simplex encephalitis. *Nat Med* 25: 1873-84

166. Zhang SY, Clark NE, Freije CA, Pauwels E, Taggart AJ, Okada S, Mandel H, Garcia P, Ciancanelli MJ, Biran A, Lafaille FG, et al. 2018. Inborn Errors of RNA Lariat Metabolism in Humans with Brainstem Viral Infection. *Cell* 172: 952-65.e18

167. Bibert S, Piret J, Quinodoz M, Collinet E, Zoete V, Michielin O, Menasria R, Meylan P, Bihl T, Erard V, Fellmann F, et al. 2019. Herpes simplex encephalitis in adult patients with MASP-2 deficiency. *PLoS Pathog* 15: e1008168

168. Menendez CM, Carr DJJ. 2017. Defining nervous system susceptibility during acute and latent herpes simplex virus-1 infection. *J Neuroimmunol* 308: 43-49

169. Lopez C. 1975. Genetics of natural resistance to herpesvirus infections in mice. *Nature* 258: 152-3

170. Reinert LS, Harder L, Holm CK, Iversen MB, Horan KA, Dagnaes-Hansen F, Ulhoi BP, Holm TH, Mogensen TH, Owens T, Nyengaard JR, et al. 2012. TLR3 deficiency renders astrocytes permissive to herpes simplex virus infection and facilitates establishment of CNS infection in mice. *J Clin Invest* 122: 1368-76

171. Wang JP, Bowen GN, Zhou S, Cerny A, Zacharia A, Knipe DM, Finberg RW, Kurt-Jones EA. 2012. Role of specific innate immune responses in herpes simplex virus infection of the central nervous system. *J Virol* 86: 2273-81

172. Mancini M, Caignard G, Charbonneau B, Dumaine A, Wu N, Leiva-Torres GA, Gerondakis S, Pearson A, Qureshi ST, Sladek R, Vidal SM. 2019. Rel-Dependent Immune and Central Nervous System Mechanisms Control Viral Replication and Inflammation during Mouse Herpes Simplex Encephalitis. *J Immunol* 202: 1479-93

173. Lima GK, Zolini GP, Mansur DS, Freire Lima BH, Wischhoff U, Astigarraga RG, Dias MF, das Gracas Almeida Silva M, Bela SR, do Valle Antonelli LR, Arantes RM, et al. 2010. Toll-like receptor (TLR) 2 and TLR9 expressed in trigeminal ganglia are critical to viral control during herpes simplex virus 1 infection. *Am J Pathol* 177: 2433-45

174. Menasria R, Boivin N, Lebel M, Piret J, Gosselin J, Boivin G. 2013. Both TRIF and IPS-1 adaptor proteins contribute to the cerebral innate immune response against herpes simplex virus 1 infection. *J Virol* 87: 7301-8

175. Mansur DS, Kroon EG, Nogueira ML, Arantes RM, Rodrigues SC, Akira S, Gazzinelli RT, Campos MA. 2005. Lethal encephalitis in myeloid differentiation factor 88-deficient mice infected with herpes simplex virus 1. *Am J Pathol* 166: 1419-26

176. Yamashiro LH, Wilson SC, Morrison HM, Karalis V, Chung JJ, Chen KJ, Bateup HS, Szpara ML, Lee AY, Cox JS, Vance RE. 2020. Interferon-independent STING signaling promotes resistance to HSV-1 in vivo. *Nat Commun* 11: 3382

177. Reinert LS, Lopusna K, Winther H, Sun C, Thomsen MK, Nandakumar R, Mogensen TH, Meyer M, Vaegter C, Nyengaard JR, Fitzgerald KA, et al. 2016. Sensing of HSV-1 by the cGAS-STING pathway in microglia orchestrates antiviral defence in the CNS. *Nat Commun* 7: 13348

178. Ramakrishna C, Cantin EM. 2018. IFNgamma inhibits G-CSF induced neutrophil expansion and invasion of the CNS to prevent viral encephalitis. *PLoS Pathog* 14: e1006822

179. Lundberg P, Welander PV, Edwards CK, 3rd, van Rooijen N, Cantin E. 2007. Tumor necrosis factor (TNF) protects resistant C57BL/6 mice against herpes simplex virus-induced encephalitis independently of signaling via TNF receptor 1 or 2. *J Virol* 81: 1451-60

180. Sergerie Y, Rivest S, Boivin G. 2007. Tumor necrosis factor-alpha and interleukin-1 beta play a critical role in the resistance against lethal herpes simplex virus encephalitis. *J Infect Dis* 196: 853-60

181. LeBlanc RA, Pesnicak L, Cabral ES, Godleski M, Straus SE. 1999. Lack of interleukin-6 (IL-6) enhances susceptibility to infection but does not alter latency or reactivation of herpes simplex virus type 1 in IL-6 knockout mice. *J Virol* 73: 8145-51

182. Menasria R, Canivet C, Piret J, Gosselin J, Boivin G. 2017. Protective role of CX3CR1 signalling in resident cells of the central nervous system during experimental herpes simplex virus encephalitis. *J Gen Virol* 98: 447-60

183. Wuest TR, Carr DJ. 2008. Dysregulation of CXCR3 signaling due to CXCL10 deficiency impairs the antiviral response to herpes simplex virus 1 infection. *J Immunol* 181: 7985-93

184. Carr DJ, Ash J, Lane TE, Kuziel WA. 2006. Abnormal immune response of CCR5-deficient mice to ocular infection with herpes simplex virus type 1. *J Gen Virol* 87: 489-99

185. Gupta S, Markham DW, Drazner MH, Mammen PP. 2008. Fulminant myocarditis. *Nat Clin Pract Cardiovasc Med* 5: 693-706

186. Roberts BJ, Moussawi M, Huber SA. 2013. Sex differences in TLR2 and TLR4 expression and their effect on coxsackievirus-induced autoimmune myocarditis. *Exp Mol Pathol* 94: 58-64

187. Kurt-Jones EA, Chan M, Zhou S, Wang J, Reed G, Bronson R, Arnold MM, Knipe DM, Finberg RW. 2004. Herpes simplex virus 1 interaction with Toll-like receptor 2 contributes to lethal encephalitis. *Proc Natl Acad Sci U S A* 101: 1315-20

188. Riad A, Westermann D, Escher F, Becher PM, Savvatis K, Lettau O, Heimesaat MM, Bereswill S, Volk HD, Schultheiss HP, Tschöpe C. 2010. Myeloid differentiation factor-88 contributes to TLR9-mediated modulation of acute coxsackievirus B3-induced myocarditis in vivo. *Am J Physiol Heart Circ Physiol* 298: H2024-31

189. Lafferty EI, Wiltshire SA, Angers I, Vidal SM, Qureshi ST. 2015. Unc93b1 -Dependent Endosomal Toll-Like Receptor Signaling Regulates Inflammation and Mortality during Coxsackievirus B3 Infection. *J Innate Immun* 7: 315-30

190. Riad A, Westermann D, Zietsch C, Savvatis K, Becher PM, Bereswill S, Heimesaat MM, Lettau O, Lassner D, Dörner A, Poller W, et al. 2011. TRIF is a critical survival factor in viral cardiomyopathy. *J Immunol* 186: 2561-70

191. Fuse K, Chan G, Liu Y, Gudgeon P, Husain M, Chen M, Yeh WC, Akira S, Liu PP. 2005. Myeloid differentiation factor-88 plays a crucial role in the pathogenesis of Coxsackievirus B3-induced myocarditis and influences type I interferon production. *Circulation* 112: 2276-85

192. Wang JP, Cerny A, Asher DR, Kurt-Jones EA, Bronson RT, Finberg RW. 2010. MDA5 and MAVS mediate type I interferon responses to coxsackie B virus. *J Virol* 84: 254-60

193. Wessely R, Klingel K, Knowlton KU, Kandolf R. 2001. Cardioselective infection with coxsackievirus B3 requires intact type I interferon signaling: implications for mortality and early viral replication. *Circulation* 103: 756-61

194. Cantin E, Tanamachi B, Openshaw H, Mann J, Clarke K. 1999. Gamma interferon (IFN-gamma) receptor null-mutant mice are more susceptible to herpes simplex virus type 1 infection than IFN-gamma ligand null-mutant mice. *J Virol* 73: 5196-200

195. Murphy AA, Rosato PC, Parker ZM, Khalenkov A, Leib DA. 2013. Synergistic control of herpes simplex virus pathogenesis by IRF-3, and IRF-7 revealed through non-invasive bioluminescence imaging. *Virology* 444: 71-9

196. Rahnefeld A, Klingel K, Schuermann A, Diny NL, Althof N, Lindner A, Bleienheuft P, Savvatis K, Respondek D, Opitz E, Ketscher L, et al. 2014. Ubiquitin-like protein ISG15 (interferon-stimulated gene of 15 kDa) in host defense against heart failure in a mouse model of virus-induced cardiomyopathy. *Circulation* 130: 1589-600

197. Gebhard JR, Perry CM, Harkins S, Lane T, Mena I, Asensio VC, Campbell IL, Whitton JL. 1998. Coxsackievirus B3-induced myocarditis: perforin exacerbates disease, but plays no detectable role in virus clearance. *Am J Pathol* 153: 417-28

198. Klingel K, Schnorr JJ, Sauter M, Szalay G, Kandolf R. 2003. beta2-microglobulin-associated regulation of interferon-gamma and virus-specific immunoglobulin G confer resistance against the development of chronic coxsackievirus myocarditis. *Am J Pathol* 162: 1709-20

199. Zaragoza C, Ocampo C, Saura M, Leppo M, Wei XQ, Quick R, Moncada S, Liew FY, Lowenstein CJ. 1998. The role of inducible nitric oxide synthase in the host response to Coxsackievirus myocarditis. *Proc Natl Acad Sci U S A* 95: 2469-74

200. Vilela MC, Lima GK, Rodrigues DH, Lacerda-Queiroz N, Pedroso VS, Miranda AS, Rachid MA, Kroon EG, Campos MA, Teixeira MM, Sellner J, et al. 2013. Absence of CCR5 increases neutrophil recruitment in severe herpetic encephalitis. *BMC Neurosci* 14: 19

201. Westermann D, Savvatis K, Lindner D, Zietsch C, Becher PM, Hammer E, Heimesaat MM, Bereswill S, Völker U, Escher F, Riad A, et al. 2011. Reduced degradation of the chemokine MCP-3 by matrix metalloproteinase-2 exacerbates myocardial inflammation in experimental viral cardiomyopathy. *Circulation* 124: 2082-93

202. Sun C, Zhang X, Yu Y, Li Z, Xie Y. 2020. CARD9 mediates T cell inflammatory response in Coxsackievirus B3-induced acute myocarditis. *Cardiovasc Pathol* 49: 107261

203. Gaaloul I, Riabi S, Harrath R, Hunter T, Hamda KB, Ghzala AB, Huber S, Aouni M. 2014. Coxsackievirus B detection in cases of myocarditis, myopericarditis, pericarditis and dilated cardiomyopathy in hospitalized patients. *Mol Med Rep* 10: 2811-8
204. Woudstra L, Juffermans LJM, van Rossum AC, Niessen HWM, Krijnen PAJ. 2018. Infectious myocarditis: the role of the cardiac vasculature. *Heart Fail Rev* 23: 583-95
205. Dec GW, Fuster V. 1994. Idiopathic dilated cardiomyopathy. *N Engl J Med* 331: 1564-75
206. Hershberger RE, Hedges DJ, Morales A. 2013. Dilated cardiomyopathy: the complexity of a diverse genetic architecture. *Nat Rev Cardiol* 10: 531-47
207. Gorbea C, Makar KA, Pauschinger M, Pratt G, Bersola JL, Varela J, David RM, Banks L, Huang CH, Li H, Schultheiss HP, et al. 2010. A role for Toll-like receptor 3 variants in host susceptibility to enteroviral myocarditis and dilated cardiomyopathy. *J Biol Chem* 285: 23208-23
208. Fairweather D, Cooper LT, Jr., Blauwet LA. 2013. Sex and gender differences in myocarditis and dilated cardiomyopathy. *Curr Probl Cardiol* 38: 7-46
209. Vidal SM, Malo D, Marquis JF, Gros P. 2008. Forward genetic dissection of immunity to infection in the mouse. *Annu Rev Immunol* 26: 81-132
210. Singer B. 1977. Sites in nucleic acids reacting with alkylating agents of differing carcinogenicity of mutagenicity. *J Toxicol Environ Health* 2: 1279-95
211. Bull KR, Rimmer AJ, Siggs OM, Miosge LA, Roots CM, Enders A, Bertram EM, Crockford TL, Whittle B, Potter PK, Simon MM, et al. 2013. Unlocking the bottleneck in forward genetics using whole-genome sequencing and identity by descent to isolate causative mutations. *PLoS Genet* 9: e1003219
212. Caignard G, Eva MM, van Bruggen R, Eveleigh R, Bourque G, Malo D, Gros P, Vidal SM. 2014. Mouse ENU Mutagenesis to Understand Immunity to Infection: Methods, Selected Examples, and Perspectives. *Genes (Basel)* 5: 887-925
213. Torre S, Polyak MJ, Langlais D, Fodil N, Kennedy JM, Radovanovic I, Berghout J, Leiva-Torres GA, Krawczyk CM, Ilangumaran S, Mossman K, et al. 2017. USP15 regulates type I interferon response and is required for pathogenesis of neuroinflammation. *Nat Immunol* 18: 54-63
214. Yuki KE, Marei H, Fiskin E, Eva MM, Gopal AA, Schwartzentruber JA, Majewski J, Cellier M, Mandl JN, Vidal SM, Malo D, et al. 2019. CYRI/FAM49B negatively regulates

RAC1-driven cytoskeletal remodelling and protects against bacterial infection. *Nat Microbiol* 4: 1516-31

215. Napetschnig J, Wu H. 2013. Molecular basis of NF-κB signaling. *Annu Rev Biophys* 42: 443-68

216. Mulero MC, Huxford T, Ghosh G. 2019. NF-κB, IκB, and IKK: Integral Components of Immune System Signaling. *Adv Exp Med Biol* 1172: 207-26

217. Gilmore TD, Gerondakis S. 2011. The c-Rel Transcription Factor in Development and Disease. *Genes Cancer* 2: 695-711

218. Martin EW, Pacholewska A, Patel H, Dashora H, Sung MH. 2020. Integrative analysis suggests cell type-specific decoding of NF-κB dynamics. *Sci Signal* 13

219. Grumont R, Lock P, Mollinari M, Shannon FM, Moore A, Gerondakis S. 2004. The mitogen-induced increase in T cell size involves PKC and NFAT activation of Rel/NF-kappaB-dependent c-myc expression. *Immunity* 21: 19-30

220. Chen Y, Sharma S, Assis PA, Jiang Z, Elling R, Olive AJ, Hang S, Bernier J, Huh JR, Sassetti CM, Knipe DM, et al. 2018. CNBP controls IL-12 gene transcription and Th1 immunity. *J Exp Med* 215: 3136-50

221. Dhamija N, Choudhary D, Ladha JS, Pillai B, Mitra D. 2015. Tat predominantly associates with host promoter elements in HIV-1-infected T-cells - regulatory basis of transcriptional repression of c-Rel. *Febs j* 282: 595-610

222. Grumont R, Hochrein H, O'Keeffe M, Gugasyan R, White C, Caminschi I, Cook W, Gerondakis S. 2001. c-Rel regulates interleukin 12 p70 expression in CD8(+) dendritic cells by specifically inducing p35 gene transcription. *J Exp Med* 194: 1021-32

223. Carmody RJ, Ruan Q, Liou HC, Chen YH. 2007. Essential roles of c-Rel in TLR-induced IL-23 p19 gene expression in dendritic cells. *J Immunol* 178: 186-91

224. Hoentjen F, Sartor RB, Ozaki M, Jobin C. 2005. STAT3 regulates NF-kappaB recruitment to the IL-12p40 promoter in dendritic cells. *Blood* 105: 689-96

225. Chen G, Hardy K, Bunting K, Daley S, Ma L, Shannon MF. 2010. Regulation of the IL-21 gene by the NF-κB transcription factor c-Rel. *J Immunol* 185: 2350-9

226. Kontgen F, Grumont RJ, Strasser A, Metcalf D, Li R, Tarlinton D, Gerondakis S. 1995. Mice lacking the c-rel proto-oncogene exhibit defects in lymphocyte proliferation, humoral immunity, and interleukin-2 expression. *Genes Dev* 9: 1965-77

227. Rao S, Gerondakis S, Woltring D, Shannon MF. 2003. c-Rel is required for chromatin remodeling across the IL-2 gene promoter. *J Immunol* 170: 3724-31

228. Poke FS, Upcher WR, Sprod OR, Young A, Brettingham-Moore KH, Holloway AF. 2012. Depletion of c-Rel from cytokine gene promoters is required for chromatin reassembly and termination of gene responses to T cell activation. *PLoS One* 7: e41734

229. Ruan Q, Kameswaran V, Zhang Y, Zheng S, Sun J, Wang J, DeVirgiliis J, Liou HC, Beg AA, Chen YH. 2011. The Th17 immune response is controlled by the Rel-RORγ-RORγ T transcriptional axis. *J Exp Med* 208: 2321-33

230. Grumont RJ, Strasser A, Gerondakis S. 2002. B cell growth is controlled by phosphatidylinosotol 3-kinase-dependent induction of Rel/NF-kappaB regulated c-myc transcription. *Mol Cell* 10: 1283-94

231. Zong WX, Edelstein LC, Chen C, Bash J, Gélinas C. 1999. The prosurvival Bcl-2 homolog Bfl-1/A1 is a direct transcriptional target of NF-kappaB that blocks TNFalpha-induced apoptosis. *Genes Dev* 13: 382-7

232. Chen C, Edelstein LC, Gelinas C. 2000. The Rel/NF-kappaB family directly activates expression of the apoptosis inhibitor Bcl-x(L). *Mol Cell Biol* 20: 2687-95

233. Sarnico I, Lanzillotta A, Boroni F, Benarese M, Alghisi M, Schwaninger M, Inta I, Battistin L, Spano P, Pizzi M. 2009. NF-kappaB p50/RelA and c-Rel-containing dimers: opposite regulators of neuron vulnerability to ischaemia. *J Neurochem* 108: 475-85

234. Gaspar-Pereira S, Fullard N, Townsend PA, Banks PS, Ellis EL, Fox C, Maxwell AG, Murphy LB, Kirk A, Bauer R, Caamaño JH, et al. 2012. The NF-κB subunit c-Rel stimulates cardiac hypertrophy and fibrosis. *Am J Pathol* 180: 929-39

235. Bunting K, Rao S, Hardy K, Woltring D, Denyer GS, Wang J, Gerondakis S, Shannon MF. 2007. Genome-wide analysis of gene expression in T cells to identify targets of the NF-kappa B transcription factor c-Rel. *J Immunol* 178: 7097-109

236. Zhernakova A, Festen EM, Franke L, Trynka G, van Diemen CC, Monsuur AJ, Bevova M, Nijmeijer RM, van 't Slot R, Heijmans R, Boezen HM, et al. 2008. Genetic analysis of innate immunity in Crohn's disease and ulcerative colitis identifies two susceptibility loci harboring CARD9 and IL18RAP. *Am J Hum Genet* 82: 1202-10

237. Ellinghaus E, Stuart PE, Ellinghaus D, Nair RP, Debrus S, Raelson JV, Belouchi M, Tejasvi T, Li Y, Tsoi LC, Onken AT, et al. 2012. Genome-wide meta-analysis of psoriatic arthritis identifies susceptibility locus at REL. *J Invest Dermatol* 132: 1133-40

238. Gregersen PK, Amos CI, Lee AT, Lu Y, Remmers EF, Kastner DL, Seldin MF, Criswell LA, Plenge RM, Holers VM, Mikuls TR, et al. 2009. REL, encoding a member of the NF-kappaB family of transcription factors, is a newly defined risk locus for rheumatoid arthritis. *Nat Genet* 41: 820-3

239. Consortium IMSG. 2013. Network-based multiple sclerosis pathway analysis with GWAS data from 15,000 cases and 30,000 controls. *Am J Hum Genet* 92: 854-65

240. Strange A, Capon F, Spencer CC, Knight J, Weale ME, Allen MH, Barton A, Band G, Bellenguez C, Bergboer JG, Blackwell JM, et al. 2010. A genome-wide association study identifies new psoriasis susceptibility loci and an interaction between HLA-C and ERAP1. *Nat Genet* 42: 985-90

241. Martins LT, Frigeri HR, de Castro CCS, Mira MT. 2020. Association study between vitiligo and autoimmune-related genes CYP27B1, REL, TNFAIP3, IL2 and IL21. *Exp Dermatol* 29: 535-38

242. Rose KL, Sherman PM, Cooke-Lauder J, Mawani M, Benchimol EI, Kaplan GG, Bernstein CN, Bitton A, Murthy SK, Nguyen GC, Lee K. 2019. The Impact of Inflammatory Bowel Disease in Canada 2018: IBD Research Landscape in Canada. *J Can Assoc Gastroenterol* 2: S81-s91

243. Visekruna A, Linnerz T, Martinic V, Vachharajani N, Hartmann S, Harb H, Joeris T, Pfefferle PI, Hofer MJ, Steinhoff U. 2015. Transcription factor c-Rel plays a crucial role in driving anti-CD40-mediated innate colitis. *Mucosal Immunol* 8: 307-15

244. Burkitt MD, Hanedi AF, Duckworth CA, Williams JM, Tang JM, O'Reilly LA, Putoczki TL, Gerondakis S, Dimaline R, Caamano JH, Pritchard DM. 2015. NF-κB1, NF-κB2 and c-Rel differentially regulate susceptibility to colitis-associated adenoma development in C57BL/6 mice. *J Pathol* 236: 326-36

245. Picard C, von Bernuth H, Ghandil P, Chrabieh M, Levy O, Arkwright PD, McDonald D, Geha RS, Takada H, Krause JC, Creech CB, et al. 2010. Clinical features and outcome of patients with IRAK-4 and MyD88 deficiency. *Medicine (Baltimore)* 89: 403-25

246. Beaussant-Cohen S, Jaber F, Massaad MJ, Weeks S, Jones J, Alosaimi MF, Wallace J, Al-Herz W, Geha RS, Chou J. 2019. Combined immunodeficiency in a patient with c-Rel deficiency. *J Allergy Clin Immunol* 144: 606-08.e4

247. Zhazykbayeva S, Pabel S, Mügge A, Sossalla S, Hamdani N. 2020. The molecular mechanisms associated with the physiological responses to inflammation and oxidative stress in cardiovascular diseases. *Biophys Rev*

248. Parra-Izquierdo I, Castaños-Mollor I, López J, Gómez C, San Román JA, Sánchez Crespo M, García-Rodríguez C. 2018. Calcification Induced by Type I Interferon in Human Aortic Valve Interstitial Cells Is Larger in Males and Blunted by a Janus Kinase Inhibitor. *Arterioscler Thromb Vasc Biol* 38: 2148-59

249. King KR, Aguirre AD, Ye YX, Sun Y, Roh JD, Ng RP, Jr., Kohler RH, Arlauckas SP, Iwamoto Y, Savol A, Sadreyev RI, et al. 2017. IRF3 and type I interferons fuel a fatal response to myocardial infarction. *Nat Med* 23: 1481-87

250. Robbins SH, Bessou G, Cornillon A, Zucchini N, Rupp B, Ruzsics Z, Sacher T, Tomasello E, Vivier E, Koszinowski UH, Dalod M. 2007. Natural killer cells promote early CD8 T cell responses against cytomegalovirus. *PLoS Pathog* 3: e123

251. Crow YJ. 2013. Aicardi-Goutières syndrome. *Handb Clin Neurol* 113: 1629-35

252. Barrett JP, Henry RJ, Shirey KA, Doran SJ, Makarevich OD, Ritzel RM, Meadows VA, Vogel SN, Faden AI, Stoica BA, Loane DJ. 2020. Interferon-β Plays a Detrimental Role in Experimental Traumatic Brain Injury by Enhancing Neuroinflammation That Drives Chronic Neurodegeneration. *J Neurosci* 40: 2357-70

253. Siednienko J, Maratha A, Yang S, Mitkiewicz M, Miggin SM, Moynagh PN. 2011. Nuclear factor kappaB subunits RelB and cRel negatively regulate Toll-like receptor 3-mediated beta-interferon production via induction of transcriptional repressor protein YY1. *J Biol Chem* 286: 44750-63

254. Chen B, Frangogiannis NG. 2020. Chemokines in Myocardial Infarction. *J Cardiovasc Transl Res*

255. Harling-McNabb L, Deliyannis G, Jackson DC, Gerondakis S, Grigoriadis G, Brown LE. 1999. Mice lacking the transcription factor subunit Rel can clear an influenza infection and have functional anti-viral cytotoxic T cells but do not develop an optimal antibody response. *Int Immunol* 11: 1431-9

256. Ramakrishna C, Newo AN, Shen YW, Cantin E. 2011. Passively administered pooled human immunoglobulins exert IL-10 dependent anti-inflammatory effects that protect against fatal HSV encephalitis. *PLoS Pathog* 7: e1002071

257. Varanasi SK, Reddy PB, Bhela S, Jaggi U, Gimenez F, Rouse BT. 2017. Azacytidine Treatment Inhibits the Progression of Herpes Stromal Keratitis by Enhancing Regulatory T Cell Function. *J Virol* 91

258. DeBiasi RL, Kleinschmidt-DeMasters BK, Richardson-Burns S, Tyler KL. 2002. Central nervous system apoptosis in human herpes simplex virus and cytomegalovirus encephalitis. *J Infect Dis* 186: 1547-57

259. Laukoter S, Rauschka H, Troscher AR, Kock U, Saji E, Jellinger K, Lassmann H, Bauer J. 2017. Differences in T cell cytotoxicity and cell death mechanisms between progressive multifocal leukoencephalopathy, herpes simplex virus encephalitis and cytomegalovirus encephalitis. *Acta Neuropathol* 133: 613-27

260. Pizzi M, Sarnico I, Lanzillotta A, Battistin L, Spano P. 2009. Post-ischemic brain damage: NF-kappaB dimer heterogeneity as a molecular determinant of neuron vulnerability. *Febs j* 276: 27-35

261. Bernard D, Quatannens B, Begue A, Vandenbunder B, Abbadie C. 2001. Antiproliferative and antiapoptotic effects of crel may occur within the same cells via the up-regulation of manganese superoxide dismutase. *Cancer Res* 61: 2656-64

262. Wang Z, Dong H, Wang J, Huang Y, Zhang X, Tang Y, Li Q, Liu Z, Ma Y, Tong J, Huang L, et al. 2020. Pro-survival and anti-inflammatory roles of NF-κB c-Rel in the Parkinson's disease models. *Redox Biol* 30: 101427

263. Parrella E, Bellucci A, Porrini V, Benarese M, Lanzillotta A, Faustini G, Longhena F, Abate G, Uberti D, Pizzi M. 2019. NF-κB/c-Rel deficiency causes Parkinson's disease-like prodromal symptoms and progressive pathology in mice. *Transl Neurodegener* 8: 16

264. Aravalli RN, Hu S, Lokensgard JR. 2008. Inhibition of toll-like receptor signaling in primary murine microglia. *J Neuroimmune Pharmacol* 3: 5-11

265. Sanchez JF, Sniderhan LF, Williamson AL, Fan S, Chakraborty-Sett S, Maggirwar SB. 2003. Glycogen synthase kinase 3beta-mediated apoptosis of primary cortical astrocytes involves inhibition of nuclear factor kappaB signaling. *Mol Cell Biol* 23: 4649-62

266. Atkins CM, Oliva AA, Jr., Alonso OF, Pearse DD, Bramlett HM, Dietrich WD. 2007. Modulation of the cAMP signaling pathway after traumatic brain injury. *Exp Neurol* 208: 145-58

267. Katzenell S, Cabrera JR, North BJ, Leib DA. 2017. Isolation, Purification, and Culture of Primary Murine Sensory Neurons. *Methods Mol Biol* 1656: 229-51

268. Leeman JR, Weniger MA, Barth TF, Gilmore TD. 2008. Deletion analysis and alternative splicing define a transactivation inhibitory domain in human oncoprotein REL. *Oncogene* 27: 6770-81

269. Deem MW, Hejazi P. 2010. Theoretical aspects of immunity. *Annu Rev Chem Biomol Eng* 1: 247-76

270. Drayman N, Patel P, Vistain L, Tay S. 2019. HSV-1 single-cell analysis reveals the activation of anti-viral and developmental programs in distinct sub-populations. *Elife* 8

271. Wyler E, Franke V, Menegatti J, Kocks C, Boltengagen A, Praktiknjo S, Walch-Rückheim B, Bosse J, Rajewsky N, Grässer F, Akalin A, et al. 2019. Single-cell RNA-sequencing of herpes simplex virus 1-infected cells connects NRF2 activation to an antiviral program. *Nat Commun* 10: 4878

272. Bongfen SE, Rodrigue-Gervais IG, Berghout J, Torre S, Cingolani P, Wiltshire SA, Leiva-Torres GA, Letourneau L, Sladek R, Blanchette M, Lathrop M, et al. 2012. An N-ethyl-N-nitrosourea (ENU)-induced dominant negative mutation in the JAK3 kinase protects against cerebral malaria. *PLoS One* 7: e31012

273. Gerondakis S, Grumont R, Gugasyan R, Wong L, Isomura I, Ho W, Banerjee A. 2006. Unravelling the complexities of the NF-kappaB signalling pathway using mouse knockout and transgenic models. *Oncogene* 25: 6781-99

274. Neznanov N, Chumakov KM, Neznanova L, Almasan A, Banerjee AK, Gudkov AV. 2005. Proteolytic cleavage of the p65-RelA subunit of NF-kappaB during poliovirus infection. *J Biol Chem* 280: 24153-8

275. Coiras M, López-Huertas MR, Mateos E, Alcamí J. 2008. Caspase-3-mediated cleavage of p65/RelA results in a carboxy-terminal fragment that inhibits IkappaBalpha and enhances HIV-1 replication in human T lymphocytes. *Retrovirology* 5: 109

276. Gregory DJ, Godbout M, Contreras I, Forget G, Olivier M. 2008. A novel form of NF-kappaB is induced by Leishmania infection: involvement in macrophage gene expression. *Eur J Immunol* 38: 1071-81

277. Hodgson A, Wier EM, Fu K, Sun X, Yu H, Zheng W, Sham HP, Johnson K, Bailey S, Vallance BA, Wan F. 2015. Metalloprotease NleC suppresses host NF-κB/inflammatory responses by cleaving p65 and interfering with the p65/RPS3 interaction. *PLoS Pathog* 11: e1004705

278. Roux KJ, Kim DI, Burke B, May DG. 2018. BioID: A Screen for Protein-Protein Interactions. *Curr Protoc Protein Sci* 91: 19.23.1-19.23.15

279. Reinhard K, Huber M, Wostl C, Hellhund A, Toboldt A, Abass E, Casper B, Joeris T, Herr C, Bals R, Steinhoff U, et al. 2011. c-Rel promotes type 1 and type 17 immune responses during Leishmania major infection. *Eur J Immunol* 41: 1388-98

280. Luu M, Romero R, Bazant J, Abass E, Hartmann S, Leister H, Fischer F, Mahdavi R, Plaza-Sirvent C, Schmitz I, Steinhoff U, et al. 2020. The NF-κB transcription factor c-Rel controls host defense against Citrobacter rodentium. *Eur J Immunol* 50: 292-94

APPENDIX

COPYRIGHT PERMISSIONS

1. As per the policies of The Journal of Immunology, I, as first co-author, retain the permission to include the final, published version of the following article in Chapter 2 of this thesis, with the following attribution:

Mathieu Mancini, Grégory Caignard, Benoît Charbonneau, Anne Dumaine, Nila Wu, Gabriel A. Leiva-Torres, Steve Gerondakis, Angela Pearson, Salman T. Qureshi, Robert Sladek, and Silvia M. Vidal. 2019. *Rel*-dependent immune and central nervous system mechanisms control viral replication and inflammation during mouse herpes simplex encephalitis. *J Immunol* 202: 1479-93.

Digital object identifier for the original work is provided here:
https://doi.org/10.4049/jimmunol.1800063.

2. In Chapter 1 of this thesis, Figures 1 and 2, and Table 1 are adapted, with modifications, from the following article, published in Mammalian Genome in 2018. As co-authors, Silvia Vidal and I hold the copyright. In addition, the article is open-access and distributed under the terms of the Creative Commons Attribution 4.0 International License (http://creativecommons.org/licenses/by/4.0/), which permits unrestricted use, distribution, and reproduction in any medium, with the following attribution:

Mathieu Mancini and Silvia M. Vidal. Insights into the pathogenesis of herpes simplex encephalitis from mouse models. 2018. *Mammalian Genome*. 29(7-8): 425-445.

Digital object identifier for the original work is provided here:
https://doi.org/10.1007/s00335-018-9772-5